BRCA1/BARD1-Dependent Ubiquitylation of Nucleosomal Histone H2A

Samuel R. Witus

A dissertation

Submitted in partial fulfilment of the

Requirements for the degree of

Doctor of Philosophy

University of Washington

2022

Reading Committee:

Rachel E. Klevit, Chair

Ning Zheng

Andrea E. Wills

Program Authorized to Offer Degree:

Department of Biochemistry

University of Washington

Abstract

BRCA1/BARD1-Dependent Ubiquitylation of Nucleosomal Histone H2A

Samuel R. Witus

Chair of the Supervisory Committee:
Professor Rachel E. Klevit
Department of Biochemistry

Breast cancer type-1 susceptibility protein (*BRCA1*) was the first gene to be linked to heritable breast and ovarian cancer over thirty years ago. Since then, remarkable progress has been made with regards to genetic testing, prophylactic measures, and treatment options available to patients with *BRCA1* mutations. However, thousands of *BRCA1* variants of unknown significance still exist, leaving doctors and patients with no clear path forward. Understanding the underlying biology of the gene product of *BRCA1* (the BRCA1 protein) is an important goal that may improve health outcomes. The BRCA1 protein forms an obligate heterodimeric complex with its binding partner, BARD1 (BRCA1/BARD1). Together, this large complex functions in the nucleus of cells, protecting the integrity of genome by helping to repair double-stranded DNA breaks and regulate the transcription of certain genes. These functions are mediated, in-part, by the sole known enzymatic function of BRCA1/BARD1 as a RING-type E3 ubiquitin (Ub) ligase. Recently, histone H2A in nucleosomes has emerged as a central substrate for BRCA1/BARD1-dependent Ub ligase activity. BRCA1/BARD1 targets specific lysine sites on the extreme C-terminal tail of histone H2A for Ub transfer which serves as a signal for DNA repair and transcriptional regulation. In this thesis, I first review what is known about the E3 ubiquitin ligase function of BRCA1/BARD1 in general (Chapter 1) and specifically at chromatin (Chapter 2). In Chapter 3, I present a cryo-EM structure of the BRCA1/BARD1 RING/RING heterodimer bound to a nucleosome substrate, with additional structural and biochemical data that provide key mechanistic insight into the basis for site-specific ubiquitylation of nucleosomal

H2A. In Chapter 4, I reveal interactions between non-RING regions of BARD1 and nucleosome substrates that enhance chromatin binding and H2A ubiquitylation, describing BRCA1/BARD1/chromatin complexes with extensive multivalency. Overall, my work uncovers a critical role for the previously underappreciated partner of BRCA1, BARD1. Together, this body of work sets the stage for additional discoveries into the biological importance of BRCA1/BARD1 H2A-specific E3 Ub ligase activity in DNA repair and transcriptional regulation. These findings may ultimately be used to predict or experimentally measure the impacts of patient mutations of unknown clinical significance in addition to explaining the effects of known pathogenic mutations. Knowledge of the molecular effects of these mutations and their underlying biology may ultimately lead to enhanced prophylactic measures or new avenues of therapeutics for patients.

TABLE OF CONTENTS

LIST OF FIGURES

LIST OF TABLES

ACKNOWLEDGEMENTS

I am lucky to be the recipient of outstanding mentorship. First, I would like to thank Rachel for giving me the latitude to explore my interests, the space to fail, and all the tools to develop into an independent, rigorous scientist. She has been the perfect mentor for me, and I will be forever grateful for my time in the Klevit Lab. Thank you to Peter Brzovic, who has been a consistent source of support, thoughtful conversation, and humor. Thank you to Justin Kollman for his support of my cryo-EM endeavors and growth as a scientist. Thank you to my undergraduate research mentor Lina Dahlberg for her continued presence in my life and career. Thank you to my thesis committee members Ning Zheng, Champak Chatterjee, Andrea Wills, and David Veesler for their supportive insights. Thank you to Erin Kirschner for keeping track of the details and caring deeply about us.

I am indebted to every scientist that I have had the opportunity to work with these past six years, of which there are too many to name individually. You know who you are. You pushed me to be better, to work collaboratively, to stay enthusiastic; you lifted me up me when things seemed bleak, and celebrated successes. I consider myself fortunate to cross paths with each one of you. I am especially thankful to those who considered me a mentor, those who I directly collaborated with, and members of the Klevit lab with whom I interacted with daily.

To my parents, who cultivated my curiosity, encouraged excellence, and have seen me through the extended journey, I would not be where I am if not for you. And finally, to my fiancé Erin. Whose undying patience (which I frequently test), encouragement, friendship, and love have kept me going. Words will never be enough. Thank you.

CHAPTER 1

The BRCA1/BARD1 ubiquitin ligase and its substrates

Samuel R. Witus[1], Mikaela D. Stewart[2], Rachel E. Klevit[1,3].

1. University of Washington School of Medicine. Department of Biochemistry. Seattle, WA, U.S.A.
2. Texas Christian University. Department of Biology. Fort Worth, TX, U.S.A.
3. Corresponding author contact: klevit@uw.edu

Reprinted with permission from: Samuel R. Witus, Mikaela D. Stewart, Rachel E. Klevit; The BRCA1/BARD1 ubiquitin ligase and its substrates. *Biochem J* 2021;
doi: https://doi.org/10.1042/BCJ20200864

Author Contributions

S.R.W. and M.D.S. wrote the first draft of the manuscript and made figures. S.R.W., M.D.S., and R.E.K. wrote and edited the final draft of the manuscript.

Abstract

Mutations in breast cancer type 1 susceptibility protein (BRCA1) and its heterodimeric binding partner BARD1 confer a high risk for the development of breast and ovarian cancers. The sole enzymatic function of the BRCA1/BARD1 complex is as a RING-type E3 ubiquitin (Ub) ligase, leading to the deposition of Ub signals onto a variety of substrate proteins. Distinct types of Ub signals deposited by BRCA1/BARD1 (i.e., degradative vs. non-degradative; mono-Ub vs. poly-Ub chains) on substrate proteins mediate aspects of its function in DNA double-stranded break repair, cell-cycle regulation, and transcriptional regulation. While cancer-predisposing mutations in both subunits lead to the inactivation of BRCA1/BARD1 ligase activity, controversy remains as to whether its Ub ligase activity directly leads to tumorigenesis. Investigation of BRCA1/BARD1 substrates using rigorous, well-validated mutants and experimental systems will ultimately clarify the role of its ligase activity in cancer and possibly establish prognostic and diagnostic metrics for patients with mutations. In this review, we discuss the Ub ligase function

of BRCA1/BARD1, highlighting experimental approaches, mechanistic considerations, and reagents that are useful in the study of substrate ubiquitylation. We also discuss the current understanding of two well-established BRCA1/BARD1 substrates (nucleosomal H2A and estrogen receptor a) and several recently discovered substrates (p50, NF2, Oct1, and LARP7). Lessons from the current body of work should provide a road map to researchers examining novel substrates and biological functions attributed to BRCA1/BARD1 Ub ligase activity.

Introduction

Mutations in the *BRCA1* gene were first linked to increased risk for familial breast cancer over 30 years ago[1–4]. Since then, *BRCA1* and its protein product BRCA1 (breast cancer type 1 susceptibility protein) have been investigated by clinical researchers and basic scientists alike. Thousands of *BRCA1* variants of unknown significance still require classification as pathogenic or benign, potentially influencing medical decisions of individuals carrying such mutations. More recently, mutations in the BARD1 gene associated with high risk for breast and ovarian cancer have been identified[5–7]. Together the two gene products form a heterodimeric protein complex, BRCA1/BARD1, that acts as a tumor suppressor by serving as a central regulator and guardian of genomic integrity throughout the cell cycle[8]. Although most past research has focused mainly on BRCA1, conditional knockout of either BRCA1 or BARD1 in mouse mammary epithelial cells leads to genomic instability and indistinguishable carcinomas, supporting the prevailing view that the proteins' critical tumor-suppressor functions arise from the heterodimer[9].

BRCA1/BARD1 is largely localized to the nucleus and is best characterized in its critical role in double-stranded DNA break repair by promoting homologous recombination (HR). It also functions in transcriptional regulation, cell-cycle control, centrosome regulation, metabolic regulation, and DNA decatenation[10–13]. In general, these functions are attributed to the molecular scaffolding properties of BRCA1/BARD1, which is a component of numerous

extremely large multi-protein complexes[14,15]. The sole biochemical function defined for BRCA1/BARD1 is as a ubiquitin (Ub) E3 ligase[16,17]. It is well established that the ligase activity is required for BRCA1/BARD1's role in the maintenance of genome integrity and transcriptional regulation, but whether the activity is required for other processes in which BRCA1/BARD1 is implicated remains unclear. A direct link between BRCA1/BARD1 E3 ligase activity and its role as a tumor suppressor is not universally accepted, with studies arriving at conflicting conclusions[18–20]. A major hurdle to a more complete understanding of BRCA1/BARD1 ligase function and its ties to tumor suppression is a lack of clarity regarding how ubiquitylation of each of the numerous cellular protein targets identified to date regulates their function and the processes in which they participate **(Table I)**. Here we focus on aspects of BRCA1/BARD1 related to its E3 ligase function, paying special attention to challenges and strategies that can address remaining gaps in knowledge.

BRCA1/BARD1 is a RING-type E3 ligase

BRCA1 and BARD1 form a large obligate heterodimer via their N-terminal RING domains, creating a structure that is an archetypal RING-type E3 ligase[21,22] **(Fig. 1a, b)**. Members of this large E3 class (more than 600 in humans) simultaneously bind a substrate and a Ub-conjugating (E2) enzyme that holds activated Ub ("E2~Ub") and must therefore contain distinct substrate-and E2-binding regions[23]. RING domains bind E2s, potentially leaving the remainder of the complex for substrate binding. Intriguingly, BRCA1 and BARD1 are the only two proteins in the human proteome that contain both an N-terminal RING (Really Interesting New Gene) domain and C-terminal tandem BRCT (BRCA1 C-terminal) domains and both contain substantial intrinsically disordered content characteristic of molecular scaffolds[24] **(Fig. 1a)**. BARD1 also has an ankyrin-repeat domain (Ank) adjacent to its BRCT domain; these are usually associated with protein-protein interactions.

A challenge faced in the study of RING E3s is that they do not possess a catalytic residue that is directly involved in the Ub transfer reaction. Instead, RINGs facilitate direct transfer of Ub from an E2~Ub to a substrate. While prevalent cancer-associated mutations in BRCA1 RING zinc-coordinating cysteine residues eliminate E3 ligase activity towards all known substrates, they do so by disrupting the structural integrity of the RING and possibly by destabilizing BRCA1 and BARD1 in cells[16,25–27]. No single mutation has been discovered that can both generate a completely "ligase-dead" BRCA1/BARD1 and leave the structure and other potential functions intact[28]. Without such a tool, it is difficult to parse out the role of ligase activity from other potential cellular functions. As discussed below, this situation has contributed to the ongoing controversy regarding the role of E3 ligase activity in BRCA1 tumor-suppressor function because a BRCA1 RING mutation presumed to be "ligase-dead" (Ile26Ala) may not be truly dead, as it retains activity with some E2 enzymes in vitro[29].

There are multiple substrate-binding regions in both subunits of BRCA1/BARD1 **(Table I)**. It is also possible, though not yet reported, that some substrates bind indirectly via other binding partners as is the case with cullin-RING ligases and their substrate adaptor proteins[30]. Numerous BRCA1/BARD1 binding partners have been identified, any of which could be substrates or substrate adaptors. However, only a subset of reported BRCA1/BARD1-binding proteins have been demonstrated explicitly to be ubiquitylated and an even smaller subset has been rigorously validated as BRCA1/BARD1-dependent substrates. Regions known to interact with established substrates are noted in Figure 1A. Although these regions are mostly localized to the ordered regions of BRCA1/BARD1, individual substrates could feasibly bind throughout the protein (including the expansive IDRs), making characterization of relevant substrates with unknown ligase binding sites challenging.

Gold standards for understanding Ub E3 ligase function are 1) the ability to reconstitute the activity of interest with high fidelity using specified components and 2) structural information for complexes containing E2, E3, and substrate. Below, we identify challenges posed by features of BRCA1/BARD1 that must be considered when designing in vitro, cellular, or animal studies.

Challenges associated with E2s.

RING E3s must assemble the relevant ubiquitylation machinery to promote substrate modification. Thus, a first step needed to understand RING E3 function requires knowing the relevant E2(s) with which it works. BRCA1/BARD1 can bind to and function with nine of the ~36 human E2s in vitro, adding complexity to the study of BRCA1/BARD1 function[31]. Despite this, the vast majority of studies use only the Ube2D family of E2s. Though general mechanistic principles are likely similar for all the E2s, there are bound to be idiosyncratic differences that can confound interpretation of results. An important case in point is the widely used I26A-BRCA1 variant. Originally reported to lack detectable activity in association with the E2 Ube2D3 (UbcH5c) *in vitro*, it has subsequently been observed that I26A-BRCA1 retains residual activity with other BRCA1/BARD1-partnering E2s[29,32]. This raises the possibility that I26A-BRCA1 has sufficient ligase activity to mask potential effects of true loss-of-function in cells or animals.

The general rule is that an E2 specifies the Ub product generated in RING E3-directed reactions: attachment of a single Ub (mono-Ub) or one of seven possible poly-Ub chain types[33]. Different ubiquitin products lead to distinct cellular outcomes (e.g., degradative and non-degradative) that alter how best to investigate them in cells. Different pairings of E2s and BRCA1/BARD1 produce mono-Ub attached to lysine sidechains (Ube2E1/2/3), mono-Ub attached to the N-terminus of a substrate (Ube2W), and several different poly-Ub chain types (Ube2D1/2/3, Ube2K, Ube2N)[31,34]. BRCA1/BARD1 preferentially catalyzes atypical, non-degradative K6-linked polyubiquitin chains with the E2 enzymes Ube2D1/2/3 in

autoubiquitylation reactions in vitro and in cells[35,36]. The molecular functions of K6-linked Ub chains synthesized by BRCA1/BARD1 remain a major unanswered question, though they likely play a role in some aspect of DNA DSB repair[37]. BRCA1/BARD1 catalyzes K48- and K63-linked chain formation with the E2s Ube2K and Ube2N/UBE2V, respectively[31]. In vitro, BRCA1/BARD1-directed synthesis of these chain linkages requires a different E2 to attach the first Ub to substrate, in a so-called priming step, as these chain-building E2s are inefficient at performing Ub transfer to a lysine that is not on an acceptor Ub. In contrast, Ube2D family members can catalyze both types of reactions, with the specificity determined at least in part by the substrate itself. For example, the E2/E3 pairing of Ube2D1/2/3 and BRCA1/BARD1 generates K6-linked chains in auto-ubiquitylation reactions but mono-ubiquitylates nucleosomal H2A and ERα[5,29,35]. This implies that BRCA1/BARD1 and Ube2D assemble into mechanistically distinct structures with the various substrates that allow for either mono- or poly-ubiquitylation. Deciphering the nature of the ubiquitin product deposited on a novel BRCA1/BARD1 substrate is likely to yield insights into the consequence of the modification as well as the E2s that may be involved. In general, this can be accomplished using mass spectrometry, ubiquitin lysine mutations, chain-linkage specific Ub antibodies, or a combination of these tools[38,39].

The BRCA1-binding E2s recognize a similar binding surface on the RING domain, making it virtually impossible to find mutations that specifically ablate one E2's interaction while leaving others intact[32]. Furthermore, no single-site mutation other than those that disrupt RING structure has been discovered that will render BRCA1/BARD1 "dead" to all its E2s. The E2s that work with BRCA1/BARD1 include several with overlapping and/or redundant activities, especially the three isoforms of Ube2D. This feature may make a strategy of using single E2 knock-out strains uninformative or, at least, confounding. Furthermore, the requirement for both a priming E2 (i.e., an E2 that can place the first Ub onto a substrate) and a chain-building E2, both of which work with BRCA1/BARD1, adds further complications to parsing out BRCA1/BARD1-dependent

substrate ubiquitylation. One way this challenge can be addressed is by testing the entire panel of E2s, alone and in pairs, with any putative substrate in vitro.

Approaches that may overcome challenges.

A triple mutant BRCA1 I26A/L63A/K65A abrogates ligase function with all BRCA1-interacting E2s and does not appear to have defects in BARD1 heterodimerization or protein stability in vitro[29] **(Fig. 1b, c)**. Introduction of the triple-mutant in cells and animals could clarify the controversial role of BRCA1/BARD1 ligase activity in DNA damage, tumor suppression, and other cellular processes. A designed BARD1 mutation (R99E) inactivates E3 activity toward all substrates tested to date for reactions using Ube2D family members as the E2[40] **(dark green, Fig. 1b, c)**. Complementary mutation of ubiquitin suggested that Arg99 helps to stabilize the more active closed state of the E2~Ub conjugate, a general mechanism of action among RING-type E3 ligases[40–42]. However, it is not known whether the BARD1 Arg99 mutation eliminates activity with all E2 partners of BRCA1/BARD1, so results obtained using this BARD1 mutant in cells should be interpreted with caution.

In addition to approaches that rely on loss of ligase activity to identify substrates and/or to assess the cellular consequences of their BRCA1-directed ubiquitylation, use of a hyperactive E3 ligase may be informative. Such species may yield increased levels of products without the potential pitfalls that over-expression at non-physiological ligase protein levels can entail. A deep mutational screen identified residues in the BRCA1 RING that, when mutated, enhance its ligase activity[29,43]. Specifically, tandem introduction of L51W and K65R in BRCA1 yields a hyperactive ligase. However, the hyperactive variant has lower specificity for E2 pairings and ubiquitin linkages (mono-Ub vs. chain building) in substrate and autoubiquitylation assays, indicating that wild-type BRCA1 ligase activity is tuned to work with specific E2s to promote different Ub linkages in a context-dependent manner (substrate vs. autoubiquitylation). Notably,

combination of hyper-activating mutations with the ligase-dead C61G mutant in cis (L51W/K65R/C61G) restores activity of the Zn^{2+}-coordinating mutant to wild-type levels in vitro, implying there could be strategies that stabilize the cancer-associated mutant protein to restore its activity.

Considerations about BRCA1/BARD1 constructs used for in vitro and cellular/in vivo investigations

A minimal BRCA1/BARD1 RING heterodimer consisting of the first ~110 residues of each subunit is sufficient to bind to an E2 and to stimulate the discharge of ubiquitin. These constructs contain the RING domain and flanking α-helices that are necessary and sufficient for formation of the BRCA1/BARD1 heterodimer[21]. Although both BRCA1 and BARD1 contain RING domains, only the BRCA1 RING binds E2s[31,32]. The minimal RING constructs of BRCA1/BARD1 have provided important biochemical and structural insights into the underlying mechanism of Ub transfer from an associated E2~Ub. However, additional BRCA1/BARD1-based reagents are required to tackle questions regarding substrate-specific modification.

Robust methodology has been developed to observe RING E3 ligase-mediated ubiquitylation in vitro and all required components to reconstitute a ubiquitylation reaction (E1, E2, Ub) are available commercially or through services such as Addgene[44]. Biochemically pure recombinant BRCA1/BARD1 heterodimer constructs can be generated by co-expression in E. coli[32]. There are two widely used versions: 1) a minimal RING construct composed of BRCA1(1-112)/BARD1(26-142) and 2) a longer construct that contains the RING heterodimer and portions of both IDRs BRCA1(1-302)/BARD1(26-327). The minimal construct is sufficient to bind to an E2 and to stimulate the discharge of ubiquitin in so-called E2~Ub discharge reactions that monitor enhancement of Ub release from an E2 by BRCA1/BARD1[45]. This construct is not detectably auto-ubiquitylated and, with the exception of nucleosomal histone H2A, does not

contain a substrate-binding region[46]. The longer construct can serve as a proxy substrate in autoubiquitylation assays, making it useful in direct assessment of the intrinsic ligase activity of point mutations on BRCA1/BARD1 or an E2 of interest. BRCA1(1-302)/BARD1(26-327) is also active in substrate-level ubiquitylation reactions with estrogen receptor-α[29,47].

The truncated BRCA1/BARD1 constructs described above likely lack recognition domains for most substrates. For example, the C-terminal BRCTs of BRCA1 or BARD1 are required for binding the substrates CtIP, RPB1, NF2, p50, and LARP7[48–53] **(Fig. 1a)**. Furthermore, substrates may interact with multiple regions of BRCA1/BARD1, necessitating thorough analysis of all possible interaction sites, for example ERα and g-tubulin[47,54,55] **(Fig. 1a)**. Production of biochemical quantities of highly purified intact full-length BRCA1/BARD1 has long been a roadblock due to the large size and high amount of intrinsic disorder of the full-length proteins. A robust expression and purification scheme to generate sub-milligram quantities of high-quality full-length BRCA1/BARD1 using a baculovirus-based expression system in insect cells is now available[56]. This important development provides a new gold standard for production of BRCA1/BARD1 for substrate ubiquitylation assays. The published protocol employs FLAG immunoprecipitation of the complex followed by ion-exchange chromatography, but this can be adapted to incorporate a twin Strep-tag appended to the N-terminus of BARD1, yielding comparable results at a significantly decreased cost[57]. The ability to generate biochemical-quality full-length BRCA1/BARD1 represents a major advance that should propel studies of native substrates.

Post-translational modifications (PTMs) either on the substrate, on BRCA1/BARD1, or both may affect ligase activity. PTMs including acetylation, phosphorylation, proline isomerization, ubiquitylation, and SUMOylation have been reported on BRCA1/BARD1[58–62]. Several have been observed to modulate ligase function in vitro and possibly in vivo. Phosphorylation and

ubiquitylation are often engaged in crosstalk and BRCA1 is modified by DNA damage checkpoint kinases throughout the protein[59,63]. Phosphorylation of BRCA1/BARD1 by aurora kinase A has been shown to dampen its ligase activity, and the cell-cycle kinase CDK2/cyclin E1 has been observed to suppress the E3 ligase activity of BRCA1/BARD1 indirectly through depletion of its protein levels[64,65]. The BRCT domains of each subunit bind to phosphorylated substrates and other binding partners, allowing for the possibility that additional BRCA1/BARD1 substrates are recruited via recognition of phosphorylated sites. In the future, methods to generate defined modified protein reagents and/or to manipulate specific sites of modification on BRCA1/BARD1 and/or its substrates will be needed to sort out these important aspects of regulation.

BRCA1/BARD1 itself can serve as a substrate for ubiquitylation, either through its own ligase activity (i.e., autoubiquitylation) or by other cellular ligases[66–71]. How or if ubiquitylation of BRCA1/BARD1 directly affects its ligase activity remains an open question. The modification could affect intrinsic ligase activity and/or could serve to recruit certain substrates. BRCA1/BARD1 autoubiquitylation is reported to enhance its ligase activity in vitro on free histones as a proxy substrate[61]. But neither a mechanism by which this effect works nor evidence that it affects ubiquitylation of a bona fide substrate are yet available. Ubiquitylated BRCA1 can be detected in cells after DNA damage. The ubiquitin binding domain of UBXN1 was shown to bind to autoubiquitylated BRCA1/BARD1 and suppress its ligase function in vitro and in cells[72]. However, the significance of ubiquitylation of BRCA1/BARD1 as a regulatory signal with an outcome other than degradation remains to be clearly defined[73].

BRCA1 is SUMOylated at lysine residues proximal to the RING domain[62]. The responsible SUMO ligases are important for HR following DNA damage, and SUMOylation of BRCA1 was found to enhance its E3 ligase activity in vitro as judged by its ability to form poly-Ub chains.

Mutation of a BRCA1 lysine targeted for SUMOylation or of part of the SUMO ligase recognition motif decreased the co-localization of BRCA1 with conjugated ubiquitin, suggesting that this modification may also contribute to its ligase activity in cells. As BRCA1/BARD1 is the target of myriad PTMs that influence its biochemical properties including Ub ligase function, a full understanding of substrate ubiquitylation will require careful and thorough parsing of these effects.

Finally, an important consideration for BRCA1/BARD1 studies is ensuring proper maintenance of the heterodimer. BRCA1/BARD1 heterodimerization is not only required for nuclear localization but also for ensuring the stability of the complex[16,74,75]. Heterodimerization is thought to mask degron sequences located near the RING domains of each subunit[70,76]. Attempts to deplete one subunit can result in concomitant depletion of the other[77]. Subsequent replacement of one subunit by overexpression via transient transfection does not necessarily restore the new BRCA1/BARD1 complex to endogenous levels[5,78,79]. Therefore, it may be necessary to co-transfect both BRCA1 and BARD1 and to confirm proper heterodimerization of the ectopically-expressed protein by immunoprecipitation when designing rescue experiments to test the effects of mutations. An alternative approach is to generate stable cell lines expressing siRNA-resistant BRCA1 or BARD1, and subsequently deplete the endogenous protein. This approach has been successfully employed for both BRCA1 and BARD1 to study ligase activity using the Flp-FRT recombination system in multiple cell-types[19,40]. Additionally, a BARD1 auxin-inducible degron (AID) system in HCT-116 cells has been developed and employed to study its function in DNA damage repair[80,81]. However, these two methods (Flp-FRT and AID) have yielded conflicting data about the requirements for BRCA1/BARD1 ligase activity in DNA damage repair using the Ube2D-deficient BARD1 Arg99Glu mutant, necessitating further comparison of the two methods and clarification of the effects of this mutant[40,80].

Cellular Substrates of BRCA1/BARD1 ligase activity

The biological outcomes of BRCA1/BARD1 ligase activity are ultimately mediated through its cellular substrates. A full understanding of the cellular function of BRCA1/BARD1 requires knowledge of its cellular substrates, the Ub signals generated, and the functional consequences of the substrate modification. In addition to the difficulty of identifying E2s associated with modification of a particular substrate, many substrates may be targeted by more than one E3 ligase, so the effects of depletion of a particular E3 may be difficult to discern. Furthermore, BRCA1/BARD1 can generate non-degradative signals, so the powerful methods that rely on changes in protein levels associated with E3 ablation will not be applicable. Finally, in vitro validation of substrate modification may require use of full-length BRCA1/BARD1 which, until recently, has not been a viable option. Despite these challenges, putative BRCA1/BARD1 substrates have been identified primarily by testing known interaction partners for BRCA1/BARD1-dependent ubiquitylation. Several previous reviews provide in-depth summaries on all but the most recently discovered substrates[82–85]. The identities of known substrates reveal that BRCA1/BARD1 can target a diverse subset of nuclear proteins and deposit different ubiquitin marks that can serve degradative, stabilizing, or signaling roles **(Table I)**. To illustrate some best practices and highlight the biological functions of several substrates, we elaborate on two exemplary BRCA1/BARD1 substrates – nucleosomal histone H2A and ERα and discuss four recently identified substrates that have not been presented in previous reviews (p50, Oct1, NF2, and LARP7).

Discovery of BRCA1/BARD1 substrates

In addition to candidate-based approaches, putative substrates have been identified by affinity enrichment of ubiquitylated proteins upon overexpression of BRCA1/BARD1 in 293T cells[86,87]. Over one-hundred proteins with increased ubiquitylation were detected, providing a rich pool of potential substrates to be validated. Among them, the histone variant macroH2A1 was identified

and mono-ubiquitylation of a specific lysine residue (K123) was shown to be involved in regulation of cellular senescence[87]. Two proteins involved in transcriptional regulation and DNA damage repair, GADD45GIP1 and HLTF, were observed to be ubiquitylated in a BRCA1/BARD1-dependent manner in the mass-spectrometry screen and verified by Western blotting, although biological roles for ubiquitylation of these putative substrates have yet to be investigated. However, increased ubiquitylation levels of previously validated BRCA1/BARD1 substrates nucleophosmin (NPM1), ERα, and canonical H2A ubiquitylated at K125/127/129 were not detected. Substrates may be missed due to transient ubiquitylation/deubiquitylation, cell-type specific effects (e.g., mammary vs. non-mammary), or lack of peptide coverage in mass spectrometry analysis.

Considerations in substrate characterization

For substrate ubiquitylation to occur, BRCA1/BARD1 must simultaneously bind an activated E2~Ub conjugate and a substrate protein, bringing the two into proximity. As mentioned previously, substrates may bind throughout BRCA1 or BARD1 or, possibly, may interact indirectly. The possibility of multiple interacting regions should be entertained when characterizing substrate ubiquitylation. Pull-down assays using isolated domains as bait can be an effective method to identify substrate binding domains. Sequential C-terminal truncation constructs of BRCA1 and BARD1 that leave the N-terminal RING heterodimer unit intact are useful reagents for in vitro ubiquitylation assays with substrate candidates. However, relevant substrate-binding interactions and ubiquitylation may be decoupled. For example, the interaction of LARP7, a 7SK RNA binding protein that controls RNAPII pausing, is likely mediated through the BARD1 C-terminal BRCT domain in a phospho-dependent manner in cells[53]. But a construct that lacked the BRCTs (BRCA1(1-304)/BARD1(26-327)) catalyzed poly-ubiquitylation of LARP7 in vitro, suggesting differential requirements for cellular recruitment compared to in vitro Ub

modification. Such considerations are especially important when characterizing the ubiquitylation of putative substrates.

An emerging feature of BRCA1/BARD1-dependent ubiquitylation is that in many cases specific substrate lysine residues are targeted, in contrast to most cases in which poly-Ub chains are attached to a substrate with no apparent lysine discrimination. Specifically-targeted residues may play a critical role in downstream signaling, so their identification using mutagenesis or mass-spectrometry analysis is a worthwhile endeavor. Lysine to arginine mutations that abrogate substrate ubiquitylation may be a viable way to characterize the effects of BRCA1/BARD1 ligase activity. Important considerations for such an approach include the possibility that other substrate lysines may be modified in the absence of its preferred target residues, or that the mutated lysine residues are also targeted for alternative PTMs such as acetylation[47,88]. An additional strategy in which substrates with Ub genetically fused to their C-terminus has been successfully employed to study substrates that are mono-ubiquitylated by BRCA1/BARD1 at or near their C-terminus. Despite the fact that the N-terminus of Ub is tethered to the substrate in the genetic fusions while bona fide products are attached to the Ub C-terminus, such chimeras have been shown to rescue the effects of BRCA1/BARD1 ligase deficiency for both nucleosomal H2A and p50[5,40,52,89,90].

Case Studies and recently discovered substrates

Below we discuss the two best-characterized BRCA1/BARD1 substrates, estrogen receptor (ERα) and histone H2A, and recently discovered substrates. The examples include substrates that are modified with non-degradative Ub signals (mono-ub and K63-linked poly-Ub) and others that are modified with degradative K48-linked chains, highlighting the spectrum of biological outcomes experienced by BRCA1/BARD1 substrates.

Estrogen Receptor-α

Although BRCA1 and BARD1 are expressed in a wide range of cell types, inherited mutations in the genes are associated with breast and ovarian cancers. Therefore, identification of substrates that might provide insight into the tissue-specificity of BRCA1-associated cancers is a key goal. The hormone-responsive estrogen receptor (ERα) was such a candidate, based on early observations that overexpression of wild-type BRCA1, but not a cancer-associated BRCA1 mutant (C61G) results in repressed ERα transcriptional activity[91,92]. A direct interaction between BRCA1/BARD1 and ERα was inferred from pull-down experiments in which the first 302 residues of BRCA1 co-purified with ERα [91].

In reconstituted systems, ERα is mono-ubiquitylated by BRCA1/BARD1 in the linker region between the ERα DNA-binding and ligand-binding domains[47]. Substitution of the modified residues identified by mass spectrometry (K302/303) with arginine did not completely suppress ERα ubiquitylation, suggesting that BRCA1 can ubiquitylate other lysine residues in the absence of its preferred targets[47]. Of the E2s that work with BRCA1/BARD1, only Ube2D family members modify ERα in collaboration with BRCA1/BARD1, revealing an E2/substrate specificity that has not been observed with other substrates[29,46] **(Table I)**.

BRCA1-dependent ERα monoubiquitylation was subsequently demonstrated in cells overexpressing BRCA1 and by ubiquitin immunoprecipitation with endogenously expressed BRCA1 and ERα[88,93]. Consistent with the E2 specificity observed *in vitro*, cells expressing the Ube2D-incompetent BRCA1 mutant (I26A-BRCA1) failed to display repressed ERα transcriptional activity[88].

ERα binding regions on BRCA1/BARD1 were mapped using in vitro ubiquitylation assays with purified components. BRCA1/BARD1 constructs that included the minimal RING heterodimer

region required for enzymatic activity and incrementally larger regions of the BRCA1/BARD1 IDRs were assayed for their ability to ubiquitylate ERα. The shortest construct that produced detectable ERα ubiquitylation contained BRCA1 residues 1-258, from which it was concluded that an ERα binding site is located between IDR residues 177 and 258[47] **(Fig. 1a)**. However, more distal regions of either BRCA1 or BARD1 have not yet been tested for ERα binding, so there may be additional sites that contribute to a higher affinity interaction.

Identification of the E3/substrate interaction sites and substrate ubiquitylation sites enabled investigation of BRCA1-dependent ERα ubiquitylation in cells. Mutation of ERα residues Lys 302/303 resulted in lower levels of mono-ubiquitylated ERα and decreased suppression of ERα transcriptional activity by BRCA1[88]. Importantly, acetylation of Lys 302/303 is involved in ERα activation, so mutation of these residues disallows both their ubiquitylation and their acetylation. The balance between acetylation and ubiquitylation may therefore modulate ERα activity in cells. Consistent with this mechanism, overexpression of wild-type BRCA1 in cells, but not I26A-BRCA1, decreases levels of acetylated ERα[88]. The ERα situation highlights caveats that need to be considered when interpreting effects of substrate lysine mutation, as loss of a ubiquitylation site could have unintended effects that may or may not be relevant to the role of the ubiquitylation process under investigation.

Nucleosomal histone H2A

Early studies identified the core histones (H2A, H2B, H3, H4) and the DNA damage-specific H2A isoform H2Ax as substrates for BRCA1/BARD1 ligase activity in vitro[61,78,94]. Although BRCA1/BARD1 can attach mono-Ub to these histone proteins when presented individually (i.e., not in the context of histone dimers, octamers, or nucleosomes), these lysine-rich polypeptides likely serve as “proxy-substrates” rather than true cellular targets[95]. In the context of the nucleosome, BRCA1/BARD1 mono-ubiquitylates histone H2A and this activity is required for

maintenance of heterochromatic centers and constitutive transcriptional repression of satellite DNA regions in mice[90,95–97]. Histone H2A ubiquitylation by BRCA1/BARD1 was subsequently shown to play a role in DNA double-strand break repair, promoting cell survival after treatment with a subset of DNA damaging agents[40]. Specifically, the H2A-Ub promotes end resection of broken DNA ends by recruitment of the SWI/SNF-like chromatin remodeler SMARCAD1 to chromatin, resulting in a repositioning of 53BP1, an opposing DNA repair factor that stimulates non-homologous end joining, at DNA breaks[40,89]. Another study observed that the BRCA1 RING domain, nucleosome binding competency, and ligase activity were required for the localization of BRCA1/BARD1 to DSB sites specifically in the absence of recruitment via the BRCA1-A complex (BRCA1-BRCTs/RAP80 interaction)[98]. Thus, BRCA1/BARD1-dependent ubiquitylation of nucleosomal H2A and ligase function in general is required for specific steps of homology-directed repair (HDR).

BRCA1/BARD1-dependent H2A-Ub also transcriptionally represses certain estrogen-metabolizing cytochrome P450 (CYP450) genes in breast epithelial cells[5]. These two enzymes catalyze quinol formation and hydroxylation of estradiol, generating metabolites that can form adducts with DNA and cause double-stranded breaks[99]. De-repression of CYP450 transcription due to BRCA1/BARD1 deficiency in BARD1+/- CRISPR MCF10a knockout cells was rescued by ectopic expression of an H2A-Ub genetic fusion, but not BARD1 cancer-predisposing RING mutants that are unable to bind H2A in nucleosomes[5] **(Fig. 1a)**. Notably, these BARD1 mutants do not affect intrinsic ligase function of the heterodimer and are active with other substrates, indicating a direct nucleosome-specific effect **(Fig. 1a)**. A comprehensive catalog of genes that are transcriptionally regulated by BRCA1/BARD1-dependent H2A-Ub and how these genes are selected remains an important outstanding question.

Nucleosomal H2A is the only BRCA1/BARD1 substrate for which atomic-level structural information is currently available[46,100]. Cryo-EM structures of a BRCA1/BARD1/Ube2D3/nucleosome complex revealed that the non-E2 binding BARD1 RING domain makes unique contacts with the nucleosomal surface **(Fig. 2)**. The interaction tilts the BRCA1 E2-binding surface upward and elevates the BRCA1-bound E2 enzyme away from the nucleosomal surface, explaining why lysine residues on the H2A C-terminal tail, rather than the surface, are targeted by the ligase complex. The highly dynamic flexible H2A C-terminal tail retains its flexibility in the E3/E2/nucleosome complex, and the native H2A lysine targets of BRCA1/BARD1 have adequate reach to access the E2 active site for efficient ubiquitin transfer. Importantly, the structure revealed that the non-E2 binding RING domain of BARD1 directs the nucleosomal H2A specificity of BRCA1/BARD1. The structure also provided an explanation for known and putative cancer-associated mutations in the BARD1 RING domain, showing why these abrogate nucleosome binding and, therefore, ubiquitylation[5,46].

Altogether, the described studies establish histone H2A as an important and specific BRCA1/BARD1 substrate. While greater detail is known about the biological functions of BRCA1/BARD1-mediated H2A ubiquitylation than most other putative cellular substrates, many questions remain. For example, how is BRCA1/BARD1 recruited to nucleosomes for H2A ubiquitylation, and does it involve other histone PTMs? Studies have established that the BARD1 C-terminal domains (Ank-BRCTs) specifically recognize nucleosomes containing H4K20me0 and H2A K13/15-Ub, and that these interactions are important for its function in DNA DSB repair[80,81,98,100–102]. The BARD1 Ank-BRCTs bind to a fully overlapping histone surface to that used by the RING heterodimer, implying that both domains cannot simultaneously bind to the same “face” of a nucleosome substrate. It is possible that these interactions encode a nucleosome read/write mechanism, and in vitro evidence suggests that nucleosomes containing H2A K13/15-Ub are better substrates for BRCA1/BARD1-dependent

H2A ubiquitylation than unmodified nucleosomes[100]. Future investigation of the H2A-Ub mark specific to BRCA1/BARD1 and its cellular ramifications are impeded by the lack of a detection system: there are currently no validated antibodies that discern this mark from other H2A-Ub marks. Development of tools and systems to study BRCA1/BARD1-dependent nucleosome ubiquitylation in cells is likely to yield rich insight into its cellular E3 functions and dysregulation in cancer.

p50

The p50 protein is a component of the transcription factor NFkB that is activated by cellular signals that includes cytokines, oxidants, free radicals, ultraviolet irradiation, and bacterial or viral products[103]. BRCA1 deficiency is associated with dysregulation of NFkB signaling and NFkB signaling is also associated with chemoresistance in BRCA1-proficient tumors[104–106]. Use of a phosphorylation-resistant p50 mutant in 293T cells revealed that phosphorylated p50 binds to the BARD1 C-terminal BRCT domain[52] **(Fig. 1a, Table I)**. The interaction facilitates BRCA1/BARD1-dependent mono-ubiquitylation near the p50 C-terminus at K354 or K356, tandem mutation of which abrogated p50 ubiquitylation[52]. Expression of a p50-Ub genetic fusion as a proxy for p50 that is mono-ubiquitylated at one of its C-terminal lysine residues revealed that mono-ubiquitylation 1) stabilizes p50, 2) decreases its recruitment to chromatin, and 3) promotes its cytoplasmic localization. Furthermore, mice injected with cells expressing a ubiquitylation-resistant mutant of p50 formed larger tumors than wild-type. Ubiquitylation of p50 was also shown to be important for genome maintenance; BARD1 cancer-predisposing mutants in the BRCT domain disrupt the interaction with p50, impair its ubiquitylation, and decrease its stability. Finally, analysis of patient neuroblastoma and breast cancer tumor samples reveal that BARD1 and p50 levels are positively correlated.

The p50 study provides a cohesive framework for the investigation of BRCA1/BARD1-dependent ubiquitylation of putative substrates[52]. The biological findings were contingent on several key insights: (1) identification of the binding sites for both BRCA1/BARD1 and the p50 substrate (including p50 PTM requirements), (2) identification of mutations that selectively disrupt the association, (3) identification of the type of Ub mark and its location on the substrate, and (4) design of Ub-resistant lys to arg mutants and a "constitutively-ubiquitylated" genetic fusion. Together, these findings helped guide design of a robust set of constructs with which to characterize the biological consequences of BRCA1/BARD1-dependent p50 ubiquitylation. While not all substrates may be amenable to all these approaches, this study presents rigorous characterization that should be employed when establishing new BRCA1/BARD1 substrates.

NF2

NF2 is a scaffolding component of the Hippo growth-signaling pathway that controls organ size development by regulating cell proliferation, apoptosis, and stem cell self-renewal[107]. While components of the Hippo pathway are known to be regulated by ubiquitylation, it has only recently been discovered that BRCA1/BARD1 ubiquitylates NF2 to keep Hippo signaling "off" in the presence of nutrient-rich media conditions[51]. Ubiquitylated NF2 is unable to interact with the kinase LATS, which in turn prevents the phosphorylation, cytosolic relocation, and proteasomal degradation of the Hippo transcriptional regulator YAP1, in a process mediated by a ligase other than BRCA1/BARD1. Consistent with these findings, luciferase assays revealed that BRCA1 is required for proper YAP1 function. Mass spectrometry analysis of ubiquitylated NF2 from cells revealed mostly non-degradative K63-linked ubiquitin modification at sites throughout the protein. Ubiquitylation of NF2 was decreased upon shRNA knockdown of BRCA1 and BARD1 independently, and a direct interaction between BRCA1 and NF2 was mapped to the C-terminal BRCTs of BRCA1 and the NF2 N-terminal FERM domain **(Fig. 1a, Table I)**. However, whether BRCA1/BARD1 collaborates with multiple E2s or other E3s to synthesize the observed K63-

linked chains on NF2 is unknown. Although YAP1 stability is contingent on BRCA1-dependent ubiquitylation of NF2, expression of a constitutively active YAP1 mutant resistant to degradation rescued growth defects in BRCA1-deficient breast epithelial cells (MCF10a) and caused invasive structure formation in 3D-culture experiments. Injection of BRCA1-deficient MCF10a cells expressing the constitutively active YAP1 mutant into mice caused tumorigenesis that was not observed upon BRCA1 knockdown alone or in conjunction with knockdown of the known tumor-suppressor p53. These findings indicate that YAP1 reactivation may confer a growth advantage in BRCA1-deficient cells and drive the formation of cancers. Together, these data reveal an important role for BRCA1/BARD1 ligase activity as a regulatory node in Hippo signaling. Remaining questions to be addressed include the relevance and function of the observed K63-linked chains and whether BRCA1/BARD1 are directly and/or solely responsible for them.

Oct1

Oct1 (also called POUF1) is a widely expressed transcription factor that is related to the pluripotency master regulator Oct4[108]. Oct1 insulates critical genes against oxidative stress, dampens reactive oxygen species, promotes glycolytic metabolism, and promotes normal and cancer stem cell phenotypes. A physical interaction between BRCA1 and Oct1 has been established that regulates the transcriptional activation of multiple genes, notably including *ESR1* that encodes ERa[109–112]. These observations prompted investigation as to whether BRCA1 regulates Oct1 through its ligase activity. An in vitro ubiquitylation assay using Oct1-containing cell lysate as substrate showed that poly-ubiquitylation of Oct1 was dependent on all components of the Ub cascade including BRCA1 and was not observed using a Ub-resistant Oct1 mutant (K9/403R)[113]. Although exogenous Ube2D was used, it cannot be ruled out that other E2s in the lysate were active in this assay. However, Oct1 levels were stabilized in cells expressing I26A-BRCA1 (Ube2D-incompetent form of BRCA1) and cells treated with

proteasome inhibitor (MG132) accumulated Oct1 with K48-linked ubiquitin chains. Taken together, the data strongly suggest that BRCA1/BARD1 serves as a degradative ligase for Oct1 by targeting specific lysine residues for Ub attachment. Important gaps in understanding regarding how this occurs remain. Does BRCA1/BARD1 perform both priming and K48-linked chain building reaction with a UBE2D, or does it use another E2 (for example, UBE2K) as the chain extender, or does it perform the critical first step (priming) and another E2/E3 pair builds the chains?

The observed stabilization of Oct1 in I26A-BRCA1-expressing MEFs enabled identification of ~1000 genes whose expression patterns were altered, with “metabolic disease” emerging as a significantly affected pathway[113]. Consistent with this, the cells had an increased glycolytic phenotype measured by a decrease in oxygen consumption, increase in extracellular acidification rates, and increase in glycolytic metabolites. Notably, Oct1 levels correlate with tumor aggressiveness and inversely correlate with BRCA1 protein levels in patient tumor samples. Overall, the findings point to a link between BRCA1/BARD1 Ub ligase activity and metabolic processes in cancer.

LARP7

La-related protein 7 (LARP7) has been reported to act as a potential tumor suppressor in gastric and breast cancers[114,115]. LARP7 binds to distinct small nuclear RNAs, stabilizes the 3’ hairpin of non-coding 7SK RNA, and is known to negatively regulate RNAPII pausing release[116]. LARP7 levels negatively correlate with cell survival upon DNA damage in MEF and HeLa cells [53]. Following IR treatment, LARP7 is rapidly shuttled from the nucleus and degraded. A potential interaction between LARP7 and BARD1 that appeared in the BioGRID database was confirmed via immunoprecipitation experiments[53]. While both the BRCA1 and BARD1 BRCTs interact independently with LARP7, only the BARD1 interaction is stimulated by IR treatment **(Fig. 1a,**

Table I). BRCA1/BARD1 binding and ubiquitylation of LARP7 was shown to be dependent upon ATM-mediated phosphorylation of LARP7 at T440. BRCA1 and BARD1 co-expression in 293T cells was associated with proteasome-dependent depletion of LARP7. Use of single-lysine Ub mutants revealed the majority of ubiquitylated LARP7 contains K48-linked Ub chains, consistent with a degradation outcome. While full-length BRCA1/BARD1 was needed to induce poly-ubiquitylation of LARP7 in cells, a truncated construct lacking the BRCTs of both E3 subunits was observed to build poly-Ub chains on LARP7 in vitro with Ube2D3 as the E2, raising questions as to why requirements differ in the two contexts. Analysis of LARP7 ubiquitylation using full-length BRCA1/BARD1 and an E2 panel may provide insight into the mechanism by which such K48-linked chains are built. As discussed for other substrates, the possibility that another E2 and/or E3 is involved in LARP7 poly-ubiquitylation remains open.

As LARP7 depletion leads to increased HDR efficiency, loss of BRCA1/BARD1 ligase function towards LARP7 might result in DNA damage defects. Indeed, high LARP7 levels are correlated with increased survival times in patients receiving chemotherapy, and LARP7-overexpressing cells are especially sensitive to ionizing radiation and cisplatin. These data suggest that LARP7 may be a useful drug target or prognostic marker in BRCA1-deficient cancers.

Concluding Remarks

An important initiative in BRCA1/BARD1 research involves the accurate classification of thousands of observed patient variants, of which a majority of missense variants remain unclassified variants of unknown significance in the ClinVar database[117]. To date, efforts towards this end have relied upon detecting processes such as HDR efficiency, drug resistance, and cell viability[118–121]. Such phenotypes may be linked to BRCA1/BARD1 function indirectly and, at the very least, the underlying mechanisms are undefined. Given that E3 ligase activity is the sole biochemical function, it is in principle possible that all, or a majority of, known

phenotypes have substrate ubiquitylation at their source. Therefore, identification of substrates whose ubiquitylation is associated with processes linked to tumor suppression will provide critical information regarding the potential effects of unclassified variants in either the BRCA1 or BARD1 genes. In principle, quantitative assessment of variant BRCA1/BARD1 species' ability to ubiquitylate relevant substrates could have the power to predict the impact of a mutation and, ultimately, inform decision-making in prophylactic treatment. Clearly, there will be more than one critical substrate, suggesting a goal in which multiple substrates are monitored in patient samples. An important intermediate step towards such a goal is the assessment of relevant substrate ubiquitylation by known BRCA1/BARD1 variants and their association with processes such as DNA damage response and transcriptional regulation. With tools and reagents currently available, we may be entering a time when this goal is achievable (though non-trivial) with the existing BRCA1/BARD1 substrates and can be pursued anew for each additional substrate identified in the future.

References

1. Friedman, L. S. *et al.* Confirmation of BRCA1 by analysis of germline mutations linked to breast and ovarian cancer in ten families. *Nat. Genet.* **8**, 399–404 (1994).
2. Hall, J. *et al.* Linkage of early-onset familial breast cancer to chromosome 17q21. *Science* **250**, 1684 (1990).
3. King, M.-C., Marks, J. H., Mandell, J. B., & New York Breast Cancer Study Group. Breast and ovarian cancer risks due to inherited mutations in BRCA1 and BRCA2. *Science* **302**, 643–646 (2003).
4. Miki, Y. *et al.* A strong candidate for the breast and ovarian cancer susceptibility gene BRCA1. *Science* **266**, 66 (1994).
5. Stewart, M. D. *et al.* BARD1 is necessary for ubiquitylation of nucleosomal histone H2A and for transcriptional regulation of estrogen metabolism genes. *Proc. Natl. Acad. Sci. U. S. A.* **115**, 1316–1321 (2018).
6. Li, W. *et al.* A synergetic effect of BARD1 mutations on tumorigenesis. *Nat. Commun.* **12**, 1243 (2021).
7. Weber-Lassalle, N. *et al.* Germline loss-of-function variants in the BARD1 gene are associated with early-onset familial breast cancer but not ovarian cancer. *Breast Cancer Res.* **21**, 55 (2019).
8. Tarsounas, M. & Sung, P. The antitumorigenic roles of BRCA1–BARD1 in DNA repair and replication. *Nat. Rev. Mol. Cell Biol.* **21**, 284–299 (2020).

9. Shakya, R. *et al.* The basal-like mammary carcinomas induced by Brca1 or Bard1 inactivation implicate the BRCA1/BARD1 heterodimer in tumor suppression. *Proc. Natl. Acad. Sci.* **105**, 7040 (2008).

10. Mullan, P. B., Quinn, J. E. & Harkin, D. P. The role of BRCA1 in transcriptional regulation and cell cycle control. *Oncogene* **25**, 5854–5863 (2006).

11. Kais, Z. & Parvin, J. D. Regulation of centrosomes by the BRCA1-dependent ubiquitin ligase. *Cancer Biol. Ther.* **7**, 1540–1543 (2008).

12. Privat, M. *et al.* BRCA1 Induces Major Energetic Metabolism Reprogramming in Breast Cancer Cells. *PLOS ONE* **9**, e102438 (2014).

13. Lou, Z., Minter-Dykhouse, K. & Chen, J. BRCA1 participates in DNA decatenation. *Nat. Struct. Mol. Biol.* **12**, 589–593 (2005).

14. Christou, C. M. & Kyriacou, K. BRCA1 and Its Network of Interacting Partners. *Biology* **2**, 40–63 (2013).

15. Savage, K. I. & Harkin, D. P. BRCA1, a 'complex' protein involved in the maintenance of genomic stability. *FEBS J.* **282**, 630–646 (2015).

16. Hashizume, R. *et al.* The RING heterodimer BRCA1-BARD1 is a ubiquitin ligase inactivated by a breast cancer-derived mutation. *J. Biol. Chem.* **276**, 14537–14540 (2001).

17. Lorick, K. L. *et al.* RING fingers mediate ubiquitin-conjugating enzyme (E2)-dependent ubiquitination. *Proc. Natl. Acad. Sci.* **96**, 11364 (1999).

18. Drost, R. *et al.* BRCA1 RING Function Is Essential for Tumor Suppression but Dispensable for Therapy Resistance. *Cancer Cell* **20**, 797–809 (2011).

19. Reid, L. J. *et al.* E3 ligase activity of BRCA1 is not essential for mammalian cell viability or homology-directed repair of double-strand DNA breaks. *Proc. Natl. Acad. Sci. U. S. A.* **105**, 20876–20881 (2008).

20. Shakya, R. *et al.* BRCA1 tumor suppression depends on BRCT phosphoprotein binding, but not its E3 ligase activity. *Science* **334**, 525–528 (2011).

21. Brzovic, P. S., Rajagopal, P., Hoyt, D. W., King, M. C. & Klevit, R. E. Structure of a BRCA1-BARD1 heterodimeric RING-RING complex. *Nat. Struct. Biol.* **8**, 833–837 (2001).

22. Clark, S. L., Rodriguez, A. M., Snyder, R. R., Hankins, G. D. V. & Boehning, D. Structure-function of the tumor suppressor. *Comput. Struct. Biotechnol. J.* **1**, e201204005 (2012).

23. Metzger, M. B., Pruneda, J. N., Klevit, R. E. & Weissman, A. M. RING-type E3 ligases: Master manipulators of E2 ubiquitin-conjugating enzymes and ubiquitination. *Ubiquitin-Proteasome Syst.* **1843**, 47–60 (2014).

24. Mark, W.-Y. *et al.* Characterization of segments from the central region of BRCA1: an intrinsically disordered scaffold for multiple protein-protein and protein-DNA interactions? *J. Mol. Biol.* **345**, 275–287 (2005).

25. Brzovic, P. S., Meza, J. E., King, M.-C. & Klevit, R. E. BRCA1 RING Domain Cancer-predisposing Mutations: Structural consequences and effects on protein-protein interactions. *J. Biol. Chem.* **276**, 41399–41406 (2001).

26. Ruffner, H., Joazeiro, C. A. P., Hemmati, D., Hunter, T. & Verma, I. M. Cancer-predisposing mutations within the RING domain of BRCA1: Loss of ubiquitin protein ligase activity and protection from radiation hypersensitivity. *Proc. Natl. Acad. Sci.* **98**, 5134 (2001).

27. Andrew C. Nelson & Jeffrey T. Holt. Impact of RING and BRCT Domain Mutations on BRCA1 Protein Stability, Localization and Recruitment to DNA Damage. *Radiat. Res.* **174**, 1–13 (2010).

28. Morris, J. R. *et al.* Genetic analysis of BRCA1 ubiquitin ligase activity and its relationship to breast cancer susceptibility. *Hum. Mol. Genet.* **15**, 599–606 (2006).

29. Stewart, M. D. *et al.* Tuning BRCA1 and BARD1 activity to investigate RING ubiquitin ligase mechanisms. *Protein Sci.* **26**, 475–483 (2017).

30. Bosu, D. R. & Kipreos, E. T. Cullin-RING ubiquitin ligases: global regulation and activation cycles. *Cell Div.* **3**, 7 (2008).

31. Christensen, D. E., Brzovic, P. S. & Klevit, R. E. E2-BRCA1 RING interactions dictate synthesis of mono- or specific polyubiquitin chain linkages. *Nat. Struct. Mol. Biol.* **14**, 941–948 (2007).

32. Brzovic, P. S. *et al.* Binding and recognition in the assembly of an active BRCA1/BARD1 ubiquitin-ligase complex. *Proc. Natl. Acad. Sci. U. S. A.* **100**, 5646–5651 (2003).

33. Stewart, M. D., Ritterhoff, T., Klevit, R. E. & Brzovic, P. S. E2 enzymes: more than just middlemen. *Cell Res.* **26**, 423–440 (2016).

34. Vittal, V. *et al.* Intrinsic disorder drives N-terminal ubiquitination by Ube2w. *Nat. Chem. Biol.* **11**, 83–89 (2015).

35. Nishikawa, H. *et al.* Mass Spectrometric and Mutational Analyses Reveal Lys-6-linked Polyubiquitin Chains Catalyzed by BRCA1-BARD1 Ubiquitin Ligase. *J. Biol. Chem.* **279**, 3916–3924 (2004).

36. Wu-Baer, F., Lagrazon, K., Yuan, W. & Baer, R. The BRCA1/BARD1 Heterodimer Assembles Polyubiquitin Chains through an Unconventional Linkage Involving Lysine Residue K6 of Ubiquitin*. *J. Biol. Chem.* **278**, 34743–34746 (2003).

37. Morris, J. R. & Solomon, E. BRCA1: BARD1 induces the formation of conjugated ubiquitin structures, dependent on K6 of ubiquitin, in cells during DNA replication and repair. *Hum. Mol. Genet.* **13**, 807–817 (2004).

38. Heap, R. E., Gant, M. S., Lamoliatte, F., Peltier, J. & Trost, M. Mass spectrometry techniques for studying the ubiquitin system. *Biochem. Soc. Trans.* **45**, 1137–1148 (2017).

39. Newton, K. *et al.* Ubiquitin Chain Editing Revealed by Polyubiquitin Linkage-Specific Antibodies. *Cell* **134**, 668–678 (2008).

40. Densham, R. M. *et al.* Human BRCA1-BARD1 ubiquitin ligase activity counteracts chromatin barriers to DNA resection. *Nat. Struct. Mol. Biol.* **23**, 647–655 (2016).

41. Pruneda, J. N. *et al.* Structure of an E3:E2~Ub complex reveals an allosteric mechanism shared among RING/U-box ligases. *Mol. Cell* **47**, 933–942 (2012).

42. Taherbhoy, A. M., Huang, O. W. & Cochran, A. G. BMI1–RING1B is an autoinhibited RING E3 ubiquitin ligase. *Nat. Commun.* **6**, 7621 (2015).

43. Starita, L. M. *et al.* Massively Parallel Functional Analysis of BRCA1 RING Domain Variants. *Genetics* **200**, 413–422 (2015).

44. Zhao, Q., Liu, L. & Xie, Q. In Vitro Protein Ubiquitination Assay. in *Plant Signalling Networks: Methods and Protocols* (eds. Wang, Z.-Y. & Yang, Z.) 163–172 (Humana Press, 2012). doi:10.1007/978-1-61779-809-2_13.

45. Buetow, L., Gabrielsen, M. & Huang, D. T. Single-Turnover RING/U-Box E3-Mediated Lysine Discharge Assays. in *The Ubiquitin Proteasome System: Methods and Protocols* (eds. Mayor, T. & Kleiger, G.) 19–31 (Springer New York, 2018). doi:10.1007/978-1-4939-8706-1_2.

46. Witus, S. R. *et al.* BRCA1/BARD1 site-specific ubiquitylation of nucleosomal H2A is directed by BARD1. *Nat. Struct. Mol. Biol.* **28**, 268–277 (2021).

47. Eakin, C. M., Maccoss, M. J., Finney, G. L. & Klevit, R. E. Estrogen receptor alpha is a putative substrate for the BRCA1 ubiquitin ligase. *Proc. Natl. Acad. Sci. U. S. A.* **104**, 5794–5799 (2007).

48. Varma, A. K., Brown, R. S., Birrane, G. & Ladias, J. A. A. Structural Basis for Cell Cycle Checkpoint Control by the BRCA1−CtIP Complex. *Biochemistry* **44**, 10941–10946 (2005).

49. Yu, X., Fu, S., Lai, M., Baer, R. & Chen, J. BRCA1 ubiquitinates its phosphorylation-dependent binding partner CtIP. *Genes Dev.* **20**, 1721–1726 (2006).

50. Starita, L. M. *et al.* BRCA1/BARD1 ubiquitinate phosphorylated RNA polymerase II. *J. Biol. Chem.* **280**, 24498–24505 (2005).

51. Verma, S. *et al.* BRCA1/BARD1-dependent ubiquitination of NF2 regulates Hippo-YAP1 signaling. *Proc. Natl. Acad. Sci.* **116**, 7363 (2019).

52. Wu, L. *et al.* p50 mono-ubiquitination and interaction with BARD1 regulates cell cycle progression and maintains genome stability. *Nat. Commun.* **11**, 5007 (2020).

53. Zhang, F. *et al.* L ARP7 Is a BRCA1 Ubiquitinase Substrate and Regulates Genome Stability and Tumorigenesis. *Cell Rep.* **32**, 107974 (2020).

54. Hsu, L.-C., Doan, T. P. & White, R. L. Identification of a γ-Tubulin-binding Domain in BRCA1. *Cancer Res.* **61**, 7713 (2001).

55. Starita, L. M. *et al.* BRCA1-dependent ubiquitination of gamma-tubulin regulates centrosome number. *Mol. Cell. Biol.* **24**, 8457–8466 (2004).

56. Zhao, W. *et al.* BRCA1-BARD1 promotes RAD51-mediated homologous DNA pairing. *Nature* **550**, 360–365 (2017).

57. Tan, W. *et al.* Preparation and purification of mono-ubiquitinated proteins using Avi-tagged ubiquitin. *PLOS ONE* **15**, e0229000 (2020).

58. Minten, E. V. *et al.* SIRT2 promotes BRCA1-BARD1 heterodimerization through deacetylation. *Cell Rep.* **34**, 108921 (2021).

59. Ouchi, T. BRCA1 phosphorylation: Biological consequences. *Cancer Biol. Ther.* **5**, 470–475 (2006).

60. Daza-Martin, M. *et al.* Isomerization of BRCA1–BARD1 promotes replication fork protection. *Nature* **571**, 521–527 (2019).

61. Mallery, D. L., Vandenberg, C. J. & Hiom, K. Activation of the E3 ligase function of the BRCA1/BARD1 complex by polyubiquitin chains. *EMBO J.* **21**, 6755–6762 (2002).

62. Morris, J. R. *et al.* The SUMO modification pathway is involved in the BRCA1 response to genotoxic stress. *Nature* **462**, 886–890 (2009).

63. Hunter, T. The Age of Crosstalk: Phosphorylation, Ubiquitination, and Beyond. *Mol. Cell* **28**, 730–738 (2007).

64. Sankaran, S., Crone, D. E., Palazzo, R. E. & Parvin, J. D. Aurora-A Kinase Regulates Breast Cancer–Associated Gene 1 Inhibition of Centrosome-Dependent Microtubule Nucleation. *Cancer Res.* **67**, 11186 (2007).

65. Hayami, R. *et al.* Down-regulation of BRCA1-BARD1 Ubiquitin Ligase by CDK2. *Cancer Res.* **65**, 6 (2005).

66. Wu, W. *et al.* HERC2 Is an E3 Ligase That Targets BRCA1 for Degradation. *Cancer Res.* **70**, 6384 (2010).

67. Wang, X. *et al.* HUWE1 interacts with BRCA1 and promotes its degradation in the ubiquitin–proteasome pathway. *Biochem. Biophys. Res. Commun.* **444**, 549–554 (2014).

68. Lu, Y. *et al.* The F-box Protein FBXO44 Mediates BRCA1 Ubiquitination and Degradation*. *J. Biol. Chem.* **287**, 41014–41022 (2012).

69. Lu, Q., Zhang, F.-L., Lu, D.-Y., Shao, Z.-M. & Li, D.-Q. USP9X stabilizes BRCA1 and confers resistance to DNA-damaging agents in human cancer cells. *Cancer Med.* **8**, 6730–6740 (2019).

70. Song, L. & Rape, M. Regulated Degradation of Spindle Assembly Factors by the Anaphase-Promoting Complex. *Mol. Cell* **38**, 369–382 (2010).

71. Liang, Y. *et al.* Structural analysis of BRCA1 reveals modification hotspot. *Sci. Adv.* **3**, e1701386 (2017).

72. Wu-Baer, F., Ludwig, T. & Baer, R. The UBXN1 protein associates with autoubiquitinated forms of the BRCA1 tumor suppressor and inhibits its enzymatic function. *Mol. Cell. Biol.* **30**, 2787–2798 (2010).

73. Choudhury, A. D., Xu, H. & Baer, R. Ubiquitination and Proteasomal Degradation of the BRCA1 Tumor Suppressor Is Regulated during Cell Cycle Progression*. *J. Biol. Chem.* **279**, 33909–33918 (2004).

74. Fabbro, M., Rodriguez, J. A., Baer, R. & Henderson, B. R. BARD1 Induces BRCA1 Intranuclear Foci Formation by Increasing RING-dependent BRCA1 Nuclear Import and Inhibiting BRCA1 Nuclear Export. *J. Biol. Chem.* **277**, 21315–21324 (2002).

75. Rodriguez, J. A., Schüchner, S., Au, W. W. Y., Fabbro, M. & Henderson, B. R. Nuclear–cytoplasmic shuttling of BARD1 contributes to its proapoptotic activity and is regulated by dimerization with BRCA1. *Oncogene* **23**, 1809–1820 (2004).

76. Lu, Y. *et al.* Ubiquitination and Proteasome-Mediated Degradation of BRCA1 and BARD1 during Steroidogenesis in Human Ovarian Granulosa Cells. *Mol. Endocrinol.* **21**, 651–663 (2007).

77. Joukov, V., Chen, J., Fox, E. A., Green, J. B. A. & Livingston, D. M. Functional communication between endogenous BRCA1 and its partner, BARD1, during Xenopus laevis development. *Proc. Natl. Acad. Sci.* **98**, 12078 (2001).

78. Xia, Y., Pao, G. M., Chen, H.-W., Verma, I. M. & Hunter, T. Enhancement of BRCA1 E3 Ubiquitin Ligase Activity through Direct Interaction with the BARD1 Protein*. *J. Biol. Chem.* **278**, 5255–5263 (2003).

79. McCarthy Ellen E., Celebi Julide T., Baer Richard, & Ludwig Thomas. Loss of Bard1, the Heterodimeric Partner of the Brca1 Tumor Suppressor, Results in Early Embryonic Lethality and Chromosomal Instability. *Mol. Cell. Biol.* **23**, 5056–5063 (2003).

80. Nakamura, K. *et al.* H4K20me0 recognition by BRCA1–BARD1 directs homologous recombination to sister chromatids. *Nat. Cell Biol.* **21**, 311–318 (2019).

81. Becker, J. R. *et al.* BARD1 reads H2A lysine 15 ubiquitination to direct homologous recombination. *Nature* **596**, 433–437 (2021).

82. Starita, L. & Parvin, J. Substrates of the BRCA1-Dependent Ubiquitin Ligase. *Cancer Biol. Ther.* **5**, 137–41 (2006).

83. Wu, W., Koike, A., Takeshita, T. & Ohta, T. The ubiquitin E3 ligase activity of BRCA1 and its biological functions. *Cell Div.* **3**, 1 (2008).

84. Parvin, J. D. The BRCA1-dependent ubiquitin ligase, γ-tubulin, and centrosomes. *Environ. Mol. Mutagen.* **50**, 649–653 (2009).

85. Ohta, T., Sato, K. & Wu, W. The BRCA1 ubiquitin ligase and homologous recombination repair. *Ubiquitin Fam. Proteins DNA Damage Response* **585**, 2836–2844 (2011).

86. Song, M., Hakala, K., Weintraub, S. T. & Shiio, Y. Quantitative Proteomic Identification of the BRCA1 Ubiquitination Substrates. *J. Proteome Res.* **10**, 5191–5198 (2011).

87. Kim, B.-J. *et al.* The Histone Variant MacroH2A1 Is a BRCA1 Ubiquitin Ligase Substrate. *Cell Rep.* **19**, 1758–1766 (2017).

88. Ma, Y. *et al.* BRCA1 Regulates Acetylation and Ubiquitination of Estrogen Receptor-α. *Mol. Endocrinol.* **24**, 76–90 (2010).

89. Uckelmann, M. *et al.* USP48 restrains resection by site-specific cleavage of the BRCA1 ubiquitin mark from H2A. *Nat. Commun.* **9**, 229 (2018).

90. Zhu, Q. *et al.* BRCA1 tumour suppression occurs via heterochromatin-mediated silencing. *Nature* **477**, 179–184 (2011).

91. Fan, S. *et al.* Role of direct interaction in BRCA1 inhibition of estrogen receptor activity. *Oncogene* **20**, 77–87 (2001).

92. Kawai, H., Li, H., Chun, P., Avraham, S. & Avraham, H. K. Direct interaction between BRCA1 and the estrogen receptor regulates vascular endothelial growth factor (VEGF) transcription and secretion in breast cancer cells. *Oncogene* **21**, 7730–7739 (2002).

93. La Rosa, P., Marino, M. & Acconcia, F. 17β-estradiol regulates estrogen receptor α monoubiquitination. *IUBMB Life* **63**, 49–53 (2011).

94. Chen, A., Kleiman, F., Manley, J., Ouchi, T. & Pan, Z.-Q. Autoubiquitination of the BRCA1-BARD1 RING ubiquitin ligase. *J. Biol. Chem.* **277**, 22085–92 (2002).

95. Kalb, R., Mallery, D. L., Larkin, C., Huang, J. T. J. & Hiom, K. BRCA1 is a histone-H2A-specific ubiquitin ligase. *Cell Rep.* **8**, 999–1005 (2014).

96. Zhu, Q. *et al.* Heterochromatin-Encoded Satellite RNAs Induce Breast Cancer. *Mol. Cell* **70**, 842-853.e7 (2018).

97. McGinty, R. K., Henrici, R. C. & Tan, S. Crystal structure of the PRC1 ubiquitylation module bound to the nucleosome. *Nature* **514**, 591–596 (2014).

98. Sherker, A. *et al.* Two redundant ubiquitin-dependent pathways of BRCA1 localization to DNA damage sites. *bioRxiv* 2021.07.21.452958 (2021) doi:10.1101/2021.07.21.452958.

99. Savage, K. I. *et al.* BRCA1 deficiency exacerbates estrogen-induced DNA damage and genomic instability. *Cancer Res.* **74**, 2773–2784 (2014).

100. Hu, Q. *et al.* Mechanisms of BRCA1–BARD1 nucleosome recognition and ubiquitylation. *Nature* **596**, 438–443 (2021).

101. Dai, L. *et al.* Structural insight into BRCA1-BARD1 complex recruitment to damaged chromatin. *Mol. Cell* **81**, 2765-2777.e6 (2021).

102. Krais, J. J. *et al.* RNF168-mediated localization of BARD1 recruits the BRCA1-PALB2 complex to DNA damage. *Nat. Commun.* **12**, 5016 (2021).

103. Yu, Y., Wan, Y. & Huang, C. The biological functions of NF-kappaB1 (p50) and its potential as an anti-cancer target. *Curr. Cancer Drug Targets* **9**, 566–571 (2009).

104. Sau, A. *et al.* Persistent Activation of NF-κB in BRCA1-Deficient Mammary Progenitors Drives Aberrant Proliferation and Accumulation of DNA Damage. *Cell Stem Cell* **19**, 52–65 (2016).

105. Buckley, N. E. *et al.* A BRCA1 deficient, NFκB driven immune signal predicts good outcome in triple negative breast cancer. *Oncotarget* **7**, 19884–19896 (2016).

106. Harte, M. T. *et al.* NF-κB is a critical mediator of BRCA1-induced chemoresistance. *Oncogene* **33**, 713–723 (2014).

107. Misra, J. R. & Irvine, K. D. The Hippo Signaling Network and Its Biological Functions. *Annu. Rev. Genet.* **52**, 65–87 (2018).

108. Vázquez-Arreguín, K. & Tantin, D. The Oct1 transcription factor and epithelial malignancies: Old protein learns new tricks. *Oct Transcr. Factor Fam.* **1859**, 792–804 (2016).

109. Fan, W. *et al.* BRCA1 Regulates GADD45 through Its Interactions with the OCT-1 and CAAT Motifs. *J. Biol. Chem.* **277**, 8061–8067 (2002).

110. Wang, R.-H., Yu, H. & Deng, C.-X. A requirement for breast-cancer-associated gene 1 (BRCA1) in the spindle checkpoint. *Proc. Natl. Acad. Sci. U. S. A.* **101**, 17108 (2004).

111. Maekawa, T. *et al.* ATF-2 controls transcription of Maspin and GADD45α genes independently from p53 to suppress mammary tumors. *Oncogene* **27**, 1045–1054 (2008).

112. Hosey, A. M. *et al.* Molecular Basis for Estrogen Receptor α Deficiency in BRCA1-Linked Breast Cancer. *JNCI J. Natl. Cancer Inst.* **99**, 1683–1694 (2007).

113. Vázquez-Arreguín, K. *et al.* BRCA1 through Its E3 Ligase Activity Regulates the Transcription Factor Oct1 and Carbohydrate Metabolism. *Mol. Cancer Res. MCR* **16**, 439–452 (2018).

114. Cheng, Y. *et al.* LARP7 is a potential tumor suppressor gene in gastric cancer. *Lab. Invest.* **92**, 1013–1019 (2012).

115. Ji, X., Lu, H., Zhou, Q. & Luo, K. LARP7 suppresses P-TEFb activity to inhibit breast cancer progression and metastasis. *eLife* **3**, e02907 (2014).

116. Markert, A. *et al.* The La-related protein LARP7 is a component of the 7SK ribonucleoprotein and affects transcription of cellular and viral polymerase II genes. *EMBO Rep.* **9**, 569–575 (2008).

117. Landrum, M. J. *et al.* ClinVar: improving access to variant interpretations and supporting evidence. *Nucleic Acids Res.* **46**, D1062–D1067 (2018).

118. Starita, L. M. *et al.* Massively Parallel Functional Analysis of BRCA1 RING Domain Variants. *Genetics* **200**, 413–422 (2015).

119. Starita, L. M. *et al.* A Multiplex Homology-Directed DNA Repair Assay Reveals the Impact of More Than 1,000 BRCA1 Missense Substitution Variants on Protein Function. *Am. J. Hum. Genet.* **103**, 498–508 (2018).

120. Findlay, G. M. *et al.* Accurate classification of BRCA1 variants with saturation genome editing. *Nature* **562**, 217–222 (2018).

121. Adamovich, A. I. *et al.* Functional analysis of BARD1 missense variants in homology-directed repair and damage sensitivity. *PLOS Genet.* **15**, e1008049 (2019).

122. Ryser, S. *et al.* Distinct Roles of BARD1 Isoforms in Mitosis: Full-Length BARD1 Mediates Aurora B Degradation, Cancer-Associated BARD1β Scaffolds Aurora B and BRCA2. *Cancer Res.* **69**, 1125 (2009).

123. Shabbeer, S. *et al.* BRCA1 targets G2/M cell cycle proteins for ubiquitination and proteasomal degradation. *Oncogene* **32**, 5005–5016 (2013).

124. Lin, S.-Y., Li, K., Stewart, G. S. & Elledge, S. J. Human Claspin works with BRCA1 to both positively and negatively regulate cell proliferation. *Proc. Natl. Acad. Sci. U. S. A.* **101**, 6484 (2004).

125. Sato, K. *et al.* A DNA-damage selective role for BRCA1 E3 ligase in claspin ubiquitylation, CHK1 activation, and DNA repair. *Curr. Biol. CB* **22**, 1659–1666 (2012).

126. Li, S. *et al.* Binding of CtIP to the BRCT Repeats of BRCA1 Involved in the Transcription Regulation of p21 Is Disrupted Upon DNA Damage*. *J. Biol. Chem.* **274**, 11334–11338 (1999).

127. Sato, K. *et al.* Nucleophosmin/B23 Is a Candidate Substrate for the BRCA1-BARD1 Ubiquitin Ligase. *J. Biol. Chem.* **279**, 30919–30922 (2004).

128. Calvo, V. & Beato, M. BRCA1 Counteracts Progesterone Action by Ubiquitination Leading to Progesterone Receptor Degradation and Epigenetic Silencing of Target Promoters. *Cancer Res.* **71**, 3422 (2011).

129. Kleiman, F. E. *et al.* BRCA1/BARD1 inhibition of mRNA 3' processing involves targeted degradation of RNA polymerase II. *Genes Dev.* **19**, 1227–1237 (2005).

130. Horwitz, A. A., Affar, E. B., Heine, G. F., Shi, Y. & Parvin, J. D. A mechanism for transcriptional repression dependent on the BRCA1 E3 ubiquitin ligase. *Proc. Natl. Acad. Sci. U. S. A.* **104**, 6614–6619 (2007).

131. Wu, W. *et al.* BRCA1 Ubiquitinates RPB8 in Response to DNA Damage. *Cancer Res.* **67**, 951 (2007).

132. Sankaran Satish, Starita Lea M., Groen Aaron C., Ko Min Ji, & Parvin Jeffrey D. Centrosomal Microtubule Nucleation Activity Is Inhibited by BRCA1-Dependent Ubiquitination. *Mol. Cell. Biol.* **25**, 8656–8668 (2005).

Figures

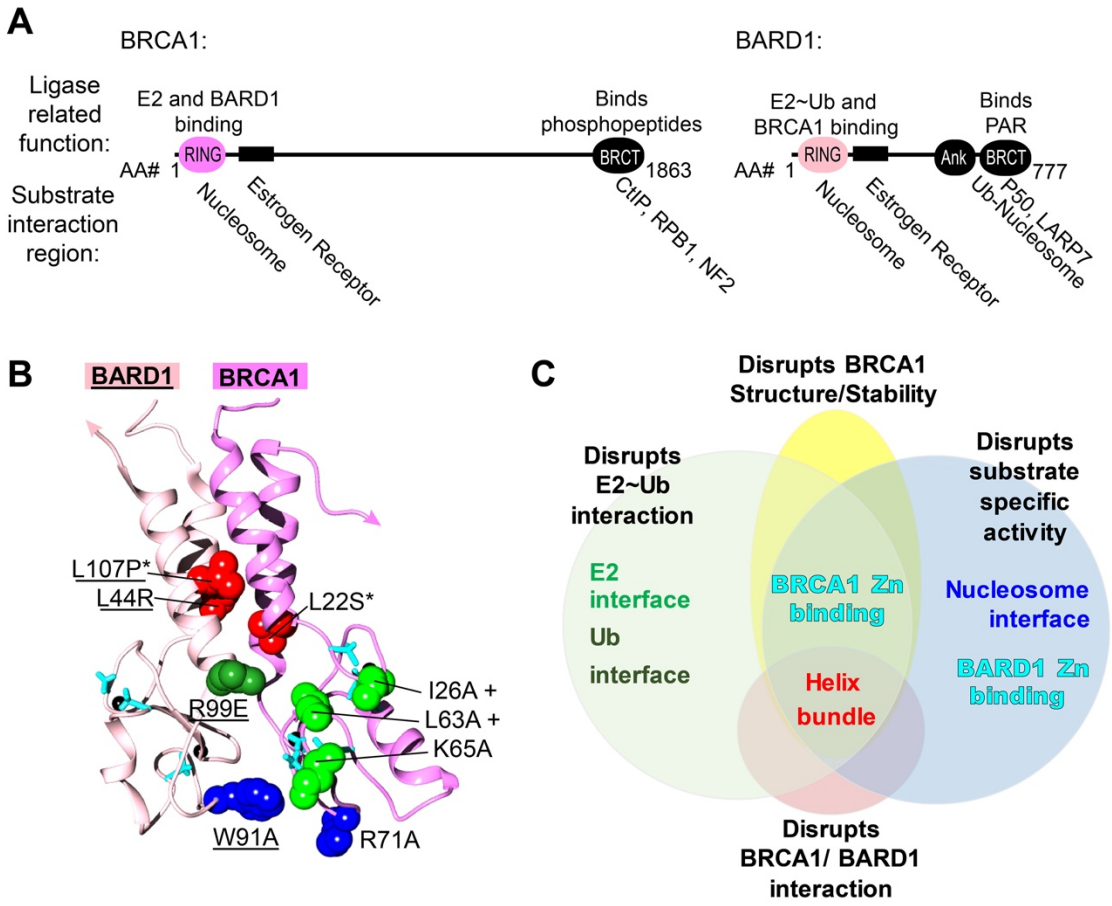

Figure 1. An overview of the features of the BRCA1/BARD1 Ubiquitin ligase. (A) The domain structure and function of BRCA1 and BARD1 domains. Folded domains of BRCA1 and BARD1 are depicted with ovals and their corresponding domain names: really interesting new gene (RING), BRCA1 C-terminal (BRCT), and ankyrin repeats (ARD). Substrate binding domains within the intrinsically disordered regions are represented with rectangles. Domain functions related to E3 ligase activity are listed above domains. Substrates are listed below the region of protein with which they interact. "Ub-nucleosome" refers specifically to nucleosome substrates with ubiquitin attached on the N-terminal tail of H2A at Lys 13/15. **(B)** The solution structure of RING domains from BRCA1 and BARD1 (PDB 1JM7) are shown in magenta and pink respectively. The sidechains at mutation sites used to study the structure/function relationship are shown in spheres or sticks: BARD1 mutations are underlined, cancer-associated mutations are either labeled with an asterisk or in the case of zinc-coordinating mutation sites depicted in cyan sticks (BRCA1 C24R, C39S/R/Y/W, C44S/Y/F, C47S/Y/F, C61G, C64R/Y/W and BARD1 C53W, C71Y, and C83R). The colors of mutation site sidechains correspond with their functions in Panel C. **(C)** Mutations are categorized in a Venn diagram according to the properties and functions they affect.

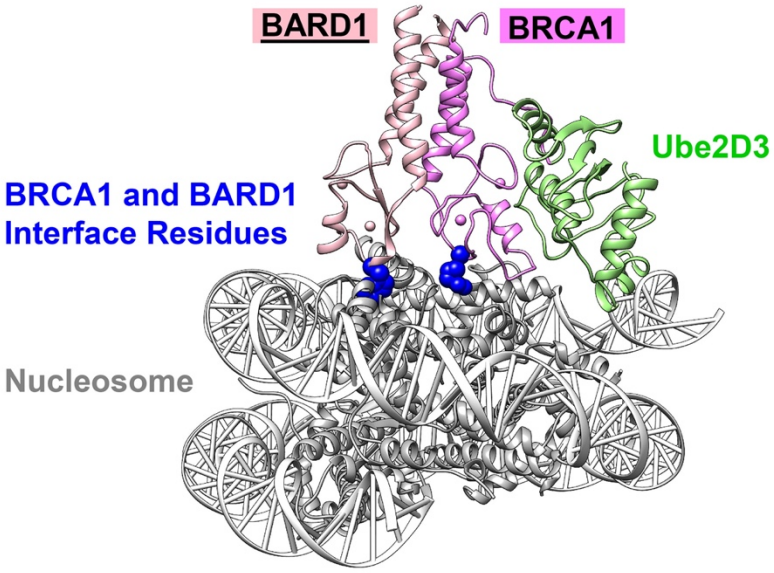

Figure 2: BRCA1 and BARD1 bind the nucleosome substrate and E2 simultaneously. The cryo-EM structure (PDB 7JZV) reveals that both BRCA1 and BARD1 RING domains (magenta and pink, respectively) contain critical residues (BRCA1 Arg 71 and BARD1 Trp 91, blue) that contact the nucleosome surface (gray). The E2, Ube2D3 (green), binds to a distinct interface on BRCA1 allowing the heterodimer to coordinate substrate and E2 simultaneously. The complex allows for transfer of ubiquitin from the E2 onto the dynamic C-terminal end of H2A (unresolved in the structure).

Tables

Table I. Characterized BRCA1/BARD1 substrates.

Substrate	Biological function(s)*	Observed in cells/in vitro?	BRCA1 (BC)/ BARD1 (BD) binding site	Substrate Ub-attachment site (linkage-type)	E2-enzyme	Substrate binding site	Ref(s)
Aurora Kinase B	CCR	Y/N	n.d.	n.d.	n.d.	n.d.	122
Cdc25C	CCR	Y/Y	BC: BRCTs	n.d. (poly-Ub, degradative)	Ube2D[a]	n.d.	123
Claspin	DDR	Y/Y	n.d.	K60/K96 (mono-Ub *in vitro*)	Ube2D[a]	1-331	124, 125
CtIP	DDR, TR	Y/Y	BC: BRCTs	n.d. (poly-Ub, non-degradative)	Ube2D[a]	322-333 (pSer327)	48, 49, 126
Cyclin B1	CCR	Y/Y	BC: BRCTs	n.d. (poly-Ub, degradative)	Ube2K, Ube2D	n.d.	123
estrogen receptor α	TR	Y/Y	BC: IDR BD: IDR	K302 (mono-Ub)	Ube2D	Ligand binding domain	29, 47, 88, 91, 92, 93
H2A	DDR, TR	Y/Y	BC: RING BD: RING	K125/127/129 (mono-Ub)	Ube2D, Ube2E	histone surface, acidic patch	40, 46, 95, 97, 99
LARP7	CCR, DDR	Y/Y	BC: BRCTs BD: BRCTs	n.d. (poly-Ub, K48-linked)	Ube2D[a]	around pThr440	53
macroH2A1	CCR, TR	Y/Y	BC: RING BD: RING	K123 (mono-Ub)	Ube2D[a]	likely same as H2A	87
NF2	Hippo growth signaling	Y/N	BC: BRCTs	K159/269/274/364/387/396/439/449 (poly-Ub K6-, K27-, K29-, K63-linked)	n.d.	FERM domain	51
Nuclephosmin	n.d. (colocalizes in mitosis)	Y/Y	BC: 1-222 BD:1-320	n.d. (poly-Ub, K6-, K29-linked)	Ube2D[a]	n.d.	127
Oct1	Metabolic regulation	Y/Y		K9/403 (poly-Ub, K48-linked)	Ube2D[a]	n.d.	108
P50	CCR, chromosome stability	Y/Y	BD: BRCTs	K354/356 (mono-Ub)	Ube2D[a]	around pSer337	52
progesterone receptor	TR	Y/Y	n.d.	n.d. (poly-Ub, degradative)	Ube2D	n.d.	128

RPB1	DDR, TR	Y/Y	BC: BRCTs	n.d. (poly-Ub, degradative)	Ube2D[a]	C-terminal domain (pSer5)	50, 129, 130
RPB8	DDR, TR	Y/Y	n.d.	n.d. (poly-Ub K6-linked)	Ube2D[a], Ube2W	n.d.	34, 131
TFIIE	TR	N/Y	n.d.	n.d. (likely mono-Ub)	Ube2D[a]	n.d.	130
Topoisomerase IIa	DNA decatenation	Y/N	n.d.	n.d. (poly-Ub, non-degradative)	n.d.	n.d.	13
γ-tubulin	CCR (centrosome regulation)	Y/Y	BC: BRCTs & IDR	K48/344 (mono-Ub)	Ube2D[a]	n.d.	54, 55, 132

(*) DDR, DNA damage repair; **TR**, transcriptional regulation; **CCR**, cell-cycle regulation. Reported functions limited to those from references reporting BRCA1/BARD1-mediated Ub of substrate.

(Ube2D[a]) other E2s not tested

CHAPTER 2

BRCA1/BARD1 is a nucleosome reader and writer

Samuel R. Witus[1], Weixing Zhao[2], Peter S. Brzovic[1], and Rachel E. Klevit[1,3]

1. University of Washington School of Medicine, Department of Biochemistry. Seattle, WA.
2. University of Texas Health Science Center at San Antonio, Department of Biochemistry and Structural Biology. San Antonio, TX.
3. Corresponding author: klevit@uw.edu

Reprinted with permission from: Witus SR, Zhao W, Brzovic PS, Klevit RE. BRCA1/BARD1 is a nucleosome reader and writer. Trends Biochem Sci. 2022 Mar 26:S0968-0004(22)00060-3. doi: 10.1016/j.tibs.2022.03.001. Epub ahead of print. PMID: 35351360.

Author Contributions:

S.R.W. wrote the initial draft of this manuscript and made the figures. The final draft of the manuscript was edited by S.R.W., W.Z., P.S.B., and R.E.K.

***** Bolded phrases are defined in a glossary following the “references” section

Abstract:

Mutations in *BRCA1* and *BARD1* predispose carriers to breast and ovarian cancers. The BRCA1 and BARD1 proteins form a heterodimeric complex (BRCA1/BARD1) that regulates many biological processes including transcription and DNA double-stranded break repair. These functions are mediated by BRCA1/BARD1’s only known enzymatic function as an E3 ubiquitin ligase and its role as a central hub for many large protein complexes. But the mechanisms by which BRCA1/BARD1 interfaces with chromatin, where it exerts its major functions, have remained unknown. Here, we review recent advancements in structural and cellular biology that have provided critical insights into how BRCA1/BARD1 serves as both a nucleosome reader and writer to facilitate transcriptional regulation and DNA repair by homologous recombination.

Main Text

BRCA1/BARD1 performs chromatin-associated functions

The breast-cancer susceptibility gene *BRCA1* was linked to heritable breast and ovarian cancers over thirty years ago[1–4]. More recently, mutations in the *BARD1* gene were also linked to breast cancer[5–7]. The BRCA1 and BARD1 proteins associate to form a large obligate heterodimeric complex (BRCA1/BARD1) that localizes to the nucleus, where it acts as a central regulator of DNA-centric activity throughout the cell cycle. Well-established roles for BRCA1/BARD1 include **transcriptional regulation (see Glossary)** and promotion of **DNA double-stranded break** (**DSB**) repair by **homologous recombination** (**HR**)[8–10].

Formation of the BRCA1/BARD1 heterodimer is essential for its nuclear function. The two proteins associate via interactions governed by their N-terminal RING domains[11] **(Fig. 1)**. This region constitutes the sole known enzymatic activity of BRCA1/BARD1 which functions as a RING-type E3 ubiquitin (Ub) ligase[12,13]. Both proteins also contain folded C-terminal domains (BRCT for BRCA1; Ank-BRCT for BARD1) and expansive intervening stretches of intrinsically disordered regions (IDR). Sites throughout both subunits of the heterodimer serve as hubs for many protein interactions, including several extremely large complexes involved in transcriptional regulation and DNA damage repair[14,15] (a relevant subset of these are indicated in **Fig. 1**). For example, BRCA1 has been shown to interact with a variety of transcription factors, including the core transcriptional machinery[16]. BRCA1/BARD1 is also recruited to DNA damage sites, forming so-called ‘foci’ with repair factors until the breaks are fixed[17–20]. What remains to be determined, however, is a detailed understanding of the molecular logic that governs the recruitment and function of BRCA1/BARD1 on chromatin, where it exerts its major functions.

Based on several recent studies, a new paradigm has emerged for BRCA1/BARD1 recruitment and enzymatic activity at **nucleosomes**, the basic organizing units of chromatin. In support of its chromatin "writer" function, the BRCA1/BARD1 RING domains bind nucleosomes directly, facilitating mono-ubiquitylation of non-canonical sites in the unstructured C-terminal tail of H2A. In support of its chromatin "reader" function, the BARD1 C-terminal domains bind to H2A K13/15-ubiquitylated nucleosomes that are unmethylated at H4K20 (H4K20me0). These marks are hallmarks of damaged chromatin in the S/G2 phase of the cell cycle when a newly replicated sister chromatid is present to be used as a template for HR. Presently, the connection between the two activities remains to be fully defined. Here, we discuss recent advances in BRCA1/BARD1 structural and cellular biology and their implications in transcriptional regulation and DNA DSB repair.

BRCA1/BARD1 is an H2A-specific Ub ligase

In its capacity as a RING-type E3 Ub ligase, BRCA1/BARD1 facilitates the direct transfer of the small signaling protein Ub from an E2 Ub-conjugating enzyme to substrate proteins. The action of BRCA1/BARD1 as a Ub ligase is two-fold; it elicits a reactive conformation of an E2~Ub conjugate and simultaneously binds a substrate for Ub transfer[21,22]. While several BRCA1/BARD1 Ub ligase substrates have been described, few have provided compelling links to its major functions in transcriptional regulation and DNA DSB repair[23]. Moreover, whether the ligase function of BRCA1/BARD1 contributes to its role as a tumor suppressor has been the subject of controversy[24–27]. Early genetic and biochemical studies revealed that highly penetrant cancer-predisposing mutations concentrated in the BRCA1 RING domain cause inactivation of E3 Ub ligase function, but also disrupt heterodimerization with BARD1 – a critical interaction for tumor suppression[12].

Providing a direct link to chromatin regulation, nucleosomal histone H2A was identified as a target for BRCA1/BARD1 Ub ligase function *in vivo*. BRCA1/BARD1-mediated H2A ubiquitylation was shown to promote heterochromatin-mediated silencing of a-satellite DNA regions in a murine model[28] **(see Figure 3a)**. These genomic regions are normally transcriptionally repressed, and the loss of BRCA1 or ectopic over-expression of a-satellite RNAs both cause genomic instability – a hallmark of BRCA1 deficiency. Expression of a-satellite RNAs was subsequently shown to induce breast cancer in mice, potentially linking BRCA1/BARD1 H2A-Ub ligase function to cancer phenotypes[29].

BRCA1/BARD1 transfers mono-ubiquitin to a region with three closely spaced sites on the unstructured extreme C-terminal tail of canonical histone H2A in nucleosomes (K125/127/129, referred to here as K127-Ub)[30]. Importantly, these lysine sites differ from those targeted by other RING Ub ligases (H2A K13/15, referred to as K15-Ub, by RNF168; K119 by RING1B/BMI1; and H2B K120 by RNF20/40), discussed later in this review. The unique lysine sites suggest that BRCA1/BARD1-dependent ubiquitylation is a novel histone post-translational modification that is functionally non-redundant with marks deposited by other RING Ub ligases. Nucleosomes harboring H2A K127-Ub are likely recognized by specific chromatin-associated factors, as has been observed for other Ub-nucleosome signals[31–34]. It is also possible that BRCA1/BARD1-dependent H2A-Ub may directly influence chromatin structure, as has been reported for chromatin fibers containing H2A K15-Ub and H2B K120-Ub[35,36].

Specialized H2A isoforms regulate DNA DSB repair and transcriptional processes and may also be substrates for BRCA1/BARD1[37]. Though the folded histone core sequences are highly conserved, isoforms contain variable sequences in the H2A C-terminal tail where BRCA1/BARD1 directs its Ub signal. Nucleosomes containing the isoform H2A.X/γH2A.X are a molecular marker of DNA damage and repair and form functional complexes with

BRCA1/BARD1[38]. Additionally, residues within the H2A.X C-terminal tail have been identified as the targets of BRCA1/BARD1 in vitro[39]. MacroH2A1 was also identified as a substrate for BRCA1/BARD1 in a screen for Ub ligase substrates[40]. MacroH2A isoforms have been shown to regulate DNA DSB repair pathway choice in cancer cells and are associated with transcriptionally repressive chromatin[41–43]. Primary human fibroblasts expressing mutant macroH2A1 lacking the BRCA1/BARD1 ubiquitylation sites were deficient in cellular senescence and exhibited increased growth rates[40]. Other H2A isoforms H2A.J, H2A.V, and H2A.Z all have lysine residues in their C-terminal tails predicted to be efficiently ubiquitylated by BRCA1/BARD1[44,45]. Ubiquitylation of H2A isoforms by BRCA1/BARD1 may mediate distinct functional outcomes in different nuclear processes.

Structural basis for site-specific H2A ubiquitylation

The H2A targeting specificity of BRCA1/BARD1 is fully encoded within the RING domains of BRCA1 and BARD1, implying that the RING/RING Ub ligase domain binds a nucleosome substrate and an E2~Ub conjugate simultaneously[30]. Although RINGs are canonically employed as E2~Ub binding units, the BARD1 RING has no E2-binding activity[46]. Cancer-predisposing mutations in the BARD1 RING domain specifically abrogate nucleosome binding and H2A ubiquitylation, revealing a substrate-binding function for this RING domain in the context of its nucleosomal activity[5]. While most RING-type Ub ligases employ auxiliary substrate binding domains or even adaptor proteins[47,48], direct substrate binding by RING domains appears to be a common feature among those that mono-ubiquitylate nucleosomes[39,44,49–51].

In addition to BRCA1/BARD1, two other RING-type Ub ligases, RNF168 and RING1B/BMI1, are known to mono-ubiquitylate distinct H2A lysine residues. RNF168-mediated H2A K15-Ub serves as a signal in the DNA DSB repair cascade that recruits repair factors to DSB sites[20]. RING1B/BMI1 is a component of the Polycomb repressive 1 (PRC1) complex that is a critical

regulator of transcription and responsible for the majority of H2A-Ub, namely H2A K119-Ub, in many cell-types[52,53]. Like BRCA1/BARD1, H2A targeting-specificity for these ligases is encoded within their RING domains[50,54].

A series of recent structural studies has revealed the basis for site-specific ubiquitylation of H2A by RNF168, RING1B/BMI1, and BRCA1/BARD1 **(Fig. 2a)**. All three ligases exploit a basic arginine anchor residue to bind to the same region of the H2A/H2B acidic patch – a surface used by many (if not most) chromatin-binding factors[55]. For the monomeric RING RNF168, additional interactions orient the E2 (UBE2D) towards the N-terminal region of H2A where K15 is located[49] **(Fig. 2a – left)**. The E2~Ub active site is oriented directly above its H2A target lysines, revealing how they are selectively ubiquitylated. In the RING1B/BMI1/UBE2D/nucleosome complex, the E2-binding RING1B contacts the acidic patch via a canonical arginine anchor[50] **(Fig. 2a – middle)**. In addition, a loop at the base of the non-E2-binding BMI1 RING domain forms interactions with the H3 α1-L1 elbow. Together, these interactions orient the RING1B E2-binding interface towards the nucleosome DNA entry/exit and position the E2~Ub active site directly over H2A K119 for Ub transfer. The RING1B-bound E2 also forms interactions with nucleosomal DNA, contributing to its affinity for the nucleosome substrate.

RNF168 and RING1B/BMI1 ubiquitylate H2A lysine residues within ordered regions of the nucleosome. In contrast, BRCA1/BARD1 mediates the transfer of Ub to lysines in a flexible disordered region of the C-terminal tail fewer than ten residues away from the target of RING1B/BMI1, calling to question how this is orchestrated **(Fig. 2b)**. Two studies reporting cryo-EM structures of BRCA1/BARD1/UBE2D/nucleosome complexes have elucidated the RING-mediated specificity determinants of site-specific H2A ubiquitylation[39,44] **(Fig. 2a – right, d, e)**. The structures show that the E2-binding BRCA1 subunit utilizes a canonical arginine-anchor to

interact with the H2A/H2B acidic patch akin to RING1B. However, the non-E2-binding BARD1 RING domain forms interactions with histones that are distinct from its counterpart, BMI1. These differences in non-E2 binding RING-histone interactions lead to a unique “stance” of the BRCA1/BARD1 RING heterodimer on the nucleosome compared to RING1B/BMI1. This stance positions the E2 bound by the BRCA1 RING away from the ordered histone surface where H2A K119 is located, providing a rationale for why this E3 ligase does not efficiently ubiquitylate the RING1B/BMI1 target lysine **(**K119, **Fig. 2c)**. Instead, the flexible H2A C-terminal tail has sufficient mobility in the complex to sample the BRCA1-bound E2 active site for Ub transfer to H2A K127[39,44]. Unlike the RING1B-bound E2, the BRCA1-bound E2 does not interact with nucleosomal DNA.

Notably, the BARD1 RING-histone interactions differ between the two published structures **(Fig. 2d, e)**. In Witus et al., the BARD1 RING binds close to the H3 a1-L1 elbow, inserting its W91 sidechain in a cleft formed by H2B and H4[44]. This interaction is consistent with the requirement for a nucleosome substrate as opposed to an H2A/H2B dimer for BRCA1/BARD1-dependent H2A ubiquitylation activity (unpublished observation). In Hu et al, the BARD1 RING domain interacts with the H2B αC helix, again using the W91 sidechain[39]. These interactions are not located near the H3 a1-L1 elbow region as observed in the Witus et al. structure. Despite these differences, the E2 is positioned away from the histone surface in both complexes, consistent with H2A K127 being selectively ubiquitylated **(Fig. 2c)**.

The source of differences in the two RING orientations in the BRCA1/BARD1 structures is unclear. Variability analysis of the Hu et al. cryo-EM map indicates a large amount of structural heterogeneity of the RING domains on the nucleosome, accounting for the lower resolution in this region compared to the histone core observed in both maps[39]. To overcome the modest affinity of the complexes, each group used a genetic fusion strategy, but the details of the

constructs employed differ. Importantly, although both groups utilized a truncated minimal RING/RING heterodimer for structural studies, the full-length BRCA1/BARD1 complex exhibits stronger binding and increased activity for a nucleosome substrate, suggesting that other regions of the ligase promote functional interactions with mono-nucleosomes[39,44]. A complete understanding of relevant regions in the full-length complex that facilitate BRCA1/BARD1-dependent H2A-Ub will be important to understand its activity and the effects of patient mutations outside the RING domains.

H2A K127-Ub in transcriptional regulation

BRCA1/BARD1 was first identified as a regulator of transcription, but this aspect of BRCA1/BARD1 activity is less well studied than its DNA damage repair function[56,57]. To date, BRCA1/BARD1-mediated H2A-Ub has primarily been associated with repressing gene expression, but studies are limited to relatively few genes identified through candidate-based approaches **(Fig. 3a, b)**.

For example, BRCA1/BARD1-mediated H2A-Ub has been implicated in the transcriptional regulation of estrogen metabolism, a process known to be disrupted in breast and ovarian cancers [58,59]. In non-cancerous breast epithelial cells (MCF10a), depletion of BRCA1 or BARD1 is associated with elevated transcript levels of certain estrogen-metabolizing cytochrome P450 (*CYP450*) genes[5] **(Fig. 3b)**. Several of these CYP450 proteins mediate the hydroxylation of estradiol, forming toxic intermediates that damage DNA and have been linked to hormone-related cancers[60]. *CYP450* transcript levels were elevated in BARD1-deficient MCF10a cells and restored to near wild-type levels by ectopic expression of wild-type BARD1 or an H2A-Ub fusion gene[5]. In another study, BRCA1 deficiency led to increased levels of toxic estrogen metabolites that induced DNA breaks in MCF10a cells[61]. While not explicitly tested, it is likely that these effects are similarly linked to BRCA1/BARD1-directed H2A-Ub. Relevant to

patient cancer phenotypes, both studies revealed substantial effects of *BRCA1* or *BARD1* **haploinsufficiency** in regulating transcription[5,61]. Together, the data indicate that transcriptional repression is a downstream effect of H2A ubiquitylation by BRCA1/BARD1. An appealing hypothesis emerging from these studies is that increased levels of specific, estrogen metabolizing CYP450 proteins (i.e., CYP1A1 and CYP3A4) resulting from transcriptional de-repression due to *BRCA1* or *BARD1* deficiency may affect the equilibrium of estrogen metabolites in tissues where estrogen is highly abundant. In turn, this will initiate DNA damage that cannot be properly repaired through HR due to BRCA1 or BARD1 deficiency, causing exacerbated DNA damage and mutational burden. To address this hypothesis, additional studies measuring and correlating CYP450 protein levels, estrogen metabolite levels, and DNA damage and repair in MCF10a cells and animals harboring *BRCA1* and *BARD1* mutations will be required. Furthermore, identification of a comprehensive set of genes regulated by BRCA1/BARD1-dependent H2A-Ub in relevant cell-types is an important goal.

BRCA1/BARD1 has also been shown to interact with other transcriptional regulators. These include the core transcriptional machinery, histone modifying enzymes, and a cadre of transcription factors[8]. Interactions with sequence-specific transcription factors (e.g., ERα, OCT1, ZBRK1, c-Myc, and others) may recruit the ligase to specific chromatin regions where it deposits H2A-Ub, thereby directly regulating transcription. It will be important to fully elucidate the role of BRCA1/BARD1 in modulating transcription via H2A-Ub, and how this process interfaces with the large and diverse array of transcriptional regulators with which it functions. It is also possible that specific histone modifications may influence BRCA1/BARD1's presence and/or H2A-Ub enzymatic activity at genomic regions to regulate transcription of target genes.

Recruitment of BRCA1/BARD1 to damaged chromatin

Double-stranded DNA breaks are mainly repaired through two competing pathways depending on the cell cycle[10]. HR is facilitated by BRCA1/BARD1 in S/G2 phases, where broken DNA ends are resected to expose single-stranded DNA and a sister chromatid serves as a template to guide high-fidelity repair. Alternatively, an error-prone repair pathway called **non-homologous end joining** (**NHEJ**) promoted by the protein **53BP1** rapidly ligates broken DNA ends to avoid catastrophic chromosome breakages. It is well established that competition between BRCA1/BARD1 and 53BP1 determines pathway choice between HR and NHEJ and, hence, the maintenance of genome integrity following DNA DSBs[62–65]. Previously, two mechanisms have been implicated in the recruitment and retention of BRCA1/BARD1 at DSB sites. These include interactions between the **BRCA1-A complex** (BRCA1/ABRAXAS1/RAP80) and K63-linked Ub chains deposited on linker histone H1 and/or interactions between the BARD1 BRCT domains and poly (ADP-ribose) (PAR; **Fig 1.**)[18,66,67]. Specifically lacking, however, is an explanation for BRCA1/BARD1's ability to compete with the NHEJ factor 53BP1 for DSB site occupancy to promote HR in S/G2 phase of the cell cycle when a sister chromatid is present.

Recent studies have elucidated a mechanism for sensing the cell cycle through multivalent interactions between the BARD1 C-terminal domains (Ank-BRCTs; **Fig. 1**) and specifically modified nucleosomes[68,69]. This is dependent on co-occurrence of the DNA DSB signal H2A K15-Ub deposited by RNF168 and the presence of H4K20me0, a marker of replicative chromatin and sister chromatid availability. Together, these marks serve to recruit the BRCA1/BARD1 complex to DNA DSBs to facilitate HR[69,70]. 53BP1 specifically binds to H2A K15-Ub and H4K20me2 nucleosomes, so this serves as a logic switch to determine whether BRCA1/BARD1 or 53BP1 is retained at DSB sites to license HR or NHEJ, respectively[32,71] **(see Fig. 5a – left pathway)**. Notably, H4K20 methylation status is a potent marker of the cell-cycle, with around 80% of post-replicative chromatin containing H4K20me1/2/3 and newly synthesized histones in S/G2 largely devoid of this mark[72].

Structures of the BARD1 Ank-BRCT C-terminal region bound to nucleosomes with H2A K15-Ub and H4K20me0 have revealed a highly specific network of interactions that are centered around an arginine anchor in the BARD1 BRCTs and the H2A/H2B acidic patch[39,73] **(Fig. 4a, b)**. The BARD1 Ank and BRCT domains also form intramolecular interactions that are not detected outside of a nucleosomal context[74]. The Ank domain binds to the H4 tail, utilizing a conserved pocket observed in other HR proteins that bind to H4K20me0[68] **(Fig. 4c)**. Mutation of binding pocket residues BARD1 E467A/N470A/D500A (called BARD1-3A) or introduction of H4K20me2 impairs nucleosome binding *in vitro*. In cells, BARD1-3A causes defects in HR by disrupting accumulation of BRCA1/BARD1 at DSBs, thereby limiting DNA end-resection[68]. Consequently, 53BP1 accumulates at DSB sites and NHEJ becomes the dominant repair pathway.

Interactions between the BARD1 BRCT domain and Ub attached to H2A K15 involve conserved, charged residues on the second BARD1 BRCT repeat termed the BRCT domain ubiquitin-directed recruitment motif (BUDR)[39,69,73] **(Fig. 4d)**. The BARD1 BUDR motif interacts with an atypical surface of Ub that spans residues N60-T66 and is distinct from the highly utilized I44 or I36 patches recognized by scores of other proteins[75]. The Ub K63 sidechain is engaged with the BARD1 BRCT, blocking extension of K63-linked chains on H2A K15-Ub by RNF8[39]. Like the BARD1-3A Ank mutation, substitution of conserved BUDR residues yields enhanced **poly (ADP-ribose) polymerase inhibitor** (**PARPi)** sensitivity and decreased recruitment to DSBs[69,73]. The putative PAR-binding pocket in BARD1 BRCT1 is unobstructed in the structure of the complex, possibly allowing for higher-order assemblies. Adding further complexity, phosphorylation of Ub-T12 in nucleosomal H2A K15-Ub decreases recognition by 53BP1 but allows for binding of BRCA1/BARD1 and other HR factors[76]. This feature is consistent with the different Ub surfaces recognized by the BARD1 BUDR and 53BP1 ubiquitin-directed recognition motif (UDR).

Finally, two redundant Ub-mediated pathways reliant on RNF168-mediated H2A K15-Ub or the BRCA1-A complex (ABRAXAS1/RAP80) serve to recruit BRCA1/BARD1 to damaged chromatin, adding an additional layer of complexity to the emerging picture[70,77] **(Fig. 5a)**. Of the two, only the RNF168-mediated pathway is dependent on BRCA1's Ub ligase activity[77]. Simultaneous disruption of the BRCA1/ABRAXAS1/RAP80 interaction and BRCA1-E2 binding (BRCA1-I26A) caused complete loss of recruitment of BRCA1/BARD1 to ionizing radiation induced foci (IRIF). Furthermore, a nucleosome-binding mutant in the RING domain of BRCA1 (K70A/R71A) also displayed defective IRIF recruitment only upon co-depletion of RAP80 as observed for the BRCA1-E2 binding mutant, although with a smaller effect[77]. Together, the data suggest that BRCA1/BARD1 Ub ligase activity functions in the same pathway as RNF168 in HR and contributes to its own retention at DSB sites. It is unclear why BRCA1/BARD1 ligase function is required for its retention at DSB sites. Hypotheses that BRCA1/BARD1 Ub ligase activity serves to displace 53BP1 and potentially influence the activities of multiple BRCA1/BARD1 substrates (including but not limited to H2A) should be entertained. Importantly, this work may provide an explanation for the lack of HR phenotypes observed in other studies using BRCA1/BARD1 Ub ligase-deficient mutants discussed in the section below, in that the effects of the BRCA1/BARD1 mutants used may be masked by intact BRCA1-A complex interactions[24,68].

H2A K127-Ub in DNA double-stranded break repair

In addition to BARD1's role as a nucleosome reader to recruit BRCA1/BARD1 to nucleosomes near DSB sites, BRCA1/BARD1-mediated ubiquitylation of nucleosomal H2A was found to promote HR after pathway commitment by facilitating long-range DNA end-resection[78] **(Fig. 5b)**. HeLa cells depleted of endogenous BARD1 by siRNA and expressing a BARD1 mutant reported to be a less effective ligase with certain E2 enzymes (BARD1-R99E) exhibited

phenotypes consistent with HR deficiency, suggesting that the E3 ligase activity of BRCA1/BARD1 is important for HR. Notably, expression of an H2A-Ub genetic fusion presumed to mimic the natural product of BRCA1/BARD1-dependent ubiquitylation restored HR in BARD1-deficient cells, implying that the H2A-Ub signal promotes DNA end-resection. The H2A modification is required to recruit SMARCAD1, a SWI/SNF-like ATP-dependent chromatin remodeler that helps reposition nucleosomes and excludes 53BP1 from DSB sites to promote DNA end-resection **(Fig. 5b)**. In a cryo-EM structure of SMARCARD1 bound to a mono-nucleosome, its ATPase domains are bound in proximity to the H2A C-terminal region, but the flexible tail is not detected in the cryo-EM image[79]. Further investigation is needed to elucidate how H2A-Ub plays a role in SMARCARD1 recruitment or remodeling activity.

Further evidence in support of a role for BRCA1/BARD1 Ub ligase function in HR comes from studies involving de-ubiquitylation. Ubiquitylation is a dynamic and reversible modification that can be removed from substrates by deubiquitylating enzymes (DUBs). The DUB USP48 was shown to be recruited to sites of DNA damage in cells and to preferentially remove BRCA1/BARD1-mediated H2A-Ub marks (K127-Ub) over those deposited by RNF168 (K15-Ub) or RING1B/BMI1 (K119-Ub) *in vitro*[80]. USP48 acts in the same pathway as BRCA1 and SMARCAD1, and its depletion resulted in over-resected DNA ends, exclusion of 53BP1 from IRIF, decreased HR efficiency, and decreased cellular survival following PARPi treatment. Together, the findings indicate that USP48 antagonizes BRCA1/BARD1 Ub ligase-dependent activities in HR, creating a balance that regulates DNA end-resection tract length[78, 80] **(Fig. 5b)**. Additional support for BRCA1/BARD1's Ub ligase activity in HR comes from studies in hTERT RPE-1 cells, where only concomitant deletion of the BRCA1 BRCT domain and introduction of an E2-binding deficient mutation in the BRCA1 RING domain caused PARPi survival defects[77]. However, whether this dependency on BRCA1/BARD1 Ub ligase function is due to H2A-Ub or other substrates remains to be determined.

Notably, the role of BRCA1/BARD1 as a Ub ligase in HR is not universally embraced, as several studies have arrived at differing observations and conclusions. Each study was performed in a different cell-type and used different methods to perturb or deplete BRCA1/BARD1 ligase functionality. For example, a study using an auxin inducible degron (AID) system to deplete endogenous BARD1 in HCT116 cells did not observe the same HR defects upon expression of BARD1 R99E (the mutant used in the study[78] described above)[68]. Additionally, in the BRCA1-deficient MDA-MB-436 cell line, several ligase-inactivating mutants did not yield PARPi survival defects and IRIF formation of HR factors was not dependent on Ub ligase function[70]. Lack of Ub ligase dependency in HR is also consistent with previous findings using a BRCA1 mutant that is defective in binding to and activity with the E2 enzyme UBE2D (BRCA1-I26A)[24,25]. Although the differences could be cell-type specific, each approach has intrinsic limitations, making it impossible to reach a unified understanding at present. Further investigation using separation-of-function mutants is warranted to clarify the requirements for BRCA1/BARD1 H2A-Ub activity in HR. Although challenging, it will be critical to examine BRCA1/BARD1 Ub ligase functions in HR in non-cancerous mammary and ovarian epithelial cells to ascertain cell-type specific dependencies. Current experimental limitations have also impeded characterization of BRCA1/BARD1-dependent H2A-Ub in cells and animals, underscoring the critical need for novel reagents and tools **(Box 1)**.

Concluding Remarks

The BARD1 C-terminal Ank-BRCT “reader” domains and the N-terminal BRCA1/BARD1 RING “writer” domains bind to a fully overlapping surface on a nucleosome, precluding their simultaneous binding to one “face” of a nucleosome. Notably, a protein species containing only the BRCA1 RING domain but full-length BARD1 has increased H2A-Ub enzymatic activity for a mono-nucleosome substrate with pre-installed H2A K15-Ub[39]. This observation implies the

possibility of a complex where the BRCA1/BARD1 RING domains and BARD1 Ank-BRCTs are simultaneously bound to opposite faces of one nucleosome through a wrapping mechanism, promoting its Ub ligase activity (i.e., the "writer" function; **Fig. 4e**). It is also possible that such interactions may occur between neighboring nucleosomes as has been observed with other nucleosome-modifying enzymes[81], but this remains to be tested. In addition to H2A K15-Ub, a variety of other histone post-translational modifications (PTMs) may influence BRCA1/BARD1-dependent H2A-Ub activity as has been reported for the H2B K120-Ub-specific Ub ligase RNF20/40[82]. A more complete understanding of BRCA1/BARD1 interactions with chromatin, the PTMs involved, and associated higher-order protein complexes will be critical to understand its many biological functions and to assess potentially pathogenic patient mutations of unknown significance **(see outstanding questions)**.

Acknowledgments:

We thank J. Pruneda for his insightful feedback on this manuscript. W.Z. was supported by V Scholar V2019.Q13 from V Foundation for Cancer Research, Young Investigator Award from Max and Minnie Tomerlin Voelcker Fund, and NIH R01GM141091. S.R.W., P.S.B., and R.E.K. were supported by NIH R01 CA260834 and R.E.K. is the Edmond H. Fischer/WRF Endowed Chair in Biochemistry.

References

1 Friedman, L.S. *et al.* (1994) Confirmation of BRCA1 by analysis of germline mutations linked to breast and ovarian cancer in ten families. *Nat. Genet.* 8, 399–404

2 Hall, J. *et al.* (1990) Linkage of early-onset familial breast cancer to chromosome 17q21. *Science* 250, 1684-1689

3 King, M.-C. *et al.* (2003) Breast and ovarian cancer risks due to inherited mutations in BRCA1 and BRCA2. *Science* 302, 643–646

4 Miki, Y. *et al.* (1994) A strong candidate for the breast and ovarian cancer susceptibility gene BRCA1. *Science* 266, 66-71

5 Stewart, M.D. *et al.* (2018) BARD1 is necessary for ubiquitylation of nucleosomal histone H2A and for transcriptional regulation of estrogen metabolism genes. *Proc. Natl. Acad. Sci. U. S. A.* 115, 1316–1321

6 Li, W. *et al.* (2021) A synergetic effect of BARD1 mutations on tumorigenesis. *Nat. Commun.* 12, 1243

7 Weber-Lassalle, N. *et al.* (2019) Germline loss-of-function variants in the BARD1 gene are associated with early-onset familial breast cancer but not ovarian cancer. *Breast Cancer Res.* 21, 55

8 Mullan, P.B. *et al.* (2006) The role of BRCA1 in transcriptional regulation and cell cycle control. *Oncogene* 25, 5854–5863

9 Zhao, W. *et al.* (2019) The BRCA Tumor Suppressor Network in Chromosome Damage Repair by Homologous Recombination. *Annu. Rev. Biochem.* 88, 221–245

10 Tarsounas, M. and Sung, P. (2020) The antitumorigenic roles of BRCA1–BARD1 in DNA repair and replication. *Nat. Rev. Mol. Cell Biol.* 21, 284–299

11 Brzovic, P.S. *et al.* (2001) Structure of a BRCA1-BARD1 heterodimeric RING-RING complex. *Nat. Struct. Biol.* 8, 833–837

12 Hashizume, R. *et al.* (2001) The RING heterodimer BRCA1-BARD1 is a ubiquitin ligase inactivated by a breast cancer-derived mutation. *J. Biol. Chem.* 276, 14537–14540

13 Lorick, K.L. *et al.* (1999) RING fingers mediate ubiquitin-conjugating enzyme (E2)-dependent ubiquitination. *Proc. Natl. Acad. Sci.* 96, 11364-11369

14 Savage, K.I. and Harkin, D.P. (2015) BRCA1, a “complex” protein involved in the maintenance of genomic stability. *FEBS J.* 282, 630–646

15 Zhao, W. *et al.* (2017) BRCA1-BARD1 promotes RAD51-mediated homologous DNA pairing. *Nature* 550, 360–365

16 Scully, R. *et al.* (1997) BRCA1 is a component of the RNA polymerase II holoenzyme. *Proc. Natl. Acad. Sci. U. S. A.* 94, 5605–5610

17 Scully, R. *et al.* (1997) Dynamic Changes of BRCA1 Subnuclear Location and Phosphorylation State Are Initiated by DNA Damage. *Cell* 90, 425–435

18 Kolas Nadine K. *et al.* (2007) Orchestration of the DNA-Damage Response by the RNF8 Ubiquitin Ligase. *Science* 318, 1637–1640

19 Sobhian Bijan *et al.* (2007) RAP80 Targets BRCA1 to Specific Ubiquitin Structures at DNA Damage Sites. *Science* 316, 1198–1202

20 Mattiroli, F. *et al.* (2012) RNF168 ubiquitinates K13-15 on H2A/H2AX to drive DNA damage signaling. *Cell* 150, 1182–1195

21 Pruneda, J.N. *et al.* (2012) Structure of an E3:E2~Ub complex reveals an allosteric mechanism shared among RING/U-box ligases. *Mol. Cell* 47, 933–942

22 Metzger, M.B. *et al.* (2014) RING-type E3 ligases: Master manipulators of E2 ubiquitin-conjugating enzymes and ubiquitination. *Ubiquitin-Proteasome Syst.* 1843, 47–60

23 Witus, S.R. *et al.* (2021) The BRCA1/BARD1 ubiquitin ligase and its substrates. *Biochem. J.* DOI: 10.1042/BCJ20200864

24 Reid, L.J. *et al.* (2008) E3 ligase activity of BRCA1 is not essential for mammalian cell viability or homology-directed repair of double-strand DNA breaks. *Proc. Natl. Acad. Sci. U. S. A.* 105, 20876–20881

25 Shakya, R. *et al.* (2011) BRCA1 tumor suppression depends on BRCT phosphoprotein binding, but not its E3 ligase activity. *Science* 334, 525–528

26 Drost, R. *et al.* (2011) BRCA1 RING Function Is Essential for Tumor Suppression but Dispensable for Therapy Resistance. *Cancer Cell* 20, 797–809

27 Shakya, R. *et al.* (2008) The basal-like mammary carcinomas induced by Brca1 or Bard1 inactivation implicate the BRCA1/BARD1 heterodimer in tumor suppression. *Proc. Natl. Acad. Sci.* 105, 7040-7045

28 Zhu, Q. *et al.* (2011) BRCA1 tumour suppression occurs via heterochromatin-mediated silencing. *Nature* 477, 179–184

29 Zhu, Q. *et al.* (2018) Heterochromatin-Encoded Satellite RNAs Induce Breast Cancer. *Mol. Cell* 70, 842-853

30 Kalb, R. *et al.* (2014) BRCA1 is a histone-H2A-specific ubiquitin ligase. *Cell Rep.* 8, 999–1005

31 Kasinath Vignesh *et al.* (2021) JARID2 and AEBP2 regulate PRC2 in the presence of H2AK119ub1 and other histone modifications. *Science* 371, eabc3393

32 Fradet-Turcotte, A. *et al.* (2013) 53BP1 is a reader of the DNA-damage-induced H2A Lys 15 ubiquitin mark. *Nature* 499, 50–54

33 Hsu, P.L. *et al.* (2019) Structural Basis of H2B Ubiquitination-Dependent H3K4 Methylation by COMPASS. *Mol. Cell* 76, 712-723

34 Worden, E.J. *et al.* (2019) Mechanism of Cross-talk between H2B Ubiquitination and H3 Methylation by Dot1L. *Cell* 176, 1490-1501

35 Fierz, B. *et al.* (2011) Histone H2B ubiquitylation disrupts local and higher-order chromatin compaction. *Nat. Chem. Biol.* 7, 113–119

36 Debelouchina, G.T. *et al.* (2017) Ubiquitin utilizes an acidic surface patch to alter chromatin structure. *Nat. Chem. Biol.* 13, 105–110

37 Shah, S. *et al.* (2020) Histone H2A isoforms: Potential implications in epigenome plasticity and diseases in eukaryotes. *J. Biosci.* 45, 4

38 Paull, T.T. *et al.* (2000) A critical role for histone H2AX in recruitment of repair factors to nuclear foci after DNA damage. *Curr. Biol. CB* 10, 886–895

39 Hu, Q. *et al.* (2021) Mechanisms of BRCA1–BARD1 nucleosome recognition and ubiquitylation. *Nature* 596, 438–443

40 Kim, B.-J. *et al.* (2017) The Histone Variant MacroH2A1 Is a BRCA1 Ubiquitin Ligase Substrate. *Cell Rep.* 19, 1758–1766

41 Sebastian, R. *et al.* (2020) Epigenetic Regulation of DNA Repair Pathway Choice by MacroH2A1 Splice Variants Ensures Genome Stability. *Mol. Cell* 79, 836-845

42 Douet, J. *et al.* (2017) MacroH2A histone variants maintain nuclear organization and heterochromatin architecture. *J. Cell Sci.* 130, 1570–1582

43 Gamble, M.J. *et al.* (2010) The histone variant macroH2A1 marks repressed autosomal chromatin, but protects a subset of its target genes from silencing. *Genes Dev.* 24, 21–32

44 Witus, S.R. *et al.* (2021) BRCA1/BARD1 site-specific ubiquitylation of nucleosomal H2A is directed by BARD1. *Nat. Struct. Mol. Biol.* 28, 268–277

45 Sarcinella Elizabeth *et al.* (2007) Monoubiquitylation of H2A.Z Distinguishes Its Association with Euchromatin or Facultative Heterochromatin. *Mol. Cell. Biol.* 27, 6457–6468

46 Christensen, D.E. *et al.* (2007) E2-BRCA1 RING interactions dictate synthesis of mono- or specific polyubiquitin chain linkages. *Nat. Struct. Mol. Biol.* 14, 941–948

47 Harper, J.W. and Schulman, B.A. (2021) Cullin-RING Ubiquitin Ligase Regulatory Circuits: A Quarter Century Beyond the F-Box Hypothesis. *Annu. Rev. Biochem.* 90, 403–429

48 Zheng, N. and Shabek, N. (2017) Ubiquitin Ligases: Structure, Function, and Regulation. *Annu. Rev. Biochem.* 86, 129–157

49 Horn, V. *et al.* (2019) Structural basis of specific H2A K13/K15 ubiquitination by RNF168. *Nat. Commun.* 10, 1751

50 McGinty, R.K. *et al.* (2014) Crystal structure of the PRC1 ubiquitylation module bound to the nucleosome. *Nature* 514, 591–596

51 Gallego, L.D. *et al.* (2016) Structural mechanism for the recognition and ubiquitination of a single nucleosome residue by Rad6-Bre1. *Proc. Natl. Acad. Sci. U. S. A.* 113, 10553–10558

52 Wang, H. *et al.* (2004) Role of histone H2A ubiquitination in Polycomb silencing. *Nature* 431, 873–878

53 Cao, R. *et al.* (2005) Role of Bmi-1 and Ring1A in H2A Ubiquitylation and Hox Gene Silencing. *Mol. Cell* 20, 845–854

54 Mattiroli, F. *et al.* (2014) The nucleosome acidic patch plays a critical role in RNF168-dependent ubiquitination of histone H2A. *Nat. Commun.* 5, 3291

55 McGinty, R.K. and Tan, S. (2021) Principles of nucleosome recognition by chromatin factors and enzymes. *Current Opinion in Structural Biology.* 71, 16–26

56 Monteiro, A.N.A. *et al.* (1996) Evidence for a transcriptional activation function of BRCA1 C-terminal region. *Proc. Natl. Acad. Sci.* 93, 13595

57 Chapman, M.S. and Verma, I.M. (1996) Transcriptional activation by BRCA1. *Nature* 382, 678–679

58 Samavat, H. and Kurzer, M.S. (2015) Estrogen metabolism and breast cancer. *Cancer Lett.* 356, 231–243

59 Mungenast, F. and Thalhammer, T. (2014) Estrogen Biosynthesis and Action in Ovarian Cancer. *Front. Endocrinol.* 5, 192

60 Fuhrman, B.J. *et al.* (2012) Estrogen Metabolism and Risk of Breast Cancer in Postmenopausal Women. *JNCI J. Natl. Cancer Inst.* 104, 326–339

61 Savage, K.I. *et al.* (2014) BRCA1 deficiency exacerbates estrogen-induced DNA damage and genomic instability. *Cancer Res.* 74, 2773–2784

62 Chen, J. *et al.* (2020) 53BP1 loss rescues embryonic lethality but not genomic instability of BRCA1 total knockout mice. *Cell Death Differ.* 27, 2552–2567

63 Bouwman, P. *et al.* (2010) 53BP1 loss rescues BRCA1 deficiency and is associated with triple-negative and BRCA-mutated breast cancers. *Nat. Struct. Mol. Biol.* 17, 688–695

64 Jaspers, J.E. *et al.* (2013) Loss of 53BP1 Causes PARP Inhibitor Resistance in Brca1-Mutated Mouse Mammary Tumors. *Cancer Discov.* 3, 68

65 Escribano-Díaz, C. *et al.* (2013) A Cell Cycle-Dependent Regulatory Circuit Composed of 53BP1-RIF1 and BRCA1-CtIP Controls DNA Repair Pathway Choice. *Mol. Cell* 49, 872–883

66 Thorslund, T. *et al.* (2015) Histone H1 couples initiation and amplification of ubiquitin signalling after DNA damage. *Nature* 527, 389–393

67 Li, M. and Yu, X. (2013) Function of BRCA1 in the DNA damage response is mediated by ADP-ribosylation. *Cancer Cell* 23, 693–704

68 Nakamura, K. *et al.* (2019) H4K20me0 recognition by BRCA1–BARD1 directs homologous recombination to sister chromatids. *Nat. Cell Biol.* 21, 311–318

69 Becker, J.R. *et al.* (2021) BARD1 reads H2A lysine 15 ubiquitination to direct homologous recombination. *Nature* 596, 433–437

70 Krais, J.J. *et al.* (2021) RNF168-mediated localization of BARD1 recruits the BRCA1-PALB2 complex to DNA damage. *Nat. Commun.* 12, 5016

71 Wilson, M.D. *et al.* (2016) The structural basis of modified nucleosome recognition by 53BP1. *Nature* 536, 100–103

72 Saredi, G. *et al.* (2016) H4K20me0 marks post-replicative chromatin and recruits the TONSL–MMS22L DNA repair complex. *Nature* 534, 714–718

73 Dai, L. *et al.* (2021) Structural insight into BRCA1-BARD1 complex recruitment to damaged chromatin. *Mol. Cell* 81, 2765-2777.e6

74 Fox, D., 3rd *et al.* (2008) Crystal structure of the BARD1 ankyrin repeat domain and its functional consequences. *J. Biol. Chem.* 283, 21179–21186

75 Winget, J.M. and Mayor, T. (2010) The Diversity of Ubiquitin Recognition: Hot Spots and Varied Specificity. *Mol. Cell* 38, 627–635

76 Walser, F. *et al.* (2020) Ubiquitin Phosphorylation at Thr12 Modulates the DNA Damage Response. *Mol. Cell* 80, 423-436

77 Sherker, A. *et al.* (2021) Two redundant ubiquitin-dependent pathways of BRCA1 localization to DNA damage sites. *EMBO Rep.* 22, e53679

78 Densham, R.M. *et al.* (2016) Human BRCA1-BARD1 ubiquitin ligase activity counteracts chromatin barriers to DNA resection. *Nat. Struct. Mol. Biol.* 23, 647–655

79 Markert Jonathan *et al.* SMARCAD1 is an ATP-dependent histone octamer exchange factor with de novo nucleosome assembly activity. *Sci. Adv.* 7, eabk2380

80 Uckelmann, M. *et al.* (2018) USP48 restrains resection by site-specific cleavage of the BRCA1 ubiquitin mark from H2A. *Nat. Commun.* 9, 229

81 Poepsel, S. *et al.* (2018) Cryo-EM structures of PRC2 simultaneously engaged with two functionally distinct nucleosomes. *Nat. Struct. Mol. Biol.* 25, 154–162

82 Wojcik, F. *et al.* (2018) Functional crosstalk between histone H2B ubiquitylation and H2A modifications and variants. *Nat. Commun.* 9, 1394

Outstanding questions:

1) Full-length BRCA1/BARD1 binds more strongly and has increased activity for unmodified nucleosomes than the isolated RING/RING complex. How do regions outside the RING domains contribute to chromatin interactions?
2) In addition to H2A K15-Ub and K4K20me0, what combinations of histone PTMs regulate BRCA1/BARD1 recruitment to nucleosomes and H2A-Ub activity?
3) What are the patterns and dynamics of the H2A K127-Ub mark in different cell-types? This requires a method for nucleosome-Ub PTM detection that is currently lacking.
4) What is the full subset of genes regulated by BRCA1/BARD1-dependent H2A-Ub? How is BRCA1/BARD1 targeted to these genomic regions to deposit H2A-Ub? How does this differ between cell types?
5) What are the direct and indirect effects of BRCA1/BARD1-dependent H2A K127-Ub on chromatin? What factors other than SMARCAD1 and USP48 recognize and regulate this mark?
6) Studies have drawn conflicting conclusions regarding BRCA1/BARD1 Ub ligase participation in DNA DSB repair. What are the requirements for BRCA1/BARD1 Ub ligase activity in DNA DSB repair and how is H2A-Ub involved? Is BRCA1/BARD1-dependent H2A K127-Ub important for tumor suppressor function?
7) What is the interplay between BRCA1/BARD1 recruitment to damaged chromatin via its C-terminal domains and its Ub ligase activity in HR?

Glossary

BRCA1-A complex – A complex composed of ABRAXAS1, RAP80, BRCC36, BRCC45, and MERIT40 that recruits BRCA1/BARD1 to DNA DSBs. This is mediated by direct binding of phosphorylated ABRAXAS1 to the BRCTs of BRCA1, and an interaction between the RAP80 Ub interaction motif (UIM) and K63-linked poly-Ub chains deposited on linker histone H1 by the Ub ligase RNF8.

DNA double-stranded break (DSB) repair – a collection of biological pathways including (but not limited to) HR and NHEJ that recognize and repair double-stranded DNA breaks. DNA DSBs are caused by a variety of chemical and environmental mutagens in addition to normal cellular processes, resulting in fragmented chromosomes. Disruptions to normal DNA DSB repair processes can introduce mutations, sometimes leading to cancer phenotypes.

Haploinsufficiency – a genetic model of dominant gene action in diploid organisms where the presence of one wild-type allele and one mutant allele does not produce a wild-type phenotype.

Homologous recombination (HR) – a DNA repair pathway that utilizes the genetic information on a sister chromatid to perform template-based repair of the damaged chromosome. DNA repair by HR generally does not produce mutations, thereby promoting genome integrity and stability. HR is facilitated by BRCA1/BARD1 and associated repair factors in S/G2 phases of the cell-cycle when a sister chromatid is present. HR and non-homologous end-joining are competing DNA repair pathways.

Non-homologous end-joining (NHEJ) – a non-templated DNA repair pathway promoted by 53BP1. In NHEJ, broken DNA ends are rapidly ligated back together to avoid catastrophic chromosomal breakage. However, this process is error-prone and can lead to mutations.

Nucleosome – The fundamental organizing unit of chromatin. A mono-nucleosome is composed of a histone octamer formed by two copies each of histones H2A, H2B, H3, and H4 wrapped by about 147 base-pairs of double-stranded DNA. The histone octamer contains an ordered core region and dynamic histone tails that are subject to a wide variety of regulatory post-translational modifications (PTMs). Mono-nucleosomes are connected in chromatin via linker DNA and may contain linker histone H1. Many chromatin-regulating factors bind to nucleosomes directly, including BRCA1/BARD1 and 53BP1.

Poly (ADP-ribose) polymerase inhibitors (PARPi) – a class of small-molecule drugs that target PARP enzymes. These drugs exacerbate DNA damage by preventing early DNA damage signaling by PARP enzymes. Cells that are deficient in HR, such as those harboring certain *BRCA1* and *BARD1* mutations, are especially sensitive to PARPi drug treatment. Therefore, PARPi treatment can be used to assess the effects of mutations on BRCA1/BARD1 function in HR.

TP53 binding-protein 1 (53BP1) – a protein that promotes DNA DSB repair by directly competing with BRCA1/BARD1 to occupy damaged chromatin sites, inhibiting DNA end-resection. 53BP1 uses its tandem Tudor domain and ubiquitin-directed recognition motif to bind to nucleosomes containing both H4K20me2 and H2A K15-Ub.

Transcriptional regulation – a collection of biological pathways that determine which and when genes are expressed in cells. In general, transcriptional regulation is influenced by the collection of histone post-translational modifications and regulatory enzymes/factors found at a particular genomic region.

Text boxes

Box 1. Current experimental limitations in understanding H2A K127-Ub. An impediment to biological characterization of BRCA1/BARD1-dependent ubiquitylation of nucleosomal H2A is the lack of tools for robust detection and manipulation of this post-translation modification. Unlike the other H2A-Ub marks (K15-Ub and K119-Ub), no commercial antibodies are currently available. The lysine-rich extreme C-terminal H2A tail also precludes traditional mass spectrometry techniques that employ trypsin digestion, which generates peptide fragments that are likely too small to detect. Furthermore, the basal cellular amount of BRCA1/BARD1-mediated H2A-Ub appears to be extremely low compared to that of PRC1-mediated K119-Ub. Although expressing an H2A-Ub C-terminal genetic fusion to bypass ligase deficiency has proven to be an effective strategy, it is possible that overexpression of this fusion construct causes global perturbation of chromatin that could introduce artifacts. Together, these circumstances indicate a critical need for the development of reagents and tools capable of monitoring and manipulating BRCA1/BARD1-dependent H2A-Ub in cells.

Figures

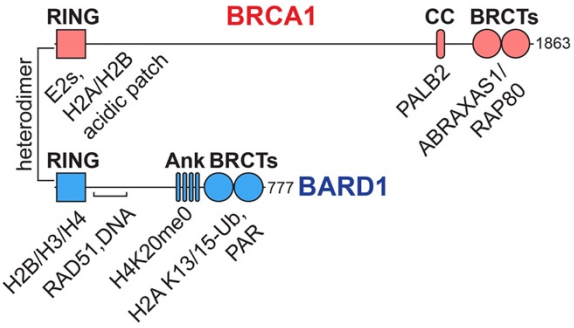

Figure 1. Domain structure of the BRCA1/BARD1 heterodimer. Folded domains are represented by shapes, with the intervening sequences composed of intrinsically disordered regions (RING, really interesting new gene; BRCT, BRCA1 C-terminal; Ank, ankyrin repeat domain; CC, coiled-coil). A subset of interacting proteins and nucleosome regions relevant to this review are labelled under the BRCA1/BARD1 domains to which they bind.

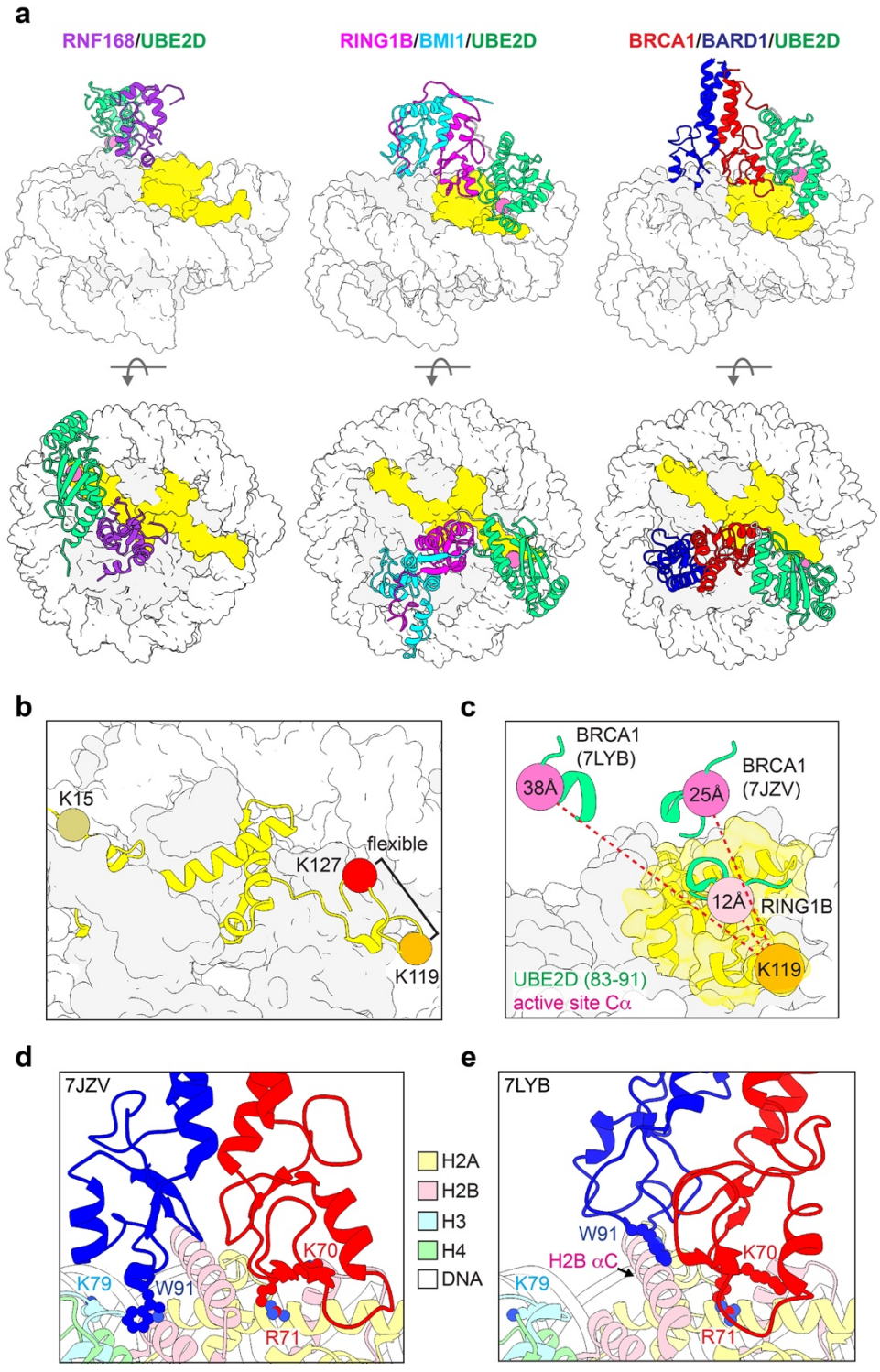

Figure 2. Structural basis for site-specific ubiquitylation of nucleosomal H2A. (a) Structural models of RING/E2/nucleosome complexes (PDB-Dev: 00000028, PDB: 4R8P, 7JZV). The active site Ca of the E2 (UBE2D, green) in each model is shown as a pink sphere and H2A is yellow. **(b)** Locations of representative target lysine residues for H2A-modifying Ub ligases on a nucleosome (PDB: 1KX5). The C-terminal tail of H2A beyond K119 is unstructured

and not observed in x-ray or cryo-EM structures but is modelled in PDB 1KX5. **(c)** Positions of the E2 active site (Cα, pink spheres) from the indicated RING/E2/nucleosome structural models (PDB: 4R8P, 7JZV, 7LYB) relative to H2A K119 in the RING1B/BMI1/nucleosome complex (PDB: 4R8P, orange sphere). The Cα-Cα distances from H2A K119 to the respective E2 active sites in the E3/E2/nucleosome complexes (dashed red lines) are reported inside the active site spheres. For the measurements, models were aligned by H2B in the nucleosome. **(d, e)** BRCA1/BARD1 RING-histone interactions from two published structural models (PDB: 7JZV and 7LYB). The models are aligned by H2B on the E3/E2-bound face of the the nucleosome (see H2B αC helix) and shown side-by-side instead of overlaid for clarity. The largest difference between the two structures is in the positioning of the BARD1 RING domain. Critical histone-binding BRCA1/BARD1 sidechains and the H3 K79 sidechain in the H3 α1-L1 elbow are shown as sticks. Histone colors are indicated in the legend, and BRCA1 is red and BARD1 is blue.

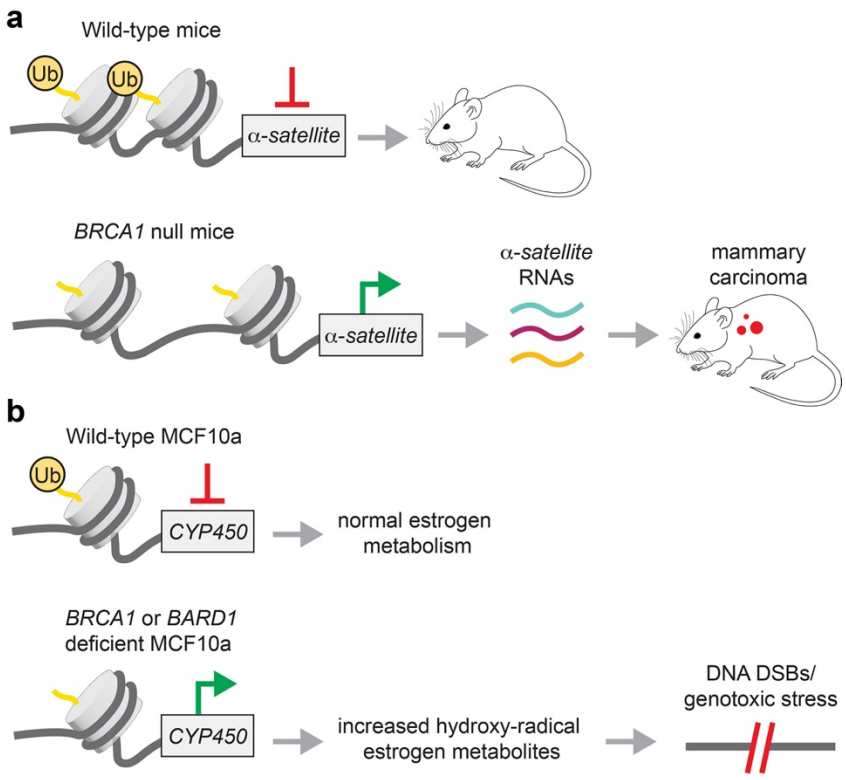

Figure 3. BRCA1/BARD1-dependent H2A-Ub in transcriptional regulation. (a) Proposed model for heterochromatin-mediated silencing of a-satellite DNA regions by BRCA1/BARD1-dependent H2A-Ub. **(b)** Proposed model for regulation of estrogen metabolism through modulation of *CYP450* expression levels in breast epithelial cells (MCF10a) by BRCA1/BARD1-dependent H2A-Ub.

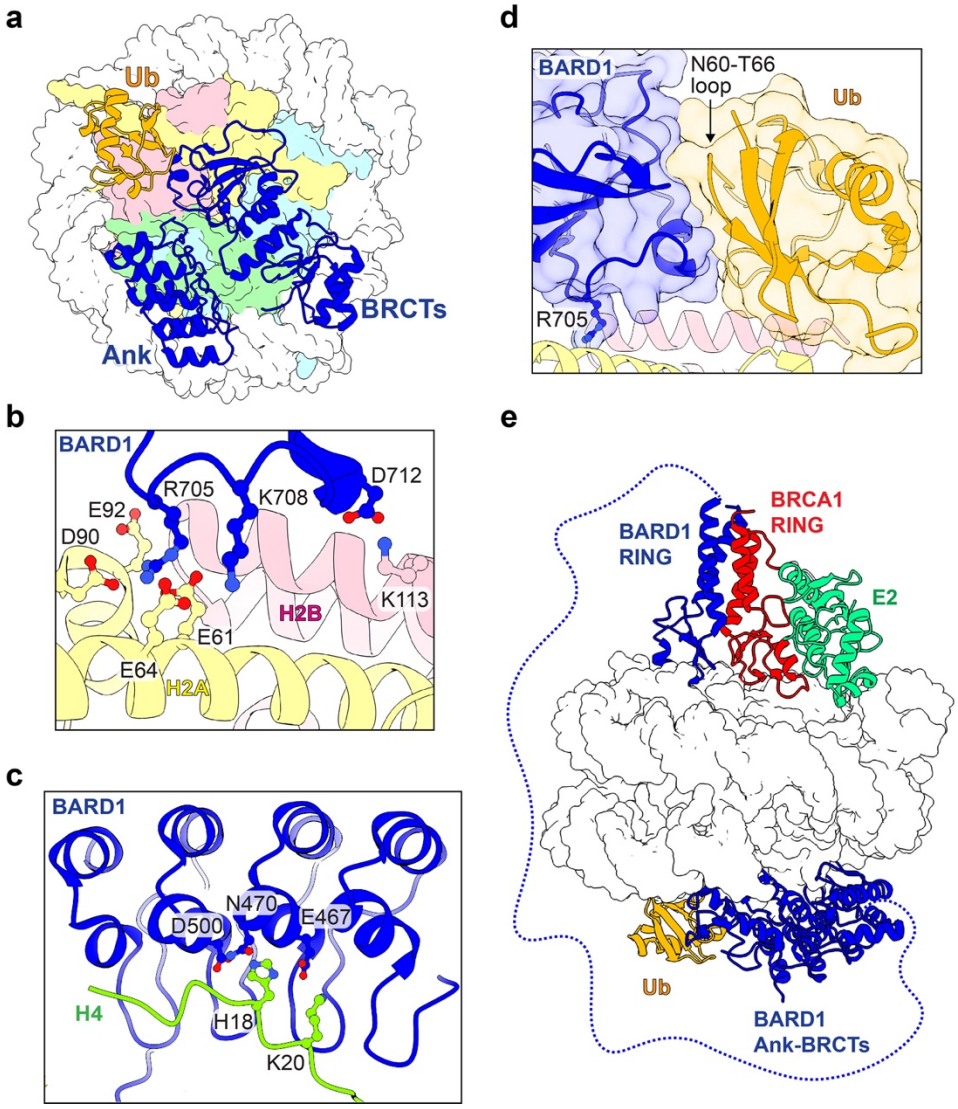

Figure 4. Recognition of damaged chromatin by BARD1. (a) Top-down view of the BARD1 Ank-BRCT domains (blue) bound to a nucleosome containing H2A K15-Ub and H4K20me0 (PDB: 7E8I). **(b)** Interactions between the BARD1 BRCT domain and the H2A/H2B acidic patch. **(c)** Interactions between the BARD1 Ank domain and the H4 N-terminal tail. Residue sidechains mutated in the "BARD1-3A" mutant are shown as blue sticks. **(d)** Interaction between the BARD1 BRCT Ub-directed recognition motif and H2A K15-Ub. The BARD1 "Arg anchor" sidechain interacting with the H2A/H2B acidic patch is shown in sticks. **(E)** Proposed model of binding for the RING heterodimer BRCA1/BARD1/E2 complex and the BARD1 Ank-BRCTs to both sides of the same nucleosome (overlay of PDB models 7JZV and 7E8I).

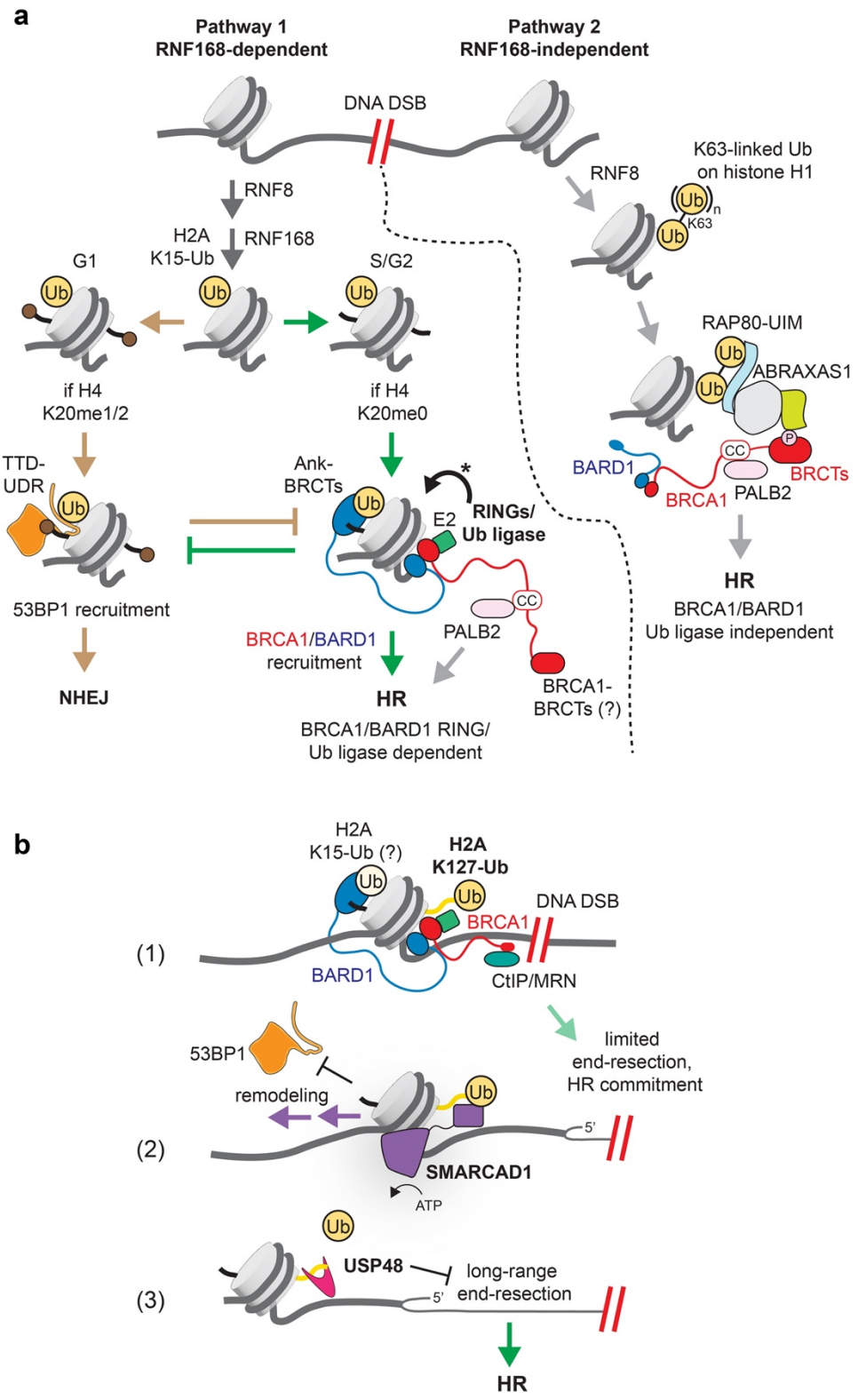
a
Pathway 1
RNF168-dependent
Pathway 2
RNF168-independent
DNA DSB
RNF8
H2A
K15-Ub
RNF168
G1
S/G2
Ub
if H4
K20me1/2
if H4
K20me0
TTD-
UDR
53BP1 recruitment
NHEJ
Ank-
BRCTs
E2
RINGs/
Ub ligase
BRCA1/BARD1
recruitment
PALB2
CC
BRCA1-
BRCTs (?)
HR
BRCA1/BARD1 RING/
Ub ligase dependent
K63-linked Ub
on histone H1
K63
RAP80-UIM
ABRAXAS1
BARD1
BRCA1
PALB2
BRCTs
P
HR
BRCA1/BARD1
Ub ligase independent
b
H2A
K15-Ub (?)
H2A
K127-Ub
DNA DSB
BRCA1
BARD1
CtIP/MRN
(1)
53BP1
remodeling
limited
end-resection,
HR commitment
(2)
SMARCAD1
ATP
5'
USP48
long-range
end-resection
(3)
HR

Figure 5. Nucleosome-based recruitment and activity of BRCA1/BARD1 in DNA DSB repair. (a) Schematic of BRCA1/BARD1 and 53BP1 recruitment pathways and retention at damaged chromatin. The left two pathways are reliant on RNF168-mediated H2A K15-Ub, while the right pathway (separated by dashed line) is reliant on RNF8-mediated K63-linked poly-Ub deposited on linker histone H1. The center pathway reliant on H2A K15-Ub and H4K20me0 requires the BRCA1 RING domain and ligase proficiency for DSB site retention and HR, indicated by the curved arrow with an asterisk. **(b)** Schematic of BRCA1/BARD1-dependent H2A-Ub activity in the DNA end-resection step of HR. BRCA1/BARD1 is recruited to DSB sites and ubiquitylates H2A K127 (1, top). HR is licensed through limited end-resection of broken DNA ends via association of BRCA1/BARD1 with CtIP and MRN (1 and 2, top and middle, light green arrow). SMARCAD1 is recruited via BRCA1/BARD1-dependent H2A K127-Ub, excludes the NHEJ factor 53BP1 from break sites, and performs ATP-dependent nucleosome repositioning to facilitate long-range DNA end-resection (2, middle). This is antagonized by the action of the deubiquitylating enzyme USP48, which specifically removes H2A K127-Ub to prevent over-resected DNA tracts and facilitate HR (3, bottom). Question marks in panels denote unknown interactions (a) or speculative complexes (b).

CHAPTER 3

BRCA1/BARD1 site-specific ubiquitylation of nucleosomal H2A is directed by BARD1

Samuel R. Witus[1], Anika L. Burrell[1], Daniel P. Farrell[1,2], Jianming Kang[1,3], Meiling Wang[4], Jesse M. Hansen[1], Alex Pravat[1], Lisa M. Tuttle[1], Mikaela D. Stewart[1,†], Peter S. Brzovic[1], Champak Chatterjee[3], Weixing Zhao[4], Frank DiMaio[1,2], Justin M. Kollman[1], and Rachel E. Klevit[1*]

1. Department of Biochemistry, University of Washington, Seattle, WA, USA.
2. Institute for Protein Design, University of Washington, Seattle, WA, USA.
3. Department of Chemistry, University of Washington, Seattle, WA, USA.
4. Department of Biochemistry and Structural Biology, University of Texas Health San Antonio, San Antonio, TX, USA.

† Current address: Department of Biology, Texas Christian University, Fort Worth, TX, USA.

*Corresponding author email: klevit@uw.edu

Reprinted with permission from: Witus, S.R., Burrell, A.L., Farrell, D.P. *et al.* BRCA1/BARD1 site-specific ubiquitylation of nucleosomal H2A is directed by BARD1. *Nat Struct Mol Biol* **28,** 268–277 (2021). https://doi-org.offcampus.lib.washington.edu/10.1038/s41594-020-00556-4

Author Contributions

S.R.W., M.D.S., P.S.B., and R.E.K. conceived the project, designed the experiments, and analyzed data. S.R.W. prepared the cryo-EM sample, imaged, and analyzed data with A.L.B., and J.M.H under the supervision of J.M.K. D.P.F. built the atomic model under supervision of F.D. with input from S.R.W. J.K. generated methylated nucleosomes under supervision of C.C. S.R.W. and L.M.T. conducted and analyzed NMR experiments. M.W. and W.Z. produced full-length BRCA1/BARD1 and performed binding assays. S.R.W. and A.P. purified proteins, performed assays, and analyzed data. S.R.W. wrote the initial draft of the manuscript. S.R.W., P.S.B., and R.E.K. wrote the final manuscript with input from all co-authors.

Abstract

Mutations in BRCA1/BARD1's E3 ubiquitin ligase RING domains predispose carriers to breast and ovarian cancers. We present the first structure of the BRCA1/BARD1 RING heterodimer

with the E2 enzyme UbcH5c bound to its cellular target, the nucleosome, along with biochemical data that explain how the complex selectively ubiquitylates lysines 125/127/129 in the flexible C-terminal tail of H2A in a fully human system. The structure reveals that a novel BARD1-histone interface couples to a repositioning of UbcH5c compared to the structurally similar PRC1 E3 ligase Ring1b/Bmi1 that ubiquitylates H2A Lys119 in nucleosomes. This interface is sensitive to both H3 Lys79 methylation status and mutations found in cancer patients. Furthermore, NMR reveals an unexpected mode of E3-mediated substrate regulation through modulation of dynamics in the C-terminal tail of H2A. Our findings provide insight into how E3 ligases preferentially target nearby lysine residues in nucleosomes by a steric occlusion and distancing mechanism.

Introduction

Germline mutations in *BRCA1* and *BARD1* predispose carriers to breast and ovarian cancer. BRCA1/BARD1 is a large heterodimeric complex best characterized for its role in DNA double-stranded break (DSB) repair by homologous recombination[1,2]. Its only known enzymatic activity is as an E3 ubiquitin (Ub) ligase, encoded by the heterodimeric N-terminal RING domains of BRCA1 and BARD1[3,4]. A variety of putative cellular targets for BRCA1/BARD1-dependent E3 ligase activity have been identified, but the functional significance for most is not well understood. Furthermore, a role for the E3 ligase activity of BRCA1/BARD1 in DNA damage repair and tumorigenesis remains controversial[5–12].

Nucleosomal histone H2A was recently discovered as a *bona fide* substrate for BRCA1/BARD1-dependent E3 ligase activity[13–15]. The heterodimeric RING domains are sufficient for preferential mono-ubiquitylation of lysine residues 125/127/129 on the flexible extreme C-terminal tail of canonical H2A[14] and Lys123 in nucleosomes containing the macroH2A1 isoform[16]. The non-E2 binding RING domain of BARD1 is required for this activity, and cancer-predisposing mutations

in this domain specifically abrogate nucleosome binding and ubiquitylation[17]. BRCA1/BARD1-dependent H2A ubiquitylation contributes to DNA DSB repair by homologous recombination[11,18] and acts as a mark of transcriptional repression[15,17].

Two other RING E3-ligases, RNF168 and the Ring1b/Bmi1 complex, bind to the nucleosome via their RING domains and facilitate mono-ubiquitylation of distinct H2A lysine residues. RNF168 ubiquitylates H2A residues Lys13/15 in the N-terminal region of H2A[19,20], a signal that recruits the DSB repair factor 53BP1 to sites of damage to facilitate repair by non-homologous end joining[21,22]. The heterodimeric E3 ligase Ring1b/Bmi1, a component of the Polycomb repressive complex 1 (PRC1), directs ubiquitylation of H2A Lys119 in nucleosomes[23,24]. This modification functions in transcriptional regulation[25] and may also contribute to the regulation of DNA DSB repair[26]. A crystal structure of the Ring1b/Bmi1[27] and an NMR-based model of the RNF168[28] E3-E2/nucleosome complexes reveal how these E3s direct site-specific H2A ubiquitylation. Surface-exposed polar residues in the RING domains orient the E3s on the face of the nucleosome, recognizing distinct regions of the H2A/H2B acidic patch. This directs the RING-bound E2 enzymes towards opposite ends of the nucleosome disc surface, placing the E2 active site directly over the H2A lysine residues targeted for modification. For RNF168 and Ring1b/Bmi1, the target lysines are located on the boundary of ordered regions of H2A ~70 Å away from each other across the nucleosome disc surface **(Fig. 1a, b)**.

The H2A lysines targeted by BRCA1/BARD1 (125/127/129) are nearby to those targeted by Ring1b/Bmi1 (118/119) but reside in the fully disordered extreme C-terminal tail of H2A. The Ring1b/Bmi1 and BRCA1/BARD1 RING heterodimers are topologically similar and share several functional features. BRCA1, like Ring1b, directly interacts with E2~Ub conjugates and has a conserved nucleosome-binding ‘arginine-anchor’ motif required to bind the nucleosome acidic patch[27] **(Fig. 1c)**. BARD1, like Bmi1, does not interact with the ubiquitylation machinery.

These two RINGs differ primarily at the base of their RING domains where Bmi1 has an extended loop that contacts the nucleosome surface. Structural comparison calls to question how these complexes differ in binding to nucleosomes **(Fig. 1d)** and specifically target closely positioned H2A lysine residues **(Fig. 1e).** Here, we report a cryo-electron microscopy (cryo-EM) structure of the BRCA1/BARD1 RING domain heterodimer with the E2 enzyme UbcH5c bound to the nucleosome. Together with biochemical and nuclear magnetic resonance (NMR) spectroscopy data, the results reveal the basis for preferential ubiquitylation of H2A Lys 125/127/129. Our findings constitute the first structural analysis of the E3 ligase domain of BRCA1/BARD1 with any of its cellular targets and provide mechanistic insight into the process of site-specific ubiquitylation by RING-type E3 ligases.

Results

Reconstitution and cryo-EM structure of the BRCA1-UbcH5c/BARD1/nucleosome complex.

To reconstitute the BRCA1-UbcH5c/BARD1/nucleosome complex, we generated a chimeric E3-E2 enzyme where the RING domain of BRCA1 was genetically fused to UbcH5c by a flexible linker (referred to as E3-E2 module; **Extended Data Fig. 1b**). We took this approach to circumvent the low affinity of UbcH5c for BRCA1/BARD1[29] that could hinder formation of a stable ternary complex with the nucleosome. The E2 enzyme UbcH5c was chosen because it has similar activity in nucleosome ubiquitylation assays with BRCA1/BARD1 to other members of the UbcH5 (Ube2d) and Ube2e families and was used to characterize the Ring1b/Bmi1[27] and RNF168[28] nucleosome complexes **(Extended Data Fig. 1c)**. Importantly, the E3-E2 module retained enzymatic activity and specificity for lysine residues 125/127/129, validating its use for structural studies **(Extended Data Fig. 1d, e)**. Consistent with a previous report[27], Ub could not be added to the active site of UbcH5c^{Cys85Lys} in the context of the E3-E2 module to form a stable isopeptide-linked E3-E2-Ub moiety **(Extended Data Fig. 2a)**. Serendipitously, we found that

substitution of the E2 active site cysteine to lysine stabilized the E3-E2/nucleosome interaction, allowing for purification of the complex by size exclusion chromatography (SEC; **Extended Data Fig. 2b, c**). This mutation appears to increase the association of the complex through non-specific, weak electrostatic interactions as a modest increase in ionic strength is sufficient to disrupt binding **(Extended Data Fig. 2d, e)**. The complex was observed to have an approximate molecular weight consistent with an expected 2:1 binding stoichiometry by SEC coupled to multi-angle light scattering **(Extended Data Fig. 2f)**. Owing to the stronger observed interaction of this complex, it was used for subsequent cryo-EM and NMR studies.

Although the complex co-purified on SEC, the E3-E2 module dissociated from the nucleosome upon cryo-EM grid preparation and was therefore stabilized by light crosslinking with glutaraldehyde immediately prior to vitrification. We obtained a cryo-EM reconstruction of the bound complex that refined to a global resolution of ~3.9 Å (3.4-7.8 Å) **(Fig. 2a, Extended Data Figs. 3 and 4, Table I)**. The structure shows the E3-E2 module associated with one face of the nucleosome, consistent with recent cryo-EM structures of similar complexes expected to bind with 2:1 stoichiometry[30,31]. The polypeptide backbone is traceable in the density map for ordered regions of the nucleosome and the BRCA1/BARD1 RING domains. Density for the E2 enzyme UbcH5c is noisier with missing regions in the C-terminal end furthest from the E3-E2 interface **(Fig. 2a and Extended Data Fig. 4)**. Importantly, map quality was sufficient for unambiguous docking with full or partial side chain density for many key interface residues. Model building was accomplished by a combination of homology modelling, *de novo* structure prediction, rigid-body docking, and all-atom refinement in Rosetta[32,33] **(Fig. 2b and Table I)**. The resulting structure shows that the BRCA1/BARD1 RING domains straddle the H2B αC helix, binding to both the H2A/H2B acidic patch and H2B/H4 cleft **(Fig. 2b)**. UbcH5c is bound to the BRCA1 RING in a canonical manner and is tilted away from the histone surface, terminating near the DNA ends without making specific interactions with the nucleosome.

BRCA1/BARD1 RING-histone interactions.

The BRCA1 RING domain shares a common nucleosome binding motif with Ring1b that is required for nucleosome ubiquitylation in *in vitro* activity assays[27]. Central to this motif is the BRCA1 Arg71 side chain that is observed to insert into a pocket in the nucleosome acidic patch composed of side chains from H2A residues Glu61, Asp90, and Glu92 **(Fig. 3a)**. Our model predicts that the conserved neighboring Lys70 of BRCA1 interacts with the side chain of H2A Glu64 that is also observed in the Ring1b-histone interface. BRCA1 Arg71Ala was the only mutant tested that abrogated detectable nucleosome ubiquitylation and the Lys70Ala mutant was also severely affected **(Fig. 3c)**. Binding to the nucleosome was also not detected for the BRCA1 Arg71Ala mutant using isothermal titration calorimetry (ITC**; Fig. 3e, Extended Data Fig. 5h)**. These data identify Arg71 as the 'arginine-anchor' common to many chromatin factors[34]. Mutation of BRCA1 RING domain residues surrounding Lys70 and Arg71 had diminishing effects on decreasing nucleosome ubiquitylation **(Extended Data Fig. 5a, d, e)**.

To further validate the BRCA1/BARD1-histone interface, we tested the activity of BRCA1/BARD1 and Ring1b/Bmi1 with nucleosomes mutated at the H2A/H2B acidic patch. Consistent with previous reports[27,28], the same canonical acidic patch surface is required for BRCA1/BARD1- and Ring1b/Bmi1-dependent nucleosome ubiquitylation **(Extended Data Fig. 6a, b)**. Residues at the N-terminal end of the H2B αC helix that line the nucleosome acidic patch are poised to make analogous interactions with residues on BRCA1/BARD1 and Ring1b/Bmi1 **(Extended Data Fig. 6c)**. H2A ubiquitylation by BRCA1/BARD1 decreased similarly for H2B Glu105Ala and Lys108Ala nucleosome mutants. In contrast, nucleosome ubiquitylation by Ring1b/Bmi1 was nearly abrogated with an H2B Glu105Ala substrate but was less affected by the Lys108Ala and His109Ala mutants **(Extended Data Fig. 6d, e)**. These

results show that BRCA1/BARD1 and Ring1b/Bmi1 have similar yet distinct interactions on the nucleosomal surface that facilitate specific H2A ubiquitylation.

Although the BRCA1 and Ring1b RINGs are structurally similar and use a common nucleosome binding motif, the non-E2 binding RING domains of BARD1 and Bmi1 are more divergent **(Fig. 1c)**. In the Ring1b-UbcH5c/Bmi1/nucleosome complex, Bmi1 binds to the C-terminal end of the H3 α1 helix using an extended loop that is largely conserved among the six human PCGF proteins that form functional heterodimers with Ring1b[35]. Our structure reveals that, lacking this extended loop, BARD1 binds to the nucleosome H2B/H4 cleft using a novel interface in which the Trp91 sidechain inserts into a pocket lined by residues H3 Phe78/Lys79, H4 Val70/Thr71/Glu74, and H2B Arg99 **(Fig. 3b)**. This interaction is facilitated by a conformational change that extends the loop containing Trp91 towards the histone surface **(Extended Data Fig. 7a)**. Mutation of BARD1 Trp91 to Ala sharply reduced nucleosome ubiquitylation and binding **(Fig. 3d, e and Extended Data Fig. 5h)**. Importantly, Trp91 is not required for the structural integrity of the BARD1 RING, as the $^{1}H^{15}N$-TROSY-HSQC NMR spectrum of BARD1 Trp91Ala RING heterodimer resembles that of wild-type BRCA1/BARD1 **(Extended Data Fig. 5i)**. Nucleosomes with mutations in the BARD1 Trp91 binding-pocket were significantly impaired toward BRCA1/BARD1 ubiquitylation **(Fig. 3f)** but had no or lesser effects with Ring1b/Bmi1 **(Extended Data Fig. 6f, g)**. Our structure shows that H3 Lys79 lines the BARD1 Trp91 binding pocket and is positioned near the C-terminal cap of BARD1 helix 2 (Gly80/Thr81) **(Fig. 3b and Extended Data Fig. 6h)**. Consistent with this, BARD1 Gly80Ala or H3 Lys79Ala mutants decreased nucleosome ubiquitylation activity **(Fig. 3d and Extended Data Fig. 6i, j)**. Mutation of surrounding residues in the BARD1 RING did not confer these effects **(Extended Data Fig. 5b, f, g)**. Unexpectedly, mutation of H3 Lys79Ala enhanced Ring1b/Bmi1-dependent nucleosome ubiquitylation, indicating unique requirements for this residue between the two E3s **(Extended Data Fig. 6i, j)**.

As H3 Lys79 methylation is generally associated with actively transcribed chromatin[36,37], we tested the activity of BRCA1/BARD1, Ring1b/Bmi1, and RNF168 for H3 Lys79me1 and Lys79me2 methyl-lysine analog nucleosomes. Ubiquitylation activity for these methylated substrates was significantly reduced for both BRCA1/BARD1 and Ring1b/Bmi1 compared to unmethylated nucleosomes, but unaffected for RNF168 that does not bind near H3 Lys79 **(Fig. 3g and Extended Data Fig. 6k-p)**. This potential mode of histone-modification crosstalk suggests that BRCA1/BARD1-dependent nucleosome ubiquitylation may occur more frequently at non-transcribed genes. Histone H3 Lys79 methylation has also been implicated in recruiting 53BP1 for DNA DSB repair by non-homologous end joining[38,39]. As BRCA1/BARD1 occupancy at DSBs antagonizes 53BP1, we speculate that H3 Lys79 methylation status may further delineate chromatin substrates for these opposing DNA repair factors.

Next, we tested the nucleosome ubiquitylation activity of a series of BARD1 RING mutants found in the expert-curated Catalogue of Somatic Mutations in Cancer (COSMIC) database[40]. Missense mutations at BARD1 Pro89 have been reported in five patient samples. BARD1 Pro89 is in close proximity to the Trp91 interface and forms an adjacent interface with residues on the H2B α3 and αC helices **(Extended Data Fig. 5c)**. The BARD1 Pro89Ala mutant significantly decreased nucleosome ubiquitylation activity **(Fig. 3h)**. A patient-derived mutant of the zinc coordinating histidine residue His68Tyr also decreased nucleosome ubiquitylation. Other reported mutants from patients did not confer deleterious effects *in vitro* **(Extended Data Fig. 5c, j, k)**. All BRCA1 and BARD1 mutants found to be highly defective in nucleosome ubiquitylation assays still retained intrinsic E3 ligase activity in E2~Ub lysine discharge assays, indicating that these residues play a critical role in the assembly of a productive RING/nucleosome complex **(Extended Data Fig. 5l-o)**. Together, these data reveal the critical contributions of the non-E2 binding BARD1 RING domain in directing specific nucleosome

ubiquitylation that is modulated by the methylation status of H3 Lys79 *in vitro*, and also uncovers potential disease mechanisms for BARD1 RING mutations found in cancer patients.

BRCA1/BARD1 RING orientation keeps the UbcH5c active site away from H2A Lys119. The Ring1b/Bmi1 and RNF168 RING complexes direct specific nucleosome ubiquitylation by binding to distinct histone surfaces and orienting the UbcH5c active site directly over H2A lysine residues 118/119 and 13/15, respectively. These lysine targets are on the boundary of ordered regions of H2A in the nucleosome. Because the H2A lysine residues (125/127/129) that are modified by BRCA1/BARD1 are in a fully disordered region of the C-terminal tail that is not visible by x-ray crystallography or cryo-EM, the mechanism of site-specific ubiquitylation by this E3-E2 pair is not revealed directly.

In our structure, BRCA1-bound UbcH5c is removed from the histone surface compared to its location in the Ring1b-UbcH5c/Bmi1/nucleosome complex **(Fig. 4a)**. Although the BRCA1 and Ring1b RINGs bind similarly, the BARD1 subunit is constrained closer to the nucleosome surface and shifted ~10 Å on an axis parallel to the H4 α2 helix compared to Bmi1 **(Fig. 4b).** This arrangement effectively tilts the BRCA1 E2 interaction site, reorienting UbcH5c away from the nucleosome surface **(Fig. 4c, d and Extended Data Fig. 7b, c)**. The result is that Cα-Cα distance between the E2 active site of BRCA1-bound UbcH5c and H2A Lys118 (last ordered residue in H2A C-terminus) is increased to ~19 Å from ~9Å for Ring1b-bound UbcH5c **(Fig. 4a)**. Although elevated from the nucleosome surface, BRCA1-bound UbcH5c extends towards the DNA ends where the flexible region of the C-terminal tail of H2A emanates from the ordered histone surface. We propose that this increased distance from H2A Lys118 accounts for the observation that BRCA1/BARD1 is unable to efficiently ubiquitylate H2A Lys118/119 in the absence of its preferred lysine targets.

Unlike Ring1b-bound UbcH5c, our structure does not predict extensive interactions between BRCA1-bound UbcH5c and nucleosomal DNA **(Extended Data Fig. 7d)**. Consistent with this, the presence of the E2 does not substantially alter the binding affinity of the BRCA1/BARD1 RING-nucleosome interaction measured by ITC (42 ± 12 μM versus 27 ± 5 μM in the absence and presence of UbcH5c, respectively; **Extended Data Fig. 7e, f**). In contrast, incorporation of UbcH5c in the Ring1b/Bmi1 nucleosome complex increased the affinity ten-fold from ~2.1 μM for the RING complex alone to ~0.23 μM for the E3-E2 module[27]. Although the BRCA1/BARD1 and Ring1b/Bmi1 affinity measurements were conducted using different methods, the roughly twenty-fold difference in affinity between RING/nucleosome complexes is supported by EMSA binding data **(Fig. 1d)**. To further test the observed difference in E2 placement, we made a series of mutations in surface exposed basic residues on UbcH5c that were shown to be important for nucleosome binding and ubiquitylation by Ring1b/Bmi1 and retain intrinsic amino-lysis activity[27]. These UbcH5c mutations impact Ring1b/Bmi1-dependent nucleosome ubiquitylation but have no or minimal effects on BRCA1/BARD1-dependent activity **(Extended Data Fig. 7g, h)**. Maintenance of near wild-type like activity in BRCA1/BARD1-containing nucleosome ubiquitylation assays supports our model in which UbcH5c is tilted away from the nucleosome surface. This changes the position of the BRCA1-bound UbcH5c active site compared to Ring1b-bound UbcH5c active site, preventing modification of H2A Lys119, while allowing ubiquitylation of lysine residues 125/127/129 in the unstructured H2A C-terminal tail.

Lysine location in the flexible C-terminal tail of H2A dictates ubiquitylation efficiency. The H2A lysine targets of BRCA1/BARD1 are in a flexible region of the C-terminal tail that is not observed by density in our structure. This region is less conserved between isoforms than ordered regions of the histone[41] **(Fig. 5a)**. We hypothesized that H2A residues Lys125/127/129 are optimally located on the flexible C-terminal tail of H2A to sample the UbcH5c active site at

high frequency. To test this, we measured the ubiquitylation efficiency of BRCA1/BARD1 for nucleosome substrates with single lysine residues placed throughout the C-terminal tail of H2A and a substrate extended by ten residues via a flexible linker. A sharp increase in nucleosome ubiquitylation efficiency was observed between lysines placed at positions 121 and 123 on the H2A tail **(Fig. 5b, c)**. Ubiquitylation efficiency peaked with a single lysine at positions 125 and 127, then decreased for each subsequent position. The lysine residue at the end of a ten-residue extension (+10-K) was ubiquitylated with similar efficiency as a lysine at position 121. These data are in agreement with the ~19 Å linear distance measured between Cα atoms of H2A Lys118 and the active site residue of UbcH5c **(Fig. 5c, d)**. Together, these results indicate that a lysine residue must have an optimal reach from the ordered histone surface to sample the UbcH5c active site to be efficiently ubiquitylated. Although the native lysine at position 125 is ubiquitylated with highest efficiency *in vitro*, only lysine residues 127 and 129 were observed to be ubiquitylated in a previously reported cellular assay[14]. This discrepancy may reflect a lack of detection by mass-spectrometry or additional modes of substrate regulation that are not preserved in our unmodified recombinant nucleosome substrates.

The C-terminal tail of H2A is uniquely flexible in complex with BRCA1-UbcH5c/BARD1. The altered position of UbcH5c in the BRCA1/BARD1 and Ring1b/Bmi1 nucleosome complexes suggests that the E2 may differentially impact interactions with the flexible C-terminal tail of H2A. Although the inherent flexibility of the H2A tails prevents observation in x-ray and cryo-EM structures, this property allows for detection by conventional NMR experiments that report on the chemical environment of backbone amide groups. We obtained backbone resonance assignments for human H2A residues 1-10, 120-121, and 125-129 in nucleosomes reconstituted with $^{2}H^{15}N^{13}C$-labeled H2A **(Extended Data Fig. 8a, b)**. $^{1}H^{15}N$-TROSY-HSQC spectra were collected for BRCA1-UbcH5c^{Cys85Lys}/BARD1 binding to $^{2}H^{15}N$-H2A-labeled nucleosomes **(Fig. 6a, left panel)**. Significant changes in chemical shifts were not observed.

Instead, predominant spectral changes correspond to specific resonance broadening relative to unbound nucleosomes (I_{com}/I_{ref}), primarily for H2A residues 120-122 and 125 **(Fig. 6b)**. Resonances corresponding to residues 126-129 were relatively unaffected, with signal broadening similar to that measured for residues 1-10 in N-terminal tail of H2A (trendline on graph represents the mean I_{com}/I_{ref} for residues -1-10). Further titration of BRCA1-UbcH5c^{Cys85Lys}/BARD1 caused uniform broadening of all observable NMR resonances indicative of non-specific binding and formation of very high molecular weight complexes **(Extended Data Fig. 8c, d)**. Spectra collected in the presence of BRCA1-UbcH5c/BARD1 with the wild-type E2 active site revealed similar trends with lesser resonance broadening consistent with sub-stoichiometric binding or a shorter complex lifetime **(Extended Data Fig. 8e, f)**.

Analogous spectra were collected for Ring1b-UbcH5c/Bmi1 binding to nucleosomes **(Fig. 6a, right panel)**. Though the concentration is lower (30 μM Ring1b-UbcH5c/Bmi1 vs. 60 μM BRCA1-UbcH5c^{Cys85Lys}/BARD1) substantially greater resonance broadening was observed affecting more residues, particularly residues 120-127 **(Fig. 6c)**. In addition, changes in chemical shifts are readily apparent for residues 121, 125, and 126, suggesting that Ring1b-UbcH5c/Bmi1 binding alters the environment of these residues to a greater extent in the nucleosome complex. Some of these effects may be attributed to tighter binding of the Ring1b-UbcH5c/Bmi1 complex. However, complementary experiments with nucleosomes reconstituted with $^{2}H^{15}N$-labeled H3 showed robust and similar loss in intensity for both complexes due to global resonance broadening at these concentrations **(Extended Data Fig. 8g, h)**. As the two E3-E2 complexes have approximately the same molecular weight, general signal broadening due to increases in complex molecular size was expected to be similar. These data are consistent with current models where UbcH5c in the Ring1b/Bmi1/nucleosome complex, located closer to the nucleosome surface and the emerging H2A tail, would have a greater impact on tail flexibility. Formation of the BRCA1-UbcH5c/BARD1/nucleosome complex does somewhat

restrict the flexibility of the H2A C-terminal tail closest to Lys119 on the ordered histone surface, while the extreme C-terminal region where lysine targets 127/129 are located retains native-like flexibility.

Full-length BRCA1/BARD1 has increased activity and affinity for nucleosomes

Although the RING domains of BRCA1/BARD1 are sufficient for binding and specific nucleosome ubiquitylation, the modest affinity of the BRCA1/BARD1 RING heterodimer for unmodified nucleosome substrates suggests that additional interactions may play a role. It has recently been suggested that the C-terminal region of BARD1 contributes to chromatin binding to facilitate DNA DSB repair[43,44]. Furthermore, both BRCA1 and BARD1 harbor DNA binding regions and interact with a variety of other chromatin-related factors[45,46] **(Fig. 7a)**. Using highly purified full-length human BRCA1/BARD1 that shows specificity for H2A Lys125/127/129 in an unmodified nucleosome substrate, we observe faster H2A ubiquitylation kinetics and a greater than 100-fold increase in nucleosome binding affinity compared to the RING heterodimer **(Fig. 7b, c and Extended Data Fig. 9)**. This observation confirms that regions outside the RING domains of BRCA1/BARD1 contribute to interactions with nucleosomes in the context of H2A ubiquitylation. These auxiliary interactions are likely to provide additional layers of regulation and recruitment *in vivo*. Furthermore, it suggests that cancer-predisposing mutations outside of the RING domains may indirectly affect nucleosome-specific E3 ligase functions of BRCA1/BARD1.

Discussion

We used cryo-EM, NMR, and biochemical methods to reveal the mechanism of site-specific nucleosomal H2A ubiquitylation by BRCA1/BARD1. Our structure shows that while the BRCA1 RING binds to the nucleosome acidic patch using an arginine anchor motif nearly identical to Ring1b and other nucleosome binding factors, BARD1 forms a distinct and novel interface with

the H2B/H4 cleft that constrains the BARD1 RING closer to the histone surface than Bmi1 and causes an upward tilt of the BRCA1 E2 binding interface. The E3-E2 complex acts like a teeter-totter, elevating UbcH5c from the histone surface and distancing its active site away from H2A Lys119. This positioning disfavors Ub transfer to Lys119 and promotes modification of lysines 125/127/129 in the disordered tail of H2A that have adequate reach distance from the histone surface to gain access to the UbcH5c active site in the complex. Another potential determinant of specificity suggested from NMR experiments is that the two heterodimeric E3-E2 complexes differentially restrict the conformation of the H2A C-terminal tail. The Ring1b-UbcH5c/Bmi1 complex, positioned closer to the nucleosome surface and the emerging H2A tail, limits the conformational space that can be explored by the C-terminal tail of H2A. This may inhibit H2A lysine residues 125/127/129 from approaching the Ring1b-bound UbcH5c active site and actively prevent off-target modification by Ring1b/Bmi1. Conversely, the retention of native-like flexibility in the BRCA1-UbcH5c/BARD1/nucleosome complex ensures that Lys 125/127/129 are able to approach the E2 active site for Ub transfer. Currently, there is little data regarding the mechanism of substrate lysine approach to E2s, and especially in the case of specific mono-ubiquitylation of disordered substrate lysines. To our knowledge, all reported cases involve substrate lysine residues that are in more ordered protein regions and are observed to be positioned or stabilized near the E2~Ub active site by specific interactions between the E3/substrate[47–49] or E2~Ub/substrate[50] complexes, and therefore are more similar to the mechanism of Ring1b/Bmi1 and RNF168 than BRCA1/BARD1.

In the structure, UbcH5c binds to the canonical E2 recognition surface of BRCA1. However, the quality of cryo-EM density map for UbcH5c is better adjacent to the BRCA1 subunit and diminishes toward the C-terminal end of the E2. This suggests that the E3/E2 interface is not rigidly fixed, consistent with the moderate affinity of the BRCA1-UbcH5c interaction[29]. Upon binding, RING E3s, especially those that function with UbcH5c, generally promote a closed

conformation of the E2~Ub conjugate to enhance Ub transfer to lysine side chains[51]. As noted for the Ring1b/Bmi1[27] and RNF168[28] E3-E2/nucleosome complexes, the BRCA1-UbcHc/BARD1/nucleosome complex is completely compatible with closed conformations of the E2~Ub conjugate (**Extended Data Fig. 10**). Indeed, tilting the UbcH5c active site away from the nucleosome surface in the BRCA1/BARD1/nucleosome complex would further remove steric restrictions that might impede formation of the closed E2~Ub conformation.

While site-specific BRCA1/BARD1-dependent nucleosome ubiquitylation has been directly observed *in vitro* for canonical H2A from multiple species and macroH2A, other specialized H2A isoforms including the DNA-damage specific H2Ax that co-localize with BRCA1/BARD1 at DNA DSB foci[52] have lysine residues that are predicted to be efficiently ubiquitylated by BRCA1/BARD1 based on our model. Ubiquitylation of these different H2A isoforms in chromatin may delineate its role in various nuclear processes. Although BRCA1/BARD1 can multi-monoubiquitylate the tail of H2A *in vitro*, a single Ub genetically fused to the C-terminus of H2A has been observed to complement defective BRCA1/BARD1 E3 ligase activity in DNA DSB repair[11] and transcriptional regulation[15,17]. Furthermore, the DUB USP48 was discovered to preferentially target the multi-ubiquitylated H2A-Ub product of BRCA1/BARD1 over Lys13/15-Ub or Lys119-Ub *in vitro* and to antagonize BRCA1 E3-ligase dependent activity at DSBs in cells[18]. Further investigation is needed to better understand the biologically relevant H2A-Ub product of BRCA1/BARD1 *in vivo* and its signaling mechanisms. We envision that downstream chromatin factors will be specifically recruited to chromatin ubiquitylated by BRCA1/BARD1 in a manner similar to the PRC1/2[53] and the RNF168/53BP1[21,22] systems.

While our data explain the basis for site-specific nucleosome ubiquitylation by the BRCA1/BARD1 RING heterodimer, we show that the full-length protein has enhanced binding and activity towards a nucleosome substrate. Other regions of BRCA1 and BARD1 are

implicated in binding to DNA[45,46], histone tails[43], and histone modifications[44]. BRCA1/BARD1 also exists as part of several discrete higher-order molecular assemblies[54], including with proteins known to specifically bind to nucleosomes such as PALB2[55]. Our findings suggest that patient mutations in regions critical for these interactions could be pathogenic by indirectly affecting the nucleosome-specific E3 ligase activity of BRCA1/BARD1. Further investigation is needed to understand the chromatin landscape that recruits BRCA1/BARD1 to bind to nucleosomes to ubiquitylate H2A, and which BRCA1/BARD1 complexes are involved in these processes. Finally, our observation that a prevalent BARD1 RING mutation found in cancer patients though not reported to be a causative agent of cancer specifically and potently disrupts H2A ubiquitylation supports the mounting evidence that BRCA1/BARD1-dependent nucleosome ubiquitylation is critical to its function as a tumor suppressor.

Acknowledgements

We thank S. Tan (Penn State University) for sharing Ring1b/Bmi1plasmids and L. Kay (University of Toronto) for sharing the 153 base-pair Widom 601 repeat plasmid. We thank N. Zheng for his insightful feedback on the manuscript and sharing laboratory equipment, T. Hinds for assistance with ITC experiments, P. Hsu for advice on nucleosome complexes, J. Quispe and Q. Beedle for technical assistance with cryo-EM data collection, and L. Walls, A. Borst, and D. Veesler for advice on single-particle cryo-EM data processing. S.R.W. acknowledges support from the NIH (T32GM008268). A.L.B. was supported by the NIH (T32GM008268 and 1F31EY030732), D.P.F. was supported through the Human Frontiers Science Program (RGP0061/2019). J.M.H. was supported by the NIH (T32GM007270). W.Z. was supported by a V Scholar Grant (V2019.Q13) from V Foundation and a Young Investigator Award from Max and Minnie Tomerlin Voelcker Fund. F.D. was supported by the NIH (GM123089). R.E.K. is the Edmond H. Fischer Endowed Chair in Biochemistry and is supported by the NIH (GM088055).

References (main text)

1. Tarsounas, M. & Sung, P. The antitumorigenic roles of BRCA1–BARD1 in DNA repair and replication. *Nat. Rev. Mol. Cell Biol.* **21**, 284–299 (2020).

2. Densham, R. M. & Morris, J. R. Moving Mountains—The BRCA1 Promotion of DNA Resection. *Front. Mol. Biosci.* **6**, 79 (2019).

3. Hashizume, R. *et al.* The RING heterodimer BRCA1-BARD1 is a ubiquitin ligase inactivated by a breast cancer-derived mutation. *J. Biol. Chem.* **276**, 14537–14540 (2001).

4. Brzovic, P. S., Rajagopal, P., Hoyt, D. W., King, M. C. & Klevit, R. E. Structure of a BRCA1-BARD1 heterodimeric RING-RING complex. *Nat. Struct. Biol.* **8**, 833–837 (2001).

5. Wu, W. *et al.* BRCA1 Ubiquitinates RPB8 in Response to DNA Damage. *Cancer Res.* **67**, 951 (2007).

6. Sato, K. *et al.* A DNA-damage selective role for BRCA1 E3 ligase in claspin ubiquitylation, CHK1 activation, and DNA repair. *Curr. Biol. CB* **22**, 1659–1666 (2012).

7. Vázquez-Arreguín, K. *et al.* BRCA1 through Its E3 Ligase Activity Regulates the Transcription Factor Oct1 and Carbohydrate Metabolism. *Mol. Cancer Res. MCR* **16**, 439–452 (2018).

8. Reid, L. J. *et al.* E3 ligase activity of BRCA1 is not essential for mammalian cell viability or homology-directed repair of double-strand DNA breaks. *Proc. Natl. Acad. Sci. U. S. A.* **105**, 20876–20881 (2008).

9. Shakya, R. *et al.* BRCA1 tumor suppression depends on BRCT phosphoprotein binding, but not its E3 ligase activity. *Science* **334**, 525–528 (2011).

10. Drost, R. *et al.* BRCA1 RING Function Is Essential for Tumor Suppression but Dispensable for Therapy Resistance. *Cancer Cell* **20**, 797–809 (2011).

11. Densham, R. M. *et al.* Human BRCA1-BARD1 ubiquitin ligase activity counteracts chromatin barriers to DNA resection. *Nat. Struct. Mol. Biol.* **23**, 647–655 (2016).

12. Densham, R. M. & Morris, J. R. The BRCA1 Ubiquitin ligase function sets a new trend for remodelling in DNA repair. *Nucleus.* **8**, 116-125 (2017).

13. Thakar, A., Parvin, J. D. & Zlatanova, J. BRCA1/BARD1 E3 Ubiquitin Ligase Can Modify Histones H2A and H2B in the Nucleosome Particle. *J. Biomol. Struct. Dyn.* **27**, 399–405 (2010).

14. Kalb, R., Mallery, D. L., Larkin, C., Huang, J. T. J. & Hiom, K. BRCA1 is a histone-H2A-specific ubiquitin ligase. *Cell Rep.* **8**, 999–1005 (2014).

15. Zhu, Q. *et al.* BRCA1 tumour suppression occurs via heterochromatin-mediated silencing. *Nature* **477**, 179–184 (2011).

16. Kim, B.-J. *et al.* The Histone Variant MacroH2A1 Is a BRCA1 Ubiquitin Ligase Substrate. *Cell Rep.* **19**, 1758–1766 (2017).

17. Stewart, M. D. *et al.* BARD1 is necessary for ubiquitylation of nucleosomal histone H2A and for transcriptional regulation of estrogen metabolism genes. *Proc. Natl. Acad. Sci. U. S. A.* **115**, 1316–1321 (2018).

18. Uckelmann, M. *et al.* USP48 restrains resection by site-specific cleavage of the BRCA1 ubiquitin mark from H2A. *Nat. Commun.* **9**, 229 (2018).

19. Mattiroli, F. *et al.* RNF168 ubiquitinates K13-15 on H2A/H2AX to drive DNA damage signaling. *Cell* **150**, 1182–1195 (2012).

20. Mattiroli, F., Uckelmann, M., Sahtoe, D. D., van Dijk, W. J. & Sixma, T. K. The nucleosome acidic patch plays a critical role in RNF168-dependent ubiquitination of histone H2A. *Nat. Commun.* **5**, 3291 (2014).

21. Fradet-Turcotte, A. *et al.* 53BP1 is a reader of the DNA-damage-induced H2A Lys 15 ubiquitin mark. *Nature* **499**, 50–54 (2013).

22. Wilson, M. D. *et al.* The structural basis of modified nucleosome recognition by 53BP1. *Nature* **536**, 100–103 (2016).

23. Wang, H. *et al.* Role of histone H2A ubiquitination in Polycomb silencing. *Nature* **431**, 873–878 (2004).

24. Cao, R., Tsukada, Y. & Zhang, Y. Role of Bmi-1 and Ring1A in H2A Ubiquitylation and Hox Gene Silencing. *Mol. Cell* **20**, 845–854 (2005).

25. Tamburri, S. *et al.* Histone H2AK119 Mono-Ubiquitination Is Essential for Polycomb-Mediated Transcriptional Repression. *Mol. Cell* **77**, 840-856.e5 (2020).

26. Vissers, J. H. A., van Lohuizen, M. & Citterio, E. The emerging role of Polycomb repressors in the response to DNA damage. *J. Cell Sci.* **125**, 3939 (2012).

27. McGinty, R. K., Henrici, R. C. & Tan, S. Crystal structure of the PRC1 ubiquitylation module bound to the nucleosome. *Nature* **514**, 591–596 (2014).

28. Horn, V. *et al.* Structural basis of specific H2A K13/K15 ubiquitination by RNF168. *Nat. Commun.* **10**, 1751 (2019).

29. Brzovic, P. S. *et al.* Binding and recognition in the assembly of an active BRCA1/BARD1 ubiquitin-ligase complex. *Proc. Natl. Acad. Sci. U. S. A.* **100**, 5646–5651 (2003).

30. Anderson, C. J. *et al.* Structural Basis for Recognition of Ubiquitylated Nucleosome by Dot1L Methyltransferase. *Cell Rep.* **26**, 1681-1690.e5 (2019).

31. Valencia-Sánchez, M. I. *et al.* Structural Basis of Dot1L Stimulation by Histone H2B Lysine 120 Ubiquitination. *Mol. Cell* **74**, 1010-1019.e6 (2019).

32. Song, Y. *et al.* High-resolution comparative modeling with RosettaCM. *Struct. Lond. Engl. 1993* **21**, 1735–1742 (2013).

33. Yang, J. *et al.* Improved protein structure prediction using predicted interresidue orientations. *Proc. Natl. Acad. Sci.* **117**, 1496 (2020).

34. McGinty, R. K. & Tan, S. Recognition of the nucleosome by chromatin factors and enzymes. *Curr. Opin. Struct. Biol.* **37**, 54–61 (2016).

35. Taherbhoy, A. M., Huang, O. W. & Cochran, A. G. BMI1–RING1B is an autoinhibited RING E3 ubiquitin ligase. *Nat. Commun.* **6**, 7621 (2015).

36. Wood, K., Tellier, M. & Murphy, S. DOT1L and H3K79 Methylation in Transcription and Genomic Stability. *Biomolecules* **8**, 11 (2018).

37. Nguyen, A. T. & Zhang, Y. The diverse functions of Dot1 and H3K79 methylation. *Genes Dev.* **25**, 1345–1358 (2011).

38. Huyen, Y. *et al.* Methylated lysine 79 of histone H3 targets 53BP1 to DNA double-strand breaks. *Nature* **432**, 406–411 (2004).

39. Wysocki, R. *et al.* Role of Dot1-dependent histone H3 methylation in G1 and S phase DNA damage checkpoint functions of Rad9. *Mol. Cell. Biol.* **25**, 8430–8443 (2005).

40. Tate, J. G. *et al.* COSMIC: the Catalogue Of Somatic Mutations In Cancer. *Nucleic Acids Res.* **47**, D941–D947 (2019).

41. Shah, S., Verma, T., Rashid, M., Gadewal, N. & Gupta, S. Histone H2A isoforms: Potential implications in epigenome plasticity and diseases in eukaryotes. *J. Biosci.* **45**, 4 (2020).

42. Carrion-Vazquez, M., Marszalek, P. E., Oberhauser, A. F. & Fernandez, J. M. Atomic force microscopy captures length phenotypes in single proteins. *Proc. Natl. Acad. Sci.* **96**, 11288 (1999).

43. Nakamura, K. *et al.* H4K20me0 recognition by BRCA1–BARD1 directs homologous recombination to sister chromatids. *Nat. Cell Biol.* **21**, 311–318 (2019).

44. Becker, J. R. *et al.* BARD1 links histone H2A Lysine-15 ubiquitination to initiation of BRCA1-dependent homologous recombination. *bioRxiv* 2020.06.01.127951 (2020) doi:10.1101/2020.06.01.127951.

45. Masuda, T., Xu, X., Dimitriadis, E. K., Lahusen, T. & Deng, C.-X. 'DNA Binding Region' of BRCA1 Affects Genetic Stability through modulating the Intra-S-Phase Checkpoint. *Int. J. Biol. Sci.* **12**, 133–143 (2016).

46. Zhao, W. *et al.* BRCA1-BARD1 promotes RAD51-mediated homologous DNA pairing. *Nature* **550**, 360–365 (2017).

47. Streich, F. C., Jr & Lima, C. D. Capturing a substrate in an activated RING E3/E2-SUMO complex. *Nature* **536**, 304–308 (2016).

48. Scott, D. C. *et al.* Structure of a RING E3 trapped in action reveals ligation mechanism for the ubiquitin-like protein NEDD8. *Cell* **157**, 1671–1684 (2014).

49. Brown, N. G. *et al.* RING E3 mechanism for ubiquitin ligation to a disordered substrate visualized for human anaphase-promoting complex. *Proc. Natl. Acad. Sci.* **112**, 5272 (2015).

50. Eddins, M. J., Carlile, C. M., Gomez, K. M., Pickart, C. M. & Wolberger, C. Mms2-Ubc13 covalently bound to ubiquitin reveals the structural basis of linkage-specific polyubiquitin chain formation. *Nat. Struct. Mol. Biol.* **13**, 915–920 (2006).

51. Pruneda, J. N. *et al.* Structure of an E3:E2~Ub complex reveals an allosteric mechanism shared among RING/U-box ligases. *Mol. Cell* **47**, 933–942 (2012).

52. Paull, T. T. *et al.* A critical role for histone H2AX in recruitment of repair factors to nuclear foci after DNA damage. *Curr. Biol. CB* **10**, 886–895 (2000).

53. Cooper, S. *et al.* Jarid2 binds mono-ubiquitylated H2A lysine 119 to mediate crosstalk between Polycomb complexes PRC1 and PRC2. *Nat. Commun.* **7**, 13661 (2016).

54. Savage, K. I. & Harkin, D. P. BRCA1, a ‘complex’ protein involved in the maintenance of genomic stability. *FEBS J.* **282**, 630–646 (2015).

55. Belotserkovskaya, R. *et al.* PALB2 chromatin recruitment restores homologous recombination in BRCA1-deficient cells depleted of 53BP1. *Nat. Commun.* **11**, 819 (2020).

Figures

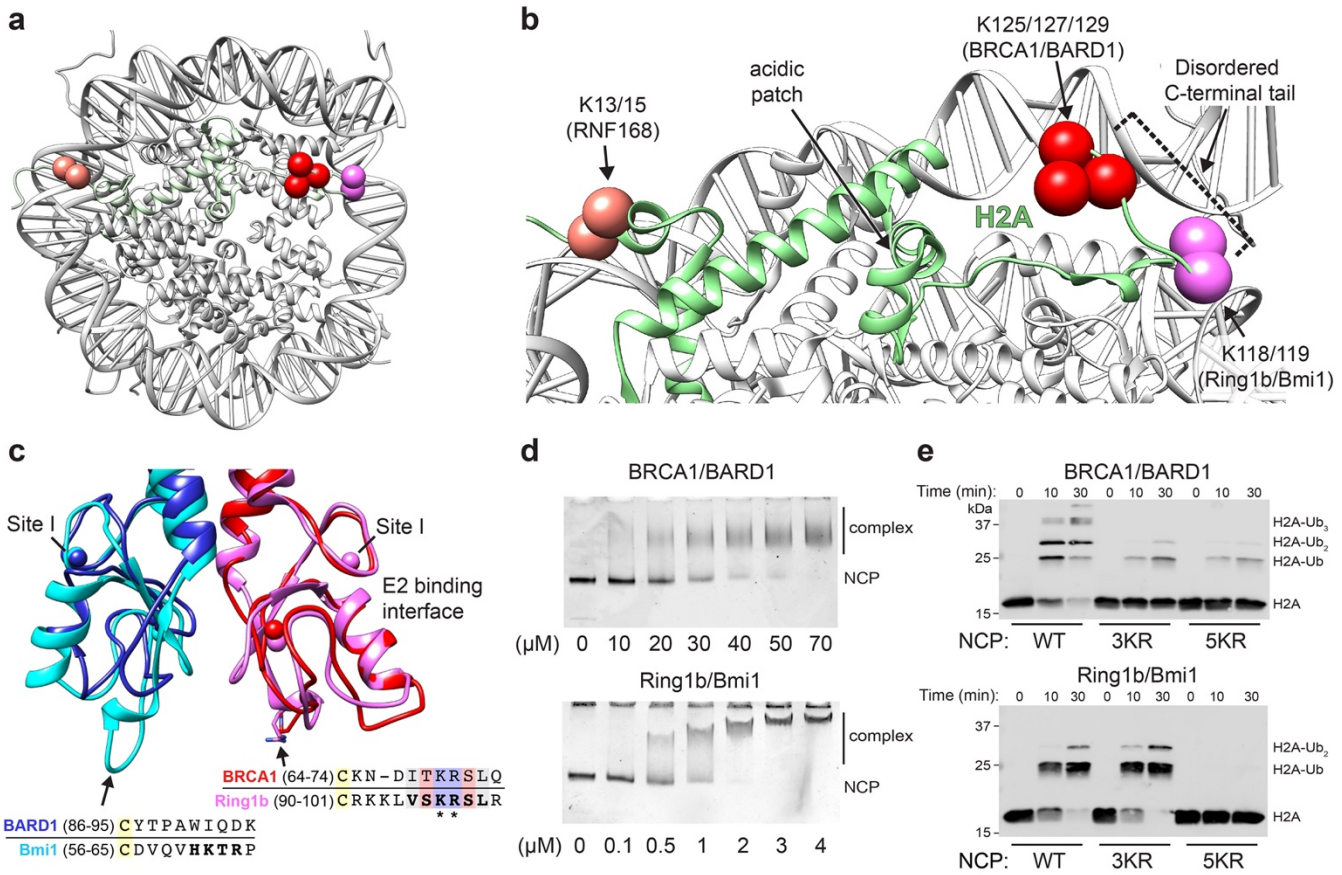

Figure 1. RING E3 ligases ubiquitylate H2A at distinct sites on the nucleosome. (a) Location of primary target lysine residues (Cαs, colored spheres) for BRCA1/BARD1 (K125/127/129, red) Ring1b/Bmi1 (K118/119, magenta), and RNF168 (K13/15, salmon) on one face of the nucleosome core particle (NCP; PDB: 1KX5). **(b)** Close-up of H2A (green) from panel a. The H2B αC helix is hidden for clarity. Residues past H2A Lys118 are disordered and generally not observed as density in X-ray or cryo-EM structures. **(c)** Structural and sequence alignment of BRCA1/BARD1 (PDB: 1JM7) and Ring1b/Bmi1 (PDB: 2CKL) RING domains with arrows pointing towards the nucleosome binding regions of Ring1b and Bmi1. Bolded residues in the sequence alignment are primary Ring1b and Bmi1 nucleosome binding loop residues. Asterisks denote arginine anchor motif residues. Yellow highlighted cysteine residues are nearest analogous Zn^{2+}-coordinating residues. Zinc atoms are shown in structures as colored spheres (partially overlapping) with zinc site I labeled for each RING domain. **(d)** Native-gel electrophoretic mobility shift assays (EMSA) measuring BRCA1/BARD1 and Ring1b/Bmi1 RING heterodimer binding to NCPs. Concentration of RING binding partner (indicated below the gels) is different between E3s. Data are representative of n=2 (Ring1b/Bmi1) or n=3 (BRCA1/BARD1) independent binding experiments. **(e)** Nucleosome ubiquitylation assays (Western blot for VSV-G tag on H2A) using either BRCA1/BARD1 or Ring1b/Bmi1 RING heterodimers and wild-type (WT), H2A Lys125/127/129Arg (3KR), or H2A Lys118/119/125/127/129Arg (5KR) NCP substrates. Data in panel e are representative of n=2 independent experiments. Uncropped gel/blot images in panels d and e are available as source data.

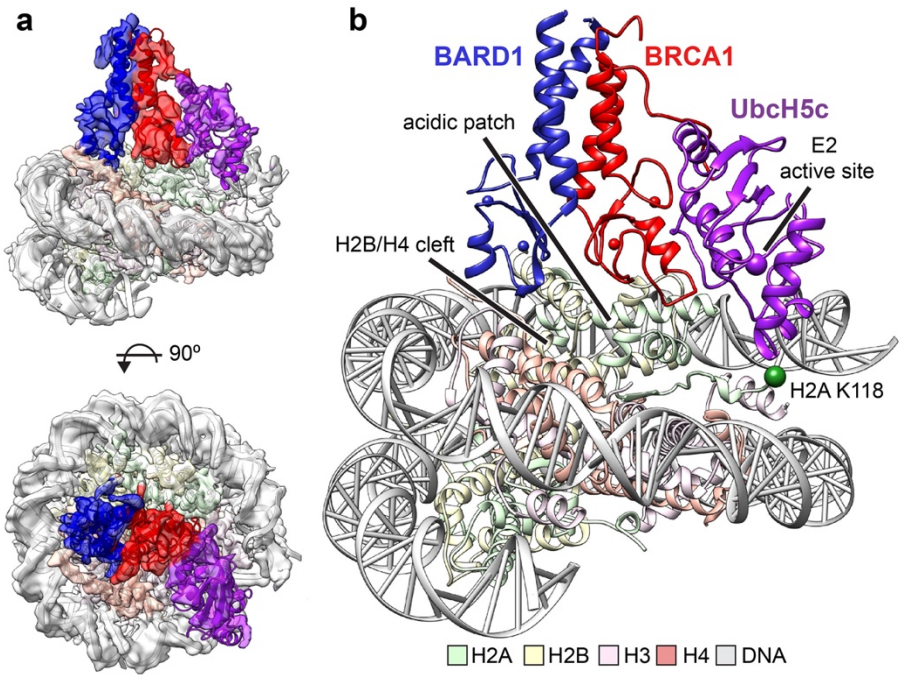

Figure 2. Cryo-EM structure of the BRCA1-UbcH5c/BARD1/nucleosome complex. (a) Cryo-EM density of the BRCA1-UbcH5c/BARD1/NCP complex (semi-transparent surface) with fit atomic model. Density map is colored coded by chain using the same scheme as in panel b. **(b)** Atomic model of BRCA1-UbcH5c/BARD1/NCP complex. The Cαs of H2A Lys118 and the active site position of UbcH5c (Lys85) are depicted at spheres.

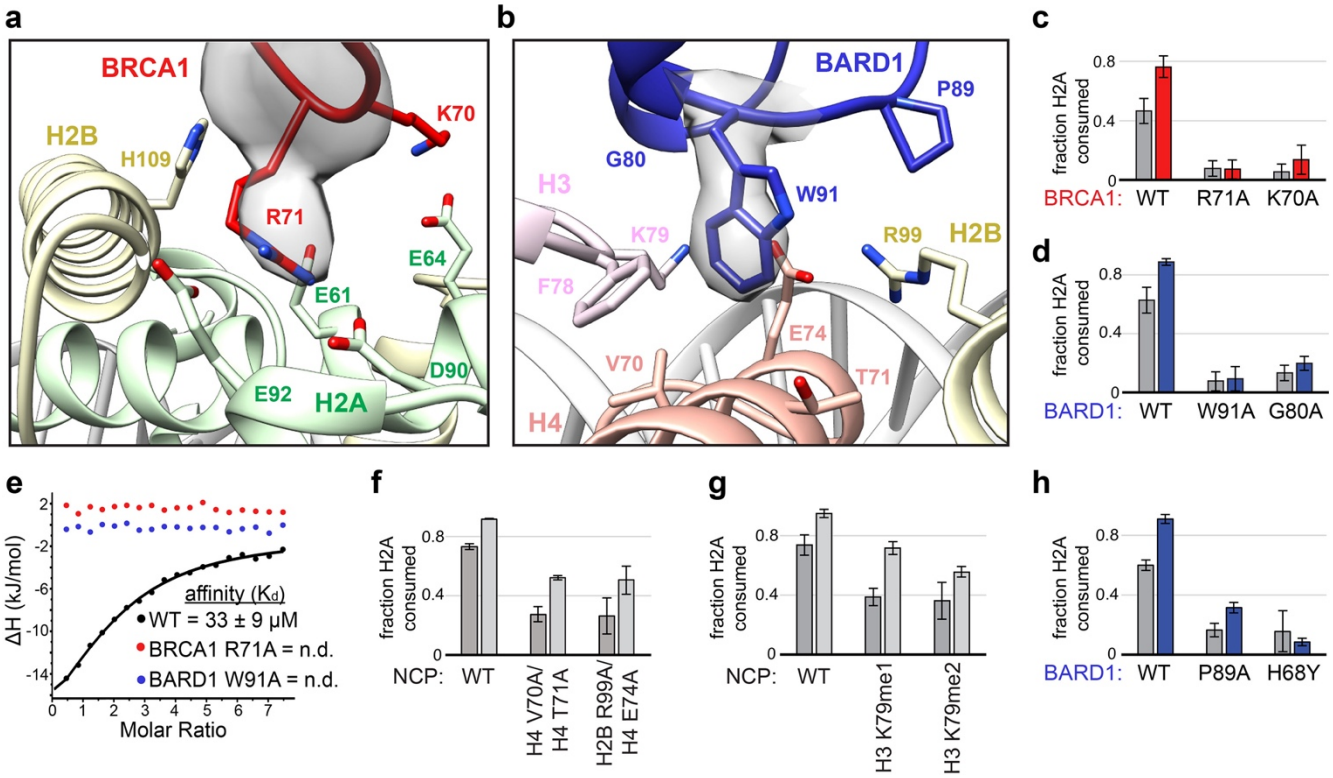

Figure 3. BRCA1/BARD1 RING-histone interactions (a) Close-up view of the BRCA1-histone interface with Arg71 side chain density shown. (**b)** Close-up view of the BARD1-histone interface with Trp91 side chain density shown. Relevant side chains in panels a and b are shown as sticks. **(c, d)** Quantified nucleosome ubiquitylation assays using the indicated BRCA1/BARD1 mutants. **(e)** Binding of BRCA1/BARD1 (wild-type and indicated mutants) to NCPs measured by isothermal titration calorimetry (ITC). Data are representative of n=2 experiments (n.d. = not detected). **(f)** Quantified nucleosome ubiquitylation assays using BRCA1/BARD1 and the indicated H2B/H4 cleft mutant NCP substrates, **(g)** H3 Lys79 methylation mimetic NCP substrates, and **(h)** BARD1 COSMIC mutants. All quantified ubiquitylation activity data show the mean; error bars are ± 1-s.d. of n=3 independent experiments for 10-minute (gray bars) and 30-minute (light gray or colored bars) time points. Data for graphs in c, d, f, g, and h are available as source data.

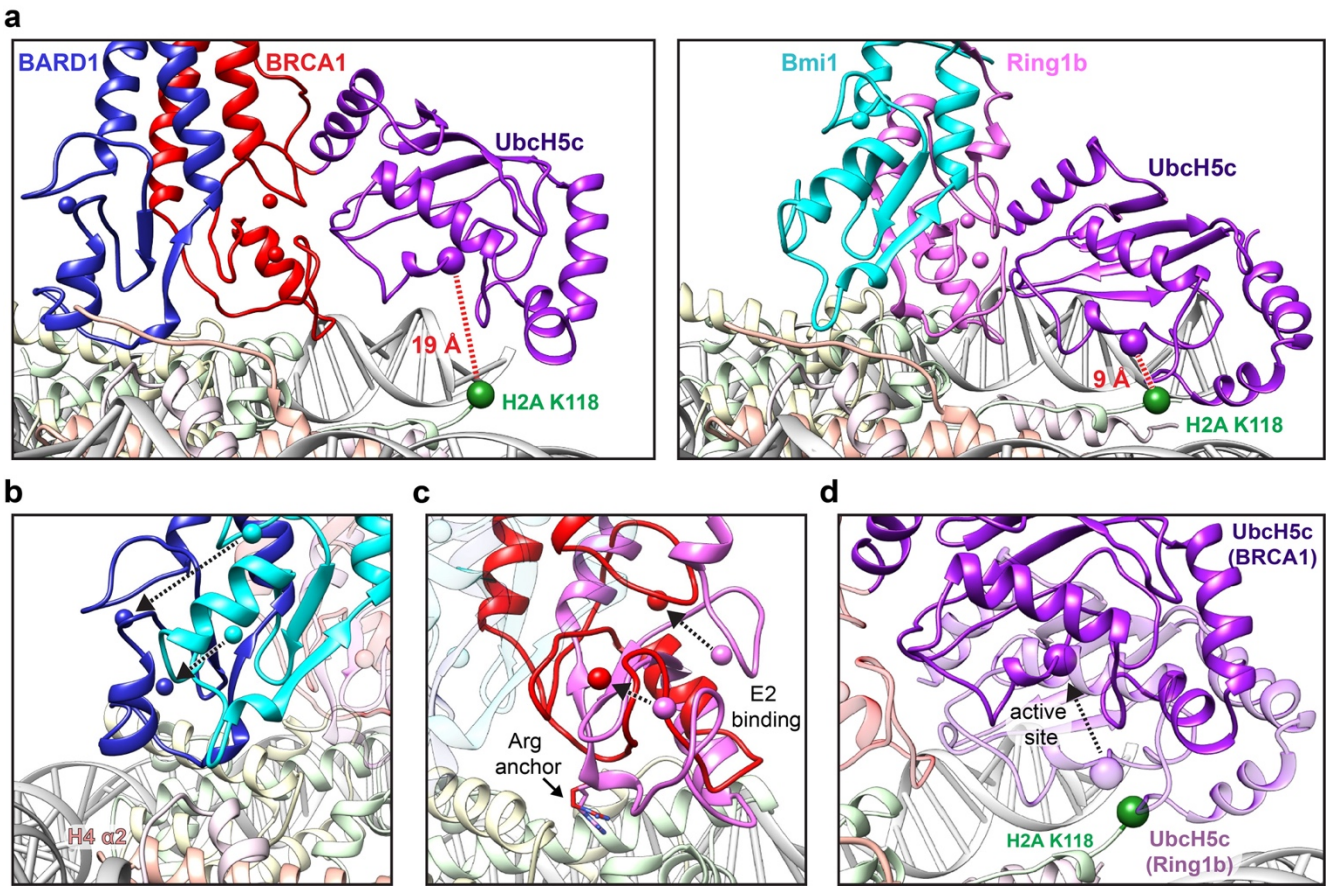

Figure 4. Comparison to the Ring1b-UbcH5c/Bmi1/nucleosome complex. (a) Close-up views of the BRCA1-UbcHc/BARD1/NCP complex (left panel) and Ring1b-UbcH5c/Bmi1/NCP complex (PDB: 4R8P, right panel) aligned by H2B on the bound face of the nucleosome. Complexes are shown side-by-side instead of overlaid for clarity. Distance measurements are shown between the Cα of H2A Lys118 (green sphere) and the active site position Cα Lys/Cys85 (purple sphere). All comparisons in this study are performed to the proximally bound side of the Ring1b-UbcH5c/Bmi1/NCP complex[27]. **(b)** View of the BARD1 and Bmi1 RING domains in the NCP complexes aligned by H2B. Only histones from the BRCA1-UbcH5c/BARD1/NCP model are depicted, but histone components from both complexes show excellent agreement (Extended Data Fig. 7b). The positions of analogous Zn^{2+} ions (colored spheres) are connected by arrows to highlight the differences in the RING domains on the histone surface. **(c)** Same alignment as in panel b comparing the location of the BRCA1 and Ring1b RING domains with the arginine anchor residue side chains shown. **(d)** Same alignment as in panel b comparing the position of BRCA1-bound UbcH5c (dark purple) to Ring1b-bound UbcH5c (light purple). The active site Cα position for each E2 is shown as a purple sphere, and the arrow between them highlights the shift of the active site of BRCA1-bound UbcH5c away from H2A Lys118 (green sphere). The Ring1b RING domain is hidden for clarity, and the BRCA1 RING is shown as partially transparent red ribbon.

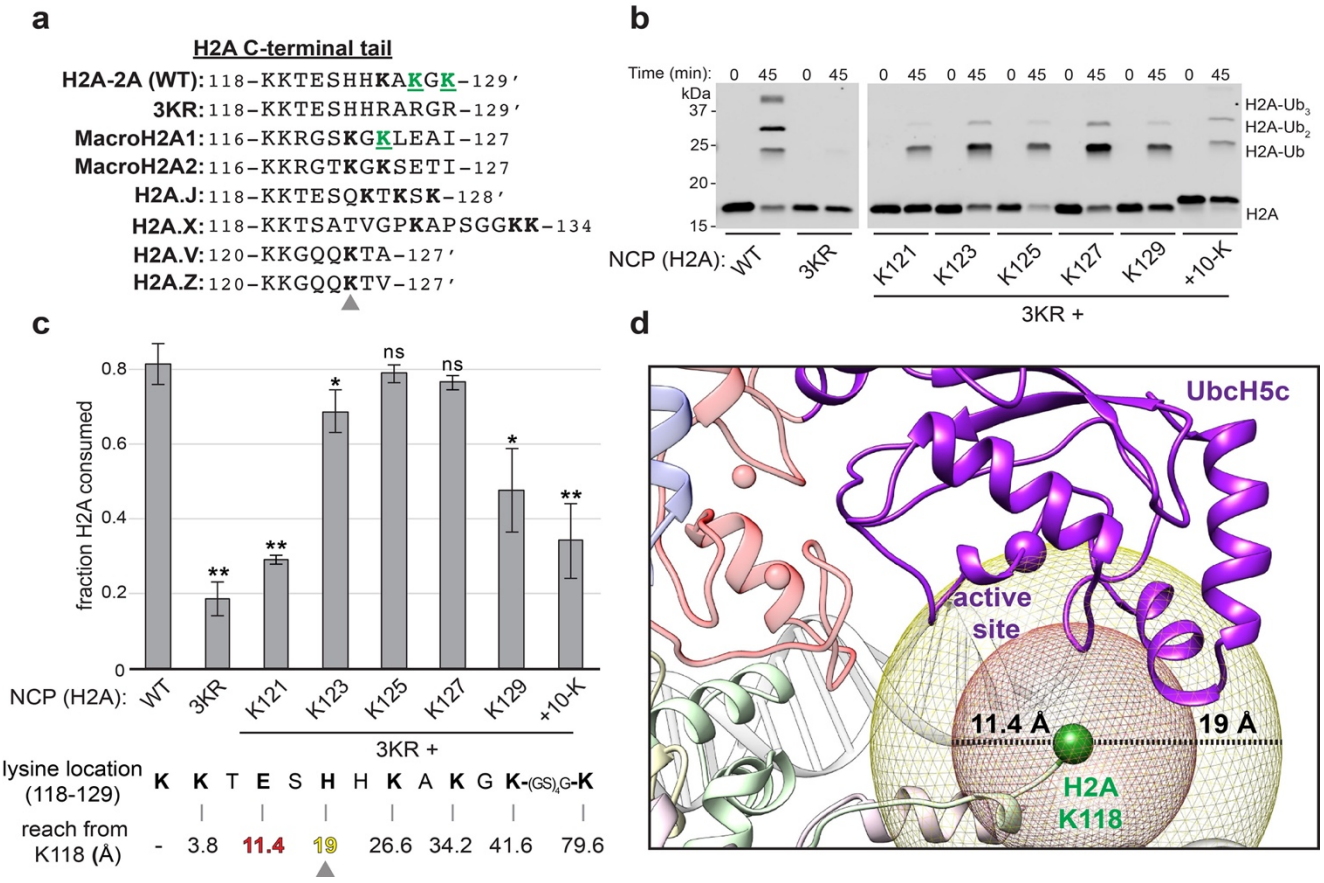

Figure 5. Lysine position along the flexible C-terminal tail of H2A dictates ubiquitylation efficiency. (a) Structure-based sequence alignment of H2A C-terminal tail regions from major histone H2A variants. An apostrophe denotes the C-terminus of the isoform. MacroH2A and H2Ax have extensions with additional lysine residues. Lysine residues located at positions equivalent or C-terminal to His123 in H2A-2A (WT) are bolded, with an arrow indicating this position. Green underlined residues have been identified as targets of BRCA1/BARD1 in cells by mass-spectrometry[14,16]. **(b)** Representative nucleosome ubiquitylation assay using BRCA1/BARD1 and NCP substrates containing wild-type or mutant single-lysine H2A substrates. **(c)** Quantified nucleosome ubiquitylation activity assays from panel b. The sequence of the H2A C-terminal tail (118-129) is below the graph, with the approximate distance from the Cα of H2A Lys118 to each single lysine position assuming an inter-residue distance equivalent to a reported contour length of 3.8 Å per amino acid[42]. Plotted data show the mean and error bars are ± 1-s.d. of n=3 independent experiments. P-values were calculated using a two-tailed Student's t-test compared to wild-type (* p≤0.05, ** p≤0.005, ns = not significant). **(d)** The position of H2A Lys118 (Cα, green sphere) relative to the active site position UbcH5c (Cα, purple sphere). Mesh spheres are centered on the Cα of H2A Lys118 with radii corresponding to the approximate linear reach of a fully disordered polypeptide to position 121 (red) or 123 (yellow) of H2A. Uncropped gels in panel b and data for graph in c are available as source data.

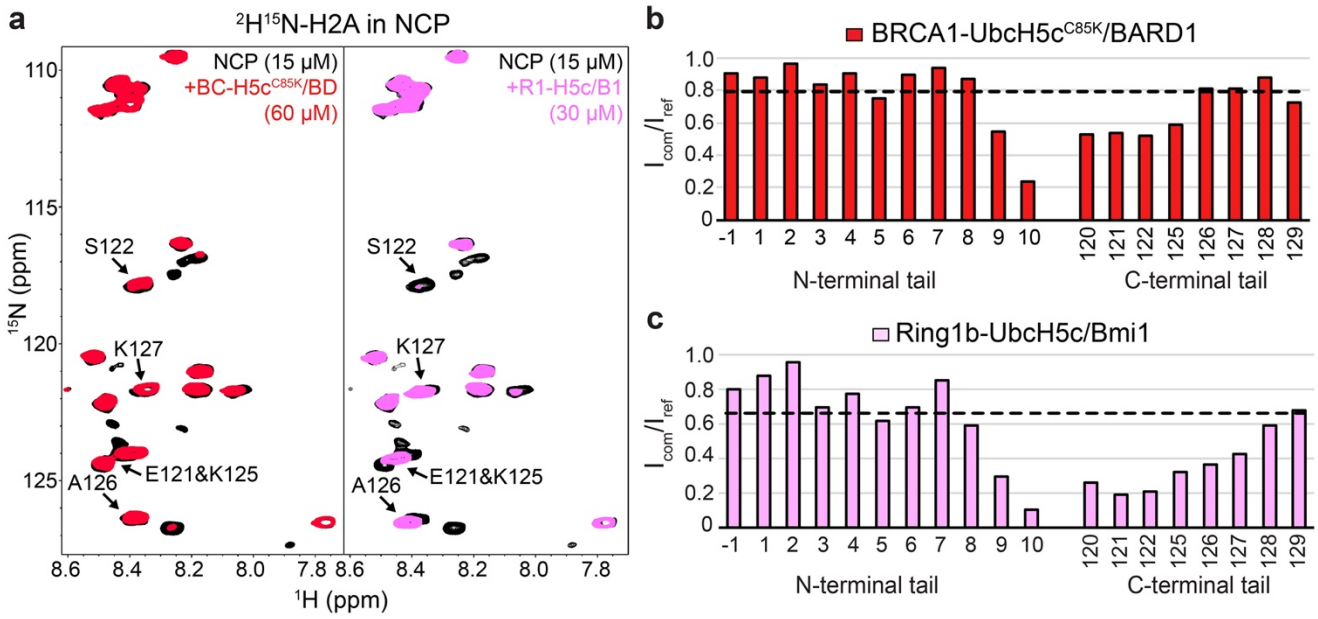

Figure 6. H2A C-terminal tail dynamics in E3-E2/nucleosome complexes. (a) Overlay of $^{1}H^{15}N$-TROSY-HSQC spectra of $^{2}H^{15}N$-H2A in the NCP (black, both panels), with BRCA1-UbcH5c^{C85K}/BARD1 added (red, left panel), or Ring1b-UbcH5c/Bmi1 added (pink, right panel). Binding experiments were performed using 15 μM $^{2}H^{15}N$-H2A NCPs with 60 μM BRCA1-UbcH5c^{C85K}/BARD1 or 30 μM Ring1b-UbcH5c/Bmi1 added. Arrows in both panels identify signals from the H2A C-terminal tail that change position or have increased signal loss in the Ring1b-UbcH5c/Bmi1/nucleosome complex spectrum. **(b)** Quantification of H2A signal intensities from the BRCA1-UbcH5c^{C85K}/BARD1/nucleosome complex in panel a comparing the bound complex spectrum to the apo reference spectrum (I_{com}/I_{ref}). The trendline represents the mean broadening (I_{com}/I_{ref}) from N-terminal tail residues -1-10. **(c)** Same analysis as in panel b for the Ring1b-UbcH5c/Bmi1/nucleosome complex. Data in panels b and c are representative of n=2 independent experiments. Data for graphs in b and c are available as source data.

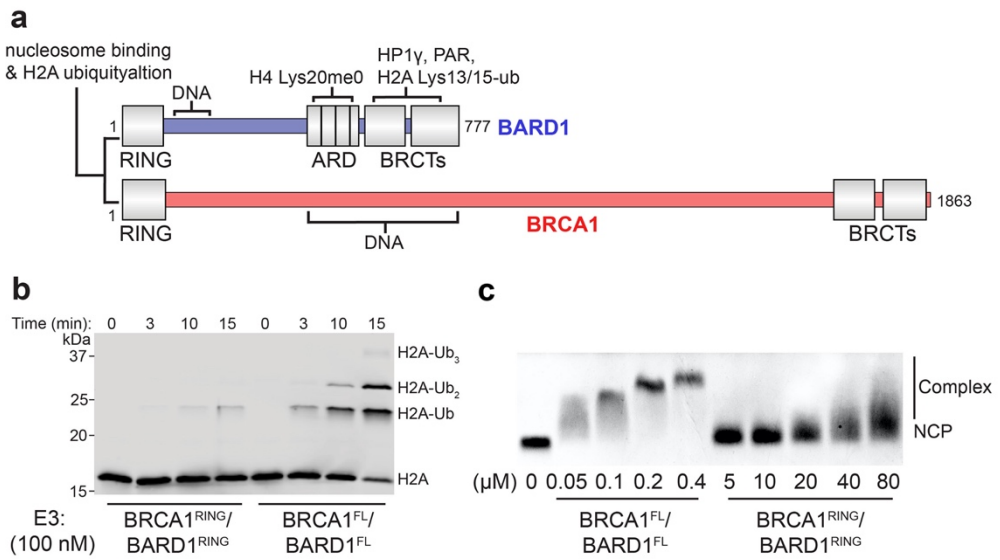

Figure 7. Enhanced nucleosome ubiquitylation activity and binding of full-length BRCA1/BARD1. (a) Domain illustration of full-length (FL) BRCA1 and BARD1 with a subset of putative chromatin and protein interactions indicated. **(b)** Nucleosome ubiquitylation assay comparing the activity of the RING heterodimer ($BRCA1^{RING}/BARD1^{RING}$) to full-length BRCA1/BARD1 ($BRCA1^{FL}/BARD1^{FL}$). The E3 concentration was lowered to 100 nM to observe ubiquitylation kinetics of $BRCA1^{FL}/BARD1^{FL}$. **(c)** EMSA assay comparing nucleosome binding of $BRCA1^{FL}/BARD1^{FL}$ to $BRCA1^{RING}/BARD1^{RING}$. The BRCA1/BARD1 concentration used in the binding experiments is reported under the gels and is ~100-fold lower for the full-length construct. Ubiquitylation activity and binding assays are representative of n=2 independent experiments. Uncropped gels in panels b and c are available as source data.

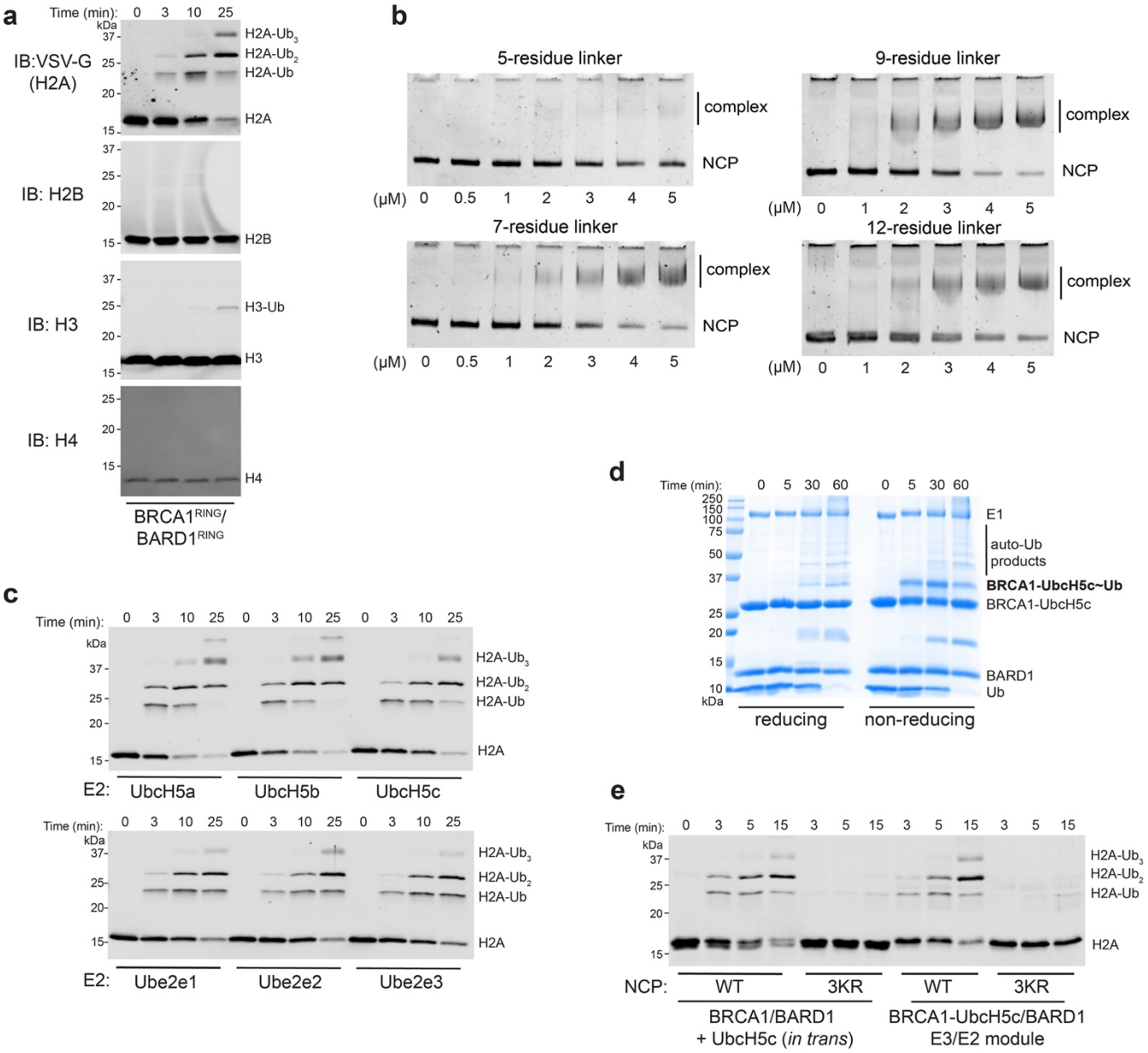

Extended Data Figure 1. Specificity of BRCA1/BARD1-dependent nucleosome ubiquitylation and validation of the E3-E2 chimera. (a) Western blot analysis of all four histone subunits from the same nucleosome ubiquitylation reaction. **(b)** Native-gel EMSA measuring NCP binding of BRCA1-UbcH5c/BARD1 constructs with various Gly/Ser-repeat linker lengths. The E3-E2 chimera with a seven-residue linker was used for structure determination and all subsequent experiments. **(c)** Nucleosome ubiquitylation assays using BRCA1/BARD1 with indicated E2 enzymes. Data are representative of n=2 experiments. **(d)** Coomassie-stained gel under reducing or non-reducing conditions of an E2 charging reaction using the BRCA1-UbcH5c/BARD1 chimera. **(e)** Nucleosome ubiquitylation activity of BRCA1/BARD1 with UbcH5c *in trans* or the BRCA1-UbcH5c/BARD1 chimera with wild-type (WT) or Lys125/127/129Arg (3KR) NCP substrates. Uncropped gels/blots in panels a-e are available as source data.

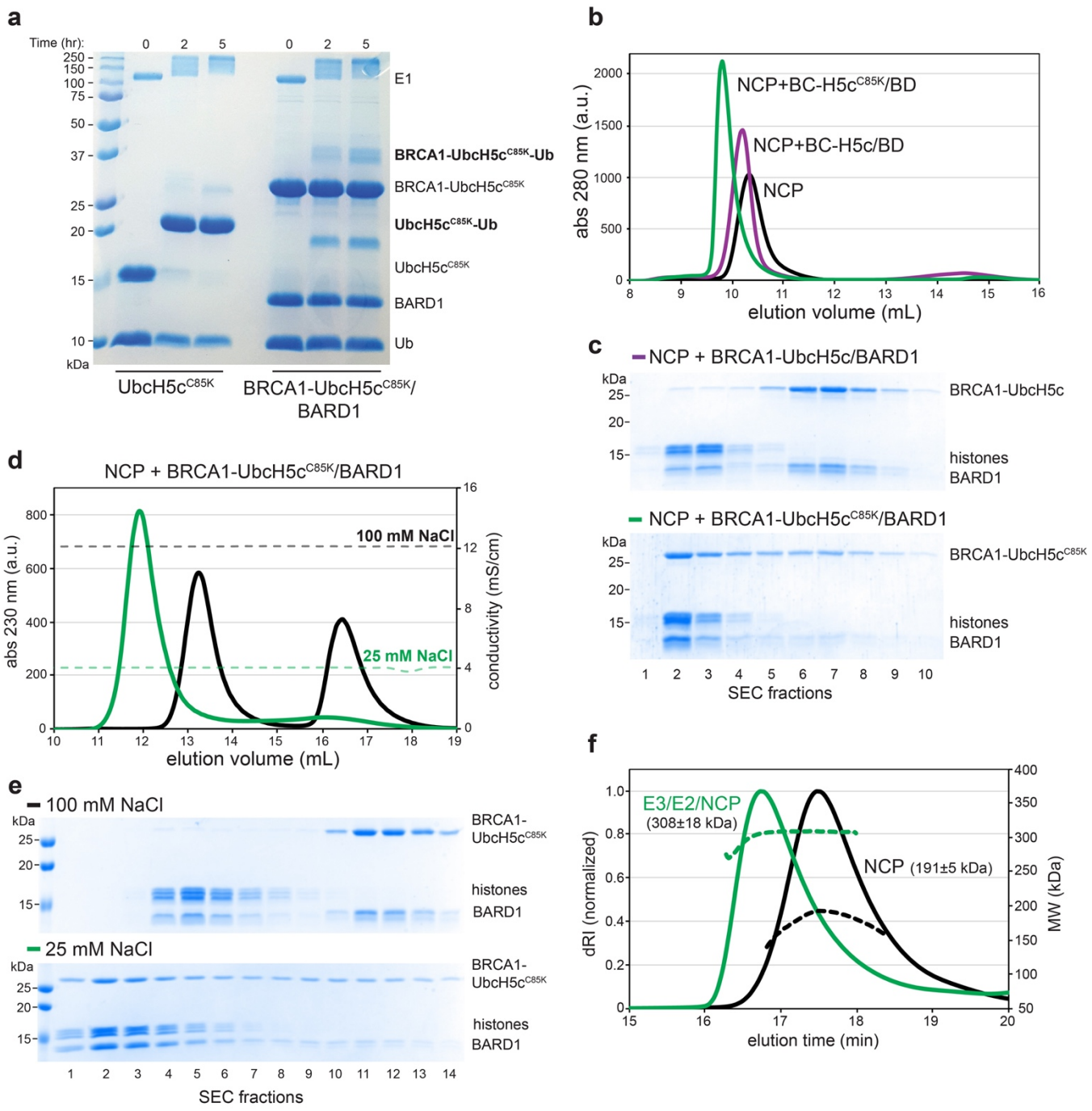

Extended Data Figure 2. Purification of a stable BRCA1-UbcH5c/BARD1/nucleosome complex. (a) Coomassie-stained gel of an E2 charging reaction using UbcH5c^{C85K} and BRCA1-UbcH5c^{C85K}/BARD1. **(b)** Size exclusion chromatography (SEC) of NCPs (black) with excess BRCA1-UbcH5c/BARD1 (purple) or BRCA1-UbcH5c^{C85K}/BARD1 (green) with 35 mM NaCl in SEC buffer. **(c)** Coomassie-stained gels of fractions from SEC binding experiments shown in panel b. **(d)** SEC of NCPs with excess BRCA1-UbcH5c^{C85K}/BARD1 with 100 mM NaCl (black) or 25 mM NaCl (green) in SEC running buffer. **(e)** Coomassie-stained gels of fractions from SEC binding experiments shown in panel d. **(f)** Size exclusion chromatography coupled to multi-angle light scattering (SEC-MALS) analysis of NCPs (black) and the BRCA1-UbcH5c^{C85K}/BARD1/NCP complex (green). Dashed lines report MALS molecular weight (MW) data. The MW value

reported is the average MW from light scattering ± 1-s.d. where error is a measure of statistical consistency of light scattering data and not an absolute bound on the error of MW. The expected MW is 203.7 kDa for the NCP and 287.2 kDa for the complex bound with 2:1 stoichiometry. Uncropped gels in panels a, c, and e are available as source data.

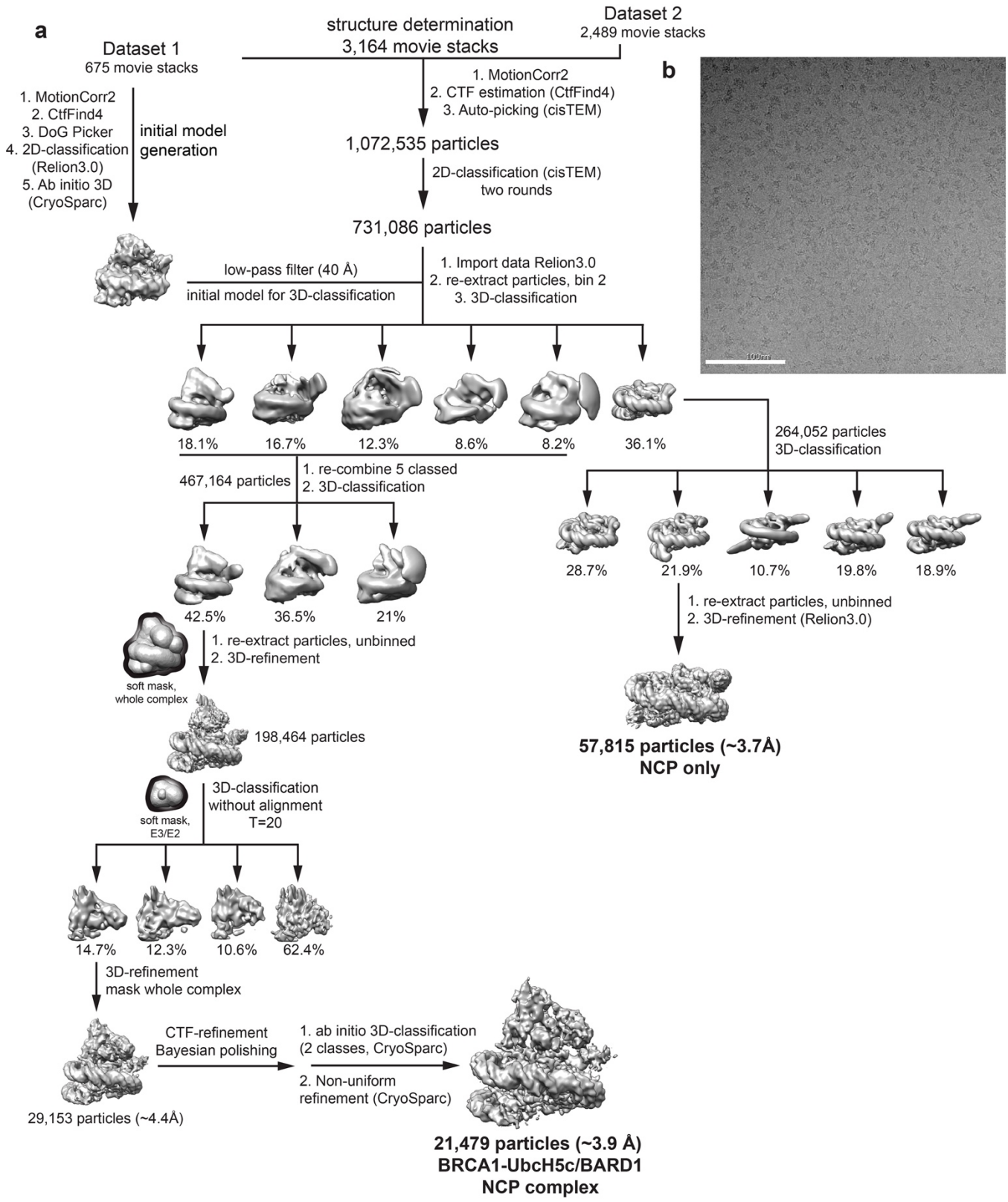
a
structure determination
3,164 movie stacks
Dataset 1
675 movie stacks
Dataset 2
2,489 movie stacks
1. MotionCorr2
2. CtfFind4
3. DoG Picker
4. 2D-classification (Relion3.0)
5. Ab initio 3D (CryoSparc)
initial model generation
1. MotionCorr2
2. CTF estimation (CtfFind4)
3. Auto-picking (cisTEM)
1,072,535 particles
2D-classification (cisTEM)
two rounds
731,086 particles
low-pass filter (40 Å)
initial model for 3D-classification
1. Import data Relion3.0
2. re-extract particles, bin 2
3. 3D-classification
18.1%
16.7%
12.3%
8.6%
8.2%
36.1%
264,052 particles
3D-classification
467,164 particles
1. re-combine 5 classed
2. 3D-classification
42.5%
36.5%
21%
28.7%
21.9%
10.7%
19.8%
18.9%
1. re-extract particles, unbinned
2. 3D-refinement (Relion3.0)
soft mask, whole complex
1. re-extract particles, unbinned
2. 3D-refinement
198,464 particles
57,815 particles (~3.7Å)
NCP only
soft mask, E3/E2
3D-classification without alignment
T=20
14.7%
12.3%
10.6%
62.4%
3D-refinement
mask whole complex
CTF-refinement
Bayesian polishing
1. ab initio 3D-classification
(2 classes, CryoSparc)
2. Non-uniform refinement (CryoSparc)
29,153 particles (~4.4Å)
21,479 particles (~3.9 Å)
BRCA1-UbcH5c/BARD1
NCP complex
b

Extended Data Figure 3. Cryo-EM processing workflow. (a) Flow chart of data processing steps. Objects with dark borders represent solvent masks and are not density maps. **(b)** Representative motion-corrected micrograph from data set. White scale bar is 100 nm.

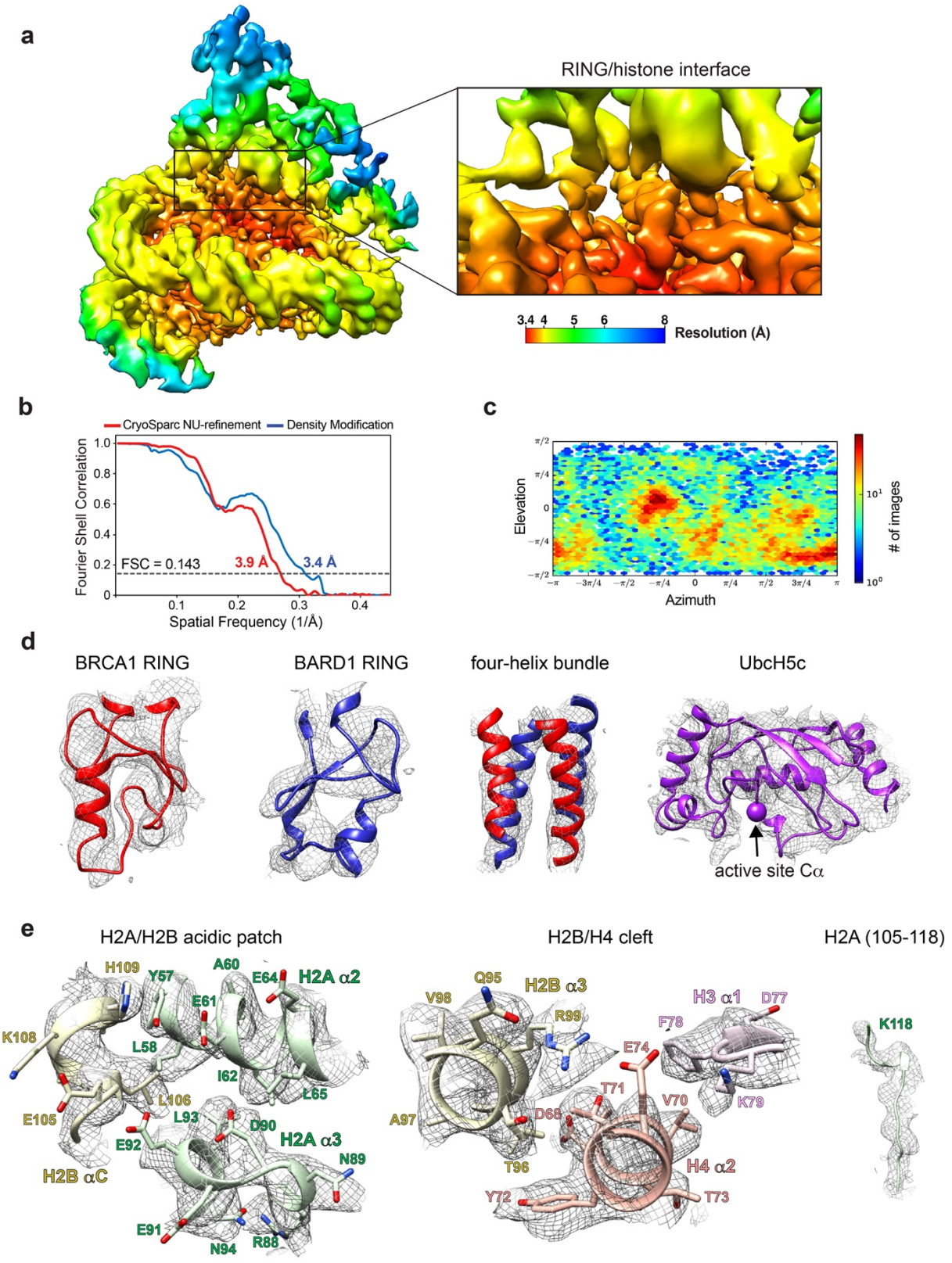

Extended Data Figure 4. Cryo-EM reconstruction validation and example density. (a) Local resolution estimate from CryoSparc after non-uniform refinement at the FSC=0.143 cutoff

plotted on the final density modified map of the whole complex (left panel) and close-up on the RING-histone interface (right panel). **(b)** Half-map Fourier shell correlation curves from CryoSparc non-uniform refinement (red) and after density modification (blue). **(c)** Euler angle distribution of refined particle subset used in final cryo-EM reconstruction. **(d)** Main chain trace of the BRCA1 RING, BARD1 RING, four-helix bundle, and UbcH5c fit into cryo-EM map. The active site position of UbcH5c (Lys 85) Cα is shown as a sphere. **(e)** Subset of important histone regions fit into the cryo-EM map with side chains shown (except for H2A C-terminal tail).

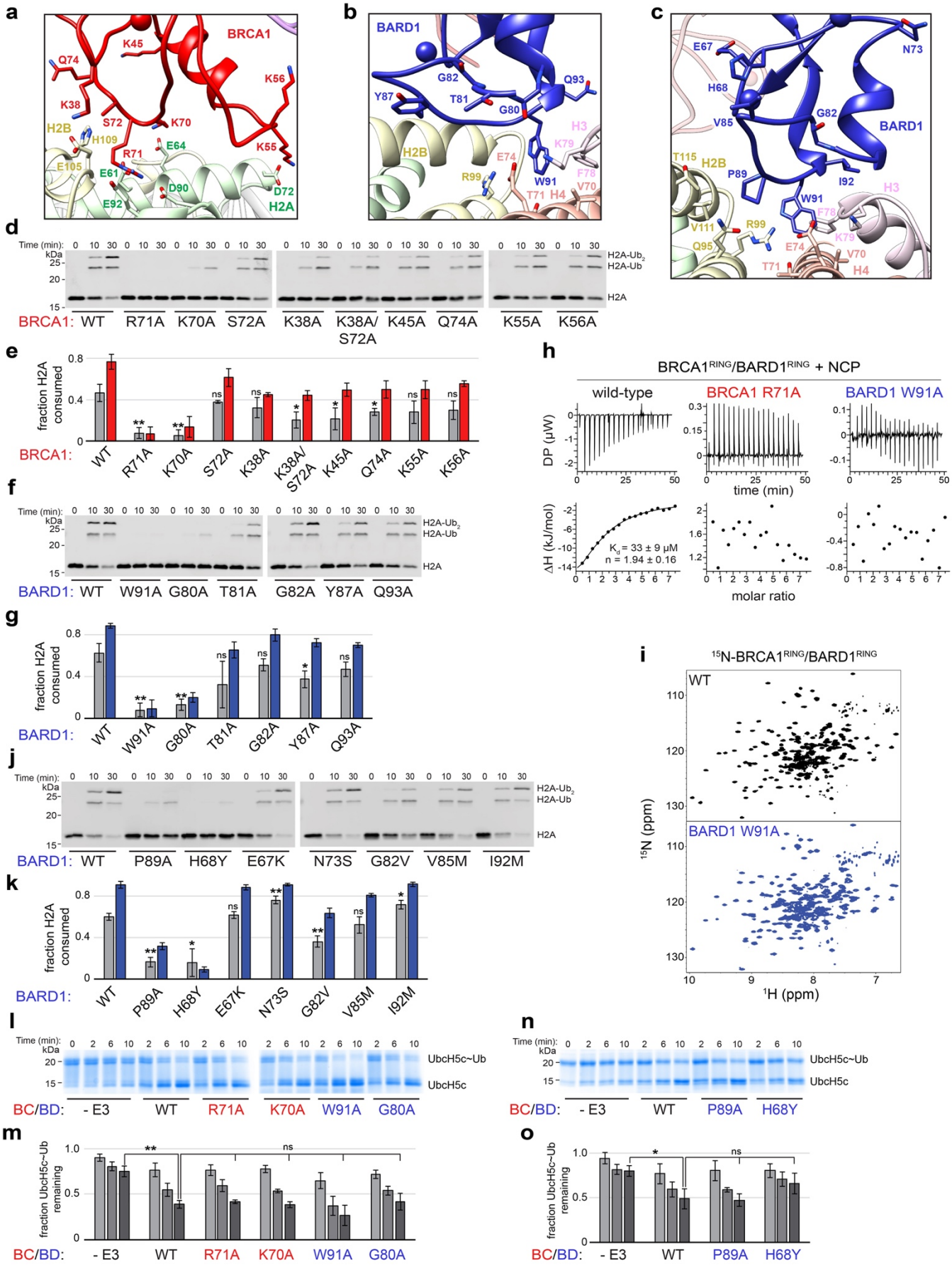
a
BRCA1
K45
Q74
K56
K38
S72
K70
H2B
H109
E64
R71
K55
E105
E61
D90
D72
E92
H2A
b
BARD1
G82
Q93
Y87
T81
G80
H3
K79
H2B
E74
R99
W91
F78
T71
H4
V70
c
E67
N73
H68
V85
G82
BARD1
T115
H2B
P89
I92
H3
W91
F78
V111
R99
K79
Q95
E74
V70
T71
H4
d
Time (min): 0 10 30 0 10 30 0 10 30 0 10 30 0 10 30 0 10 30 0 10 30 0 10 30 0 10 30 0 10 30 0 10 30 0 10 30
kDa
25
20
15
H2A-Ub2
H2A-Ub
H2A
BRCA1: WT R71A K70A S72A K38A K38A/ S72A K45A Q74A K55A K56A
e
fraction H2A consumed
0.8
0.4
0
**
**
ns
ns
*
*
*
ns
ns
BRCA1: WT R71A K70A S72A K38A K38A/ S72A K45A Q74A K55A K56A
f
Time (min): 0 10 30 0 10 30 0 10 30 0 10 30 0 10 30 0 10 30 0 10 30 0 10 30 0 10 30 0 10 30 0 10 30 0 10 30
kDa
25
20
15
H2A-Ub2
H2A-Ub
H2A
BARD1: WT W91A G80A T81A G82A Y87A Q93A
g
fraction H2A consumed
0.8
0.4
0
**
**
ns
ns
*
ns
BARD1: WT W91A G80A T81A G82A Y87A Q93A
h
BRCA1RING/BARD1RING + NCP
wild-type
BRCA1 R71A
BARD1 W91A
DP (μW)
0
-1
-2
0.3
0.15
0
0.1
0
-0.1
0 25 50
time (min)
ΔH (kJ/mol)
-2
-6
-10
-14
Kd = 33 ± 9 μM
n = 1.94 ± 0.16
2
1.6
1.2
0
-0.4
-0.8
0 1 2 3 4 5 6 7
molar ratio
i
15N-BRCA1RING/BARD1RING
WT
BARD1 W91A
15N (ppm)
110
120
130
10 9 8 7
1H (ppm)
j
Time (min): 0 10 30 0 10 30 0 10 30 0 10 30 0 10 30 0 10 30 0 10 30 0 10 30 0 10 30 0 10 30 0 10 30 0 10 30
kDa
25
20
15
H2A-Ub2
H2A-Ub
H2A
BARD1: WT P89A H68Y E67K N73S G82V V85M I92M
k
fraction H2A consumed
0.8
0.4
0
**
*
ns
**
ns
**
*
BARD1: WT P89A H68Y E67K N73S G82V V85M I92M
l
Time (min): 0 2 6 10 2 6 10 2 6 10 2 6 10 2 6 10 2 6 10 2 6 10
kDa
20
15
UbcH5c~Ub
UbcH5c
BC/BD: - E3 WT R71A K70A W91A G80A
n
Time (min): 0 2 6 10 2 6 10 2 6 10 2 6 10 2 6 10 2 6 10
kDa
20
15
UbcH5c~Ub
UbcH5c
BC/BD: - E3 WT P89A H68Y
m
fraction UbcH5c~Ub remaining
1.0
0.5
0
**
ns
BC/BD: - E3 WT R71A K70A W91A G80A
o
fraction UbcH5c~Ub remaining
1.0
0.5
0
*
ns
BC/BD: - E3 WT P89A H68Y

Extended Data Figure 5. Extensive analysis of BRCA1/BARD1 RING-histone interface. (a-c) Close-up view of BRCA1 and BARD1 RING domains in the complex showing side chains of residues mutated in nucleosome ubiquitylation assays in panels d-g and j-k **(d)** Representative nucleosome ubiquitylation assay using the indicated BRCA1 RING mutants. **(e)** Quantified nucleosome ubiquitylation assays for BRCA1 mutants shown in panel d. **(f, g)** Same experimental set-up as panels d-e using the indicated BARD1 mutants. **(h)** ITC binding data for BRCA1/BARD1 and indicated mutants with NCPs. Summarized data are also shown in figure 3e. **(i)** $^{1}H^{15}N$-TROSY-HSQC spectra of wild-type (WT) BRCA1/BARD1 and BRCA1(WT)/BARD1(Trp91Ala). **(j, k)** Same experimental set-up as panels d-e using BARD1 mutants reported on the COSMIC database. **(l)** E2~Ub lysine discharge assay using the indicated BRCA1/BARD1 mutants. **(m)** Quantified E2~Ub lysine discharge assays using the BRCA1/BARD1 mutants shown in panel l. **(n, o)** Same experimental set-up as panels l and m using BARD1 COSMIC mutants. Quantified nucleosome ubiquitylation assay data show the mean and error bars are ± 1-s.d. of n=3 independent experiments at 10-minute (gray bars) and 30-minute (colored bars) time points. Statistical analysis is compared to wild-type at the 10-minute time point. Quantified E2 lysine discharge data show the mean and error bars are ± 1-s.d. of n=3 independent experiments at 2-, 6- and 10- minute time points (light, medium, and dark gray bars). Statistical comparisons are indicated with lines above the graphs. All p-values were calculated using a two-tailed Student's t-test (* $p \leq 0.05$, ** $p \leq 0.005$, ns = not significant). Uncropped gels/blots in panels d, f, j, l, and n and data from graphs in panels e, g, k, m, and o are available as source data.

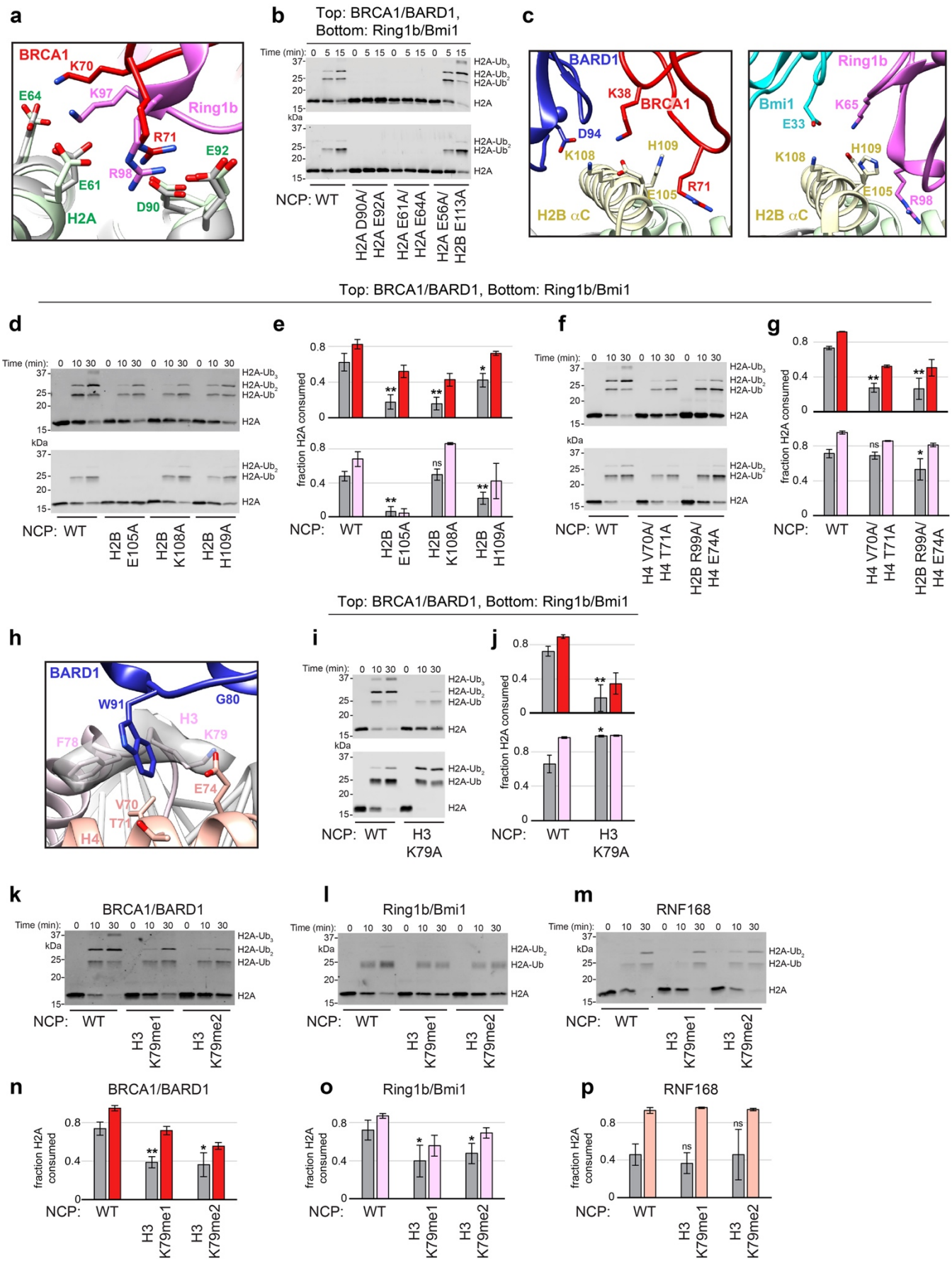
a
BRCA1
K70
E64
K97
Ring1b
R71
E92
R98
E61
D90
H2A
b
Top: BRCA1/BARD1,
Bottom: Ring1b/Bmi1
Time (min): 0 5 15 0 5 15 0 5 15 0 5 15
H2A-Ub3
H2A-Ub2
H2A-Ub
H2A
kDa
NCP: WT
H2A D90A/ H2A E92A
H2A E61A/ H2A E64A
H2A E56A/ H2B E113A
c
BARD1
K38
BRCA1
D94
H109
K108
R71
E105
H2B αC
Ring1b
Bmi1
K65
E33
H109
K108
E105
R98
H2B αC
Top: BRCA1/BARD1, Bottom: Ring1b/Bmi1
d
Time (min): 0 10 30 0 10 30 0 10 30 0 10 30
H2A-Ub3
H2A-Ub2
H2A-Ub
H2A
kDa
NCP: WT
H2B E105A
H2B K108A
H2B H109A
e
fraction H2A consumed
NCP: WT
H2B E105A
H2B K108A
H2B H109A
f
Time (min): 0 10 30 0 10 30 0 10 30
NCP: WT
H4 V70A/ H4 T71A
H2B R99A/ H4 E74A
g
fraction H2A consumed
NCP: WT
H4 V70A/ H4 T71A
H2B R99A/ H4 E74A
Top: BRCA1/BARD1, Bottom: Ring1b/Bmi1
h
BARD1
W91
G80
H3
K79
F78
E74
V70
T71
H4
i
Time (min): 0 10 30 0 10 30
NCP: WT
H3 K79A
j
fraction H2A consumed
NCP: WT
H3 K79A
k
BRCA1/BARD1
Time (min): 0 10 30 0 10 30 0 10 30
NCP: WT
H3 K79me1
H3 K79me2
l
Ring1b/Bmi1
Time (min): 0 10 30 0 10 30 0 10 30
NCP: WT
H3 K79me1
H3 K79me2
m
RNF168
Time (min): 0 10 30 0 10 30 0 10 30
NCP: WT
H3 K79me1
H3 K79me2
n
BRCA1/BARD1
fraction H2A consumed
NCP: WT
H3 K79me1
H3 K79me2
o
Ring1b/Bmi1
fraction H2A consumed
NCP: WT
H3 K79me1
H3 K79me2
p
RNF168
fraction H2A consumed
NCP: WT
H3 K79me1
H3 K79me2

Extended Data Figure 6. Comparison of nucleosome requirements for H2A-modifying E3s. (a) Comparison of the conserved BRCA1 and Ring1b arginine anchor motif interactions (PDB: 4R8P). Complexes were aligned by H2B on the bound face of the NCP. H2A from the Ring1b-UbcH5c/Bmi1 nucleosome complex is shown in gray. **(b)** Nucleosome ubiquitylation assays using the indicated H2A/H2B acidic patch NCP mutants with BRCA1/BARD1 (top) and Ring1b/Bmi1 (bottom). **(c)** Comparison of interactions between the RING domains of BRCA1/BARD1 and Ring1b/Bmi1 with the H2B αC helix residues assayed in panels d and e. **(d)** Representative nucleosome ubiquitylation assays using the indicated H2B αC helix NCP mutants with BRCA1/BARD1 (top) or Ring1b/Bmi1 (bottom). **(e)** Quantified assays using the NCP mutants and E3s from panel d **(f, g)** Same experimental set-up as in panels d and e using H2B/H4 cleft NCP mutants. **(h)** BARD1-histone binding interface with side chain density for H3 Lys79 and Phe78 shown as semi-transparent surface. **(i-j)** Same experimental set-up as panels d-e using H3 Lys79Ala NCP mutant. **(k-m)** Representative nucleosome ubiquitylation assays using H3 Lys79me1 and Lys79me2 mimetic NCP substrates with the indicated E3s. **(n-p)** Quantified assays using H3 Lys 79 methylation mimetic nucleosome substrates and the indicated E3s. Quantified ubiquitylation assays show the mean and error bars are $\pm$ 1-s.d. of n=3 independent experiments (except panel g where n=6 for wild-type) plotted for 10-minute (gray bars) and 30-minute (colored bars) time points. P-values for each mutant were calculated using a two-tailed Student's t-test compared to wild-type (* $p \leq 0.05$, ** $p \leq 0.005$, ns = not significant). Panels g (top), and n are also shown in figure 3. Uncropped blots in panels b, d, f, i, and k-m and data from graphs in panels e, g, j, and n-p are available as source data.

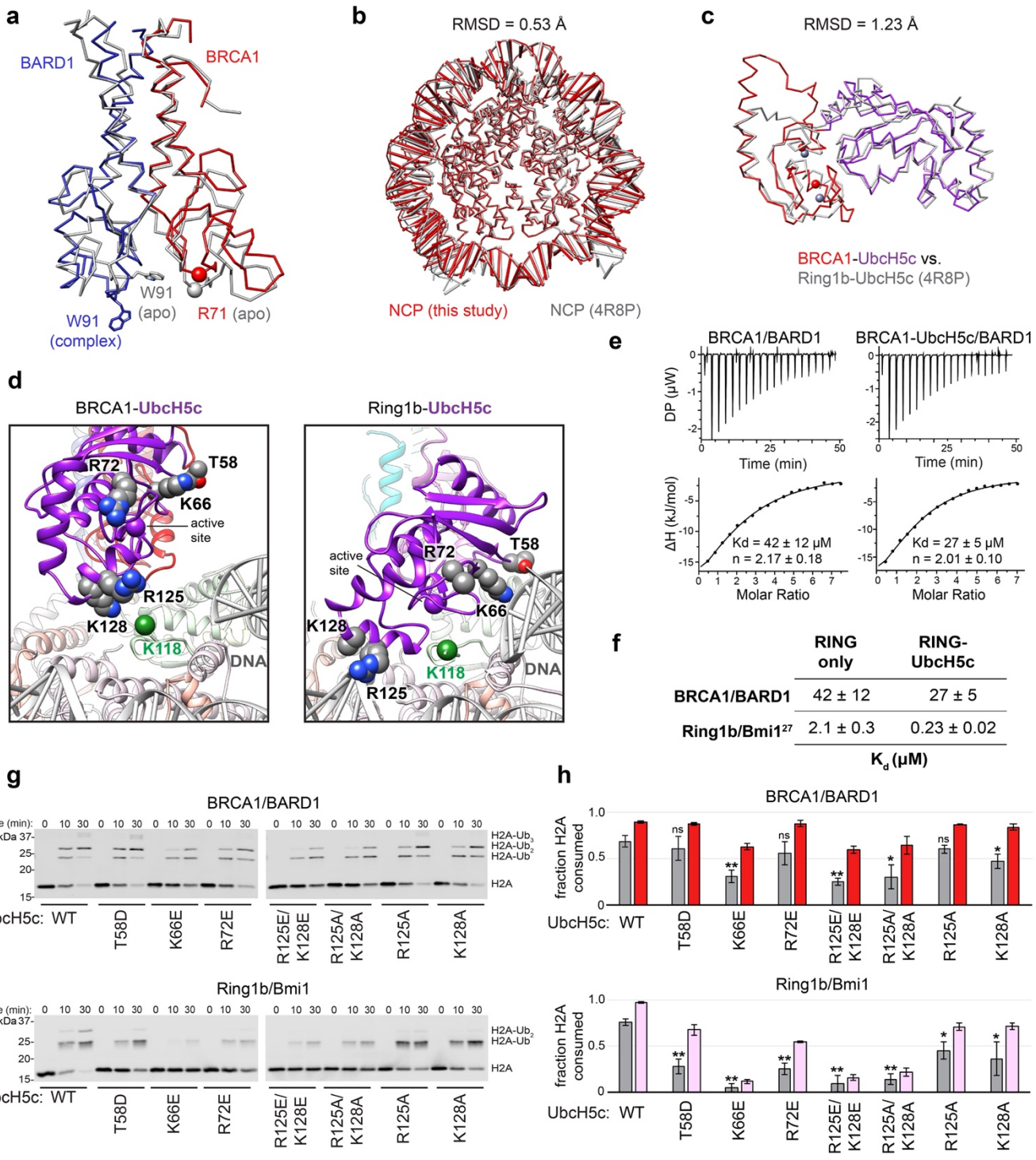

Extended Data Figure 7. Comparison to the unbound RING and Ring1b-UbcH5c/Bmi1/nucleosome complexes. (a) Structural alignment of the BRCA1/BARD1 RING from the NCP complex and the unbound structure (PDB: 1JM7, NMR ensemble model 1) aligned by the four-helix bundle. **(b)** Structural alignment of the NCP from the indicated complexes by H2B on the E3-E2-bound side. **(c)** Structural alignment of BRCA1-UbcH5c and

Ring1b-UbcH5c from E3-E2/NCP complexes. **(d)** Comparison of BRCA1-bound and Ring1b-bound UbcH5c in NCP complexes showing side chains mutated in panels g and h. Some atoms for Arg72 and Lys128 are not modelled in the Ring1b-bound structure. Green spheres are Cα of H2A Lys118. **(e)** Analysis of NCP binding by the BRCA1/BARD1 RING heterodimer and the BRCA1-UbcH5c/BARD1 (WT UbcH5c active site) chimera by ITC. Data are representative of n=2 experiments. **(f)** Comparison of NCP binding strength for BRCA1/BARD1 and Ring1b/Bmi1 RING and E3-E2 chimeras. Affinities for BRCA1/BARD1 were determined using ITC while affinities for Ring1b/Bmi1 were measured using a fluorescence based binding assay. **(g)** Representative nucleosome ubiquitylation assays using BRCA1/BARD1 or Ring1b/Bmi1 with indicated UbcH5c mutants. **(h)** Quantification of nucleosome ubiquitylation using the UbcH5c mutants and E3s from panel g. Data show the mean and error bars are ± 1-s.d. of n=3 independent experiments plotted for 10-minute (gray bars) and 30-minute (colored bars) time points of the reactions. P-values for each mutant were calculated using a two-tailed Student's t-test compared to wild-type (* $p \leq 0.05$, ** $p \leq 0.005$, ns = not significant). Uncropped blots in panel g and data from graphs in panel h are available as source data.

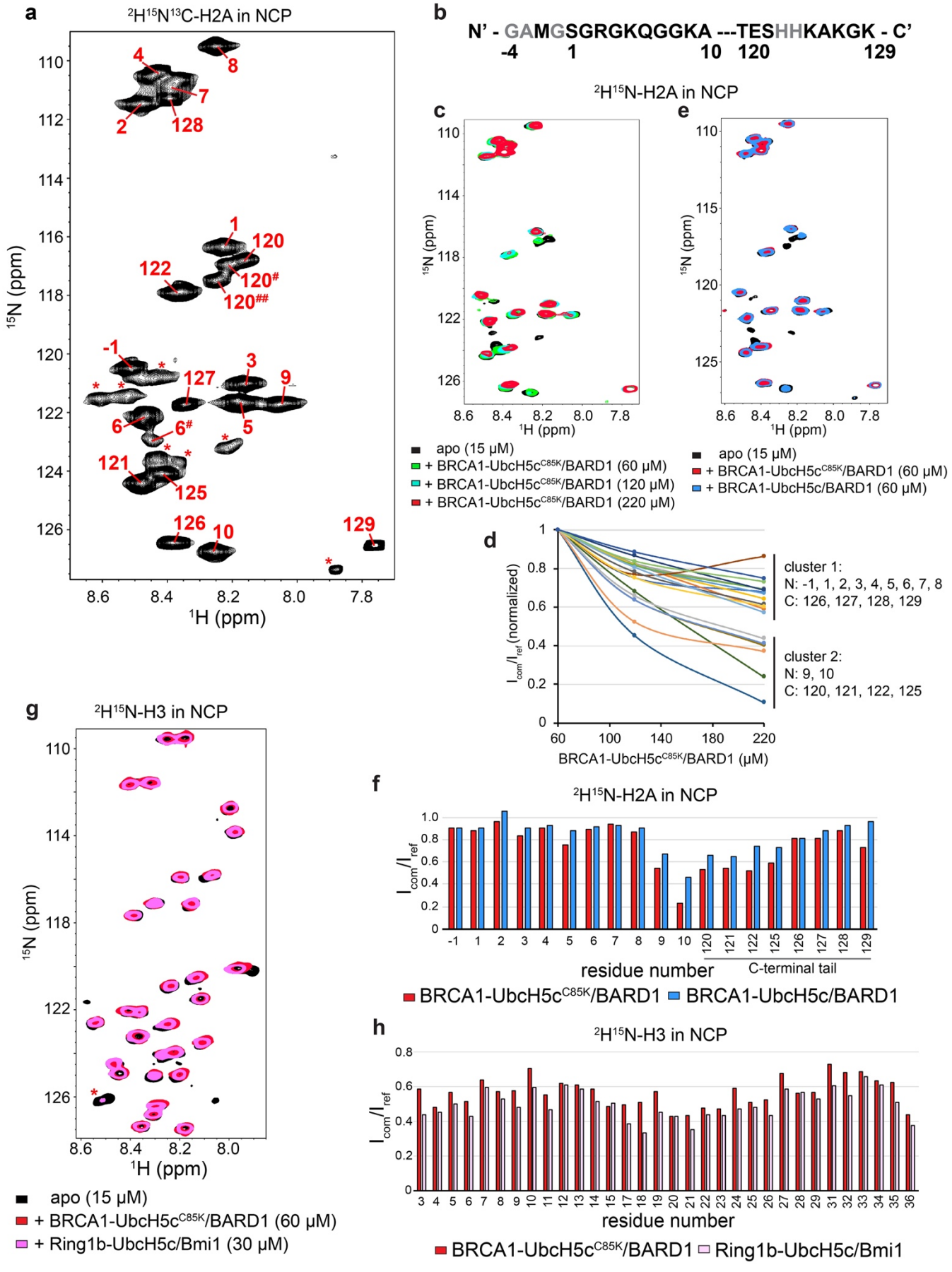
a
$^{2}H^{15}N^{13}C$-H2A in NCP
^{15}N (ppm)
^{1}H (ppm)
b
N' - GAMGSGRGKQGGKA ---TESHHKAKGK - C'
-4 1 10 120 129
$^{2}H^{15}N$-H2A in NCP
c
e
apo (15 μM)
+ BRCA1-UbcH5c^{C85K}/BARD1 (60 μM)
+ BRCA1-UbcH5c^{C85K}/BARD1 (120 μM)
+ BRCA1-UbcH5c^{C85K}/BARD1 (220 μM)
+ BRCA1-UbcH5c/BARD1 (60 μM)
d
I_{com}/I_{ref} (normalized)
BRCA1-UbcH5c^{C85K}/BARD1 (μM)
cluster 1:
N: -1, 1, 2, 3, 4, 5, 6, 7, 8
C: 126, 127, 128, 129
cluster 2:
N: 9, 10
C: 120, 121, 122, 125
f
$^{2}H^{15}N$-H2A in NCP
I_{com}/I_{ref}
residue number
C-terminal tail
BRCA1-UbcH5c^{C85K}/BARD1
BRCA1-UbcH5c/BARD1
g
$^{2}H^{15}N$-H3 in NCP
apo (15 μM)
+ BRCA1-UbcH5c^{C85K}/BARD1 (60 μM)
+ Ring1b-UbcH5c/Bmi1 (30 μM)
h
$^{2}H^{15}N$-H3 in NCP
I_{com}/I_{ref}
residue number
BRCA1-UbcH5c^{C85K}/BARD1
Ring1b-UbcH5c/Bmi1

Extended Data Figure 8. NMR analysis of E3-E2/nucleosome complexes. (a) $^{1}H^{15}N$**-**TROSY-HSQC spectrum of $^{2}H^{15}N^{13}C$-H2A in NCP (~180 μM sample) with residue assignments plotted. Signals with asterisks were not able to be assigned. Residues $120^{\#}$ and $120^{\#\#}$ appear to be alternate confirmations of 120 based on Cα chemical shifts of 119 and 120 in the HNCA and HNCOCA spectra. Assignment of the minor population for $6^{\#}$ was based on the similar back bone H, N, and Ca chemical shifts as compared to the major residue 6 population. **(b)** Sequence of H2A N- and C-terminal tails observable in NMR spectrum in panel a with assigned residues bolded. **(c)** Overlay of $^{1}H^{15}N$**-**TROSY-HSQC spectra of $^{2}H^{15}N$-H2A in NCP, with BRCA1-UbcH5c^{C85K}/BARD1 added at increasing concentrations. **(d)** Quantification of signal broadening from spectra in panel c as a function of BRCA1-UbcH5c^{C85K}/BARD1 added, normalized to the first titration point (60 μM addition). Signal behavior clusters into two groups, where resonances from the extreme N- and C- terminal tails lose signal at a similar rate indicative of non-specific broadening (cluster 1). **(e)** Overlay of $^{1}H^{15}N$**-**TROSY-HSQC spectra of $^{2}H^{15}N$-H2A in NCP (black, bottom), with BRCA1-UbcH5c^{C85K}/BARD1 added (red, middle), or BRCA1-UbcH5c/BARD1 (blue, top). **(f)** Quantification of intensity for H2A signals from spectra in panel e comparing the bound complexes to the apo reference spectrum (I_{com}/I_{ref}). **(g)** Overlay of $^{1}H^{15}N$**-**TROSY-HSQC spectra of $^{2}H^{15}N$-H3 in NCP (black, bottom), with BRCA1-UbcH5c^{C85K}/BARD1 added (red, middle), or Ring1b-UbcH5c/Bmi1 (pink, top). **(h)** Quantification of intensity for H2A signals from spectra in panel g comparing the bound complexes to the apo reference spectrum (I_{com}/I_{ref}). Concentrations of E3-E2 complexes added as well as labelled NCPs in the experiment are indicated in the figure. Data from graphs in panels d, f, and h are available as source data.

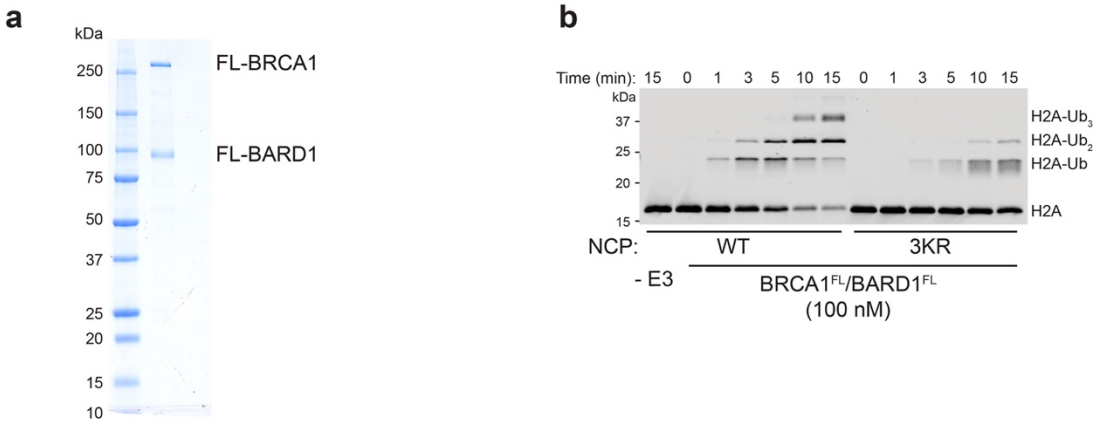

Extended Data Figure 9. Biochemical purity and nucleosome ubiquitylation specificity of full-length BRCA1/BARD1. (a) Coomassie-stained gel of purified full-length BRCA1/BARD1. **(b)** Nucleosome ubiquitylation assay using full-length BRCA1/BARD1 and wild-type (WT) or H2A Lys125/127/129Arg (3KR) nucleosome substrates**.** Uncropped gels/blots in panels a and b are available as source data.

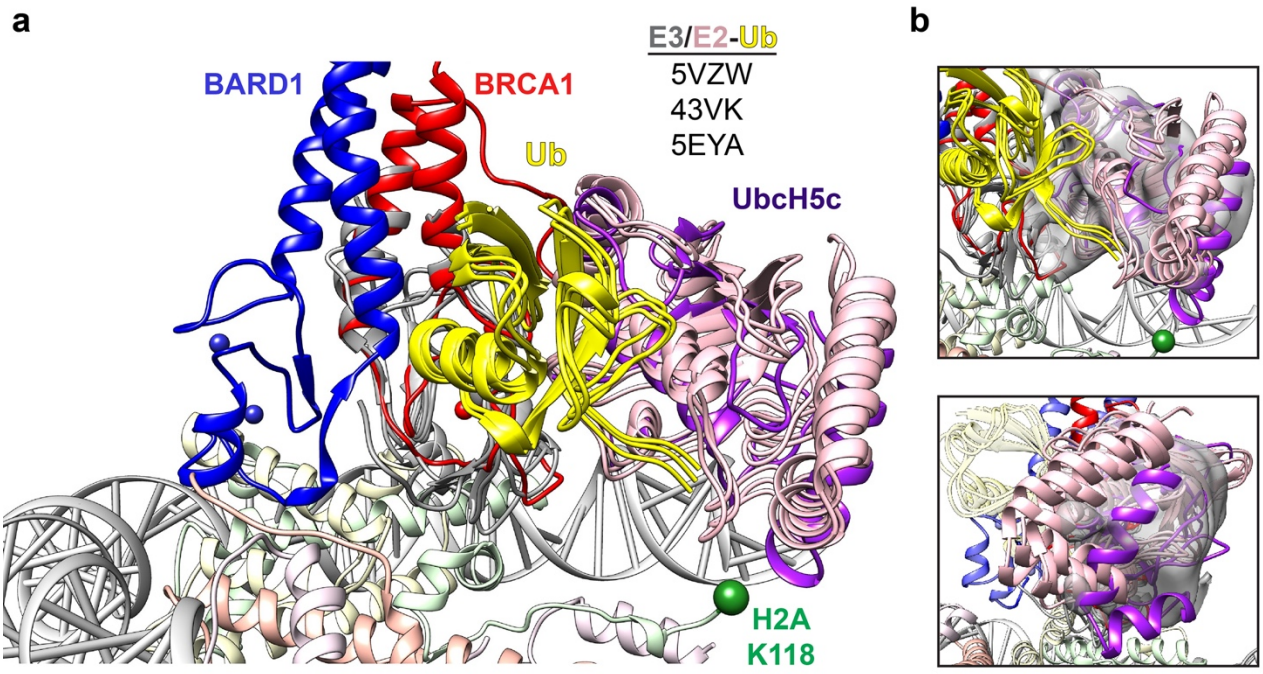

Extended Data Figure 10. Compatibility of closed E2~Ub conformations. (a) Structural overlay of BRCA1-UbcH5c/BARD1/nucleosome complex with indicated RING/E2-Ub crystal structures aligned to the RING domain of BRCA1. **(b)** Comparison of UbcH5c location in the nucleosome complex (purple) and indicated reported RING/E2-Ub structures from panel a with cryo-EM density for UbcH5c shown as gray volume. Density for the E2 is shown from a map that was locally filtered in CryoSparc to decrease excessive noise introduced from map sharpening.

Tables

Table I. Cryo-EM data collection, refinement and validation statistics

	BRCA1-UbcH5c/BARD1 nucleosome complex (EMD-22581, PDB 7JZV)
Data collection and processing	
Magnification	130,000
Voltage (kV)	300
Electron exposure (e^{-}/Å^2)	90
Defocus range (μm)	-0.7 to -2.7
Pixel size (Å)	1.05
Symmetry imposed	*C*1
Initial particle images (no.)	1,072,535
Final particle images (no.)	21,479
Map resolution (Å)	3.9
FSC threshold	0.143
Map resolution range (Å)	3.4-7.8
Refinement	
Map sharpening *B* factor (Å^2)	-85
Model composition	
Non-hydrogen atoms	14,339
Protein residues	1,093
Nucleotides	278
Ligands	Zn^{2+}(4)
R.m.s. deviations	
Bond lengths (Å)	0.012
Bond angles (°)	1.28
Validation	
MolProbity score	0.80
Clashscore	1.02
Poor rotamers (%)	0.22
Ramachandran plot	
Favored (%)	98.32
Allowed (%)	1.49
Disallowed (%)	0.19

Methods

DNA manipulation and protein purification

The BRCA1(1-104)-$(GS)_n$-UbcH5c(2-147) E3-E2 chimeras were constructed using splicing by overlap extension (SOE) PCR[56]. The GS-linker and an N-terminal precision protease (H3C) cleavage site were added by incorporation into primer sequences. The assembled fragment was sub-cloned into a pCOT7n expression vector downstream of 6xHis tag. After comparison of linker length by EMSA, a construct with sequence BRCA1(1-104)-GSGSGSG-UbcH5c(2-147)/BARD1(26-140) with either Cys85 or Cys85Lys UbcH5c active site was selected for all subsequent biochemical, cryo-EM, and NMR experiments. An H3C cleavage site was also added onto the BRCA1(1-112) construct and cloned into the same pCOT7n expression vector. Untagged human H2A type-2A was inserted into pTEV19 to make the 6xHis-TEV-H2A construct. A VSV-G epitope tag was introduced on a primer to make the 6xHis-TEV-VSV-G-H2A construct. UbcH5c(2-147) was sub-cloned into a modified pET28 vector downstream of a 6xHis-SUMO tag. All mutants were generated by QuikChange site-directed mutagenesis (Agilent) or SOE PCR and sub-cloning. All constructs were verified by Sanger sequencing. Human Uba1 (E1), UbcH5a, UbcH5b, UbcH5c (untagged), Ube2e1, Ube2e2, Ube2e3, ubiquitin, and BRCA1(1-112)/BARD1(26-140) were purified as previously described[29,57,58]. GST-RNF168(1-189) was purified as previously described without cleaving off the GST tag[20]. All BRCA1/BARD1 RING heterodimer constructs were expressed by co-transformation of two plasmids containing BRCA1 (pCOT7n vector) and BARD1 (pET28n vector). For BRCA1(1-112)/BARD1(26-140) used in cryo-EM, ITC, and NMR experiments, an additional step was added to remove the 6xHis-tag on BRCA1 with GST-H3C protease on-column overnight as described for the BRCA1-UbcH5c/BARD1 E3-E2 chimera in detail below. The cleaved product was concentrated before a final SEC step using a Superdex 75 column equilibrated in 20 mM HEPES pH 7.5, 150 mM NaCl, 1 mM DTT on an Akta FPLC (GE Healthcare). Full-length BRCA1/BARD1 was co-

expressed using the Bac-to-Bac expression system in Hi5 insect cells and purified as previously described in extensive detail[46].

For E2 and E3 expression, *Escherichia coli* (BL21 DE3) cultures were grown to an optical density at 600 nm (OD_{600nm}) of 0.6-0.8 in LB or MOPS media supplemented with ^{15}N-NH_4Cl for NMR isotopic labelling (Cambridge Isotope Labs). Media was supplemented with 100 μM $ZnCl_2$ for RING constructs. Protein expression was induced with 0.2 mM IPTG at 16 °C for 16-18 hours. Bacterial pellets were harvested by centrifugation, resuspended in lysis buffer (25 mM Tris-HCl pH 7.6, 500 mM NaCl, 10 mM imidazole) supplemented with SIGMAFAST EDTA-free protease inhibitor cocktail (Sigma) and 1 mM PMSF, lysed by 2 passages through a French pressure cell, and clarified by centrifugation at 17,000xg at 4 °C using a Sorvall LYNX 6000 centrifuge (Thermo Fisher). The supernatants containing 6xHis-SUMO-UbcH5c or 6xHis-H3C-BRCA1-UbcH5c/BARD1 were bound to a 5 mL HisTrap Ni^{2+}-NTA column (GE Healthcare). After extensive washing with lysis buffer containing 50 mM imidazole, proteins were cleaved on-column using GST-SENP1 or GST-H3C protease (prepared in-house) overnight at 4 °C in 25 mM Tris-HCl pH 7.6, 200 mM NaCl, 10 mM imidazole, 1 mM DTT supplemented with protease inhibitors leupeptin, pepstatin A, and aprotinin (1 μg/mL each). Cleaved protein was washed off the column, concentrated, and purified by SEC using a Superdex 75 column (GE Healthcare) equilibrated in 25 mM HEPES-NaOH pH 7.5, 150 mM NaCl, 1 mM DTT (BRCA1-UbcH5c/BARD1) or 25 mM phosphate pH 7.0, 150 mM NaCl (UbcH5c). To purify Ring1b/Bmi1 constructs (gift from Dr. Song Tan), bacterial supernatants containing STR-10xHis-TEV-Ring1b(2-116)/Bmi1(2-109) or STR-10xHis-TEV-Ring1b(2-116)-GSGSRS-UbcH5c(2-147)/Bmi1(2-109) were bound to a 5 mL HisTrap Ni^{2+}-NTA column (GE Healthcare) in lysis buffer, washed with buffer containing 50 mM imidazole, and eluted in buffer containing 300 mM imidazole. Affinity tags were removed by incubating with 6xHis-TEV protease (prepared in-

house) overnight at 4 °C in TEV cleavage buffer (20 mM Tris pH 7.4, 10 μM $ZnCl_2$, 200 mM NaCl, 5 mM citrate, 2 mM 2-mercaptoethanol, 10 mM imidazole). Cleaved product was filtered over Ni^{2+}-NTA resin to re-capture the affinity tag, 6xHis-TEV, and impurities. The flow-through was concentrated and further purified using a Superdex 75 column (GE Healthcare) equilibrated in 25 mM HEPES-NaOH pH 7.5, 150 mM NaCl, 1 mM DTT.

Wild-type and mutant human histones 6xHis-TEV-H2A type-2A (± N-terminal VSV-G tag), untagged H2A type-2A, H2B type-1K, H3.2 (C110A), and H4 were expressed separately in *E. coli* (BL21 or BL21 pLysS) to an OD_{600nm} of 0.6-0.8 in LB or M9 minimal media and induced with 0.5 mM IPTG for 3 hours (LB) or overnight (M9) at 37 °C. For NMR, M9 media was made in deuterium oxide (D_2O) and supplemented with ^{15}N-NH_4Cl and fully deuterated ^{12}C-D_7-glucose or ^{13}C-D_7-glucose to generate perdeuterated histone protein (Cambridge Isotope Labs). Histone octamer formation and purification was performed using the one-pot refolding method[59]. Briefly, *E. coli* cell pellets containing all four histones (including 6xHis-TEV-H2A) were mixed together, lysed by sonication in lysis buffer (20 mM Tris-HCl pH 7.5, 500 mM NaCl, 1 mM DTT) then centrifuged (17,000xg, 4 °C) for 30 minutes. The pellet was washed once with lysis buffer, resuspended in extraction buffer (sodium acetate pH 5.2, 7M guanidinium-HCl, 5 mM TCEP) and insoluble debris were removed by centrifugation. Octamers were refolded by dialysis in refolding buffer (20 mM Tris-HCl pH 7.5, 2M NaCl, 10 mM Imidazole, 2 mM ß-mercaptoethanol). After centrifugation, the supernatant containing octamers was purified using a 5 mL HisTrap Ni^{2+}-NTA column in refolding buffer according to manufacturer's instructions (GE healthcare). The 6xHis-tag was removed using TEV protease (produced in-house) overnight at 4 °C in refolding buffer without imidazole. Octamers were further purified using a Superdex 200 column in 20 mM Tris-HCl pH 7.5, 2 M NaCl, 1 mM DTT (GE Healthcare). For assays with H3 K79 methylation mimetic nucleosomes, wild-type and H3 K79C histones were individually purified using well-established protocols[60,61]. H3 K79C methylation mimetics were generated as

previously described[62]. Assembled octamers were flash frozen and stored at -80 °C in 20 mM Tris-HCl pH 7.5, 2 M NaCl, 1 mM DTT. Large-scale 153 base-pair Widom 601 DNA (gift from Dr. Lewis Kay) purification was performed essentially as described[63] using a plasmid containing 32 tandem repeats separated by *EcoRV* sites, and NCPs were reconstituted using the standard salt-dialysis method[63]. As a final step, NCPs were purified by SEC using a Superdex 200 increase 10/300 column (GE Healthcare) equilibrated with 20 mM HEPES-NaOH pH 7.5, 10-50 mM NaCl, 0.01% NaN_3, concentrated, and stored on ice for up to two weeks. NCP concentrations were determined by dilution in 0.25 M NaOH and measurement of ultraviolet absorbance at 260 nm using the extinction coefficient 2,866,600 $M^{-1}cm^{-1}$ to quantify the DNA component. Protein concentrations were determined by their ultraviolet absorbance at 280 nm and confirmed with Coomassie-stained SDS-PAGE.

Electrophoretic mobility shift assays (EMSA)

For EMSA assays in Figs. 1 and Extended Data Fig. 1, 50 nM NCPs were incubated with indicated amount of BRCA1/BARD1 or BRCA1-UbcH5c/BARD1 for 20 mins on ice in 10 mM Tris-HCl pH 7.5, 75 mM NaCl, 1 mM DTT. Sucrose was added to a final concentration of 6%, and samples were run on a pre-chilled 5% polyacrylamide 0.5X TBE gel (40 mM Tris pH 8.3, 45 mM boric acid, 1 mM EDTA) at 140 V for 45 minutes at 4°C. Gels were stained with gel-red dye (Biotium) and visualized using a BioRad gel dock. For assays including full-length BRCA1/BARD1 (Fig. 7), 50 nM NCP were incubated with the indicated amount of $BRCA1^{FL}$/$BARD1^{FL}$ or $BRCA1^{RING}$/$BARD1^{RING}$ in 10 μL of buffer (10 mM Tris-HCl, pH 7.5, 0.125 mM DTT, 0.0025% Igepal, 70 mM KCl) on ice for 20 mins. After the addition of 2 μl of gel loading buffer (50% glycerol, 20 mM Tris-HCl, pH 7.4, and 0.05% orange G), NCP complexes were resolved by 1% agarose gel electrophoresis in TAE buffer (40 mM Tris, 20 mM Acetate and 1 mM EDTA) at 4°C with 140 V for 30 mins. The gels were stained in fresh ethidium bromide solution and imaged using a ChemiDocTM MP Imaging System.

SEC-MALS and Analytical SEC binding assays

For SEC-MALS, NCPs (15 μM) were incubated with or without BRCA1-UbcH5c^{C85K}/BARD1 (45 μM) in 20 mM HEPES-NaOH pH 7.5, 35 mM NaCl, 0.5 mM TCEP and injected onto a Agilent HPLC with a Sepax SRT-SEC column equilibrated in the same buffer coupled to a Wyatt miniDAWN TREOS and Optilab T-rEX differential refractive index detector. Molar mass was calculated from the Raleigh ratio based on multi-angle (static) light scattering and protein concentration from the change in refractive index (dn/dc = 0.185). Analysis was performed using Wyatt Astra 7 software. For SEC binding experiments, 10 μM NCPs were incubated with 30 μM of the indicated BRCA1-UbcH5c/BARD1 construct at room temperature for 30 mins in 300 μL binding buffer (20 mM HEPES-NaOH pH 7.5, 25-100 mM NaCl, 0.5 mM TCEP). Samples were then injected onto a Superdex 200 increase (10/300) column equilibrated in binding buffer with the indicated amount of NaCl (25-100 mM) using an Akta FPLC system (GE Healthcare).

Nucleosome ubiquitylation assays

Unless explicitly noted in figure legends, NCP ubiquitylation assays were performed in a reaction mixture containing 0.2 μM E1 (Uba1), 1 μM E2 (UbcH5c), 2 μM E3, 20 μM ubiquitin, and 0.5 μM NCPs in 25 mM HEPES-NaOH pH 7.5, 150 mM NaCl. Several assays (Extended Data Figs 1e and 6b) were performed in a reaction mixture containing 1 μM E1 (Uba1), 4 μM E2 (UbcH5c), 8 μM E3, 20 μM ubiquitin, and 0.5 μM NCPs in 25 mM phosphate pH 7.0, 150 mM NaCl. Unless noted, reactions were performed with wild-type and mutant BRCA1$^{1-112}$/BARD1$^{26-140}$ (referred to as RING heterodimer or BRCA1^{RING}/BARD1^{RING}) as the E3. After collecting zero time-point samples, reactions were brought to 37 °C and 5 mM $MgCl_2$/ATP were added. Reactions were quenched at indicated time points by 1:1 dilution with 4x reducing SDS loading buffer and analyzed by Western blot using rabbit anti-VSV-G (Sigma, V4888), mouse anti-H2A

(EMD Millipore, 07-146), mouse anti-H2B (BioRad, VPA00384), rabbit anti-H3 (Abcam, ab1791), or rabbit anti-H4 (Abcam, ab31830) antibodies. Blots were incubated with fluorophore-conjugated anti-mouse (Invitrogen, A21058) or anti-rabbit (Cell Signaling, 5151S) secondary antibodies and visualized using a Licor Odyssey scanner. Quantification was performed using Image Studio software (Licor) by drawing a box measuring the total band intensity for unmodified H2A at each time-point, subtracting background signal, and normalizing to the zero time-point of each reaction.

E2~Ub formation and lysine reactivity assays

For E2 lysine discharge assays, E2~Ub was formed in a reaction consisting of 0.3 μM E1 (Uba1), 60 μM UbcH5c, 120 μM Ubiquitin, 10 mM $MgCl_2$/ATP in 25 mM sodium phosphate, pH 7.0, 150 mM NaCl (PBS) at 37 °C for 30 minutes. The reaction was quenched by addition of 50 mM EDTA, pH 7.4 for 10 minutes, and the lysine discharge reaction was initiated by a 1:1 dilution of the charging reaction into PBS supplemented with 50 mM lysine with or without 3 μM of the indicated E3 at 30 °C. Time-points were taken by mixing the reaction 1:1 with 4x load dye without reducing agent, resolved on an SDS-PAGE gel and stained with Coomassie blue, and visualized on a BioRad gel dock. Quantification was performed in ImageJ (NIH) by drawing a box around the E2~Ub conjugate and measuring the total area of signal and normalizing to the zero time-point. E2 charging experiments were performed using a reaction mixture of 40 μM UbcH5c or BRCA1-UbcH5c/BARD1 (WT or Cys85Lys active site), 2 μM E1 (Uba1), 80 μM Ub, and 10 mM $MgCl_2$/ATP in 50 mM sodium phosphate pH 7.0, 150 mM NaCl (UbcH5c WT active site) or 50 mM CAPS pH 10, 150 mM NaCl (UbcH5c Cys85Lys active site). Reactions were quenched at indicated time points by 1:1 dilution into 4x SDS-PAGE loading dye (± β-mercaptoethanol) and analyzed by Coomassie stained SDS-PAGE gel.

Isothermal Titration Calorimetry (ITC)

For ITC analysis, all proteins were extensively buffer exchanged by dialysis into 20 mM HEPES-NaOH pH 7.5, 50 mM NaCl, 0.5 mM TCEP. Measurements were performed on a MicroCal PEAQ-ITC (Malvern) at 25 °C spanning 19 injections with a stirring speed of 750 rpm. The cell contained 20 μM NCPs and the syringe contained ~800 μM of indicated ligand. Control experiments where ligand was injected into buffer were performed. Binding isotherms were fit to a one-site binding model and figures formatted in the Malvern PEAQ-ITC analysis software package.

Cryo-EM sample preparation, image acquisition, data processing, and model building

Extensive methods related to cryo-EM structure determination can be found as a supplementary note attached to the end of this document.

Molecular graphics and structural and sequence alignments

All figures depicting molecular structures were prepared using UCSF Chimera[64] or ChimeraX[65] software. Alignments were performed using the MatchMaker function in Chimera by best aligning chain, specific chains, or specified residues depending on the analysis. BRCA1/BARD1 and Ring1b/Bmi1 sequence alignments were performed using BLAST[66] (NCBI). For structure based alignment of H2A variants, atomic models of nucleosomes containing canonical H2A (PDB id: 5B0Z), macroH2A1 (1U35), H2A.J (6KVD), H2A.X (6K1J), H2A.V (3WAA), H2A.Z (5B33) were aligned and inspected to confirm overlap in the position equivalent to Lys118 from canonical H2A.

NMR sample preparation and data collection

All NMR experiments were collected on an Avance 600 MHz spectrometer equipped with a cryoprobe. Data were processed with the NMRpipe[67] package and visualized in NMRviewJ[68]. All

spectra of labelled NCP samples were collected at 25 °C in 20 mM MOPS pH 7.0, 50 mM NaCl, 0.5 mM TCEP in the presence of 10% D_2O. Spectra of BRCA1/BARD1 RING heterodimers were collected at 30 °C in 25 mM phosphate pH 7.0, 150 mM NaCl, 10% D_2O. To assign the H2A tails in the NCP, a standard set of multidimensional TROSY NMR experiments (HNCA, HNCOCA, HNCACB) were used. Triple-resonance experiments were performed with 180 μM $^{2}H^{15}N^{13}C$-H2A NCPs where all other histones and DNA contained natural abundance isotopes. The H2A construct for NMR contained a short, non-native N-terminal sequence after TEV cleavage (GAMG). Assignments were performed by correlating peaks among the triple resonance experiments in NMRViewJ.

For $^{1}H^{15}N$-TROSY-HSQC NMR binding experiments, concentrated NCPs were buffer exchanged into 20 mM MOPS pH 7.0, 10 mM NaCl, 0.5 mM TCEP. BRCA1-UbcH5c/BARD1 and Ring1b-UbcH5c/Bmi1 constructs were buffer exchanged into 20 mM MOPS pH 7.0, 150 mM NaCl, 0.5 mM TCEP to prevent self-association in the absence of NCP binding partner in low-salt. NMR samples containing 15 μM $^{2}H^{15}N$-H2A NCPs were assembled by stepwise addition of E3-E2 binding partner over ~30 minutes until saturation of the complex. The final salt concentration of all NMR samples was adjusted to 50 mM NaCl and supplemented with 10% D_2O. For the Ring1b-UbcH5c/Bmi1/NCP complex, irreversible aggregation was observed immediately after saturation (30 μM), resulting in minimal sample loss. BRCA1-UbcH5c^{C85K}/BARD1 did not aggregate with the NCP and was added to a final concentration of 60 μM (or more) to account for its weaker binding affinity. NMR samples with $^{2}H^{15}N$-H3 NCPs were assembled identically to H2A-labelled samples. Resonance assignments for the N-terminal tail of H3 were directly transferred from a previous study[69]. Peak intensities were measured using NMRViewJ, and the intensity of resonances in the bound complex spectrum were compared to those in the apo reference spectrum (I_{com}/I_{ref}).

Data Availability Statement

The cryo-EM map of the BRCA1-UbcH5c/BARD1/nucleosome complex was deposited to the Electron Microscopy Data Bank under accession code EMD-22581 and the atomic model to the Protein Data Bank under accession code 7JZV. NMR chemical shift assignments were deposited to the Biological Magnetic Resonance Data bank under accession code 50604. Uncropped gels/blots and statistical source data are available online linked to this article. Plasmid reagents generated in this study can be obtained upon request from the corresponding author Dr. Rachel Klevit.

References (Methods Only)

56. Aiyar, A., Xiang, Y. & Leis, J. Site-directed mutagenesis using overlap extension PCR. *Methods Mol. Biol. Clifton NJ* **57**, 177–191 (1996).

57. Christensen, D. E., Brzovic, P. S. & Klevit, R. E. E2-BRCA1 RING interactions dictate synthesis of mono- or specific polyubiquitin chain linkages. *Nat. Struct. Mol. Biol.* **14**, 941–948 (2007).

58. Lazar, G. A., Desjarlais, J. R. & Handel, T. M. De novo design of the hydrophobic core of ubiquitin. *Protein Sci. Publ. Protein Soc.* **6**, 1167–1178 (1997).

59. Lee, Y.-T., Gibbons, G., Lee, S. Y., Nikolovska-Coleska, Z. & Dou, Y. One-pot refolding of core histones from bacterial inclusion bodies allows rapid reconstitution of histone octamer. *Protein Expr. Purif.* **110**, 89–94 (2015).

60. Luger, K., Rechsteiner, T. J. & Richmond, T. J. Preparation of nucleosome core particle from recombinant histones. *Methods Enzymol.* **304**, 3–19 (1999).

61. Dhall, A. *et al.* Sumoylated human histone H4 prevents chromatin compaction by inhibiting long-range internucleosomal interactions. *J. Biol. Chem.* **289**, 33827–33837 (2014).

62. Simon, M. D. *et al.* The site-specific installation of methyl-lysine analogs into recombinant histones. *Cell* **128**, 1003–1012 (2007).

63. Dyer, P. N. *et al.* Reconstitution of nucleosome core particles from recombinant histones and DNA. *Methods Enzymol.* **375**, 23–44 (2004).

64. Pettersen, E. F. *et al.* UCSF Chimera--a visualization system for exploratory research and analysis. *J. Comput. Chem.* **25**, 1605–1612 (2004).

65. Goddard, T. D. *et al.* UCSF ChimeraX: Meeting modern challenges in visualization and analysis. *Protein Sci. Publ. Protein Soc.* **27**, 14–25 (2018).

66. Altschul, S. F., Gish, W., Miller, W., Myers, E. W. & Lipman, D. J. Basic local alignment search tool. *J. Mol. Biol.* **215**, 403–410 (1990).

67. Delaglio, F. *et al.* NMRPipe: a multidimensional spectral processing system based on UNIX pipes. *J. Biomol. NMR* **6**, 277–293 (1995).

68. Johnson, B. A. Using NMRView to visualize and analyze the NMR spectra of macromolecules. *Methods Mol. Biol. Clifton NJ* **278**, 313–352 (2004).

69. Morrison, E. A., Bowerman, S., Sylvers, K. L., Wereszczynski, J. & Musselman, C. A. The conformation of the histone H3 tail inhibits association of the BPTF PHD finger with the nucleosome. *eLife* **7**, e31481 (2018).

Supplementary Notes

Supplementary Note 1: Cryo-EM Methods

Sample preparation and image acquisition

BRCA1-UbcH5c^{C85K}/BARD1 (200 μM) was mixed with NCPs (30 μM) at a final volume of 400 μL in 20 mM HEPES-NaOH pH 7.5, 35 mM NaCl, 1 mM DTT (reconstitution buffer) and incubated at room temperature for 30 mins. The complex was purified using a Superdex 200 increase 10/300 column (GE Healthcare) equilibrated in reconstitution buffer. Pooled fractions were concentrated to ~30 μM (Amicon) and stored on ice for up to two days. The complex was crosslinked by diluting 10 μL of concentrated complex directly into 80 μL of reconstitution buffer supplemented with 0.1% glutaraldehyde (Electron Microscopy Sciences) and incubated at room temperature for 10 minutes. Crosslinking was quenched by addition of 10 μL of 500 mM Tris-HCl pH 7.5, then buffer exchanged into reconstitution buffer using a pre-equilibrated 0.5 mL Zeba desalting spin column (GE Healthcare). The crosslinked complex (3 μL at ~2.5 μM) was immediately applied to glow-discharged C-Flat 400 mesh copper 2/2 grids (Protochips), blotted for 4 seconds with an FEI Vitrobot (20 °C, 100% humidity) and plunged into liquid ethane. Grids were stored under liquid nitrogen until imaging. Data were collected in two sessions on a Titan Krios (FEI) operating at 300 kV at a nominal magnification of 130,000x and equipped with a Quantum GIF energy filter (Gatan) operating in zero-loss mode with a 20 eV slit width. Movies were recorded on a K2 Summit Direct Detection camera operating in super-resolution mode with a calibrated pixel side of 0.525 Å per super-resolution pixel (1.05 Å physical pixel) and fractionated into 50 frames over a 10 second exposure with a total fluence of 90 $e^-/Å^2$ corresponding to a dose rate of 8.9 $e^-/Å^2/s$ using a defocus range of -0.7 to -2.7 μm. Leginon software was used for automated data collection.

Image processing and reconstructions

As data were collected in two sessions, dataset 1 was first used to generate an initial model, then combined with dataset 2 to generate the final structure. For initial model generation, pre-processing was performed in the Appion framework[1]. Movie frame alignment and dose-weighted summation of all 50 frames from 675 movies was performed using MotionCor2 binning images by a factor of two (1.05 Å per pixel)[2]. CTF parameters were estimated using CtfFind4[3]. Particles were automatically picked using DoG Picker[4], extracted using a box size of 256 pixels^2 binned to 128 pixels^2, and subjected to two rounds of 2D classification in Relion 3.0[5]. A refined particle subset was un-binned, imported into CryoSparc[6], and used for ab-initio reconstruction with 4 classes. A class representing the bound complex was selected, low-pass filtered to 40 Å, and used as an initial model for initial 3D classification in Relion 3.0 using the full-dataset as described below.

For structure determination, 675 movies from dataset 1 and 2,489 movies from dataset 2 were selected after manually inspecting the motion-corrected micrographs and their respective power spectra for vitreous ice quality and isotropic frame alignment. Movie frame alignment and dose-weighted summation of all 50 frames was performed using the Relion 3.0 implementation of MotionCor2 binning images by a factor of two (1.05 Å per pixel). Motion-corrected micrographs were imported into cisTEM for the remaining pre-processing steps[7]. CTF parameters were estimated using CtfFind4. Particles were picked using the reference-free ab initio blob-picker algorithm in cisTEM and particles over carbon areas were manually de-selected. Particles were extracted in a box size of 324 pixels^2 and subjected to two rounds of reference-free 2D-classification in cisTEM that produced a refined subset of 731,086 particles. Particles were imported into Relion 3.0 and re-extracted using a box size of 256 pixels^2 binned to 128 pixels^2. 3D classification into six classes was performed using the initial model from dataset 1 described above. One class containing ~263,000 unbound nucleosome particles was selected and sub-classified into five classes. About 58,000 particles from a well-aligning class were re-extracted

into a 256 pixels^2 box without binning and 3D refined with C1 symmetry to and estimated global resolution of ~3.7 Å. All particles that did not fall into the unbound nucleosome class (~468,000) were subjected to another round of 3D classification into three classes. A prominent BRCA1-UbcH5/BARD1/NCP bound class with ~199,000 particles was selected and re-extracted using a box size of 256 pixels^2 without binning. Particles were subjected to 3D refinement without imposing symmetry using the map of the complex from 3D classification as a new initial model and a soft mask encompassing the entire bound complex. This ensured that all bound E3-E2 particles were aligned on the same side of the pseudo-symmetrical NCP. The resulting map was well-aligned on the NCP while the E3-E2 density was low-resolution and noisy. Another round of 3D classification with four classes and regularization parameter T=20 was performed without refining particle Euler angles and shifts and using a soft mask that encompassed only the E3-E2 and some interface histone density. A class containing ~29,000 particles with well-defined BRCA1/BARD1 and UbcH5c density was selected and subjected to 3D refinement with a soft mask encompassing the entire E3-E2/NCP complex. CTF-refinement and Bayesian polishing were iteratively performed in Relion 3.0. Particles were imported into CryoSparc and subjected to one round of ab initio 3D-classification, yielding 21,479 particles with better-defined density in the BARD1 RING domain. The final particle subset was subjected to non-uniform (NU) refinement in CryoSparc[8] with C1 symmetry and a soft mask encompassing the whole complex. Local resolution from the non-uniform refinement half-maps was estimated at the 0.143 FSC cut-off using CryoSparc. Global resolution was estimated using half-maps from CryoSparc NU-refinement or density modification sharpening using the 3D-FSC server[9].

To address large variations in local-resolution, post-processing was carried out using Phenix density modification for cryo-EM[10]. Local sharpening was accomplished by setting the “blur_by_resolution_factor = 25” to decrease over sharpening artifacts. The input for density modification was both half-maps, the full map, the refined solvent mask from CryoSparc non-

uniform refinement, along with a molecular weight of 240,000 Da. A schematic flowchart of cryo-EM image processing strategy is outlined in Extended data Fig. 4, and additional details of cryo-EM data collection and structure determination are provided in Table I.

Model building

The structure of BRCA1-UbcH5c fusion and the nucleosome core particle were built using only comparative modeling, while the structure of BARD1 required additional de-novo modeling in order to properly accommodate the cryoEM density. To model the NCP, the Rosetta partial_thread application was used with alignments generated from hhblits and hhalign[11] to thread the histone sequences onto the template pdb 3LZ1. This threaded model was then docked unambiguously into the cryoEM density using UCSF Chimera[12]. To model the BRCA1-UbcH5c fusion, a multi-step process was used where initially comparative models were built for each domain separately without density. Hhblits was used to search for homology modeling templates for BRCA1 and UbcH5c separately, and then using the partial_thread application and the hhblits alignments the target BRCA1 and UbcH5c sequences were threaded onto each of the templates. The selected BRCA1 templates used were (PDB id, chain id), (1JM7, A), (2C2L, C), (6QU1, A) and the selected UbcH5c templates were: (PDB id, chain id), (4R8P, N), (5LBN, A), (2PE6, A), (4JUE, D), (2R0J, A), (2UCZ, A), (5A31, Q), (1AYZ, A), (2F4Z, A), (6CP0, B), (3VON, S), (3ONG, B), (4Q5E, C), (1YRV, A), (5BNB, B), (5V0R, A), (2KJH, A), (3FN1, B), (2EDI, A), (4YII, U). Then comparative models were made for both BRCA1 and UbcH5c by generating 2000 models with RosettaCM[13] using their respective templates. The top scoring model for both peptides were selected based on their Rosetta energy and each was docked into the density using UCSF Chimera.

The initial model of BARD1 was generated using a slightly modified version of the methods used on BRCA1 and UbcH5c. In addition to using hhblits to search for templates, trRosetta[14]

was used in order to predict the structure of the BARD1 model. The trRosetta prediction, was then used as a template in addition to the hhblits discovered templates (PDB id, chain id) (4CFG, A), (1JM7, B), and (2C2L, A) for RosettaCM. Again, 2000 models were generated with RosettaCM, the top scoring model was selected based on the rosetta energy and then was docked into the density using UCSF Chimera. After building coarse models that approximately fit the cryoEM density RosettaES[15] was used to refine residues 75-100 of BARD1, 36-40 of BRCA1, and to extend the N-terminus of H4 on the bound side of the NCP to residue 16. Next, RosettaCM was used to refine the entire complex in addition to closing the loop between BRCA1 and UbcH5c. 200 models were built, and the top scoring model as selected by Rosetta energy was selected.

Finally, the zinc ions were added with a custom pyRosetta script. Briefly, the script enforces the tetrahedral geometries of the cysteine and histidine residues that coordinate the Zn ions in addition to deprotonating the coordinating atoms. Histidine tautomers were selected based on Brzovic et al.[16], and then a combination of angle, distance, and dihedral constraints with values selected based on Tuow et al.[17], were added as restraints throughout Rosetta's FastRelax protocol[18]. Due to the inability of Rosetta to properly accommodate the heterogeneous density, the script also works to freeze side chains in the high/low resolutions (manually selected) so that incorrect rotamers would not be sampled separately at different interpreted densities and subsequently applies the Rosetta FastRelax. The script is available in the Rosetta macromolecular modeling package at: Rosetta/pyrosetta_scripts/apps/metal_coordination/danpf/brca1bard1-modeling/brca1bard1_model.py.

References (supplementary note)

1. Lander, G. C. *et al.* Appion: an integrated, database-driven pipeline to facilitate EM image processing. *J. Struct. Biol.* 166, 95–102 (2009).

2. Zheng, S. Q. *et al.* MotionCor2: anisotropic correction of beam-induced motion for improved cryo-electron microscopy. *Nat. Methods* 14, 331–332 (2017).

3. Rohou, A. & Grigorieff, N. CTFFIND4: Fast and accurate defocus estimation from electron micrographs. *J. Struct. Biol.* 192, 216–221 (2015).

4. Voss, N. R., Yoshioka, C. K., Radermacher, M., Potter, C. S. & Carragher, B. DoG Picker and TiltPicker: software tools to facilitate particle selection in single particle electron microscopy. *J. Struct. Biol.* 166, 205–213 (2009).

5. Zivanov, J. *et al.* New tools for automated high-resolution cryo-EM structure determination in RELION-3. *eLife* 7, e42166 (2018).

6. Punjani, A., Rubinstein, J. L., Fleet, D. J. & Brubaker, M. A. cryoSPARC: algorithms for rapid unsupervised cryo-EM structure determination. *Nat. Methods* 14, 290–296 (2017).

7. Grant, T., Rohou, A. & Grigorieff, N. cisTEM, user-friendly software for single-particle image processing. *eLife* 7, e35383 (2018).

8. Punjani, A., Zhang, H. & Fleet, D. J. Non-uniform refinement: Adaptive regularization improves single particle cryo-EM reconstruction. *bioRxiv* 2019.12.15.877092 (2019) doi:10.1101/2019.12.15.877092.

9. Tan, Y. Z. *et al.* Addressing preferred specimen orientation in single-particle cryo-EM through tilting. *Nat. Methods* 14, 793–796 (2017).

10. Terwilliger, T. C., Ludtke, S. J., Read, R. J., Adams, P. D. & Afonine, P. V. Improvement of cryo-EM maps by density modification. *bioRxiv* 845032 (2020) doi:10.1101/845032.

11. Steinegger, M. *et al.* HH-suite3 for fast remote homology detection and deep protein annotation. *BMC Bioinformatics* 20, 473 (2019).

12. Pettersen, E. F. *et al.* UCSF Chimera--a visualization system for exploratory research and analysis. *J. Comput. Chem.* 25, 1605–1612 (2004).

13. Song, Y. *et al.* High-resolution comparative modeling with RosettaCM. *Struct. Lond. Engl. 1993* 21, 1735–1742 (2013).

14. Yang, J. *et al.* Improved protein structure prediction using predicted interresidue orientations. *Proc. Natl. Acad. Sci.* 117, 1496 (2020).

15. Frenz, B., Walls, A. C., Egelman, E. H., Veesler, D. & DiMaio, F. RosettaES: a sampling strategy enabling automated interpretation of difficult cryo-EM maps. *Nat. Methods* 14, 797–800 (2017).

16. Brzovic, P. S., Rajagopal, P., Hoyt, D. W., King, M. C. & Klevit, R. E. Structure of a BRCA1-BARD1 heterodimeric RING-RING complex. *Nat. Struct. Biol.* 8, 833–837 (2001).

17. Touw, W. G., van Beusekom, B., Evers, J. M. G., Vriend, G. & Joosten, R. P. Validation and correction of Zn-Cys(x)His(y) complexes. *Acta Crystallogr. Sect. Struct. Biol.* 72, 1110–1118 (2016).

18. Tyka, M. D. *et al.* Alternate states of proteins revealed by detailed energy landscape mapping. *J. Mol. Biol.* 405, 607–618 (2011).

CHAPTER 4

Multivalent BARD1-nucleosome interactions facilitate H2A ubiquitylation by BRCA1/BARD1

Samuel R. Witus[1], Lisa M. Tuttle[1], Alex Zelter[1], Klaiten E. Kermoade[1], Damien B. Wilburn[2], Weixing Zhao[3], Trisha N. Davis[1], Peter S. Brzovic[1], Rachel E. Klevit[1,*]

1. Department of Biochemistry, University of Washington, Seattle, WA, USA.
2. Department of Genome Sciences, University of Washington, Seattle, WA, USA.
3. University of Texas Health Science Center at San Antonio, Department of Biochemistry and Structural Biology. San Antonio, TX

* Corresponding author email: klevit@uw.edu

*This is an early version of a manuscript to be submitted soon after completion of thesis requirements.

Author Contributions

S.R.W., P.S.B., and R.E.K. conceived of the study. S.R.W., L.M.T., and K.E.K. performed experiments and analyzed data. D.B.W. analyzed data. A.Z. performed chemical crosslinking and mass spectrometry and associated data processing under the supervision of T.N.D. S.R.W. wrote the initial draft of the manuscript.

Abstract

BRCA1/BARD1 is a tumor suppressor E3 ubiquitin (Ub) ligase complex with distinct roles in DNA damage repair by homologous recombination and transcriptional regulation. To perform these functions, the BRCA1/BARD1 heterodimer directly interacts with nucleosomes through multiple binding interfaces, transferring mono-Ub signals to distinct lysine residues on the extreme C-terminal tail of histone H2A. Although the minimal enzymatic RING domains of BRCA1/BARD1 are sufficient for its H2A-Ub activity, full-length BRCA1/BARD1 forms stronger complexes with chromatin and leads to enhanced H2A-Ub activity. The molecular basis for this enhanced binding and activity is unknown. Here, we describe the presence of extensive, multivalent interactions between BRCA1/BARD1 and nucleosomes that lead to high-affinity chromatin binding and increased H2A-Ub activity. We identify an intrinsically disordered DNA-

binding region of BARD1 that supports these interactions and can be regulated by the presence of specialized DNA structures that are present during homologous recombination. We also describe the ability of BRCA1/BARD1 to form distinct higher order chromatin complexes in the presence of the DNA damage signal H2A K15-Ub and H4K20me0. Together, our findings provide a detailed understanding of how BRCA1/BARD1 interfaces with chromatin, identifying novel regions of BARD1 that are critical to the formation and regulation of these complexes.

Introduction

Mutations in BRCA1 and BARD1 lead to a high risk for the development of breast and ovarian cancer. BRCA1 and BARD1 form a large, obligate heterodimeric complex (BRCA1/BARD1) with distinct roles in DNA damage repair by homologous recombination (HR), transcriptional regulation, and other nuclear processes[1–3]. These functions are mediated, at least in-part, through its direct association with chromatin. Upon DNA damage, BRCA1/BARD1 is recruited to damaged chromatin and segregates into foci with DNA repair factors[4–7]. Cancer-predisposing mutations can disrupt these dynamics, leading to DNA damage hypersensitivity and genomic instability[8]. BRCA1/BARD1 also has distinct roles in both stimulation and repression of transcription, likely through diverse mechanisms[3]. Therefore, it is important to obtain a full understanding of how BRCA1/BARD1 interfaces with chromatin, where it exerts its major biological functions.

BRCA1/BARD1 directly interacts with nucleosomes, the organizing unit of chromatin, through multiple direct binding interfaces[9]. The N-terminal RING domains of BRCA1 and BARD1 form a heterodimer that constitutes the sole known enzymatic activity of BRCA1/BARD1 as a RING-type E3 ubiquitin (Ub) ligase[10–12]. The RING domains bind to the histone surface of one pseudo-symmetrical ‘face’ of a nucleosome, facilitating the site-specific transfer of mono-Ub to specific lysine residues on the extreme C-terminal tail of histone H2A (K125, K127, and K129; referred

to as K127)[13–15]. H2A lysine specificity is determined by the binding orientation of the RING heterodimer on the nucleosome surface that causes the BRCA1-bound E2~Ub conjugate to tilt away from the histone surface. This allows the E2~Ub active-site to be accessible to the flexible C-terminal tail of H2A for Ub transfer. This specificity is largely determined by the non-E2-binding RING domain of BARD1 that binds to a unique histone surface compared to structurally similar Ub ligase complexes that target other lysine residues on H2A (e.g., K119 by RING1B/BMI1)[16]. The H2A-Ub activity of BRCA1/BARD1 is thought to contribute to its function in DNA damage repair by HR by promoting long range resection of broken DNA ends[17,18]. BRCA1/BARD1-dependent H2A-Ub activity is also implicated in the transcriptional repression of certain estrogen-metabolizing cytochrome P450 genes and the constitutive repression of α-satellite DNA regions[19–21].

In addition to the N-terminal RING domains, the BARD1 C-terminal domains (CTDs) bind to nucleosomes to facilitate DNA DSB repair by HR[15,22–25]. The BARD1 CTDs specifically recognize nucleosomes containing H2A K15-Ub and unmethylated H4 K20 (H4K20me0). Together, these signals serve as a binding platform to recognize damaged chromatin in G2/S phases when a sister chromatid is available to template high-fidelity DNA repair by HR. The BARD1 CTDs and N-terminal BRCA1/BARD1 RING domains bind to a fully overlapping histone surface, precluding their simultaneous binding to one nucleosome ‘face’. However, mono-nucleosomes with ubiquitin pre-installed at H2A K15 have been observed to serve as better substrates for BRCA1/BARD1-dependent ubiquitylation of H2A K127 *in vitro*, indicating that both domains may bind to the same nucleosome unit (with one domain on each ‘face’)[15]. It has also been observed that full-length BRCA1/BARD1 heterodimers form stronger complexes that lead to increased H2A-Ub activity than truncated RING/RING complexes using unmodified nucleosome substrates[14,15]. Additionally, regions throughout the expansive intrinsically disordered segments of both BRCA1 and BARD1 have been also shown to bind to DNA, but the

functional significance with regards to chromatin association and H2A-Ub activity remains to be determined[26–28]. Together, these findings suggest the existence of BRCA1/BARD1/nucleosome complexes with extensive multivalent interactions that have implications for its H2A-Ub activity.

Here, we describe functional interactions between BRCA1/BARD1 and chromatin substrates that support enhanced nucleosome binding and H2A-Ub activity. We identify an intrinsically disordered region of BARD1 distal to its RING domain that strongly binds to both nucleosomal and extra-nucleosomal DNA, dramatically enhancing the affinity of the complex and leading to increased H2A-Ub activity. These interactions can be regulated by specialized DNA structures that are present during DNA damage and repair and directly compete with BARD1 binding to nucleosomal DNA, for which we describe a molecular mechanism of recognition. Finally, we provide evidence for higher-order chromatin complexes containing H2A K15-Ub nucleosomes that support the presence of both a 'wrapped' complex where the BRCA1/BARD1 RING domains and BARD1 CTDs bind to opposite sides of one nucleosome unit, as well a complex where these domains bind to adjacent nucleosome units. Throughout, we evaluate the contribution of BARD1 DNA binding to nucleosome affinity and H2A-Ub activity. Together, our findings reveal an extensive network of multivalent BARD1/nucleosome interactions that serve as a platform for BRCA1/BARD1-associated functions on chromatin.

Results

Identification of a BARD1 region supporting increased H2A ubiquitylation activity

BRCA1/BARD1 is a large, obligate heterodimeric complex with distinct functional domains **(Fig. 1a)**. A minimal N-terminal RING/RING heterodimer fragment containing BRCA1 (1-110) and BARD1 (26-140; $BRCA1^{RING}$/$BARD1^{RING}$) is sufficient to direct site-specific mono-ubiquitylation of nucleosomal histone H2A[13]. However, we and others previously reported that full-length BRCA1/BARD1 (~300 kDa) exhibits faster ubiquitylation kinetics and stronger binding to

nucleosomes than the minimal RING/RING complex (~25 kDa)[14,15]. To reveal which regions of BRCA1 or BARD1 are responsible for this increase in activity and binding affinity, we generated a series of heterodimers with C-terminal truncations in the BRCA1 and BARD1 subunits **(Extended Data Fig. 1a and Extended Data Table I)**. In agreement with previous observations, full-length BRCA1/BARD1 exhibited faster H2A ubiquitylation kinetics in a nucleosome ubiquitylation assay and increased nucleosome binding affinity by electrophoretic mobility shift assay (EMSA) than the minimal RING/RING heterodimer **(Fig. 1b and Extended Data Fig. 1b-d)**. To map the regions responsible for these effects, we performed *in vitro* nucleosome ubiquitylation and binding assays using a panel of truncated BRCA1/BARD1 heterodimers.

To measure the effects of BRCA1 subunit truncation on H2A ubiquitylation and nucleosome binding, we tested three heterodimers containing full-length BARD1. These include full-length BRCA1 ($BRCA1^{FL}$), a clinically relevant allele missing ~1000 residues in the IDR region ($BRCA1^{\Delta 11q}$), and a minimal BRCA1 RING-containing fragment capable of forming a heterodimeric complex with BARD1 **(**$BRCA1^{RING}$; **Fig. 1b, d)**. All three heterodimers exhibited faster H2A ubiquitylation kinetics than the minimal $BRCA1^{RING}$/$BARD1^{RING}$ complex **(Fig. 1b)**. Notably, complexes containing truncated BRCA1 ($BRCA1^{RING}$ and $BRCA1^{\Delta 11q}$) exhibited faster ubiquitylation kinetics than the $BRCA1^{FL}$-containing heterodimer, possibly indicative of inhibitory interactions in the full-length complex. In agreement with its increased activity, the $BRCA1^{RING}$/$BARD1^{FL}$ heterodimer bound to the nucleosome with ~1000-fold increased affinity than the $BRCA1^{RING}$/$BARD1^{RING}$ complex **(Fig. 1d)**. The reported difference in affinities is likely underestimated, as we collected the minimal RING/RING heterodimer binding data at a lower ionic strength than the rest of the constructs to obtain well-behaved binding data (50 mM vs.

100 mM NaCl). Together, these data indicate that the full BRCA1 C-terminal region is dispensable for H2A ubiquitylation and binding to an unmodified nucleosome substrate.

Next, we generated a series of BARD1 truncations in the context of BRCA1^{RING}-containing heterodimers. Truncation of the BARD1 Ank-BRCT C-terminal domains (BARD1$^{\Delta CTD}$) and to residue 216 in the putative intrinsically disordered region (IDR, BARD1^{216}) had minimal impact on H2A ubiquitylation kinetics and nucleosome binding affinity **(Fig. 1c, 1d)**. However, truncation to BARD1 residue 193 (BARD1^{193}) caused a substantial decrease in H2A ubiquitylation kinetics and ~10-fold reduction binding affinity. Supporting this, deletion of the first half of the BARD1 IDR (BARD1$^{\Delta 140\text{-}270}$) greatly diminished H2A-Ub activity **(Extended Data Fig. 1e)**. A more targeted deletion (BARD1$^{\Delta 194\text{-}216}$) modestly decreased H2A-Ub activity, suggesting the presence of additional or compensatory interaction sites in BARD1. The diminished activity of the BARD1$^{\Delta 140\text{-}270}$ was correlated with a ~3-fold decrease in nucleosome binding affinity, still considerably stronger than the minimal RING/RING heterodimer or BARD1^{193} truncation **(Extended Data Fig. 1f)**. Retention of binding affinity in this internal deletion construct is consistent with both isolated 'halves' of the BARD1 IDR binding to nucleosomes in an EMSA experiment and may indicate a requirement for specific types of interactions that lead to increased H2A ubiquitylation that are not fully detectable in our binding assay **(Extended Data Fig. 1g)**. Together, these data identify a region distal to the BRCA1/BARD1 RING domains (BARD1 194-216) that is important for productive nucleosome binding that leads to increased H2A-Ub activity. Although truncation to BARD1^{193} is defective in nucleosome binding and H2A-Ub activity, it retains higher activity and stronger nucleosome binding than the minimal RING/RING heterodimer. This suggests that additional regions within BARD1 141-193 may support functional interactions with nucleosomes.

To further investigate regions outside of the RING domains of BRCA1/BARD1 that may interact with nucleosomes, we performed chemical crosslinking with mass-spectrometry (MS) analysis on a complex containing $BRCA1^{RING}$/$BARD1^{FL}$ and a minimal nucleosome substrate **(Fig. 1e and Extended Data Fig. 2a)**. For these experiments, we used the bi-functional crosslinkers disuccinimydal suberate (DSS) and bissulfosuccinimidyl suberate (BS3) that covalently link lysine sidechains or amino termini via a ~15 Å spacer arm. We observed crosslinks from the RING domain of BRCA1 to regions within this histone core consistent with previously determined high-resolution structures **(Extended Data Fig. 2b, c)**. Although the BARD1 RING domain is lysine-depleted and lacked crosslinks, the remainder of BARD1 (residues 124-777) contains many lysine residues that are reactive with the DSS and BS3 crosslinkers. In agreement with our H2A-Ub activity and nucleosome binding data using truncated heterodimers, we observed robust intermolecular crosslinks between the BARD1 IDR (124-424) and histones **(Fig. 1e – left)**. The observed intermolecular crosslinks mostly couple to the flexible histone tails with several crosslinks to ordered regions of the histone core, including the H2B αC helix. Although the BARD1 CTDs (425-777) had good MS peptide coverage with lysine residues that reacted with the crosslinkers (indicated by mono-links, loop-links, and self-crosslinks), we observed relatively sparse crosslinking to histones **(Fig. 1e – right and Extended Data Fig. 2d)**. Together, these data suggest that the region of BARD1 that is distal to the RING domain (124-270) and contributes to increased H2A ubiquitylation activity and binding is tethered to the nucleosome, while the ordered CTDs of BARD1 do not localize around the nucleosome.

Additional BARD1-nucleosome interactions are mediated through DNA binding

Having identified non-RING regions of BARD1 that facilitate increased H2A ubiquitylation activity and nucleosome binding, we sought to characterize the molecular interactions involved. BARD1 residues 141-216 are in a large internal segment that is predicted to be mostly

intrinsically disordered (124-424)[29]. To our knowledge, whether this region of BARD1 is fully disordered has not been explicitly tested. We generated ^{15}N-labelled BARD1 fragments containing residues 124-270, 269-424, and 124-424 and collected ^{1}H^{15}N-HSQC nuclear magnetic resonance (NMR) spectra **(Extended Data Fig. 3a, 3b)**. All three spectra exhibit a narrow range of ^{1}H chemical shifts, consistent with an IDR. Furthermore, the spectra corresponding to the two halves (124-270 and 269-424) overlay well with the spectrum of the full region, indicating that the two halves behave independently of one another **(Extended Data Fig. 3b)**. Overall, these data support that the BARD1 region 124-424 is largely an IDR as predicted.

Next, we examined the region of BARD1 that supports high affinity nucleosome binding and increased H2A-Ub activity (BARD1 141-216) in the context of its surrounding amino acid sequence (BARD1 124-270). This region has been reported to bind to double-stranded DNA and specialized DNA structures containing base-pair mismatch (discussed below)[26]. The sequence of BARD1 124-270 is largely conserved, and its amino acid identity is strongly basic across a subset of homologs **(Extended Data Fig. 3c)**. Therefore, we hypothesized that additional interactions may be mediated through nucleosomal DNA. Many nucleosome modifying enzymes such as the methyltransferases DOT1L and COMPASS utilize DNA binding regions adjacent to their catalytic domains that are required for full activity[30–34]. In support of this, we observed strong binding of BARD1 124-270 to either free 147-bp '601' dsDNA or nucleosomes by EMSA **(Extended Data Fig. 4a)**.

To gain residue-level information, we performed NMR binding experiments with ^{15}N-labelled BARD1 124-270 and either a 147-bp nucleosome or 36-bp dsDNA fragment **(Fig. 2a and Extended Data Fig. 4b)**. The ^{1}H^{15}N-HSQC spectral perturbations are notably similar between the two conditions, indicating that BARD1 is using similar surfaces to recognize nucleosomes

and free dsDNA. Due to spectral overlap, we were unable to fully assign BARD1 residue identities for the fragment spanning residues 124-270. Therefore, we assigned a smaller BARD1 region that encompasses the putative DNA binding region identified in our H2A-Ub activity and binding assays (BARD1 141-216). Many resonance assignments for BARD1 141-216 were transferrable to the longer segment, allowing us to analyze binding in either context **(Fig. 2a, b and Extended Data Fig. 4b, c)**. Overall, the regions of BARD1 that were most affected by dsDNA binding as judged by backbone amide NMR chemical shift perturbations (CSPs) and dynamics measurements were BARD1 146-161 and 194-216 **(Fig. 2b and Extended Data Fig. 4b-d)**. We also observed helical secondary structure propensity for BARD1 191-199 that becomes more disordered upon DNA binding **(Fig. 2c)**. In addition, at least one signal that was absent in the unbound spectrum appears in the BARD1-DNA complex spectrum, indicative of altered IDR dynamics upon DNA binding **(Extended Data Fig. 4c)**. Importantly, residues between 162-191 of BARD1 were relatively unaffected in the BARD1-dsDNA complex, suggestive of specific DNA-binding region interactions. Due to solubility and concentration limitations, we were unable to perform these analyses on nucleosome-bound samples. However, given the similar $^{1}H^{15}N$-HSQC spectral perturbations between nucleosome-bound and dsDNA-bound BARD1, we expect the binding modes to be similar **(Extended Data Fig. 4b)**. Together, these data identify two regions of BARD1 (146-161 and 194-216) adjacent to the enzymatic RING domains that contribute to BARD1 DNA-binding and are consistent with our H2A-Ub activity and nucleosome binding data.

Having established that the isolated BARD1 IDR fragment binds to free DNA and nucleosomes similarly by NMR, we sought to observe these interactions within the context of an active enzymatic complex. We incorporated the photoactivatable crosslinker p-Benzoyl-L-phenylalanine (Bpa) at locations throughout the BARD1 IDR in RING-containing Ub ligase complexes (L120Bpa, W146Bpa, Y180Bpa, A195Bpa and W218Bpa) **(Extended Data Fig. 5a)**.

Due to the need to co-express a Bpa-specific aminoacyl tRNA transferase, we designed a genetic fusion where BRCA1 residues 1-104 were fused to the BARD1 residues 26-221 through a 12-residue GlySer-linker (BRCA1-f-BARD1^{221}). Wild-type BRCA1-f-BARD1^{221} and BPA-incorporated mutants retained similar H2A ubiquitylation activity to each other and to unfused heterodimers **(Extended Data Fig. 5b)**. For crosslinking experiments, we opted to use a nucleosome substrate with extra-nucleosomal linker DNA **(**NCP^{185}; **Extended Data Fig. 5c)**. We observed that the Bpa crosslinker incorporated at the BARD1 W146 and A195 positions formed enhanced crosslinks with nucleosomal DNA, supporting the presence of specific DNA interactions in the enzymatically active complex that are consistent with our NMR findings **(Fig. 2d)**. We observed weaker crosslinks from the Y182 and W218 positions. These were comparable to crosslinks observed from the L120 position that is located close to the RING domains and not expected to contribute to productive DNA interactions. Similar crosslinking patterns were observed with free DNA compared to nucleosomes **(Extended Data Fig. 5d)**. Together, these data support a direct interaction between the BARD1 IDR and nucleosomal DNA in the context of an enzymatically active complex.

Contribution of DNA-binding to enhanced H2A-Ub activity

Next, we assessed the contribution of BARD1 DNA-binding to overall enzymatic activity. We asked whether the DNA-binding activity of full-length BARD1 could support H2A-Ub activity in the presence of highly disruptive BARD1 RING histone-interface mutations **(**BARD1 P89A/W91A; **Fig. 3a)**[14,15]. Although high-affinity binding and auto-ubiquitylation activity were retained, heterodimers containing full-length BARD1 (P89A/W91A) were unable to support H2A-ub activity **(Fig. 3b-d)**. This indicates that the RING-histone interface is absolutely required for activity, while the DNA-binding properties of BARD1 serve a supportive role to promote the formation of a high-affinity complex that leads to enhanced H2A ubiquitylation activity.

We then asked whether the sequence identity of the BARD1 DNA-binding C-terminal extension is critical for supporting increased H2A-ub activity. To address this, we generated a chimeric BRCA1/BARD1 heterodimer in which a previously identified DNA-binding site from the BRCA1 IDR (498-663) was appended onto C-terminus of the BARD1 RING[27]. We found that this chimera supported increased H2A-Ub activity compared to the minimal RING/RING complex, although not to the levels of the native BARD1 sequence **(Fig. 3e)**. These data indicate that a major contributor to increased H2A-Ub activity is the location of a disordered, high-affinity DNA-binding region near the enzymatic RING domains.

Finally, we sought to explore potential modes of regulation of the BARD1-DNA interaction. post-translational modifications deposited on BRCA1 and BARD1 are known to regulate its biological activities. Phosphorylation of BARD1 residues S148 and S186 that are adjacent to basic DNA-binding stretches have been observed in low-throughput mass-spectrometry studies[35]. We generated single phosphomimetic mutants of $BRCA1^{RING}/BARD1^{216}$ containing S148D or S186D and tested their activity in a nucleosome ubiquitylation assay **(Fig. 3f)**. Both mutants led to diminished H2A-Ub activity, possibly due to repulsive charge interactions with nucleosomal DNA nearby to binding sites that span BARD1 146-161 and 194-216. Together, these findings confirm that DNA binding serves an auxiliary role to enhance H2A-ub activity and may serve as a point of regulation for BRCA1/BARD1-chromatin complexes.

Specialized DNA structures bind to the BARD1 IDR and inhibit H2A-Ub activity

The BARD1 DNA-binding region spanning residues 141-216 enhances the intrinsic H2A-ub activity of the BRCA1/BARD1 RING heterodimer by interacting with nucleosomal DNA and increasing the affinity of the complex. It was previously observed that this region of BARD1 preferentially binds to partially unwound DNA structures (bubble-DNA) and HR intermediates (D-loop DNA) compared to double-stranded or single-stranded DNA[26]. These interactions with

specialized DNA structures help to promote HR through assembly of a functional complex consisting of BARD1, the recombinase RAD51, and DNA. Therefore, we hypothesized that the interaction between the BARD1 DNA-binding region and bubble-DNA or D-loop DNA may modify its ability to interact with nucleosomal DNA, thereby altering nucleosome binding and H2A-Ub proficiency. As the molecular features that BARD1 is recognizing between bubble- and D-loop- DNA substrates are likely to be similar given the reported near-identical affinities of the BARD1-DNA complexes, we chose to use the simpler bubble-DNA substrate in our assays.

We assembled minimal DNA fragments containing various patterns of base-pair mismatch and performed single time-point ubiquitylation assays using full-length BRCA1/BARD1 in the presence of DNA competitors **(Fig. 4a, b and Extended Data Fig. 6a, b)**. We observed that bubble-DNA specifically inhibits H2A-Ub activity compared to the other DNA substrates tested. We hypothesized that inhibition of H2A-Ub activity is mediated through competing interactions between bubble-DNA and nucleosomal DNA for binding to BARD1 141-216. Supporting this, truncation of $BRCA1^{RING}$/$BARD1^{216}$ to the minimal RING heterodimer completely abrogated sensitivity to bubble-DNA-mediated inhibition of H2A-Ub activity **(Extended Data Fig. 6c, d)**. Indicative of a binding-competition mechanism, UV-induced Bpa crosslinks between $BRCA1^{RING}$-f-$BARD1^{221}$ and nucleosomal DNA were specifically inhibited in the presence of a bubble-DNA competitor compared to dsDNA **(Fig. 4c)**.

To further characterize the interactions between BARD1 141-216 and bubble-DNA, we turned to NMR. We compared the spectra of BARD1 IDR-DNA complexes bound to bubble-DNA and dsDNA fragments of comparable sequence and size. CSPs and changes in dynamics within BARD1 194-216, the region we previously showed to be the major site of double-stranded and nucleosomal DNA binding, were similar between the bubble-DNA and dsDNA complexes **(Fig. 4d and Extended Data Fig. 4c, d)**. However, in addition to these interactions, we observed

bubble-DNA-specific interactions with BARD1 143-157 that caused many backbone amide NMR signals to disappear, indicative of drastic changes in chemical environment and dynamics. Supporting this, we observed a large CSP for the W146Ne sidechain signal that was not present in the dsDNA-bound spectrum **(Extended Data Fig. 4c)**. We also identified several signals corresponding to methyl groups of residues within BARD1 143-157 in the $^{1}H^{13}C$-HSQC spectrum of the bubble-DNA bound complex **(Fig. 4e and Extended Data Fig. 4e)**. These signals showed large CSPs that were not present in the dsDNA bound spectrum. Together, these data support that bubble-DNA structures strongly and specifically engage an additional DNA-binding site within the BARD1 IDR that spans residues 143-157. Based on our NMR findings, we hypothesized that targeted deletion of these DNA binding regions would confer resistance to inhibition of H2A-Ub activity by a bubble-DNA competitor. Consistent with this, concomitant deletion of basic residues in both IDR regions (BARD1$^{\Delta 150\text{-}155/\Delta 194\text{-}216}$) was required to alleviate H2A-Ub activity inhibition by bubble-DNA **(Fig. 4f and Extended Data Fig. 6e)**. Together, our findings indicate that BARD1 specifically recognizes bubble-DNA through additional interactions within BARD1 143-157 that are dissimilar to those formed with dsDNA. These interactions compete with BARD1-nucleosome interactions and inhibit enhanced H2A-Ub activity.

Extra-nucleosomal linker DNA enhances H2A ubiquitylation

Given the extended domain topology of both BRCA1 and BARD1, it is possible that additional interactions may occur in higher-order chromatin substrates that are not present in the minimal mono-nucleosome substrate used in initial experiments. For example, chromatin factors such as PRC2, LSD1, and VRK1 require linker DNA or adjacent nucleosome units for optimal binding and enzymatic activity[36–39]. Therefore, we asked whether there are similar chromatin substrate requirements for BRCA1/BARD1 dependent H2A ubiquitylation. To test this, we generated nucleosome substrates with extra-nucleosomal linker DNA (NCP^{185}) and tri-nucleosomes (tri-

NCP) with linker DNA only between nucleosome units **(Fig. 5a and Extended Data Fig. 7a)**. We observed faster H2A-Ub kinetics for full-length BRCA1/BARD1 using the NCP^{185} substrate with linker DNA compared to the minimal NCP^{147} substrate **(Fig. 5b)**. We did not observe an additional increase in H2A-Ub activity using a tri-NCP substrate, indicating that in the absence of histone PTMs, functional interactions are likely limited to one mono-nucleosome unit.

In addition to full-length BRCA1/BARD1, we also tested the H2A-Ub activity of the $BRCA1^{RING}$/$BARD1^{216}$ truncation that retains BARD1 DNA-binding competency **(Fig. 5c)**. This protein species exhibited considerably faster H2A ubiquitylation kinetics using either a NCP^{185} or a tri-NCP substrate compared to a minimal NCP^{147} substrate, again indicating a dependency on the presence of linker DNA. We then asked whether the activity difference between the nucleosomes with and without linker DNA were due to differences in binding affinity. To do so, we measured nucleosome binding affinity at two different ionic strengths using the NCP^{147} and NCP^{185} substrates **(**100 mM vs. 150 mM NaCl; **Fig. 5d**). Although nucleosome complexes exhibited considerably weaker binding (~5-fold reduction) at higher buffer salt concentration, there was only a modest increase in binding affinity with the NCP^{185} substrate at both ionic strengths. This observation contrasts with other chromatin factors that exhibit affinity and activity differences on the order of magnitudes in the presence or absence of linker DNA and may reflect the different types of interactions (i.e., ordered vs disordered DNA-binding regions)[36,38]. Together, our results indicate that the BARD1 DNA-binding region can associate with both histone-associated nucleosomal DNA and extra-nucleosomal linker DNA that leads a to similar apparent binding affinity. However, interactions with linker DNA support an additional enhancement of H2A ubiquitylation kinetics.

H2A K15-Ub-mediated enhancement of BRCA1/BARD1 H2A-Ub activity

In addition to the RING domains and the BARD1 DNA-binding region, the ordered C-terminal domains (CTDs) of BARD1 bind to nucleosomes containing both H2A K15-Ub and H4K20me0 [15,25]. These BARD1 CTD-nucleosome interactions serve to recruit BRCA1/BARD1 to damaged chromatin to facilitate DNA DSB repair by homologous recombination [22–24]. The BARD1 CTDs use an overlapping histone binding surface to the enzymatic RING domains, precluding binding of both domains to the same nucleosome 'face'. However, it was previously shown that nucleosomes containing both H2A K15-Ub and H4K20me0 form a stronger complex with $BRCA1^{RING}/BARD1^{FL}$ and are better substrates for its ubiquitylation of H2A K127, implying that the BRCA1/BARD1 RING domains and BARD1 CTDs can simultaneously bind to opposite sides of the same nucleosome [15]. We sought to further characterize these complexes using our suite of BRCA1/BARD1 truncation constructs and chromatin substrates.

We assembled homogenously mono-ubiquitylated nucleosomes containing ubiquitin preinstalled at H2A positions K15, K119, and K127 using a non-hydrolyzable dichloroacetone crosslinker **(Extended Data Fig. 7b, c)**[40]. In agreement with previous observations, ubiquitin preinstalled at H2A K15 uniquely increased $BRCA1^{FL}/BARD1^{FL}$-dependent H2A-Ub activity **(Fig. 6a and Extended Data Fig. 7d)**. Ubiquitin preinstalled at either C-terminal position (K119 or K127) decreased BRCA1/BARD1-dependent H2A-Ub activity, possibly indicative of E3 exclusivity between BRCA1/BARD1 and RING1/PCGF complexes that modify the C-terminal tail of H2A. As expected, the BARD1 CTDs were required for enhancement of BRCA1/BARD1-dependent H2A-Ub activity using H2A K15-Ub nucleosome substrates **(Fig. 6b)**.

Next, we asked whether the DNA-binding properties of BARD1 are important for enhancement of H2A-Ub activity observed using H2A K15-Ub nucleosome substrates **(Fig. 6b)**. We observed slower ubiquitylation kinetics using $BRCA1^{RING}/BARD1^{\Delta 140\text{-}270}$ than the $BRCA1^{RING}/BARD1^{FL}$ complex. However, deletion of BARD1 140-270 still supported greater activity than the

BRCA1^{RING}/BARD1$^{\Delta CTD}$ complex, indicating that BARD1-DNA interactions are secondary to BARD1 CTDs-nucleosome binding in this context. The histone-binding BARD1 RING mutant BRCA1^{RING}/BARD1$^{FL\text{-}P89A/W91A}$ was unable to support BRCA1/BARD1-dependent H2A-Ub activity using H2A K15-Ub nucleosomes, supporting a model where the BRCA1/BARD1 RINGs and CTDs bind to either side of a nucleosome **(Fig. 6b)**. These findings indicate that BARD1-DNA interactions are important for stimulation of activity by H2A K15-Ub and support the presence of a 'wrapped' multivalent complex where three points of contact between BARD1 and nucleosomes (RING-histone, IDR-DNA, and CTDs-histone) are required for full BRCA1/BARD1-dependent H2A-Ub activity **(Fig. 7a, b)**.

To obtain structural insights into enhanced H2A-Ub activity in the presence of an H2A K15-Ub modification, we performed chemical crosslinking with MS analysis on a complex between BRCA1^{RING}/BARD1^{FL} and H2A K15-Ub nucleosomes **(Fig. 6c and Extended Data Fig. 2a)**. This was done side-by-side with crosslinking experiments using unmodified nucleosomes (discussed above) to facilitate direct comparison between the two conditions. We observed increased intermolecular crosslinking (judged by unique crosslinks and peptide spectral mapping counts) between the BARD1 CTDs and histones using nucleosomes containing H2A K15-Ub compared to unmodified nucleosomes **(Fig. 6c – top circle plots and Extended Data Fig. 2e)**. These crosslinks are consistent with high-resolution structures of the BARD1 CTDs bound to nucleosomes containing H2A K15-Ub **(Extended Data Fig. 2f)**. We also observed increased crosslinking between the RING and IDR domains of BARD1 to histones in samples containing H2A K15-Ub nucleosomes **(Fig. 6C – bottom circle plots and Extended Data Fig. 2e)**. These data are consistent with the reported increased binding affinity of the complex. The data also suggest that interactions between the CTDs and H2A K15-Ub nucleosomes directly facilitate BARD1 RING and IDR interactions with nucleosomes that lead to the observed increased H2A-Ub activity.

The BRCA1/BARD1 N-terminal RING domains and BARD1 CTDs are separated by ~300 intrinsically disordered residues, endowing ~1000 Å of separation between the two ordered domains. Therefore, it is possible that in addition to a 'wrapped' complex with H2A K15-Ub nucleosomes, the BARD1 CTDs may anchor the Ub ligase complex by binding to one nucleosome unit, while the RING domains are recruited to a nearby nucleosome unit on chromatin to facilitate H2A-Ub activity. To explicitly test this possibility, we assembled asymmetric di-nucleosomes (di-NCPs) where one nucleosome unit contained H2A K15-Ub ($H2A^{silent}$) and an adjacent nucleosome unit contained unmodified H2A with a fluorophore conjugated to its N-terminus to facilitate specific detection in a nucleosome ubiquitylation assay **(**$H2A^{observe}$; **Fig. 6d and Extended Data Fig. 7e-g)**. Using $BRCA1^{RING}/BARD1^{FL}$ heterodimers, we observed that an asymmetric di-NCP substrate containing H2A K15-Ub ($H2A^{silent}$) uniquely facilitate enhanced H2A-Ub modification of an adjacent nucleosome unit containing unmodified H2A **(**$H2A^{observe}$; **Fig. 6e and Extended Data Fig. 7h)**. Truncation of the BARD1 CTDs led to a large decrease in H2A-Ub activity that was comparable to that of a di-NCP substrate where both nucleosome units contain unmodified H2A. Consistent with observations made using H2A K15-Ub mono-nucleosomes, $BRCA1^{RING}/BARD1^{FL\text{-}P89A/W91A}$ did not support H2A-Ub activity using di-NCPs **(Fig. 6e)**. Additionally, deletion of BARD1 DNA-binding residues (Δ140-270) substantially decreased H2A-Ub activity **(Fig. 6f)**. Together, our results support the presence of a higher-order chromatin complex where BARD1 binding spans adjacent nucleosome units. This is mediated through binding of the BRCA1/BARD1 RING domains and BARD1 CTDs to neighboring nucleosome units, with the BARD1 IDR binding to intervening linker or nucleosomal DNA **(Fig. 7c)**.

Discussion

Here, we describe a mechanism for enhanced chromatin binding and H2A-Ub activity of full-length BRCA1/BARD1 compared to the minimal RING/RING heterodimer. This is mediated through a highly basic, intrinsically disordered region of BARD1 (primarily residues 194-216) adjacent to the enzymatic RING domains that binds to nucleosomal and extra-nucleosomal linker DNA. These strong, charge-based interactions increase the overall binding-strength of the complex from the mM- to the nM-affinity binding regime that is likely more conducive to supporting the physiological functions of BRCA1/BARD1 on chromatin. Our data indicate that DNA-binding plays a supporting role in the ability of BRCA1/BARD1 to modify H2A. A BARD1 RING-domain mutant (BARD1 P89A/W91A) that disrupts histone binding and is unable to support H2A-Ub activity with any chromatin substrate tested retains strong nucleosome binding affinity and intrinsic Ub ligase activity. Therefore, BARD1 (P89A/W91) likely constitutes a separation-of-function mutant that may be useful in cellular studies investigating BRCA1/BARD1-dependent H2A-Ub function.

Additionally, we observed increased H2A-Ub activity using truncated BRCA1-complexes ($BRCA1^{RING}$ and $BRCA1^{\Delta 11q}$) compared to true full-length heterodimers. One possible explanation for this is the presence of intramolecular interactions within BRCA1/BARD1 heterodimers that are inhibitory to nucleosome binding and H2A-Ub. Another possibility is the existence of competing nucleosome interactions from internal regions of BRCA1 that do not lead to increased H2A-Ub activity. In support of the second possibility, we observed increased H2A-Ub kinetics using a BRCA1/BARD1 chimera where a previously identified DNA binding region within BRCA1 (498-663 in the IDR) was fused directly adjacent to the minimal RING/RING heterodimer. This indicates that at least one DNA-binding region within the BRCA1 IDR can form functional interactions with nucleosomal DNA when located next to the enzymatic RING domains. Further investigation is warranted into chromatin complexes containing full-length BRCA1/BARD1 and the many protein assemblies and binding partners it associates

with[41]. Overall, we conclude that the major determinant of increased nucleosome binding-strength and H2A-Ub activity is the presence of a strong, intrinsically disordered DNA-binding region adjacent to the enzymatic RING domains that can bind to nucleosomal DNA. The ability of this region to associate with both histone-bound and extra-nucleosomal linker DNA delineates it from other chromatin-modifying enzymes that have stringent requirements for binding to linker DNA to support their enzymatic activity[36,38].

Although BRCA1^{RING}-containing heterodimers with BARD1 truncations (i.e., to BARD1^{193} and BARD1^{RING}) exhibited strongly decreased nucleosome binding affinity and H2A-Ub activity **(Fig. 1c, d)**, targeted internal deletion of basic BARD1 residues (Δ150-155 and Δ194-216) caused a much smaller effect **(Extended Data Fig. 1e)**. This may be explained by compensatory interactions from basic residues outside of these regions with nucleosomal DNA. In support of this, we observed strong binding of the second half of the BARD1 IDR region to nucleosomes and dsDNA **(**269-424; **see Extended Data Fig. 1g, 4f)**, although these interactions were less effective at supporting H2A-Ub activity than the wild-type BARD1 sequence. These results indicate a degree of plasticity in DNA recognition by BARD1 regions. As BRCA1/BARD1 serves as a large protein interaction hub that forms many complexes, it is possible that the accessibility of DNA binding regions in BARD1 are determined by the landscape of binding partners it is associated with. Consistent with this idea, we identified specific DNA competitor structures (bubble-DNA) that inhibit nucleosome binding and H2A-Ub activity by binding to the BARD1 IDR and competing with nucleosome binding. We describe a mechanism of preferential recognition for these bubble-DNA structures by BARD1 through engagement of a second binding interface in the BARD1 IDR (143-157 in addition to 194-216). This mechanism of recognition is likely similar for D-loop DNA structures that are important intermediates in HR[26]. It is possible that binding of the BARD1 IDR region to either nucleosomal DNA or specialized DNA structured

serves to control its spatial and temporal involvement in HR and other processes where these types of specialized DNA structures may be present (e.g., stalled replication fork protection)[42].

Finally, we used higher order chromatin substrates that contain ubiquitin preinstalled at H2A K15 and H4K20me0 to investigate the contribution of interactions between the BARD1 CTDs to RING-mediated H2A-Ub activity. Our findings support the presence of a 'wrapped' complex where the BARD1 CTDs and the RING heterodimer are bound to opposite sides of the same nucleosome, with BARD1 IDR-DNA interactions playing a supporting role **(Fig. 7b)**. We also provide evidence for a complex where the BARD1 CTDs and the enzymatic RING domains occupy adjacent nucleosomes separated by linker DNA **(Fig. 7c)**. Given that the BARD1 IDR region endows ~1000 Å of intrinsically disordered separation between the enzymatic RING domains and BARD1 CTDs, it is possible that the RING domains may reach nucleosome units considerably further away than the adjacent unit while anchored to chromatin via the BARD1 CTDs. This may lead to BRCA1/BARD1-dependent H2A-Ub of multiple nucleosomes in the vicinity of the K15-Ub anchor nucleosome. An important unanswered question is how the presence of additional histone PTMs may influence the chromatin binding and H2A-Ub activity of BRCA1/BARD1. Together, our results establish an extensive multivalent network of interactions that facilitate BRCA1/BARD1 chromatin binding and H2A-Ub activity. These interactions are likely critical for many functions of BRCA1/BARD1 in the nucleus that are not limited to H2A-Ub activity and may be disrupted by pathogenic mutations that cause cancer.

Acknowledgements

We thank K. Luger (University of Colorado Boulder) for sharing the plasmids for the 147-bp and NLE-trimer '601' DNA, S. Tan (Penn State University) for sharing the plasmid for the 185-bp '601' DNA, and G. Debelouchina (UC San Diego) for the MMTV DNA plasmid. We thank D.

Veelser for sharing equipment, and M. Morgan for insights into dichloroacetone crosslinking of H2A-Ub.

References (main text)

1. Tarsounas, M. & Sung, P. The antitumorigenic roles of BRCA1–BARD1 in DNA repair and replication. *Nat. Rev. Mol. Cell Biol.* **21**, 284–299 (2020).
2. Densham, R. M. & Morris, J. R. Moving Mountains—The BRCA1 Promotion of DNA Resection. *Front. Mol. Biosci.* **6**, 79 (2019).
3. Mullan, P. B., Quinn, J. E. & Harkin, D. P. The role of BRCA1 in transcriptional regulation and cell cycle control. *Oncogene* **25**, 5854–5863 (2006).
4. Scully, R. *et al.* Dynamic Changes of BRCA1 Subnuclear Location and Phosphorylation State Are Initiated by DNA Damage. *Cell* **90**, 425–435 (1997).
5. Kolas Nadine K. *et al.* Orchestration of the DNA-Damage Response by the RNF8 Ubiquitin Ligase. *Science* **318**, 1637–1640 (2007).
6. Sobhian Bijan *et al.* RAP80 Targets BRCA1 to Specific Ubiquitin Structures at DNA Damage Sites. *Science* **316**, 1198–1202 (2007).
7. Mattiroli, F. *et al.* RNF168 ubiquitinates K13-15 on H2A/H2AX to drive DNA damage signaling. *Cell* **150**, 1182–1195 (2012).
8. Gudmundsdottir, K. & Ashworth, A. The roles of BRCA1 and BRCA2 and associated proteins in the maintenance of genomic stability. *Oncogene* **25**, 5864–5874 (2006).
9. Witus, S. R., Zhao, W., Brzovic, P. S. & Klevit, R. E. BRCA1/BARD1 is a nucleosome reader and writer. *Trends Biochem. Sci.* (2022) doi:10.1016/j.tibs.2022.03.001.
10. Lorick, K. L. *et al.* RING fingers mediate ubiquitin-conjugating enzyme (E2)-dependent ubiquitination. *Proc. Natl. Acad. Sci.* **96**, 11364 (1999).
11. Brzovic, P. S., Rajagopal, P., Hoyt, D. W., King, M. C. & Klevit, R. E. Structure of a BRCA1-BARD1 heterodimeric RING-RING complex. *Nat. Struct. Biol.* **8**, 833–837 (2001).
12. Witus, S. R., Stewart, M. D. & Klevit, R. E. The BRCA1/BARD1 ubiquitin ligase and its substrates. *Biochem. J.* 3467–3483 (2021) doi:10.1042/BCJ20200864.
13. Kalb, R., Mallery, D. L., Larkin, C., Huang, J. T. J. & Hiom, K. BRCA1 is a histone-H2A-specific ubiquitin ligase. *Cell Rep.* **8**, 999–1005 (2014).
14. Witus, S. R. *et al.* BRCA1/BARD1 site-specific ubiquitylation of nucleosomal H2A is directed by BARD1. *Nat. Struct. Mol. Biol.* **28**, 268–277 (2021).
15. Hu, Q. *et al.* Mechanisms of BRCA1–BARD1 nucleosome recognition and ubiquitylation. *Nature* **596**, 438–443 (2021).
16. McGinty, R. K., Henrici, R. C. & Tan, S. Crystal structure of the PRC1 ubiquitylation module bound to the nucleosome. *Nature* **514**, 591–596 (2014).
17. Densham, R. M. *et al.* Human BRCA1-BARD1 ubiquitin ligase activity counteracts chromatin barriers to DNA resection. *Nat. Struct. Mol. Biol.* **23**, 647–655 (2016).

18. Uckelmann, M. *et al.* USP48 restrains resection by site-specific cleavage of the BRCA1 ubiquitin mark from H2A. *Nat. Commun.* **9**, 229 (2018).

19. Stewart, M. D. *et al.* BARD1 is necessary for ubiquitylation of nucleosomal histone H2A and for transcriptional regulation of estrogen metabolism genes. *Proc. Natl. Acad. Sci. U. S. A.* **115**, 1316–1321 (2018).

20. Zhu, Q. *et al.* BRCA1 tumour suppression occurs via heterochromatin-mediated silencing. *Nature* **477**, 179–184 (2011).

21. Zhu, Q. *et al.* Heterochromatin-Encoded Satellite RNAs Induce Breast Cancer. *Mol. Cell* **70**, 842-853.e7 (2018).

22. Nakamura, K. *et al.* H4K20me0 recognition by BRCA1–BARD1 directs homologous recombination to sister chromatids. *Nat. Cell Biol.* **21**, 311–318 (2019).

23. Becker, J. R. *et al.* BARD1 reads H2A lysine 15 ubiquitination to direct homologous recombination. *Nature* **596**, 433–437 (2021).

24. Krais, J. J. *et al.* RNF168-mediated localization of BARD1 recruits the BRCA1-PALB2 complex to DNA damage. *Nat. Commun.* **12**, 5016 (2021).

25. Dai, L. *et al.* Structural insight into BRCA1-BARD1 complex recruitment to damaged chromatin. *Mol. Cell* **81**, 2765-2777.e6 (2021).

26. Zhao, W. *et al.* BRCA1-BARD1 promotes RAD51-mediated homologous DNA pairing. *Nature* **550**, 360–365 (2017).

27. Mark, W.-Y. *et al.* Characterization of segments from the central region of BRCA1: an intrinsically disordered scaffold for multiple protein-protein and protein-DNA interactions? *J. Mol. Biol.* **345**, 275–287 (2005).

28. Masuda, T., Xu, X., Dimitriadis, E. K., Lahusen, T. & Deng, C.-X. 'DNA Binding Region' of BRCA1 Affects Genetic Stability through modulating the Intra-S-Phase Checkpoint. *Int. J. Biol. Sci.* **12**, 133–143 (2016).

29. McGuffin, L. J., Bryson, K. & Jones, D. T. The PSIPRED protein structure prediction server. *Bioinformatics* **16**, 404–405 (2000).

30. Worden, E. J., Hoffmann, N. A., Hicks, C. W. & Wolberger, C. Mechanism of Cross-talk between H2B Ubiquitination and H3 Methylation by Dot1L. *Cell* **176**, 1490-1501.e12 (2019).

31. Hsu, P. L. *et al.* Structural Basis of H2B Ubiquitination-Dependent H3K4 Methylation by COMPASS. *Mol. Cell* **76**, 712-723.e4 (2019).

32. Worden, E. J., Zhang, X. & Wolberger, C. Structural basis for COMPASS recognition of an H2B-ubiquitinated nucleosome. *eLife* **9**, e53199 (2020).

33. McGinty, R. K. & Tan, S. Recognition of the nucleosome by chromatin factors and enzymes. *Curr. Opin. Struct. Biol.* **37**, 54–61 (2016).

34. McGinty, R. K. & Tan, S. Principles of nucleosome recognition by chromatin factors and enzymes. *Catal. Regul. ● Protein Nucleic Acid Interact.* **71**, 16–26 (2021).

35. Hornbeck, P. V. *et al.* PhosphoSitePlus, 2014: mutations, PTMs and recalibrations. *Nucleic Acids Res.* **43**, D512–D520 (2015).

36. Wang, X. *et al.* Molecular analysis of PRC2 recruitment to DNA in chromatin and its inhibition by RNA. *Nat. Struct. Mol. Biol.* **24**, 1028–1038 (2017).

37. Poepsel, S., Kasinath, V. & Nogales, E. Cryo-EM structures of PRC2 simultaneously engaged with two functionally distinct nucleosomes. *Nat. Struct. Mol. Biol.* **25**, 154–162 (2018).

38. Kim, S.-A., Chatterjee, N., Jennings, M. J., Bartholomew, B. & Tan, S. Extranucleosomal DNA enhances the activity of the LSD1/CoREST histone demethylase complex. *Nucleic Acids Res.* **43**, 4868–4880 (2015).

39. Budziszewski, G. R. *et al.* Multivalent DNA and nucleosome acidic patch interactions specify VRK1 mitotic localization and activity. *Nucleic Acids Res.* **50**, 4355–4371 (2022).

40. Morgan, M., Jbara, M., Brik, A. & Wolberger, C. Chapter One - Semisynthesis of ubiquitinated histone H2B with a native or nonhydrolyzable linkage. in *Methods in Enzymology* (ed. Hochstrasser, M.) vol. 618 1–27 (Academic Press, 2019).

41. Savage, K. I. & Harkin, D. P. BRCA1, a 'complex' protein involved in the maintenance of genomic stability. *FEBS J.* **282**, 630–646 (2015).

42. Schlacher, K., Wu, H. & Jasin, M. A Distinct Replication Fork Protection Pathway Connects Fanconi Anemia Tumor Suppressors to RAD51-BRCA1/2. *Cancer Cell* **22**, 106–116 (2012).

Figures

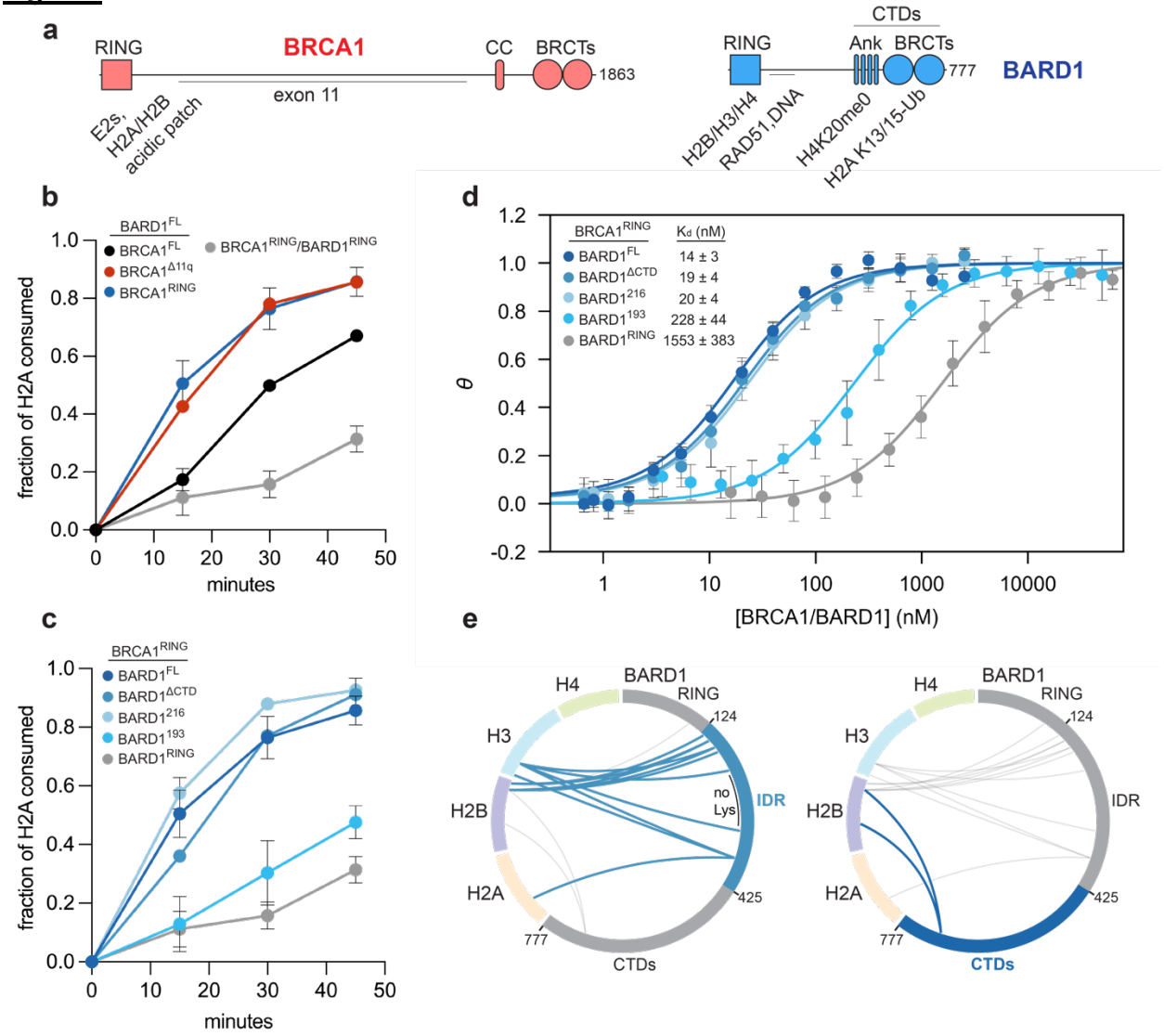

Figure 1. Contributions of BRCA1 and BARD1 regions to nucleosome binding and H2A-Ub activity. (a) Domain organization of BRCA1 and BARD1. The domain names are indicated above the cartoons (RING, really interesting new gene; CC, coiled-coil; BRCT, BRCA1 C-terminal; Ank, Ankyrin repeat domain; CTD, C-terminal domain). Binding sites of interacting partners previously described and relevant to this work are indicated below the domain illustrations. **(b, c)** Quantification of time-course H2A-Ub assays using the indicated BRCA1/BARD1 truncations. Data show the mean; error bars are ± 1-s.d. of n=3 independent experiments. **(d)** Comparison of nucleosome binding affinity from fluorescence-quenching based measurements using the indicated BRCA1/BARD1 constructs. Data show the mean; error bars are ± 1-s.d. of n=4 independent experiments. **(e)** Intermolecular crosslinks observed by chemical crosslinking and mass-spectrometry analysis between BARD1 and histones using wild-type nucleosomes and $BRCA1^{RING}/BARD1^{FL}$ heterodimers. Crosslinks to histones emanating from the intrinsically disordered region (IDR) and CTDs of BARD1 are shown in side-by-side plots. A lysine depleted region of the BARD1 IDR is labelled and indicated by a black bar.

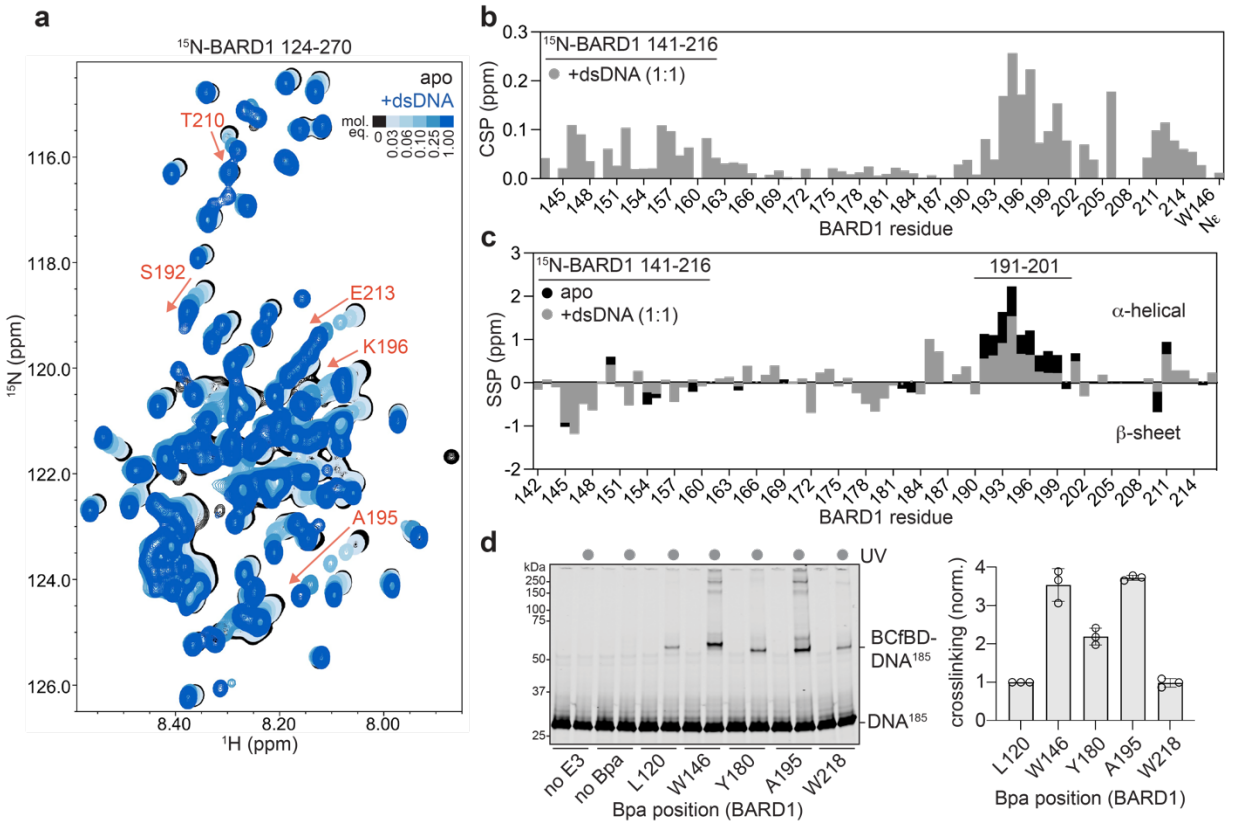

Figure 2. The BARD1 IDR binds to nucleosomes via DNA. (a) $^{1}H^{15}N$-HSQC NMR spectra of BARD1$^{124-270}$, titrating in a 36-bp dsDNA fragment. A subset of highly affected signals are labelled with their residue identities, with arrows showing their trajectories. **(b)** $^{1}H^{15}N$-HSQC NMR chemical shift perturbations (CSPs) observed to ^{15}N-BARD1$^{141-216}$ signals when bound to a 36-bp dsDNA fragment (in 1:1 complex). **(c)** Changes in secondary structural propensity (SSP) of ^{15}N-BARD1$^{141-216}$ when bound to a 36-bp dsDNA fragment (in 1:1 complex). **(d)** Representative SDS-PAGE gel monitoring in-gel fluorescence (labelled DNA) of UV-induced Bpa crosslinking of BRCA1-f-BARD1^{221} to nucleosomes (left). Quantification of Bpa crosslinking experiments with nucleosomes (right). The intensity of each crosslinked band was normalized to the intensity of the L120Bpa crosslinked band for each replicate experiment. Data bars show the mean; error bars are ± 1-s.d. and the open circles are the values of individual replicates for of n=3 independent experiments.

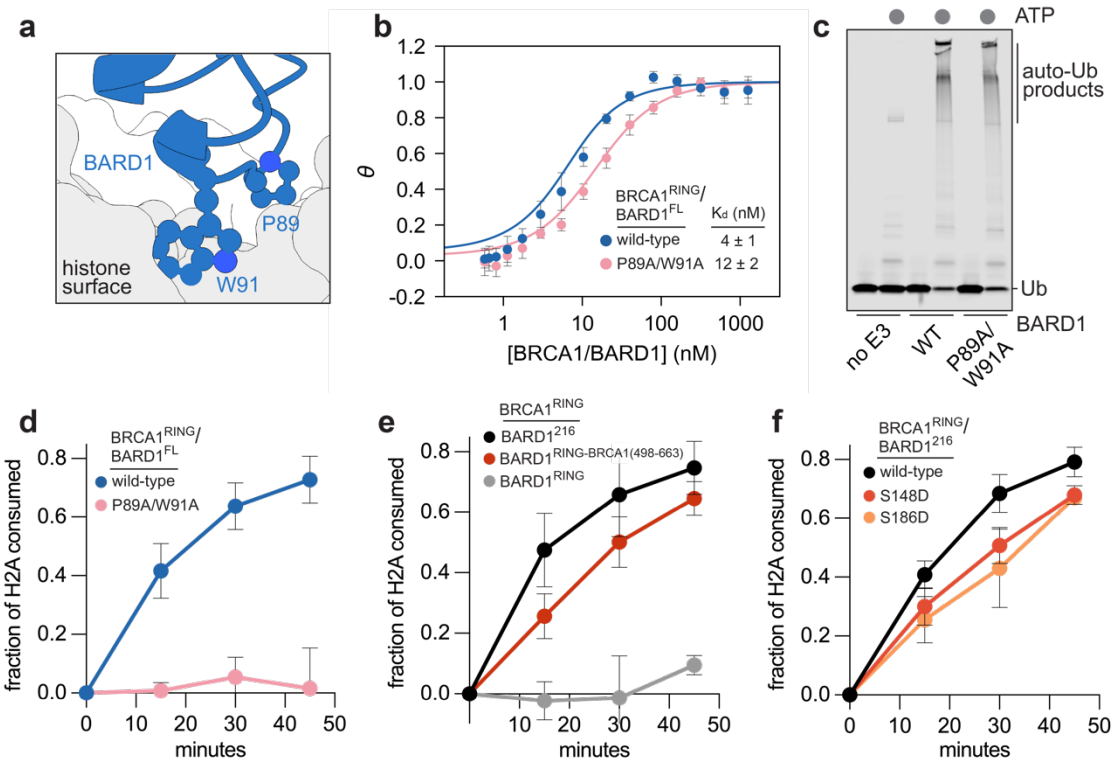

Figure 3. Contribution and regulation of BARD1 DNA binding in H2A-Ub activity. (a) The BARD1 RING-histone interface showing the locations of BARD1 P89A and W91 relative to the histone surface (PDB: 7JZV). **(b)** Comparison of nucleosome binding affinity using the indicated BRCA1/BARD1 constructs. Data show the mean; error bars are ± 1-s.d. of n=3 independent experiments. **(c)** Auto-ubiquitylation assay using $BRCA1^{RING}/BARD1^{FL}$ (wild-type or P89A/W91A). The assay monitors depletion of Ub and appearance of high molecular weight auto-Ub products in the presence of BRCA1/BARD1. Data shown is representative of n=2 independent experiments. **(d-f)** Quantification of time-course H2A-Ub assays using NCP^{147} substrates and the indicated BRCA1/BARD1 constructs. Data show the mean; error bars are ± 1-s.d. of n=3 independent experiments.

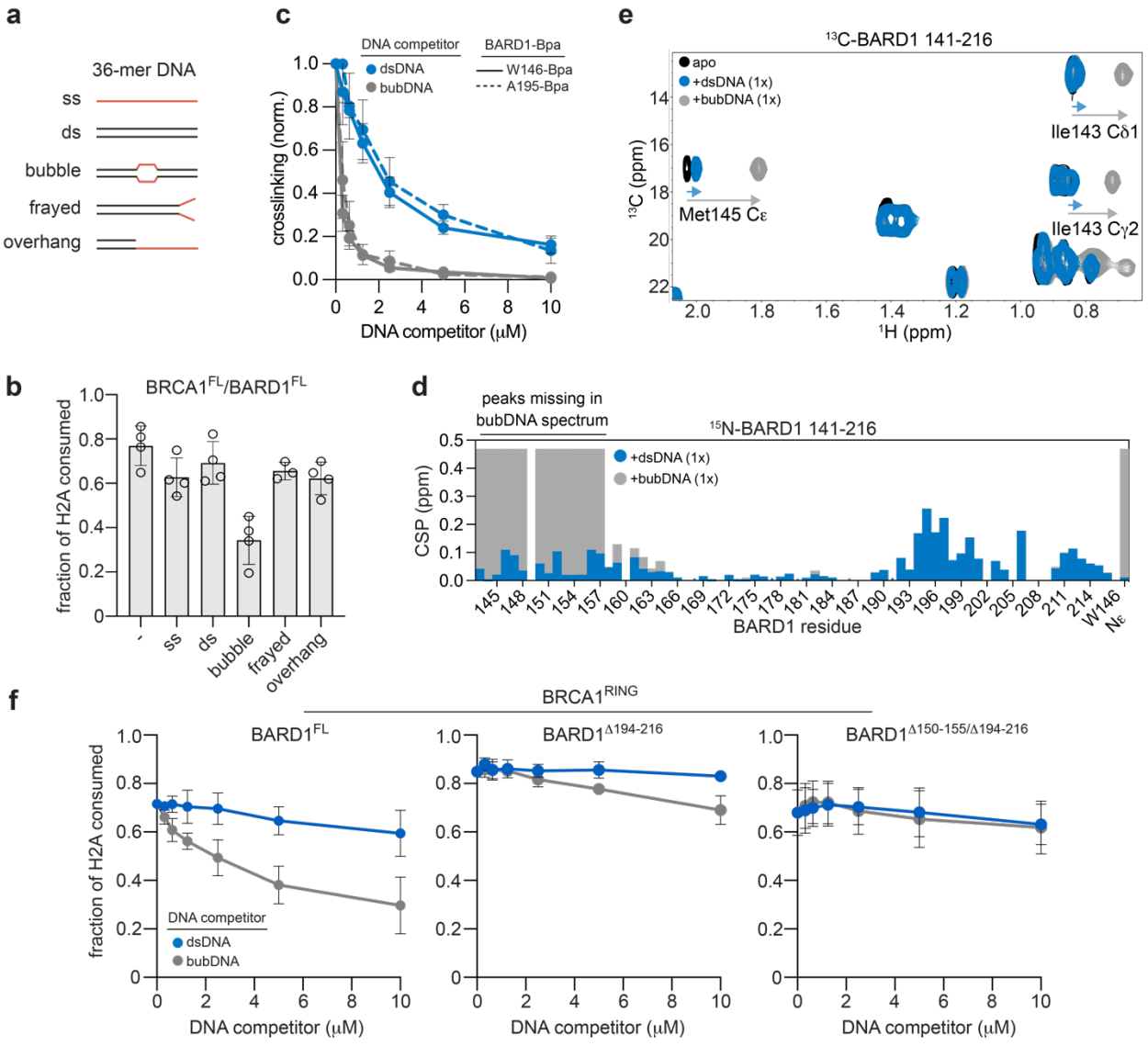

Figure 4. Inhibition of nucleosome binding and H2A-Ub by specialized DNA structures. **(a)** Design of 36-mer DNA competitor fragments. Red indicates non-base-paired regions. **(b)** Single time-point H2A-Ub inhibition assays using BRCA1^{FL}/BARD1^{FL} (100 nM) and the indicated competitor DNA (2.5 mM). Data show the mean; error bars are ± 1-s.d.; and open circles are individual data points of n=4 independent experiments. One outlier point for "frayed-DNA" was excluded from the analysis. **(c)** Inhibition of UV-induced Bpa crosslinking between the indicated BRCA1-f-BARD1^{221} Bpa-incorporated constructs and NCP^{185} substrates in the presence of increasing amounts of dsDNA or bubble-DNA competitor. Data show the mean; error bars are ± 1-s.d. of n=3 (W146Bpa) or n=4 (A195Bpa) independent experiments. **(d)** ^{1}H^{15}N-HSQC NMR chemical shift perturbations (CSPs) observed to ^{15}N-BARD1$^{141-216}$ signals when bound to a 36-mer dsDNA (blue) or bubble-DNA (gray) fragment (1:1 complex). Signals for residues 143-157 are missing in the bubble-DNA-bound spectrum, and gray bars are equal to the CSP value for the W146Nε CSP that was observed (see Extended Data Figure 4c). **(e)** Selected region of ^{13}C-HSQC spectra of ^{13}C-BARD1$^{141-216}$ in 1:1 complex with dsDNA fragment or bubble-DNA

fragment. Signal trajectories in bound specta are indicated by arrows. **(f)** Single time-point H2A-Ub inhibition assays using heterodimers containing $BRCA1^{RING}$/$BARD1^{FL}$ (left) or the indicated BARD1 internal deletion mutant (50 nM E3) and increasing amounts of dsDNA or bubble-DNA competitor. Data show the mean; error bars are ± 1-s.d. of n=3 independent experiments.

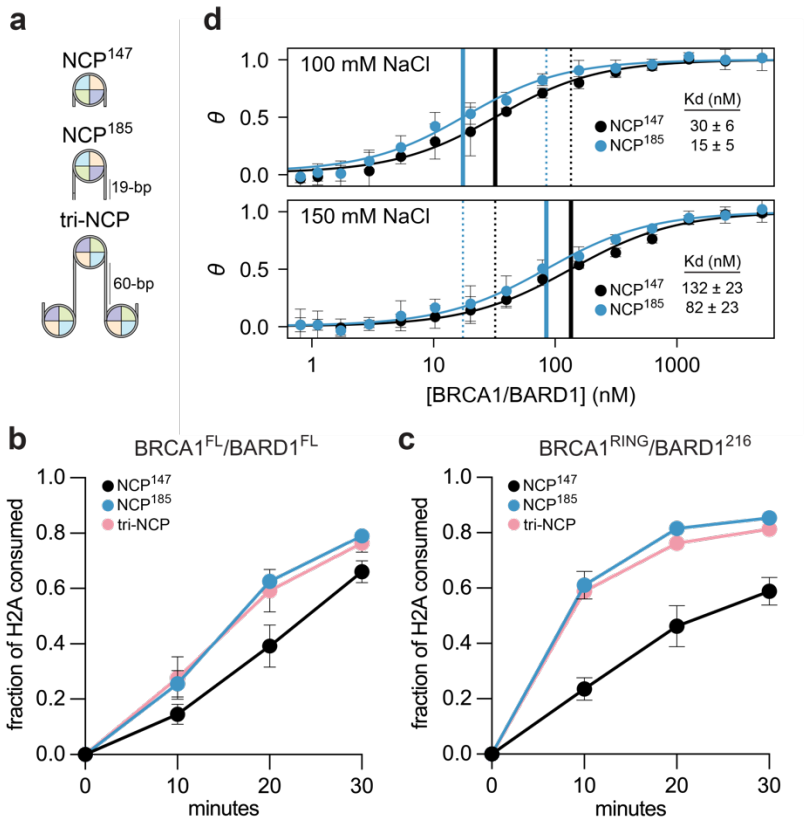

Figure 5. An unmodified mono-nucleosome with linker DNA is an optimal substrate for BRCA1/BARD1. (a) Schematic of chromatin substrates used for H2A-Ub activity and nucleosome binding assays in panels b-d. The length of linker-DNA is indicated next to the NCP^{185} and tri-NCP. **(b, c)** Quantification of time-course H2A-Ub assays using the indicated BRCA1/BARD1 constructs and chromatin substrates. Data show the mean; error bars are ± 1-s.d. of n=3 independent experiments. **(d)** Comparison of nucleosome binding affinity between $BRCA1^{RING}/BARD1^{216}$ and NCP^{147} and NCP^{185} substrates at 100 mM (top) and 150 mM (bottom) buffer-salt concentration (NaCl). Solid vertical lines denote the position of K_d values for the indicated buffer-salt concentration, and the dotted vertical lines denote the position of K_d values from the other buffer-salt concentration. Data show the mean; error bars are ± 1-s.d. of n=3 independent experiments using both NCP^{147} and NCP^{185}, with an additional replicate (total of n=4) for NCP^{147}.

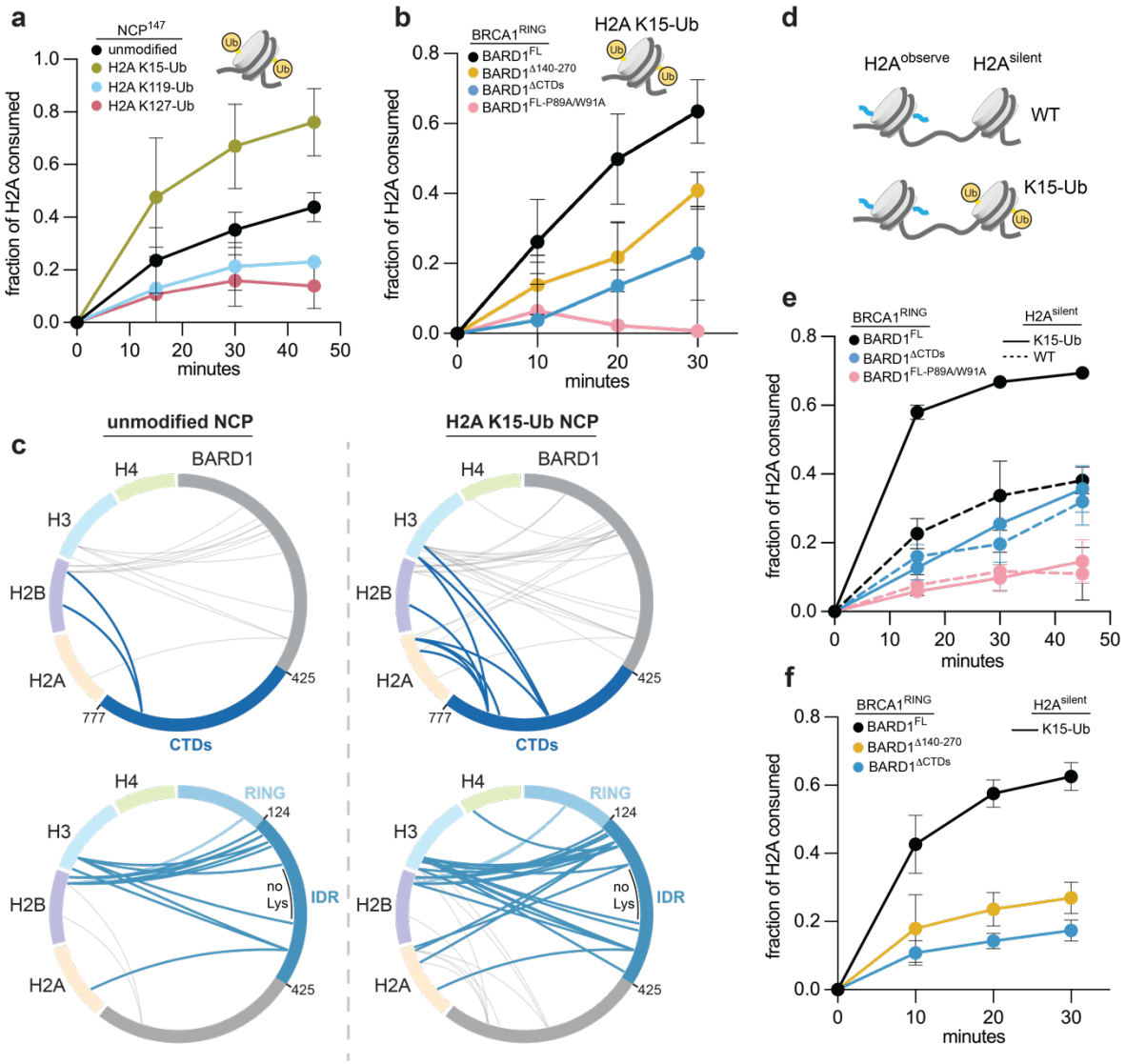

Figure 6. Enhancement of H2A-Ub activity by nucleosomes containing H2A K15-Ub. (a) Quantification of time-course H2A-Ub assays using unmodified or preinstalled H2A-Ub chromatin substrates and BRCA1^{FL}/BARD1^{FL}. **(b)** Quantification of time-course H2A-Ub assays using H2A K15-Ub chromatin substrates and indicated BRCA1/BARD1 constructs. **(c)** Intermolecular crosslinks observed by chemical crosslinking and MS analysis between BARD1 and histones using wild-type (left) and H2A K15-Ub (right, separated by dashed line) 147-bp '601' nucleosomes and BRCA1^{RING}/BARD1^{FL} heterodimers. Crosslinks to histones emanating from the CTDs of BARD1 (top) and IDR (bottom) from the same reactions are shown as stacked circle plots. A lysine depleted region of the BARD1 IDR is labelled and indicated by a black bar. **(d)** Design of di-NCP substrates. **(e, f)** Quantification of time-course H2A-Ub assays using the indicated combinations of di-NCP substrate and BRCA1/BARD1 heterodimer. For panels a, b, e, and f, data show the mean; error bars are ± 1-s.d. of n=3 independent experiments.

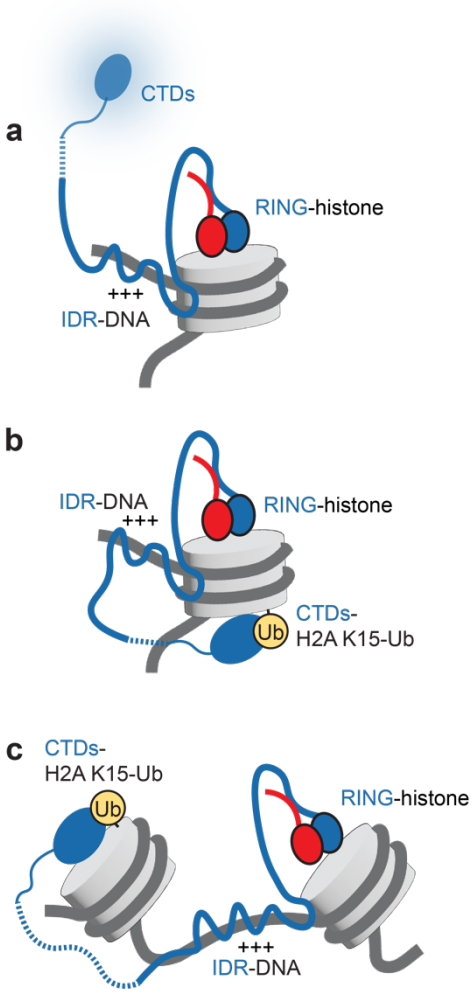

Figure 7. Models of BRCA1/BARD1/chromatin complexes supported by this study. (a) Model of BRCA1/BARD1 association with an unmodified mono-nucleosome substrate. The fuzziness of the BARD1 CTDs is representative of not being associated with the nucleosome. **(b)** Model of BRCA1/BARD1 binding to an H2A K15-Ub mono-nucleosome substrate and **(c)** asymmetric di-nucleosome substrate across nucleosome units.

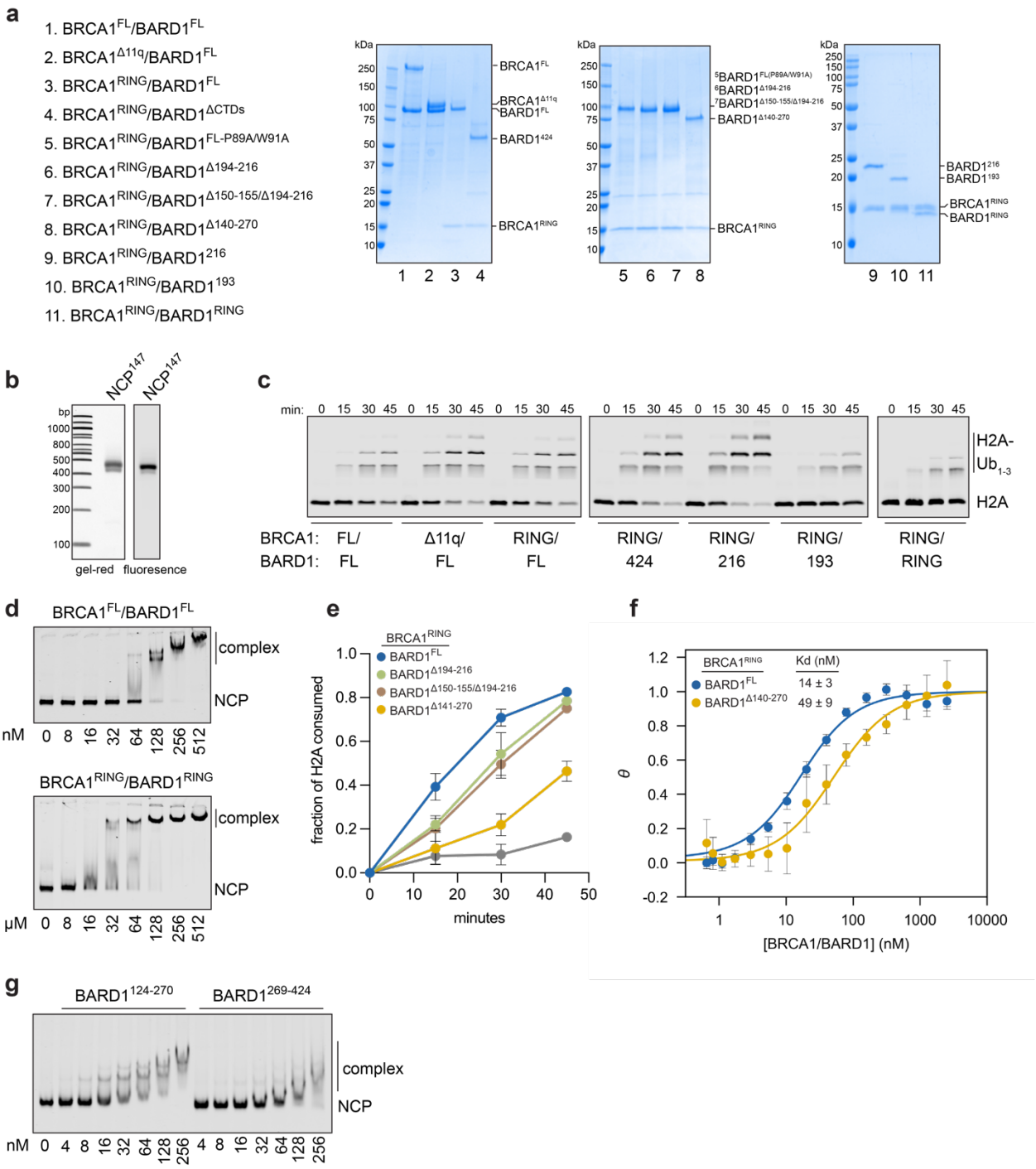

Extended Data Figure 1. Characterization of BRCA1/BARD1 constructs. (a) Coomassie-stained SDS-PAGE gels of BRCA1/BARD1 constructs used int this study. **(b)** Native gel showing an example of the minimal mono-nucleosomes substrates (NCPs) wrapped by 147-bp of '601' DNA with a fluorophore conjugated to the N-terminus of H2A used in *in vitro* ubiquitylation assays. **(c)** Representative time-course nucleosome ubiquitylation assays monitoring H2A-Ub efficiency of different BRCA1/BARD1 constructs quantified in Figure 1a and 1b. These data are representative of the basic assay set-up for other time-course H2A-Ub

assays in this study. **(d)** Electrophoretic mobility shift assay (EMSA) comparing the nucleosome binding of full-length BRCA1/BARD1 (top) to the minimal RING heterodimer (bottom). Data shown are representative of n=2 independent experiments. **(e)** Quantification of H2A-Ub assays using the indicated BRCA1/BARD1 constructs. Data show the mean; error bars are ± 1-s.d. of n=3 independent experiments. **(f)** Comparison of nucleosome binding affinity from fluorescence-quenching based measurements using the indicated BRCA1/BARD1 constructs. Data show the mean; error bars are ± 1-s.d. of n=4 independent experiments. **(g)** EMSA monitoring nucleosome binding by the indicated BARD1 IDR fragments. Data shown are representative of n=2 independent experiments.

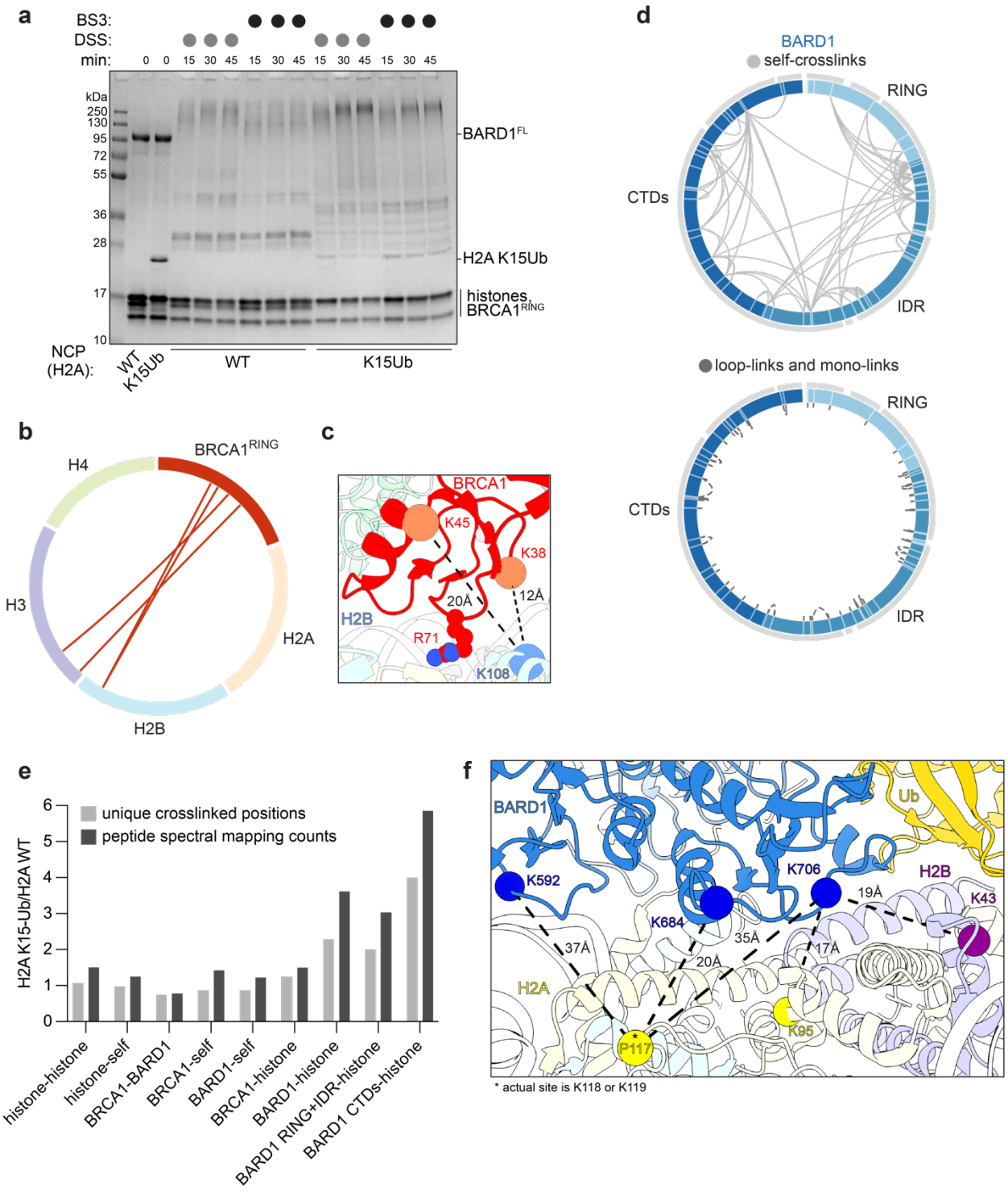

Extended Data Figure 2. Analysis of BRCA1/BARD1 chromatin complexes by chemical crosslinking and mass-spectrometry. (a) Coomassie-stained SDS-PAGE gel of chemical crosslinking reactions used in mass spectrometry analysis **(b)** Circle-plot of crosslinks observed from the RING domain of BRCA1 to histones (red). **(c)** Crosslinks observed from the RING domain of BRCA1 to ordered regions histones mapped on a high-resolution structure of the complex (PDB: 7JZV). Cα-Cα distances are indicated in the figure. **(d)** BARD1 intramolecular

crosslinks (top) and loop-links/mono-links (bottom) from the unmodified H2A NCP data set. **(e)** Quantitative comparison of crosslinking from reactions with unmodified and H2A K15-Ub NCPs. Different subsets of crosslinks were quantified for the number of unique observed crosslinks and total peptide spectral mapping counts for all crosslinks within a given subset. **(f)** Crosslinks observed from the CTDs of BARD1 to ordered regions histones in the H2A K15-Ub NCP sample mapped on a high-resolution structure (PDB: 7E8I). Cα-Cα distances are indicated. The P117 Ca serves as a proxy for the true crosslinking sites of K118 and K119 that are not modelled, denoted by an asterisk.

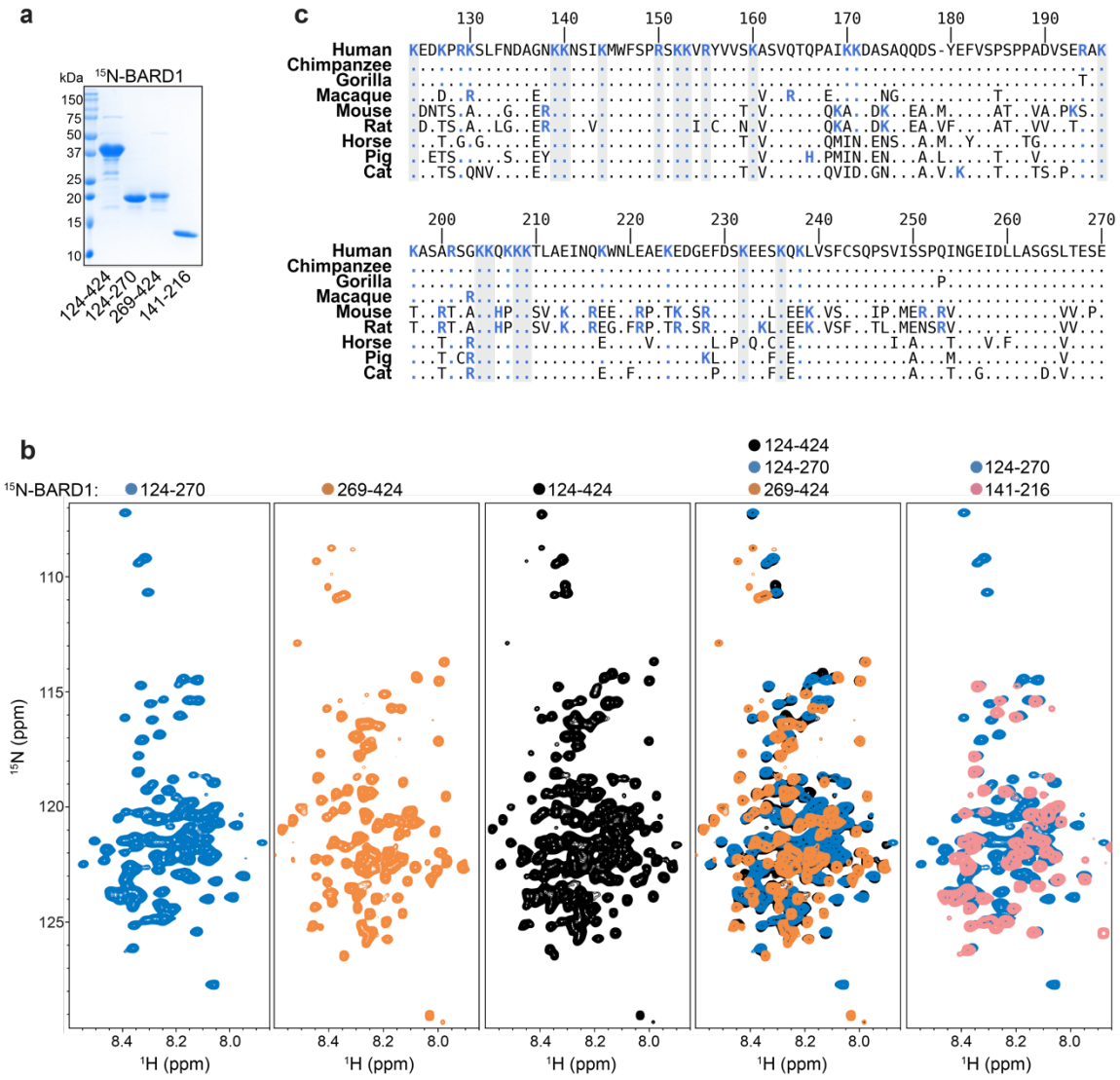

Extended Data Figure 3. Characterization of the BARD1 intrinsically disordered region. **(a)** Coomassie-stained SDS-PAGE gel of BARD1 fragments used in NMR experiments. **(b)** $^{1}H^{15}N$-HSQC NMR spectra of the indicated BARD1 fragments. **(c)** multiple-sequence alignment of BARD1 124-270 with a representative subset of homologs. Residue identities that are conserved to the human sequence are indicated by the presence of a period in place of a residue letter. Basic residues (Lys, Arg, His) are color coded in blue, and basic positions that are fully conserved across all species are highlighted with a gray background.

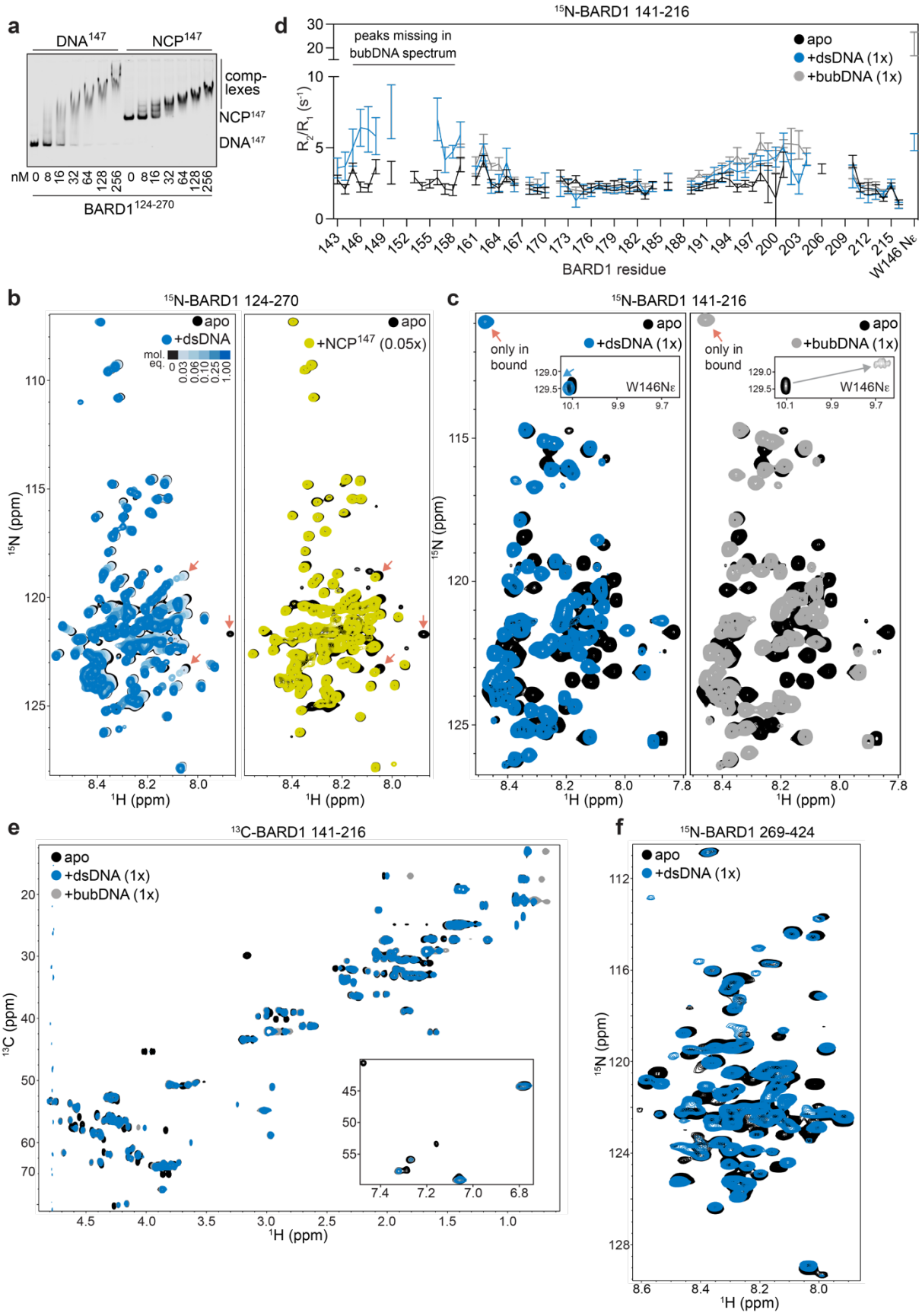
a
DNA147
NCP147
comp-lexes
NCP147
DNA147
nM 0 8 16 32 64 128 256 0 8 16 32 64 128 256
BARD1124-270
d
15N-BARD1 141-216
peaks missing in bubDNA spectrum
apo
+dsDNA (1x)
+bubDNA (1x)
R2/R1 (s-1)
BARD1 residue
W146 Nε
b
15N-BARD1 124-270
apo
+dsDNA
mol. eq. 0 0.03 0.06 0.10 0.25 1.00
+NCP147 (0.05x)
15N (ppm)
1H (ppm)
c
15N-BARD1 141-216
only in bound
+dsDNA (1x)
+bubDNA (1x)
W146Nε
e
13C-BARD1 141-216
13C (ppm)
f
15N-BARD1 269-424

Extended Data Figure 4. NMR analysis of BARD1 IDR-DNA and IDR-nucleosome complexes. (a) EMSA comparing DNA and nucleosome binding by BARD1$^{124-270}$. Data shown are representative of n=2 independent experiments. **(b)** $^{1}H^{15}N$-HSQC NMR spectra of BARD1$^{124-270}$, titrating a 36-bp dsDNA fragment (left), and a single titration point with nucleosomes (right). The red arrows point to signals that are similarly affected between the dsDNA- and nucleosome-bound samples. **(c)** $^{1}H^{15}N$-HSQC NMR spectra of ^{15}N-BARD1$^{141-216}$, in 1:1 complex with a 36-mer dsDNA fragment (left), or a 36-mer bubble-DNA fragment with 8-bp of mismatch (right). The W146Ne signals are inlaid, and the red arrows point to a signal that is present exclusively in the DNA-bound spectra. **(d)** T1/T2 dynamics measurements for amide signals of ^{15}N-BARD1$^{141-216}$ in apo form and bound to dsDNA or bubble-DNA. **(e)** Full ^{13}C-HSQC spectra of ^{13}C-BARD1$^{141-216}$ in 1:1 complex with a 36-mer dsDNA fragment or a 36-mer bubble-DNA fragment with 8-bp of mismatch. **(f)** $^{1}H^{15}N$-HSQC NMR spectra of ^{15}N-BARD1$^{269-424}$ and in 1:1 complex with a 26-mer dsDNA fragment.

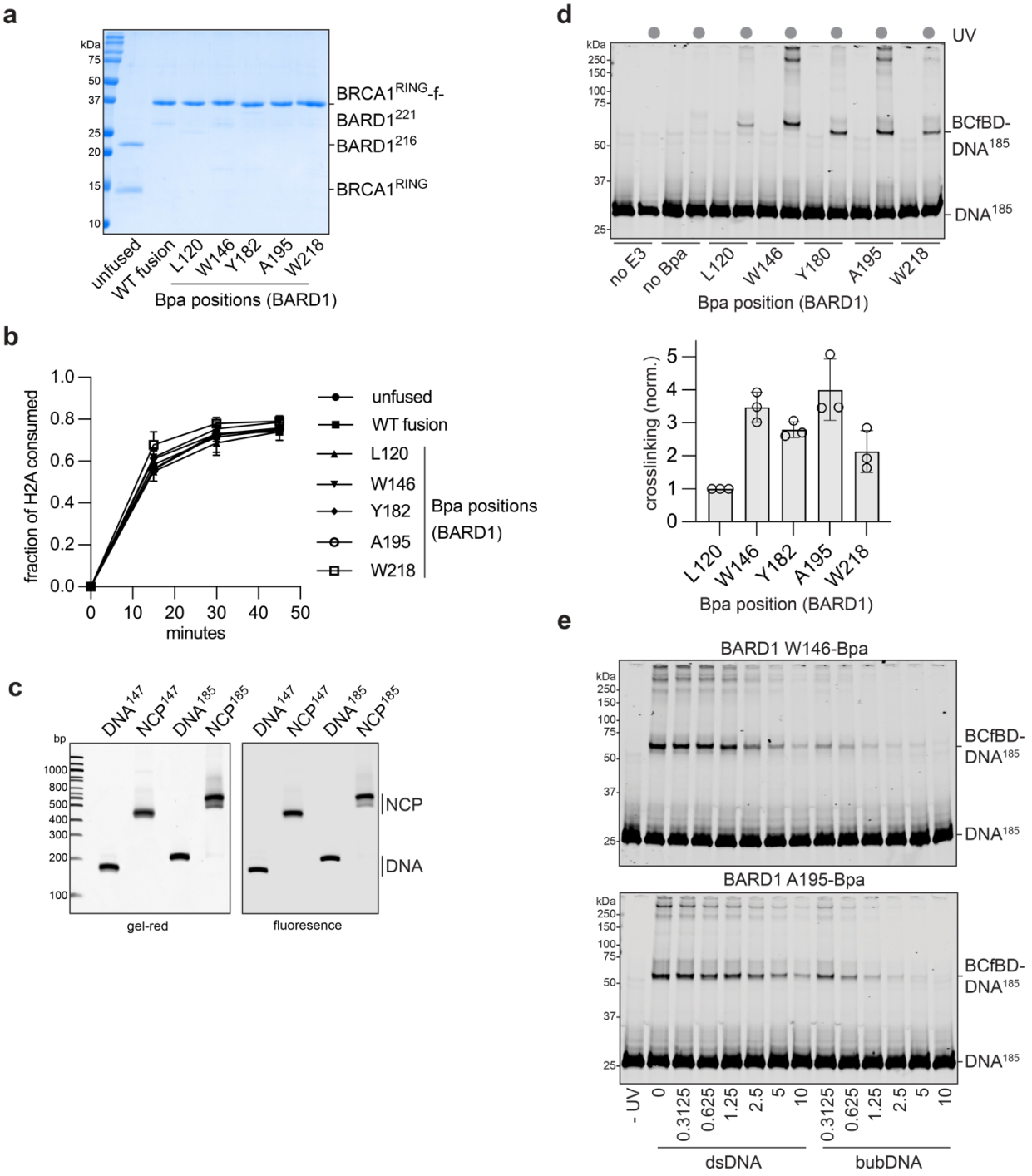

Extended Data Figure 5. UV-induced Bpa crosslinking of BRCA1/BARD1 to nucleosomal DNA. (a) Coomassie-stained SDS-PAGE gel of unfused $BRCA1^{RING}/BARD1^{216}$ heterodimers and BRCA1-f-$BARD1^{221}$ constructs with and without Bpa incorporation. **(b)** H2A-Ub activity of unfused heterodimers compared to wild-type and Bpa-incorporated BRCA1-f-$BARD1^{221}$. Data show the mean; error bars are ± 1-s.d. of n=3 independent experiments. **(c)** Native gel of fluorescently labelled DNA and nucleosomes used in Bpa crosslinking experiments. **(d)** Representative data of in-gel fluorescence signal from of a UV-induced crosslinking reaction to free 185-bp '601' DNA (DNA^{185}, top) and quantification of crosslinking experiments (bottom).

The intensity of each crosslinked band was normalized to the L120Bpa crosslinked band intensity for each replicate experiment. Data bars show the mean; error bars are ± 1-s.d. and the open circles are the values of individual replicates for of n=3 independent experiments. **(e)** Representative data of in-gel fluorescence signal from a UV-induced Bpa crosslinking reaction between W146Bpa (top) and A195Bpa (bottom) BRCA1-f-BARD1^{221} to 185-bp '601' nucleosomes (NCP^{185}) in the presence of dsDNA and bubble-DNA competitors. Quantified data from n=3 replicate experiments are shown in Figure 4c.

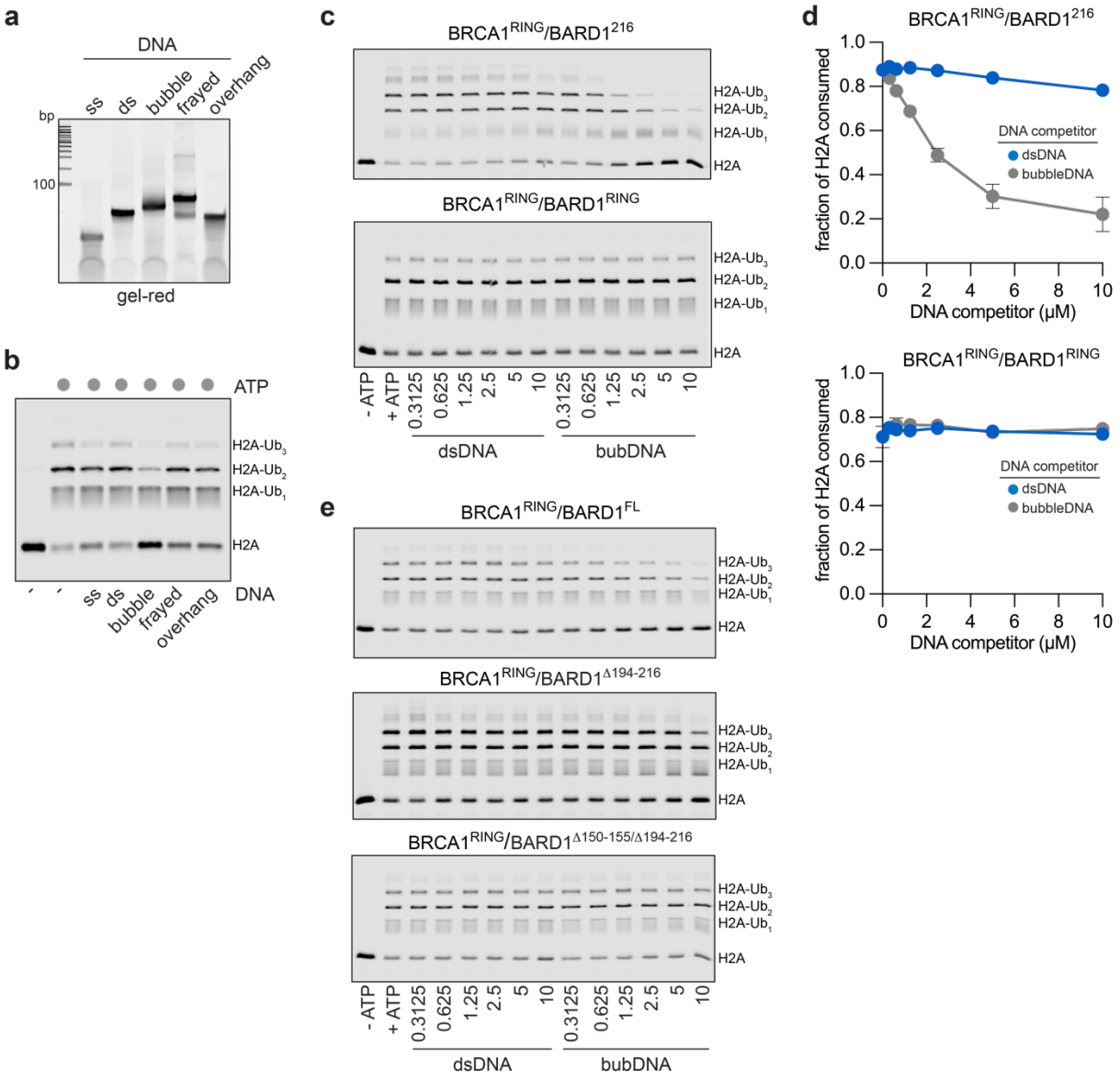

Extended Data Figure 6. Assembly of competitor DNA fragments and inhibition of H2A-Ub activity. (a) DNA-stained native-gel of annealed DNA competitor fragments. Amounts loaded were normalized to show similar band-intensity for each fragment. **(b)** Representative gel data of H2A-Ub inhibition assay using full-length BRCA1/BARD1 (100 nM) and the indicated DNA competitor fragment (2.5 mM) **(c)** Representative gel data of single time-point (20 min) H2A-Ub inhibition assays using BRCA1^{RING}/BARD1^{216} (top, 50 nM E3) and BRCA1^{RING}/BARD1^{140} (bottom, 750 nM E3) and indicated amounts of dsDNA and bubble-DNA competitors. **(d)** Quantification of H2A-Ub DNA-competitor inhibition assays from panel b using the indicated BRCA1/BARD1 constructs. Data show the mean; error bars are ± 1-s.d. of n=3 independent experiments. **(e)** Representative gel data of single time-point H2A-Ub inhibition assays using BRCA1^{RING}/BARD1^{FL} (top, 50 nM E3, 12 min endpoint), BRCA1^{RING}/BARD1$^{Δ194-216}$ (middle, 50 nM E3, 20 min endpoint), and BRCA1^{RING}/BARD1 $^{Δ150-155/Δ194-216}$ (bottom, 50 nM E3, 20 min endpoint) and indicated amounts of dsDNA and bubble-DNA competitors.

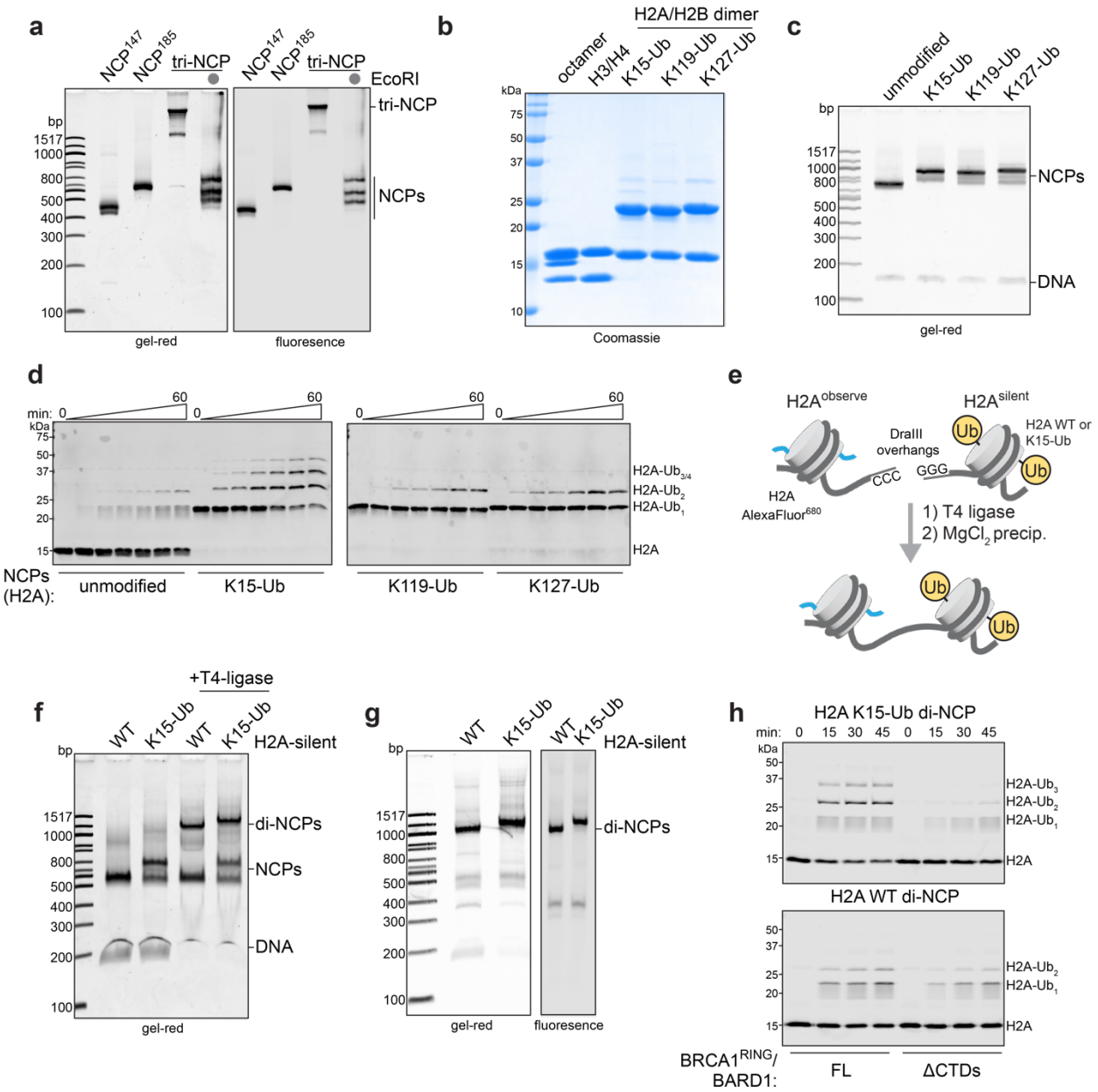

Extended Data Figure 7. Design, assembly, and quality control of higher-order chromatin substrates. (a) DNA-stained (left) and fluorescence (right) native gel of chromatin substrates used for H2A-Ub activity assays in Figure 5b and c. EcoRI digestion of tri-NCPs is used to confirm octamer binding saturation. **(b)** Coomassie-stained SDS-PAGE gel of wild-type histones and dichloroacetone linked H2A-Ub/H2B dimers. **(c)** DNA-stained native gel of mono-nucleosomes with and without H2A-Ub incorporation at the indicated positions. **(d)** Example data of H2A-Ub activity assay using full-length BRCA1/BARD1 and preinstalled H2A-Ub NCP substrates. Western blots were probed for H2A. **(e)** Schematic of asymmetric di-NCP assembly strategy. **(f)** DNA-stained native gel of di-NCP ligation reaction. **(g)** DNA-stained (left) and fluorescence (right) native gels of di-NCP substrates after purification by $MgCl_2$ precipitation. **(h)** Example gel data of H2A-Ub activity assay using di-NCP substrates and indicated BRCA1/BARD1 constructs.

Tables

Extended Data Table I. Details about BRCA1/BARD1 constructs used in this study.

Construct	BRCA1 bounds*	BRCA1 tags	BARD1 bounds*	BARD1 tags	Expression system
$BRCA1^{FL}$/ $BARD1^{FL}$	1-1863	N-FLAG	1-777	N-TwinStrepII	*Sf9*
$BRCA1^{\Delta 11q}$/ $BARD1^{FL}$	1-264, 1366-1863	N-FLAG	1-777	N-TwinStrepII	*Sf9*
$BRCA1^{RING}$/ $BARD1^{FL}$	1-112	N-FLAG	1-777	N-TwinStrepII	*Sf9*
$BRCA1^{RING}$/ $BARD1^{DCTDs}$	1-112	N-FLAG	1-424	N-TwinStrepII	*Sf9*
$BRCA1^{RING}$/ $BARD1^{\Delta 194-216}$	1-112	N-FLAG	1-193, 217-777	N-TwinStrepII	*Sf9*
$BRCA1^{RING}$/ $BARD1^{\Delta 150-155/\Delta 194-216}$	1-112	N-FLAG	1-149, 156-193, 217-777	N-TwinStrepII	*Sf9*
$BRCA1^{RING}$/ $BARD1^{\Delta 140-270}$	1-112	N-FLAG	1-139, 271-777	N-TwinStrepII	*Sf9*
$BRCA1^{RING}$/ $BARD1^{216}$	1-110	N-6xHis	26-216	none	*E. coli*
$BRCA1^{RING}$/ $BARD1^{193}$	1-110	N-6xHis	26-193	none	*E. coli*
$BRCA1^{RING}$/ $BARD1^{RING}$	1-110	N-6xHis	26-140	none	*E. coli*

* BRCA1 UniProt sequence ID: P38398-1; BARD1 UniProt sequence ID: Q99728-1

Methods

Protein, nucleosome, and experimental reagent production

Ubiquitylation machinery: Human E1 (UBA1), E2 (UBE2D3), and ubiquitin (wild-type and Q2C mutant) were expressed and purified as previously described[43–45]. For a full list of BRCA1/BARD1 truncation constructs, their residue bounds, purification/epitope tags, and expression system, see Extended Data Table I.

BRCA1/BARD1 from E. coli: For purification of truncated BRCA1/BARD1 heterodimers from *E. coli* expression ($BRCA1^{RING}/BARD1^{RING}$, $BRCA1^{RING}/BARD1^{193}$, and $BRCA1^{RING}/BARD1^{216}$), plasmids containing 6xHis-tagged BRCA1 (pCOT7n) and untagged BARD1 (pET28n) were co-transformed into *E. coli* BL21 (DE3) cells, grown in LB media at 37 °C to OD_{600nm} of 0.6-0.8, supplemented with 100 mM $ZnCl_2$ and induced with 0.2 mM IPTG for ~16 hours at 16 °C. The cell pellets were resuspended in 30 mL of Ni^{2+} start buffer (25 mM Tris-HCl pH 7.5, 500 mM NaCl, 10 mM imidazole) supplemented with DNase, RNase, EDTA-free protease inhibitors (Roche) and 1 mM PMSF, lysed by French press, centrifuged, and the supernatant was applied to a 5 mL HisTrap FF crude column (Cytiva). After extensive washing with Ni^{2+} start buffer containing 10 mM imidazole and 30 mM imidazole, protein was eluted using the same buffer supplemented with 500 mM imidazole. The $BRCA1^{RING}/BARD1^{RING}$ and $BRCA1^{RING}/BARD1^{193}$ constructs were concentrated and further purified using a 120 mL Superdex 75 column on an AKTA FPLC system in SEC buffer (25 mM HEPES-NaOH pH 7.5, 150 mM NaCl, 1 mM DTT; GE Healthcare). For the $BRCA1^{RING}/BARD1^{216}$, HisTrap elutions were dialyzed into ion-exchange buffer (25 mM Tris-HCl pH 7.5, 250 mM NaCl, 1 mM DTT) and applied to a 5 mL HiTrap SP HP column (Cytiva) and eluted over a 12 column-volume (CV) gradient (0.25-1 M NaCl). Peak fractions were concentrated, aliquoted, and flash frozen.

For Bpa crosslinking experiments, 6xHis-BRCA1$^{1-104}$-$(GS)_6$-BARD1$^{26-221}$ was sub-cloned using Gibson assembly into a pET28n vector. Constructs for Bpa incorporation were generated via site-directed mutagenesis to install amber stop codons in place of BARD1 L120, W146, Y180, A195, and W218. Bpa-mutant Pet28n-6xHis-BRCA1$^{1-104}$-$(GS)_6$-BARD1$^{26-221}$ plasmids were co-transformed with a pEVOL-Bpa plasmid encoding an evolved Bpa aminoacyl tRNA synthetase (gift from P. Schultz, Addgene #31190) in *E. coli* BL21 (DE3) cells[46]. At OD_{600nm}=0.4-0.5, cells were shifted from 37 °C to 16 °C and supplemented with 1 mM Bpa (dissolved in 1M NaOH; Bachem) and 100 mM $ZnCl_2$. After 30 minutes, protein expression was induced by addition of 0.02% L-arabinose and 0.2 mM IPTG for ~16 hours at 16 °C. Proteins were purified as described for the BRCA1^{RING}/BARD1^{216} construct. Truncations that did not incorporate Bpa were separated via the SP column.

BRCA1/BARD1 from insect cells: For insect cell expression, truncation and deletion constructs were derived from full-length BRCA1 (pFastBac-FLAG-BRCA1$^{1-1863}$; gift from W. Zhao, UT Health Sciences Center at San Antonio) and insect cell codon-optimized full-length BARD1 (pFastBac-Twin-StrepII-BARD1$^{1-777}$; gift from A. Deans, Addgene plasmid #137166) [47] using Gibson assembly cloning (NEB). Baculovirus was generated using the Bac-to-Bac system in suspension culture *Sf9* cells according to the manufacturers protocols (Invitrogen). For general *Sf9* growth and virus amplification, SF900-II media (ThermoFisher) was supplemented with 5% FBS (HyClone) and 1x antibiotic-antimycotic (Gibco). For protein expression, 15 mL of BRCA1- and 15 mL of BARD1-containing P3 baculoviruses were added to 650 mL of *Sf9* cells at ~1.5x10^6 cells/mL in SF900-II media supplemented with 1% FBS and 1x antibiotic-antimycotic. Protein expression was carried out for 48-72 hours at 27 °C, shaking at 110 RPM. Following expression, cells were spun down at 150 x g for 10 minutes. The pellet was resuspended in 30 mL of Strep-start buffer (50 mM Tris-HCl pH 8, 10% glycerol, 150 mM NaCl, 1 mM DTT)

supplemented with EDTA-free protease inhibitors and 1 mM PMSF and flash-frozen. Following freeze-thawing in a 37 °C water bath, additional EDTA-free protease inhibitors and PMSF were added in addition to 2 µL of benzonase (Sigma Aldrich). All subsequent steps were performed on ice or in a cold room over a short timeframe to prevent proteolysis (<3 hours total). Lysis was performed by sonication using a Branson Sonifier 250 (VWR Scientific) by applying 2x15 pulses at 70% duty on power level 8, ensuring that the cell mixture stayed cold. PMSF was added throughout the lysis protocol. The lysed cells were centrifuged at 41,000 x g for 15 minutes, filtered through a 0.45 mM low protein-binding PVDF filter (Millipore) and applied to a 1 mL StrepTrap HP column pre-equilibrated in Strep-start buffer (Cytiva). The column was washed with 8 mL Strep-start buffer supplemented with protease inhibitors, 8 mL wash buffer (25 mM Tris-HCl pH 7.5, 300 mM NaCl, 0.01% Igepal-CA630, 1 mM DTT, 5 mM MgCl2, 2 mM ATP, 10% glycerol, EDTA-free protease inhibitors), and an additional 5 mL of Strep-start buffer. The column was eluted using 6 mL of Strep-start buffer supplemented with 3 mM d-Desthiobiotin (Sigma). The elution was diluted with 20 mL of ion-exchange buffer (25 mM HEPES-NaOH pH 7.5, 10% glycerol, 1 mM DTT) and applied to a 1 mL SP HP column pre-equilibrated in ion-exchange buffer containing 75 mM NaCl. The SP column was eluted over 12-CV (75-500 mM NaCl). Peak fractions were combined and concentrated using a 30K MWCO concentrator (Amicon), and flash-frozen in small aliquots. Concentrations were estimated by measuring absorbance at 280 nM using molar extinction coefficients obtained from ProtParam (Expasy). Concentration estimates were verified by SDS-PAGE and Coomassie staining, and slight adjustments in concentration were applied to best equalize the amounts of E3 in activity and binding assays.

BARD1 intrinsically disordered region: BARD1 124-270, 141-216, 269-424, and 124-424 were sub-cloned from pFastBac-6xHis-BARD1$^{1-777}$ (gift from W. Zhao, UTHCSCA) into a modified pET28 vector containing an N-terminal 6xHis-SUMO tag using Gibson assembly cloning.

Plasmids were transformed into BL21 (DE3) *E. coli*, grown at 37 °C in M9 media supplemented with appropriate combination of isotopes (^{15}N-NH_4Cl, ^{13}C-glucose; Cambridge Isotopes) to an OD_{600nm} of 0.6-0.8, and induced with 0.2 mM IPTG for ~16 hours at 16 °C. HisTrap Ni^{2+} purification was performed as described above for BRCA1/BARD1 constructs expressed in *E. coli*. Elutions were dialyzed into ion exchange buffer (25 mM Tris pH 8.0, 200 mM NaCl, 0.5 mM EDTA, 1 mM DTT) in the presence of GST-SENP1 (produced in-house) to cleave the SUMO tag, leaving a non-native serine residue preceding the N-terminus except in the case of 269-424. The cleaved product was applied at a HiTrap Q column preceding a HiTrap SP column in-tandem to capture the non-specifically bound DNA (Cytiva). After application, the Q column was removed, and the SP column was eluted using a 12-CV gradient (0.2-1M NaCl). The peak fractions were combined, concentrated, and further purified using a Superdex 75 column equilibrated in NMR buffer (25 mM MOPS-NaOH pH 7.0, 100 mM NaCl, 1 mM EDTA, 0.5 mM TCEP (tris(2- carboxyethyl)phosphine)).

Histone purification: Wild-type and mutant human histones were transformed in *E. coli* BL21 (DE3) *pLysS* cells, grown at 37 °C to an OD_{600nm} of 0.5-0.6, and induced with 0.5 mM IPTG for 2 hours (H4) or 3 hours (H2A-2A, H2B-1K, H3.2) at 37 °C. Histone octamers used for fluorescence labeling were purified using the one-pot refolding protocol as described previously using 6xHis-TEV-H2A [14,48]. For nucleosome ubiquitylation assays, a glycine within the TEV cleavage scar was mutated to a cysteine for fluorophore conjugation (H2A G-1C) via site-directed mutagenesis. For fluorescence based binding assays, a cysteine was introduced at H2B D51 via site-directed mutagenesis.

For reconstituting chemically modified H2A-Ub nucleosomes, histones were purified individually essentially as described [49]. Briefly, inclusion bodies from 6-8L of histone expression in LB media

were lysed in buffer T (50 mM Tris-HCl pH 7.4, 1 mM EDTA, 100 mM NaCl), washed by sonication twice in buffer TW (50 mM Tris-HCl pH 7.4, 1 mM EDTA, 100 mM NaCl, 1% v/v Triton-X100), and then twice again in buffer T. Inclusion bodies were softened by stirring with a small volume of DMSO (2-3 mL), and extracted with 60 mL of extraction buffer (25 mM Tris-HCl pH 7.5, 7 M guanidinium-HCl, 0.5 mM EDTA, 10 mM DTT). After centrifugation, the supernatant was dialyzed overnight into ion-exchange buffer (25 mM Tris-HCl pH 7.5, 7 M deionized urea, 100 mM NaCl, 0.5 mM EDTA, 10 mM DTT), and applied to 2x5 mL HiTrap Q columns preceding 2x5 mL HiTrap SP columns in-tandem to capture the non-specifically bound DNA (Cytiva). After sample application, the Q columns were removed, and the SP columns were eluted using a 12-CV salt gradient (0.1-1M NaCl for H2A and H2B, 0.2-1M NaCl for H3 and H4). The peak fractions were assessed by Coomassie stained SDS-PAGE gel and Abs_{260}/Abs_{280} value, and the purest fractions were extensively dialyzed into water, aliquoted, flash frozen, and lyophilized. Lyophilized histones were reconstituted into H2A/H2B dimers, H3/H4 tetramers, and octamers as previously described [50], and purified via SEC using Superdex 75 (H2A/H2B) or Superdex 200 (H3/H4 and octamers) columns in SEC buffer (25 mM Tris-HCl pH 7.5, 2M NaCl, 1 mM DTT).

Fluorophore conjugation to histones and ubiquitin: For fluorophore conjugation, Alexa Fluor 680 C_2 maleimide (ThermoFisher), IRDye 680LT maleimide (Li-Cor), and Oregon green 488 maleimide (AAT Bioquest) were reconstituted in DMSO to 10 mM. Fluorophore maleimides were mixed with octamers containing single cysteine mutants H2A G-1C for H2A-Ub activity assays (with Alexa Fluor 680 C_2 maleimide or IRDye 680LT maleimide) or H2B D51C for binding assays (with Oregon green 488 maleimide). Conjugation reactions were performed using 20 mM octamer and 100 mM fluorophore overnight at 4 °C in conjugation buffer (25 mM Tris-HCl pH 7.5, 2M NaCl, 1 mM EDTA, 0.5 mM TCEP), and stopped by addition of 10 mM DTT and flash frozen. Excess fluorophore was removed after nucleosome reconstitution by SEC using a Superdex 200 increase 10/300 GL column or extensive buffer exchange in a 30K

MWCO concentrator (Amicon). Typical labelling efficiency was ~70%. For labelling of Ub Q2C, 100 mM Alexa Fluor 680 C_2 maleimide was mixed with ~1 mM of Ub Q2C in buffer (25 mM Tris-HCl pH 7.5, 1 mM EDTA, 0.5 mM TCEP) at 4 °C overnight. The reaction was quenched with 10 mM DTT, and buffer exchanged into reducing buffer (25 mM Tris-HCl pH 7.5, 1 mM EDTA, 10 mM DTT) in a concentrator to remove unconjugated dye, and stored at -80 °C. The fluorophore labelling efficiency of Ub was calculated to be ~5%.

Ubiquitin G76C and dichloroacetone crosslinking of H2A-Ub: H2A K15C, K119C, and K127C were generated by site-directed mutagenesis and purified as described above for individual histones. His-TEV-ubiquitin G76C was a gift from C. Wolberger (Addgene plasmid #75299) and purified as previously described [40,51]. Dichloroacetone crosslinking of Ub G76C to H2A single cysteine mutants was performed as previously described in detail [40], with the exception that the final product containing Ub, Ub-Ub dimers, and H2A-Ub was not purified by RP-HPLC to remove unconjugated Ub. Instead, it was lyophilized, and mixed with a slight excess of H2B in unfolding buffer (25 mM Tris-HCl pH 7.5, 7 M guanidinium-HCl, 0.5 mM EDTA, 1 mM DTT), refolded into H2A/H2B dimers in refolding buffer (25 mM Tris-HCl pH 7.5, 2M NaCl, 1 mM DTT), and purified by SEC using a 24 mL Superdex 75 column (GE Healthcare) to separate the H2A-Ub from Ub species.

'601' and MMTV DNA: For large scale purification of 147-bp '601' (gift from K. Luger, CU Boulder), 185-bp '601' (gift from S. Tan, Penn State Univ.), MMTV (gift from G. Debelouchina, (UC San Diego), and NLE-trimer '601' (for tri-NCP; gift from K. Luger) DNA, repeat plasmids from 8-12L of DH5a cells in LB media were subjected to alkaline lysis, phenol-chloroform extraction, PEG precipitation, EcoRV digestion (NEB), and ion exchange of the excised

fragment by HiTrap DEAE (147-bp '601', 185-bp '601', and MMTV; Cytiva) or mono-Q (NLE-trimer '601'; GE Healthcare) according to established protocols [50].

For UV-induced Bpa crosslinking and EMSA experiments, fluorophore labelled '601' DNA was generated using large-scale PCR with Phusion polymerase (produced in-house) from a pGEM-3z/601 plasmid containing one copy of '601' DNA (gift from J. Widom, Addgene plasmid #26656) [52] with 5'-IRdye700 labelled forward primers (IDT). Following PCR, the reactions were purified using a 1 mL mono-Q column equilibrated in ion-exchange buffer (25 mM Tris-HCl pH 8.0, 200 mM NaCl, 1 mM EDTA) over a 10-CV gradient (0.2-1M NaCl). Peak fractions containing purified 147- and 185-bp DNA fragments were dialyzed into storage buffer (10 mM Tris-HCl pH 8.0, 1 mM EDTA), concentrated, and stored at -20 °C. The primer sequences were as follows: 147-fwd: ctggagaatcccggtgccgagg; 147-rev: acaggatgtatatatctgacacg; 185-fwd: atccctatacgcggccgccctggagaatcccggtgccgagg
; 185-rev: atcgctgttcaatacatgcacaggatgtatatatctgacacg.

For generation of DNA fragments with DraIII sticky ends for dinucleosome assembly, large scale PCR was performed as described for the fluorophore-labelled DNA fragments above. Primer sequences containing DraIII cut-sites were based off those used by Poepsel *et al*. to make dinucleosomes with 35-bp of linker DNA [37]. Fragments used to reconstitute nucleosomes containing fluorophore-labelled H2A nucleosomes ($H2A^{observe}$) were generated using the "147-fwd" primer (sequence above) and the di-NCP reverse primer sequence (taggtatcgtatCACGGGGTGagatcgctacaggatgtatatatctgacacg). The fragment for the $H2A^{silent}$ nucleosomes were generated using the "147-rev" and the di-NCP-forward primer sequence (ctgacttattgaCACCCCGTGatgctcgatactgtcatactggagaatcccggtgccgag). The DraIII sites in the primers are underlined and uppercase. Following PCR purification by 1 mL mono-Q, DNA fragments were dialyzed into TE/0.1 buffer (10 mM Tris-HCl, 0.1 mM EDTA) and digested with

DraIII-HF in 1x CutSmart buffer for ~20 hr at 37 °C (NEB). Fragments with DraIII sticky ends were re-purified by 1 mL mono-Q ion-exchange, dialyzed into storage buffer (10 mM Tris-HCl, 1 mM EDTA), concentrated, and stored at -20 °C.

Nucleosome reconstitution: mono-nucleosomes (NCPs) were reconstituted by the standard salt-dialysis method by mixing histone octamers (or H3/H4 tetramers and H2A/H2B dimers) with '601' DNA in high salt buffer (25 mM Tris-HCl pH 7.5, 2M NaCl, 0.1 mM EDTA, 1 mM DTT) in a slide-a-lyzer mini dialysis unit (0.1 mL, ThermoFisher) [50]. Low-salt buffer (25 mM Tris-HCl pH 7.5, 0.1 mM EDTA, 1 mM DTT) was pumped in over ~24 hours in a cold room with stirring. A final dialysis was performed into NCP storage buffer (25 mM HEPES-NaOH, 10 mM NaCl, 0.1 mM EDTA, 1 mM DTT). Fluorophore-labelled nucleosomes were further purified by SEC using a 24 mL Superdex 200 increase 10/300 column equilibrated in NCP storage buffer or by extensive buffer exchange in a concentrator to remove excess fluorophore. For tri-NCPs, salt dialysis was performed as described for mono-NCPs using ~1.4x octamer to '601' sites in the presence of 0.2 equivalents of MMTV competitor DNA. Following dialysis into TEK10 (10 mM Tris-HCl pH 7.5, 0.1 mM EDTA, 10 mM KCl), trimers were precipitated by adding 4 mM $MgCl_2$, incubating on ice for 10 minutes and pelleted by centrifugation at 17,000 x g at 4 °C. The supernatant was discarded, and the pellet was gently resuspended in TEK10, and dialyzed overnight into NCP storage buffer. Tri-NCP assembly was verified by EcoRI digestion of sites located between nucleosome units.

For di-NCP assembly, mono-NCPs with DraIII sticky ends were assembled as described above. The strategy to make asymmetric di-NCPs was based on previously described methods [37,53]. 100 nM of each NCP was mixed in T4 ligase buffer (50 mM Tris-HCl pH 7.5, 10 mM $MgCl_2$, 1 mM ATP, 10 mM DTT) on ice. T4 ligase (NEB) was added to a final concentration of 20 U/µL,

the reaction was incubated for 30 minutes at 16 °C, and dialyzed into TEK10 for 4 hours at 4 °C. Following dialysis, $MgCl_2$ was added to a final concentration of 18 mM, incubated at room temperature for 15 minutes, and pelleted at 17,000 x g at 4 °C. The pellet containing di-NCPs was resuspended in 50 µL of TEK10 and dialyzed overnight into NCP storage buffer. All chromatin substrates were analyzed for quality on 5% polyacrylamide 0.5x TBE gels monitoring fluorescence and/or DNA-staining, ensuring minimal free DNA or contaminating species. Chromatin substrates were stored on ice for no longer than one month.

Design and assembly of DNA competitor fragments: single-stranded, double-stranded, bubble, frayed, and single-stranded overhang DNA fragments were assembled by annealing ssDNA oligos (IDT) in duplex buffer (30 mM HEPES-NaOH pH 7.5, 100 mM potassium acetate). Oligo mixtures were heated to 95 °C and slowly cooled to 25 °C stepwise over 1 hour in a thermocycler. For NMR experiments, dsDNA and bubble-DNA were buffer exchanged into NMR buffer in a spin concentrator (Amicon). The sequence of the bubble-DNA substrate was optimized from initial, longer substrates to generate a minimal substrate with the smallest stretch of mismatch and double-stranded annealing portions that (1) formed a discreet species on a DNA-stained native gel and (2) produced a robust effect of selective H2A-Ub inhibition in a nucleosome ubiquitylation assay. The sequences of oligos used are as follows. For ssDNA, dsDNA, bubbleDNA, and ssOverhang a common “bottom” oligo was used (ggtacacaattgcgctggtaccccaggcgtcgtagg). The oligos annealed to the “bottom” oligo were as follows: (dsDNA-top: cctacgacgcctggggtaccagcgcaattgtgtacc; bubbleDNA-top: cctacgacgcctggctctttcccgcaattgtgtacc; ssOverhang-top: ccgcaattgtgtac). For the frayed DNA, the annealed oligos were as follows: (frayedDNA-top: ggtacacaattgcgccaggcgtcgtaggctggtacc; frayedDNA-bottom: ctctttcccctacgacgcctggcgcaattgtgtacc).

Nucleosome ubiquitylation assays

Time-course H2A-Ub assays: The general setup for time-course H2A-Ub assays was a reaction mixture containing 0.2 mM E1 (UBA1), 1 mM E2 (UBE2D3), 30 mM ubiquitin, 0.5 mM NCP substrate, and 12.5-100 nM E3 (depending on the assay), assembled in 30 µL of reaction buffer (25 mM HEPES-NaOH pH 7.5, 150 mM NaCl). For assays containing di-NCPs, 10 nM of fluorophore-labelled di-NCP substrate was mixed with 0.5 mM unlabeled NCP^{147} substrate in the same reaction tube to facilitate quantifiable reaction kinetics. Critically, the salt concentration of each reaction within an assay was rigorously controlled, as H2A-Ub kinetics are extremely sensitive to differences in buffer ionic strength. 5 µL of each reaction was mixed 1:1 with 2x SDS-PAGE load dye as a zero time-point. The mixtures were brought to 37 °C in a heat block, and 1 µL of 100 mM $MgCl_2$/ATP was added (4 mM final concentration) to initiate the reaction, and the indicated time-points were obtained by diluting 5 µL the reaction 1:1 with 2x SDS-PAGE load dye. For experiments with tri-NCPs, the concentration of nucleosome units in the reaction was normalized to NCP^{147} and NCP^{185} (0.5 mM NCP unit or 0.17 mM tri-NCP), and reactions were initiated with 2 mM ATP and 1 mM $MgCl_2$.

Gel samples were run on 15% SDS-PAGE gels and visualized by in-gel fluorescence monitoring a fluorophore conjugated to the N-terminus of H2A. Alternatively, some assays were visualized by Western blot for H2A (EMD Millipore, 07-146) or a VSVG epitope tag on the N-terminal tag of H2A (Sigma, V4888) and a fluorescently labelled secondary antibody (Cell Signaling, 5151S). Gels and blots were imaged on a Li-Cor Odyssey imager (Li-Cor). Band quantification was performed using Image Studio software (Li-Cor) by drawing a box encompassing the unmodified H2A band to measure its intensity, performing background subtraction, and normalizing to the zero time-point of the reaction.

Inhibition of H2A-Ub by competitor DNA: A reaction mixture containing 0.2 mM E1 (UBA1), 3 mM E2 (UBE2D3), 30 mM ubiquitin, 0.5 mM NCP substrate, and 50 nM E3 (or 750 nM for $BRCA1^{RING}$/$BARD1^{RING}$) was assembled in 9 µL of reaction buffer (25 mM HEPES-NaOH pH 7.5, 100 mM NaCl) in PCR strips. To that, 1 µL of dsDNA or bubble-DNA competitor at 10x concentration was added. Reactions were brought to 37 °C in a thermocycler, started by addition of 5 µL of 10 mM ATP/$MgCl_2$, and allowed to proceed for 12-20 minutes depending on the E3. Reactions were stopped by addition of 10 µL of 4x fluorescence sample load dye (Li-Cor), resolved on a 15% SDS-PAGE gel, and visualized using a Li-Cor Odyssey imager. Quantification was performed as described above, monitoring the intensity of unmodified H2A, and normalizing each reaction to a -ATP reaction.

Auto-ubiquitylation assay: Reactions were assembled with 0.2 mM E1 (UBA1), 1 mM E2 (UBE2D3), 10 mM ubiquitin (Q2C-Alexa Fluor 680), and 0.2 mM of the indicated E3 in buffer (25 mM HEPES-NaOH pH 7.5, 50 mM NaCl), and were initiated by addition of 5 mM ATP/$MgCl_2$. After 60 minutes at 37 °C, reactions were quenched by mixing 1:1 with 4x fluorescence sample load dye (Li-Cor), resolved on a 4-20% SDS-PAGE gel (BioRad), and visualized using a Li-Cor Odyssey imager.

Nucleosome binding assays

Electrophoretic mobility shift assay: For EMSA experiments, 5 µL of 10 nM of substrate (NCPs with either H2A G-1C labelled with Alexa Fluor 680 or DNA/NCPs labelled with IRDye700) were mixed with 5 µL of indicated RING/RING heterodimer or BARD1 IDR constructs (2x concentrated) in EMSA buffer (15 mM Tris-HCl pH 7.5, 90 mM NaCl, 1 mM DTT, 0.1 mg/mL BSA, 0.05% triton X-100) in PCR strips. Binding was allowed to proceed for 10 minutes at room temperature, followed by 5 minutes on ice. 5 µL of 25% sucrose was added to each tube, and

15 µL of sample was loaded onto 5% polyacrylamide native gels (0.5x TBE) in pre-chilled 0.5x TBE buffer. Gels were run at 4 °C for 90-120 minutes at 110V and visualized using a Li-Cor Odessey scanner (Li-Cor).

Fluorescence-quenching binding experiments: Assay set up was performed essentially as previously described[15]. 10 µL of 10 nM NCPs with Oregon green 488 conjugated to H2B D51C in low-salt fluorescence buffer (25 mM Tris-HCl pH 7.5, 10 mM NaCl, 0.01% CHAPS, 0.01% NP40, 0.1 mg/ml BSA, 1 mM DTT) were mixed with the 10 µL of the indicated BRCA1/BARD1 construct at 2x concentration in high-salt fluorescence buffer containing either 90 mM, 190 mM, or 290 mM NaCl, depending on the assay, in a 384-well low volume black round bottom polystyrene non-binding surface microplate (Corning). Plates were briefly mixed, incubated at 22 °C for 10-15 minutes, and scanned using a BioTek Synergy Neo2 plate reader equipped with a fluorescence filter (excitation: 485/20 nm, emission: 528/20 nm). The gain was set to 100 for all experiments. Two technical replicates for each independent replicate experiment (fresh NCP and BRCA1/BARD1 dilutions) were performed, and the readings from two scans were averaged. BRCA1/BARD1/nucleosome binding interactions were quantitatively analyzed by fluorescence quenching assuming the following systems of equations:

$$\theta = \frac{K_D + [NCP] + [BCBD] - \sqrt{(K_D + [NCP] + [BCBD])^2 - 4 \times [NCP] \times [BCBD]}}{2 \times [NCP]}$$

$$F = [NCP] \times F_{NCP} \times (1 - q_{BCBD} \times \theta) + N(0, error)$$

where θ is the fraction of nucleosome bound by BRCA1/BARD1 (BCBD), F_{NCP} is the fluorescence per nucleosome, q_{BCBD} is the fraction of fluorescence quenching per BRCA1/BARD1 binding, and fluorescence measurements are gaussian distributed with mean 0. Maximum likelihood parameter estimates were determined using custom Python scripts with optimization by a differential evolution algorithm implemented in

Scipy (https://scipy.org/citing-scipy/). K_d and q_{BCBD} were separately estimated for each BRCA1/BARD1 construct, and NCP concentration was treated as a random effect per individual dilutions from higher concentration stock solutions, with the total number of model parameters being equal to number of NCP dilutions + (2 x number of BCBD constructs) + 2. The 95% confidence limits were estimated by computing the profile likelihood with an applied Bonferroni correction.

UV-induced Bpa crosslinking

NCPs and DNA for UV-induced crosslinking assays were reconstituted using a 185-bp '601' sequence labeled with an IRdye700 fluorophore (described above). 50 nM NCPs or DNA were incubated with 500 nM of the BRCA1$^{1-104}$-$(GS)_6$-BARD1$^{26-221}$ fusion (wild-type or with different Bpa-incorporated sites L120Bpa, W146Bpa, Y180Bpa, A195Bpa, W218Bpa) for 15 minutes at 4°C in 30 uL UV Crosslinking buffer (20 mM HEPES-NaOH pH 7.5, 100 mM NaCl) in a 96-well clear round bottom polystyrene non-treated microplate (Corning). Following incubation, 5 µL was added to 5 µL 2X SDS-PAGE gel-loading dye for the -UV sample. Samples were then subjected to UV irradiation (365 nm) using a Blak-Ray B-100AP/R High Intensity UV Lamp (UVP) from 20 cm for 30 minutes at 4°C. Following irradiation, 5 µL was added to 5 µL of 2x SDS-PAGE gel-loading dye. Samples were heated at 60°C for 5 minutes and separated on 10% SDS-PAGE gels. Gels were visualized using a Li-Cor Odyssey scanner (Li-Cor). Band quantification was performed using Image Studio software (Li-Cor) by drawing a box measuring the total band intensity for each cross-linked product, subtracting the background signal, and normalizing to the cross-linked band of the L120Bpa fusion mutant. For the Bpa UV crosslinking DNA competition assays, 50 nM NCPs were incubated with 500 nM BRCA1-f-BARD1^{221} (W146Bpa or A195Bpa) with varying amounts of competitor 36-mer dsDNA or bubble-DNA (0,

0.3125, 0.625, 1.25, 2.5, 5, or 10 μM) for 15 minutes at 4°C, and assays were performed as described above.

Chemical Cross-linking and Mass Spectrometry Analysis

Sample preparation: Chemical cross-linking and mass spectrometry analysis was carried out as described[54]. Reactions were 90 μL of protein/nucleosome mix containing 2 mM $BRCA1^{RING}$/$BARD1^{FL}$ and 2 mM of unmodified H2A or H2A K15-Ub nucleosomes wrapped with 147-bp '601' DNA in crosslinking bufffer (25 mM HEPES-NaOH pH 7.5, 150 mM NaCl, 1% glycerol, 1 mM DTT) plus 3.06 μL of 14.5 mM DSS or BS3 (final concentration 0.5 mM) (DSS: disuccinimidyl suberate, BS3: bis(sulfosuccinimidyl)suberate, ThermoFisher). Crosslinking was carried out for 10, 30 or 45 mins at room temperature before removing 30 μL and quenching by addition of 3 μL of 1 M ammonium bicarbonate at room temperature for 30 minutes. Four separate reaction conditions were performed: (1) WT-NCP DSS; (2) WT-NCP BS3; (3) K15Ub-NCP DSS; (4) K15Ub-NCP BS3. After quenching, 9 μL of each sample at each timepoint was analyzed by SDS-PAGE **(see Extended Data Fig 1a)** and the remainder was stored at -80°C until processing for mass spectrometry analysis.

Reactions were prepared for MS analysis by bringing them up to 0.1% PPS silent surfactant (Expedion Inc.), 5 mM TCEP. Samples were reduced for 60 mins at 60°C in an Eppendorf Thermomixer with shaking (1200 rpm). Alkylation was performed at room temperature in the dark for 30 mins with 6 mM iodoacetamide. Excess iodoacetamide was quenched by addition of 5 mM DTT and samples were then digested by trypsin digestion (Sequencing Grade Modified Trypsin, Promega Corp) at 37°C for 6 hours in a Thermomixer with shaking (1000 rpm) at a substrate to enzyme ratio of 15:1 prior to acidification with 250 mM HCl (final concentration). Acidified samples were incubated for 1 hour at room temperature, spun at max speed in a

microfuge and supernatants containing peptides were transferred to autosampler vials and stored at -80°C until analysis.

Chromatography: Mass spectrometry and data analysis were performed as previously described[54]. For each injection, 3 µl of protein digests were loaded by autosampler onto a 150-µm Kasil fritted trap packed with 2 cm of Reprosil-Pur C18-AQ (3-µm bead diameter, Dr. Maisch) at a flow rate of 2.5 µl/min. After desalting with 8 µl of 0.1% formic acid plus 2% acetonitrile, the trap was brought online with a Self-Packed PicoFrit Column (New Objective part number PF360-75-10-N-5, 75 µm i.d.) packed with 30 cm of Reprosil-Pur C18-AQ (3-µm bead diameter, Dr. Maisch) mounted to a heated nanospray ionization source (CorSolutions LLC) set at 50°C and placed in line with a Thermo Scientific EASY-nLC 1200 UPLC pump plus autosampler.

Peptides were eluted from the column at 0.25 µL/min using an acetonitrile gradient consisting of the following steps: (1) 0-10 mins; 6-10% B; (2) 10-90 mins; 10-32% B; (3) 100-130 mins; 32-75% B; (4) 130-135 mins; 75% B; (5) 135-136 mins; 75-100% B; (6) 136-151 mins; 100% B, followed by re-equilibration to 0% buffer B prior to the subsequent injection. Buffer A was: 0.1% formic acid in water and buffer B was 0.1% formic acid 80% acetonitrile.

Data acquisition: Thermo Fisher Scientific Exploris 480 was used to perform mass spectrometry in positive ion mode with the following settings. Data dependent acquisition (DDA) mode was used with a maximum of 20 tandem MS (MS/MS) spectra acquired per MS spectrum (scan range of *m/z* 400–1,600). The resolution for MS and MS/MS was 60,000 at *m/z* 200. The normalized automatic gain control targets for both MS and MS/MS were set to 100%, and the maximum injection times were 50 and 100 ms for MS and MS/MS scans, respectively. MS/MS spectra were acquired using an isolation width of 2 *m/z* and a normalized collision energy of 27.

MS/MS acquisitions were prevented for +1, +2, ≥+6 or undefined precursor charge states. Dynamic exclusion was set for 10 seconds. MS and MS/MS spectra were collected in centroid mode.

DDA data processing – identification of cross-linked peptides: Acquired spectra were converted into mzML using ProteoWizard's msconvert[55]. All proteins in the sample were identified using Comet[56] searching against a database including the entire *S. frugiperda*, *E. coli* and *H. sapiens* proteomes (Uniprot 7108, 83333 and 9606, respectively) plus common contaminants (https://www.thegpm.org/crap/) along with the sequences of all heterologously expressed proteins (FLAG-BRCA1, P38398; TwinStrepII-BARD1, Q99728; H2A-2A, Q99728; H2B-1K, O60814 ; H3.2 (C110A), Q71DI3; H4, P62805; Ub G76C, sequence derived from P0CG48). Smaller search databases were made for subsequent XL searching consisting only of proteins identified in initial comet searches by at least 3 peptides with a Percolator assigned q-value of ≤ 0.01. Decoy databases consisted of the corresponding set of reversed protein sequences. Cross-linked peptides were identified within these proteins by Kojak version 2.0.0-alpha8 available at (http://www.kojak-ms.org/)[57]. A statistically meaningful q-value was assigned to each peptide spectrum match (PSM) through analysis of the target and decoy PSM distributions using Percolator version 2.08[58]. All data reported in this paper were filtered to show hits to the target proteins that had a Percolator assigned peptide level q value ≤ 0.05.

NMR experiments and resonance assignments.

All spectra were collected at 25° C in NMR buffer (25 mM MOPS-NaOH, 100 mM NaCl, 1 mM EDTA, and 0.5 mM TCEP, pH 7.0) with 7% D_2O. NMR HSQC and titration data were completed on a Bruker 800 MHz Avance III spectrometer with cyroprobe. (^{1}H,^{15}N)-HSQC spectra were collected on the following ^{15}N-BARD1 IDR constructs: BARD1 Ser-124-424, Ser-124-270, 269-424, and Ser-141-216.

(^{1}H,^{15}N)- and (^{1}H,^{13}C)-HSQC titration experiments were completed for BARD1 IDR + 36mer-dsDNA or 36mer-bubDNA by adding unlabeled DNA to 150 μM [^{13}C,^{15}N]-BARD1 124-270 or 150 μM [^{13}C,^{15}N]-BARD1 Ser-141-216, maintaining a constant concentration of the labeled species. Only apo and 1:1 spectra for the [^{13}C,^{15}N] BARD1 Ser-141-216 construct were obtained since intermediate titration points resulted in loss of sample. Additionally, titration spectra with nucleosome were collected for 150 μM [^{13}C,^{15}N]-BARD1 124-270 + 0.05x NCP[147]. A (^{1}H,^{15}N)-HSQC was collected on 150 μM ^{15}N-BARD1 269-424 + 150 μM 28mer-dsDNA.

Dynamics experiments were collected on a Bruker 500 MHz Avance III spectrometer with a room temperature probe. T_1 and T_2 ^{15}N-Trosy HSQC experiments for 150 μM [^{13}C,^{15}N]-BARD1 Ser-141-216, 150 μM [^{13}C,^{15}N]-BARD1 Ser-141-216 + 150 μM 36mer-dsDNA, and 150 μM [^{13}C,^{15}N]-BARD1 Ser-141-216 + 150 μM 36mer-bubble-DNA were collected in an interleaved manner with 8 points each[59]. T_1 delays were 10, 40, 80, 120, 160, 320, 640, and 1000 ms; T_2 cpmg loop delays were 8.48, 16.96, 25.44, 25.44, 42.40, 50.88, 67.84, and 84.80 ms. T_1 and T_2 for each residue were fitted to a single exponential with errors reflecting the quality in the fit. Residues corresponding to peaks with overlapping intensities were excluded from the analysis.

Backbone chemical shift assignments were determined from standard backbone triple-resonance experiments (HNCA, HNCOCA, HNCOCACB, HNCACB, HNCO, and HNCACO) and an HNHA experiment using a Bruker 800 MHz Avance III spectrometer with cryoprobe. The 3D data were collected for 500 μM [^{13}C,^{15}N]-BARD1 Ser-124-270 and 500 μM [^{13}C,^{15}N]-BARD1 Ser-141-216. Assignments from the shorter construct were transferred as appropriate to the longer BARD1 construct. HNCACB and HNCOCACB spectra were collected on the 1:1 samples of 150 μM [^{13}C,^{15}N]-BARD1 Ser-141-216 with either 36mer dsDNA or 36mer bubble-DNA.

The NH chemical shift perturbation was calculated according to $\Delta\delta_{NH}$ (ppm) = sqrt [$\Delta\delta_H^2$ + ($\Delta\delta_N$/5)^2]. Component ^{1}H and ^{15}N chemical shift differences are (free – bound) in ppm. The CaCb CSP was calculated according to $\Delta\delta_{CaCb}$ (ppm) = 0.25*[(Cα-Cβ)$_{free}$-(Cα-Cβ)$_{bound}$]. Secondary structure propensity (SSP) was determined from Δδ(Cα-Cβ) = (Cα-Cβ)$_{measured}$ - (Cα-Cβ)$_{random\ coil}$, where the random coil shifts were generated from BARD1 IDR sequence using a webserver (https://spin.niddk.nih.gov/bax/nmrserver/Poulsen_rc_CS/)[60].

Multiple Sequence Alignment

Mammalian BARD1 ortholog sequences were downloaded from Ensembl (v106), globally aligned using MAFFT[61], and trimmed to BARD1 residues 124-270.

Data availability Statement

Raw binding and H2A-Ub data as well as uncropped gels and blots are included as supplemental files. For crosslinking mass-spectrometry analysis, the complete unfiltered list of all PSMs and their Percolator assigned q values are available on the ProXL web application[62,63] https://proxl.yeastrc.org/proxl/p/bard1nucleosome along with the raw MS spectra and search parameters used. In addition, complete search algorithm configuration files, fasta search databases, raw search output and raw MS data files were deposited to the ProteomeXchange Consortium via the PRIDE[64] partner repository with the dataset identifier XXXXXX. NMR chemical shift assignments for BARD1 Ser-141-216 have been deposited to the Biological Magnetic Resonance Bank with dataset identifier YYYYYY. Plasmid reagents generated in this study can be obtained upon request from the corresponding author Dr. Rachel Klevit.

References (methods only)

43. Brzovic, P. S. *et al.* Binding and recognition in the assembly of an active BRCA1/BARD1 ubiquitin-ligase complex. *Proc. Natl. Acad. Sci. U. S. A.* **100**, 5646–5651 (2003).

44. Christensen, D. E., Brzovic, P. S. & Klevit, R. E. E2-BRCA1 RING interactions dictate synthesis of mono- or specific polyubiquitin chain linkages. *Nat. Struct. Mol. Biol.* **14**, 941–948 (2007).
45. Lazar, G. A., Desjarlais, J. R. & Handel, T. M. De novo design of the hydrophobic core of ubiquitin. *Protein Sci. Publ. Protein Soc.* **6**, 1167–1178 (1997).
46. Chin Jason W., Martin Andrew B., King David S., Wang Lei, & Schultz Peter G. Addition of a photocrosslinking amino acid to the genetic code of Escherichia coli. *Proc. Natl. Acad. Sci.* **99**, 11020–11024 (2002).
47. Tan, W. *et al.* Preparation and purification of mono-ubiquitinated proteins using Avi-tagged ubiquitin. *PLOS ONE* **15**, e0229000 (2020).
48. Lee, Y.-T., Gibbons, G., Lee, S. Y., Nikolovska-Coleska, Z. & Dou, Y. One-pot refolding of core histones from bacterial inclusion bodies allows rapid reconstitution of histone octamer. *Protein Expr. Purif.* **110**, 89–94 (2015).
49. Luger, K., Rechsteiner, T. J. & Richmond, T. J. Preparation of nucleosome core particle from recombinant histones. *Methods Enzymol.* **304**, 3–19 (1999).
50. Dyer, P. N. *et al.* Reconstitution of Nucleosome Core Particles from Recombinant Histones and DNA. in *Methods in Enzymology* vol. 375 23–44 (Academic Press, 2003).
51. Morgan Michael T. *et al.* Structural basis for histone H2B deubiquitination by the SAGA DUB module. *Science* **351**, 725–728 (2016).
52. Lowary, P. T. & Widom, J. New DNA sequence rules for high affinity binding to histone octamer and sequence-directed nucleosome positioning11Edited by T. Richmond. *J. Mol. Biol.* **276**, 19–42 (1998).
53. Dao, H. T., Dul, B. E., Dann, G. P., Liszczak, G. P. & Muir, T. W. A basic motif anchoring ISWI to nucleosome acidic patch regulates nucleosome spacing. *Nat. Chem. Biol.* **16**, 134–142 (2020).
54. Zelter, A. *et al.* The molecular architecture of the Dam1 kinetochore complex is defined by cross-linking based structural modelling. *Nat. Commun.* **6**, 8673 (2015).
55. Chambers, M. C. *et al.* A cross-platform toolkit for mass spectrometry and proteomics. *Nat. Biotechnol.* **30**, 918–920 (2012).
56. Eng, J. K., Jahan, T. A. & Hoopmann, M. R. Comet: An open-source MS/MS sequence database search tool. *PROTEOMICS* **13**, 22–24 (2013).
57. Hoopmann, M. R. *et al.* Kojak: Efficient Analysis of Chemically Cross-Linked Protein Complexes. *J. Proteome Res.* **14**, 2190–2198 (2015).
58. Käll, L., Canterbury, J. D., Weston, J., Noble, W. S. & MacCoss, M. J. Semi-supervised learning for peptide identification from shotgun proteomics datasets. *Nat. Methods* **4**, 923–925 (2007).
59. Zhu, G., Xia, Y., Nicholson, L. K. & Sze, K. H. Protein Dynamics Measurements by TROSY-Based NMR Experiments. *J. Magn. Reson.* **143**, 423–426 (2000).
60. Kjaergaard, M. & Poulsen, F. M. Sequence correction of random coil chemical shifts: correlation between neighbor correction factors and changes in the Ramachandran distribution. *J. Biomol. NMR* **50**, 157–165 (2011).
61. Katoh, K. & Standley, D. M. MAFFT Multiple Sequence Alignment Software Version 7: Improvements in Performance and Usability. *Mol. Biol. Evol.* **30**, 772–780 (2013).

62. Riffle, M., Jaschob, D., Zelter, A. & Davis, T. N. ProXL (Protein Cross-Linking Database): A Platform for Analysis, Visualization, and Sharing of Protein Cross-Linking Mass Spectrometry Data. *J. Proteome Res.* **15**, 2863–2870 (2016).

63. Riffle, M., Jaschob, D., Zelter, A. & Davis, T. N. Proxl (Protein Cross-Linking Database): A Public Server, QC Tools, and Other Major Updates. *J. Proteome Res.* **18**, 759–764 (2019).

64. Vizcaíno, J. A. *et al.* A guide to the Proteomics Identifications Database proteomics data repository. *PROTEOMICS* **9**, 4276–4283 (2009).

SUMMARY OF MAJOR FINDINGS AND OUTLOOK

BRCA1 was the first breast cancer susceptibility gene to be identified over thirty years ago. Since then, great progress has been made in screening patients for harmful mutations, implementation of prophylactic measures, and treatment options. Moreover, study of the basic biology of BRCA1 has led to vastly increased understanding of its roles in DNA damage repair and transcriptional regulation, as well as these processes in general. Recently, attention has been drawn towards the heterodimeric binding partner of BRCA1, BARD1, as more than just a passive player in its tumor suppressive functions. This is partially due to the discovery of families with cancer predisposing BARD1 mutations, many of which are localized to that BARD1 RING domain. Together with the BRCA1 RING domain, the BRCA1/BARD1 RING/RING heterodimer constitutes the enzymatic core of the protein as an E3 ubiquitin ligase. However, given that the BRCA1 RING domain is the “active” RING that binds to E2~Ub conjugates while BARD1 does not, the impact of mutations in the BARD1 RING has remained unclear. In this thesis, I have described a critical function for the BARD1 RING domain in directing site-specific transfer of ubiquitin onto the substrate H2A in nucleosomes. This signal has emerging roles in BRCA1/BARD1-mediated DNA repair and transcriptional regulation. More generally, I have provided insight into how the full-length BRCA1/BARD1 protein associates with chromatin, where it performs most of its functions in the nucleus. Together, my findings provide insight into possible mechanistic underpinnings for cancer-predisposing mutations and establish a basis for future studies investigating the cellular biology of BRCA1/BARD1-mediated processes.

In Chapter 3 of this Thesis, I have described a mechanism of site-specific ubiquitin transfer to H2A Lys residues 125, 127, and 129 in the extreme flexible C-terminal tail of H2A in nucleosomes, which is likely a preeminent cellular substrate for BRCA1/BARD1. Major insights into site-specificity comes from a cryo-EM structure of the BRCA1/BARD1/UbcH5c/nucleosome complex. The structure reveals that the BRCA1 and BARD1 RING domains each make distinct

contacts with the histone surface. Although the BRCA1-histone contacts are similar to those observed by other RING-type E3s that target different residues on H2A for Ub transfer, the BARD1 RING domain binds to a unique surface of the histone core. This causes a distinct binding orientation of the BRCA1/BARD1 RING domains on the nucleosome histone surface compared to other RING-type E3s that modify H2A. This RING binding orientation causes the BRCA1-bound E2 enzyme to be removed from the histone surface, rendering it unable to access the canonical H2A-Ub site (H2A K119) for ubiquitin transfer. However, the highly dynamic C-terminal tail of H2A where Lys 125, 127, and 129 reside can sample the E2 active site for Ub transfer. This study provides critical new insight into the function of the BARD1 RING domain. Importantly, it establishes BARD1 as an active player in binding to substrates (the nucleosome) for Ub transfer. This provides insight into the potential effects of cancer predisposing BARD1 RING mutations that abrogate the ability of BRCA1/BARD1 to bind to nucleosomes and ubiquitylate H2A *in vitro*. Together with previously published work, these findings delineate strategies that RING-type E3s use to target specific lysine residues on the same substrate to perform biologically non-redundant functions.

In Chapter 4, I describe extensive multivalent interactions between BARD1 and nucleosomes that facilitate enhanced H2A ubiquitylation and nucleosome binding. By using full-length BRCA1/BARD1 and truncation mutants, in addition to higher order chromatin substrates, I present a model where BARD1 engages nucleosomes through two to three points of contact, depending on the existing histone post-translational modifications. These include (1) the enzymatic BRCA1/BARD1 RING domains with the histone surface as described in Chapter 3, (2) a strong DNA-binding region within the BARD1 intrinsically disordered region (IDR), and (3) the BARD1 CTDs with the histone surface only in the presence of nucleosomes with preinstalled H2A K15-Ub and H4 K20me0 (a signal of DNA damage and repair). These additional interactions boost the affinity of the complex, yielding strong binding in the nanomolar

affinity regime that leads to increased H2A-Ub activity. This work also identifies specialized DNA structures that are found in DNA damage repair that can compete with the nucleosomal DNA for binding to the BARD1 DNA-binding region, providing a potential mechanism for spatiotemporal regulation of chromatin occupancy and localization. Although this work examines chromatin association of BRCA1/BARD1 through the lens of H2A-Ub activity, we describe complexes with nucleosomes that span almost the entirety of the BARD1 sequence and are likely to be important in multiple processes where BRCA1/BARD1 binds to chromatin. Furthermore, these results help to contextualize recent findings that were obtained using the isolated BARD1 RING domains (such as in Chapter 3) and the isolated BARD1 CTDs within the full-length BRCA1/BARD1 protein.

My studies and others have illuminated the structural and biochemical features of BRCA1/BARD1 interactions with chromatin that lead to H2A-Ub activity *in vitro*. However, a comprehensive understanding of what this histone mark is doing in cells remains largely unknown and even disputed in the field. BRCA1/BARD1-mediated H2A-Ub has been linked to its functions in DNA repair by homologous recombination. However, follow-up studies using the same BRCA1/BARD1 mutants were unable to replicate these original findings, casting doubt on their validity and on the importance of BRCA1/BARD1-dependent H2A-Ub activity in DNA repair. This compounds on a history of published findings that report on the dispensability of BRCA1/BARD1 E3 Ub ligase activity in DNA repair processes, potentially using flawed experimental systems and mutants as described in more detail in Chapter 1 of this Thesis (for example, BRCA1-I26A). Together, this disagreement in the scientific community necessitates additional studies with the clear aim of investigating the role of BRCA1/BARD1-mediated H2A-Ub and Ub ligase activity in general in DNA damage repair processes.

Several recent advancements described in this work and others will aid in this: (1) generation of a truly “ligase dead” BRCA1 mutant (BRCA1-3A) and (2) identification of BRCA1 and BARD1 separation-of-function mutants that disrupt H2A-Ub (BARD1 P89A/W91A and BRCA1 K70A/R71A). Additionally, studies have begun to reveal nuanced requirements for various domains of BRCA1/BARD1 in recruitment to damaged chromatin, all of which must be considered when designing experiments. Due to clear patterns of tissue-specificity in BRCA1/BARD1 cancers, future studies must also not be limited to cancer cell lines with obvious and convenient DNA damage sensitivity phenotypes. In addition to these experimental considerations, a roadblock to understanding BRCA1/BARD1-mediated H2A-Ub in cells is a current inability to detect this mark in cells and animals. Experimental reagents and technologies (i.e., H2A-Ub antibodies, mass-spectrometry protocols, etc.) should be developed to monitor these marks in cells and animals. This must not be limited to canonical H2A isoforms, as emerging evidence supports that specialized H2A isoforms may also be the primary target for BRCA1/BARD1 (i.e., H2A.X, H2A.Z, macroH2A1). Although many researchers in the BRCA1/BARD1 field believe that it it’s Ub ligase activity is unimportant in DNA damage repair processes, this authors’ opinion is that the current lines of reasoning are incomplete, and at least partially based on deeply flawed experiments. With recent advancements in understanding of the BRCA1/BARD1 RING heterodimer, as well as a sustained investment in developing critical, missing reagents and technologies, these questions will be able to be addressed in a rigorous and nuanced manner.

In addition to the role of BRCA1/BARD1 in DNA damage repair, several additional important questions remained to be answered. First, how is BRCA1/BARD1 targeted to genomic locations to deposit H2A-Ub? Although H2A K15-Ub is a robust marker of DNA damage, there is also support for a role of BRCA1/BARD1-mediated H2A-Ub in transcriptional regulation. Therefore, it is likely that histone PTMs other than H2A K15-Ub may recruit or inhibit BRCA1/BARD1

occupancy at genomic regions to deposit its H2A-Ub signal. An example of this is inhibition of H2A-Ub in the presence of H3 K79me2 described in Chapter 3 of this work, which is generally a signal of actively transcribed chromatin. An unbiased screen of BRCA1/BARD1-dependent H2A-Ub and nucleosome-binding using available libraries of chemically modified nucleosome substrates containing a variety of histone PTMs may provide insight into under how BRCA1/BARD1 is targeted to specific regions of chromatin. These studies will generate hypotheses to investigate BRCA1/BARD1-dependent H2A-Ub in cells and animals. In addition to investigating the role of H2A-Ub in DNA repair, studies of this mark in transcriptional regulation and other processes should be pursued. A major unanswered question is what are the subsets of genes regulated by H2A-Ub in relevant cell types? So far, genes have been identified through a candidate-based approach. But with the availability of sequencing technologies, identification of additional genes controlled by BRCA1/BARD1-mediated H2A-Ub is within reach. To this end, another important effort is to identify histone “readers” that specifically recognize BRCA1/BARD1-mediated H2A K127-Ub signals. Identification of these binding factors is likely to illuminate biological pathways associated with this histone mark and provide additional experimental footholds for investigation.

In conclusion, while great progress has been made to understand the biological processes attributable to BRCA1/BARD1, much remains unknown. With a concerted effort, the field is now poised to answer questions that have evaded researchers for decades. Ultimately, these findings may establish new methods and criteria to evaluate BRCA1/BARD1 variants of unknown clinical significance and produce insights into deeply complicated and intertwined biological processes that are required for its tumor suppressive functions.